

A Molecular Investigation of the Antimicrobial Functions of the Human S100 Host-Defense Proteins

by

Lisa Stephanie Cunden

B. A. Chemistry
Smith College, 2013

Submitted to the Department of Chemistry in Partial Fulfillment of the Requirements of the Degree of

DOCTOR OF PHILOSOPHY IN CHEMISTRY

at the
Massachusetts Institute of Technology

February 2019

©Massachusetts Institute of Technology, 2019
All Rights Reserved

Signature of Author: _____ **Signature redacted**

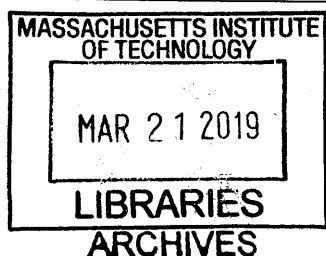
Department of Chemistry
January 15, 2019

Certified by: _____ **Signature redacted**

Elizabeth M. Nolan
Associate Professor of Chemistry
Thesis Supervisor

Accepted by: _____ **Signature redacted**

Robert W. Field
Haslam and Dewey Professor of Chemistry
Chairman, Departmental Committee for Graduate Students



This doctoral thesis has been examined by a committee of the Department of Chemistry as follows:

Signature redacted

Bradley L. Pentelute
Associate Professor of Chemistry
Committee Chairperson

Signature redacted

Elizabeth M. Nolan
Associate Professor of Chemistry
Thesis Supervisor

Signature redacted

Catherine L. Drennan
HHMI Professor and Investigator and Professor of Chemistry and Biology
Committee Member

A Molecular Investigation of the Antimicrobial Functions of the Human S100 Host-Defense Proteins

by

Lisa Stephanie Cunden

Submitted to the Department of Chemistry
On 01/15/2019 in Partial Fulfillment of the
Requirements of the Degree of
Doctor of Philosophy in Chemistry

ABSTRACT

The human host is continually exposed to potentially harmful organisms and the innate immune response is the first line of defense against microbial invasion. One strategy employed by the human innate immune system includes the release of antimicrobial host-defense proteins (HDPs). The goal of this thesis is to understand the antimicrobial functions of four host-defense proteins of the S100 family of proteins: calprotectin (CP), S100A12, S100A7, and S100A15. In the first half of this thesis, we elucidate the Zn(II)-binding and antimicrobial properties of S100A12 and S100A7 through the use of solution and microbiology studies. We evaluate the affinity of S100A12 for Zn(II), the scope of its antimicrobial activity, and put forward a model whereby S100A12 uses Ca(II) ions to tune its Zn(II)-chelating properties and antimicrobial activity. Our work with S100A7 demonstrates that the protein may exist in more than one redox state under physiological conditions, and that unlike CP and S100A12, the antimicrobial properties of S100A7 are not directly modulated by Ca(II) ions. We report a model whereby the local redox environment of S100A7 tunes its Zn(II)-sequestration capacity through intramolecular disulfide-bond redox chemistry, and that Ca(II) ions exert an indirect modulatory effect on the Zn(II)-binding properties of this protein. In the second half of this thesis, we examine the bactericidal properties of the four S100 proteins. Our results agree with prior work on the bactericidal properties of S100A7. Furthermore, we show that CP and S100A15, but not S100A12, possess bactericidal activity at pH 5, and that CP is a broad-spectrum Gram-negative bactericidal factor that functions through a mechanism of membrane permeabilization. Taken together, our studies provide new insights into the multifunctionality of the antimicrobial S100 HDPs.

Thesis Supervisor: Elizabeth M. Nolan
Title: Associate Professor of Chemistry

Chapter Abstracts

Chapter 1: A Molecular Investigation of the Antimicrobial Functions of the Human S100 Host-Defense Proteins

The innate immune system is the first line of defense against microbial invasion. This chapter reviews the roles that host-defense peptides (HDPs) play in preventing pathogenic colonization, with a focus on select members of the family of S100 HDPs, which include CP (calprotectin), S100A7 (psoriasin), S100A15 (koebnerisin), and S100A12 (calgranulin C). These relatively small (≈ 10 kDa) α -helical Ca(II)-binding host-defense peptides are multifaceted and at least two distinct mechanisms of action have been proposed to explain their antimicrobial activities. The first mechanism is one of metal sequestration, whereby the proteins starve pathogens of essential metal nutrients, including Mn, Fe, Cu, Ni, and Zn. The second mechanism involves microbicidal activity, resulting in direct killing of pathogens. The molecular details for the antimicrobial functions of CP, S100A7, S100A15, and S100A12 are discussed in this chapter.

Chapter 2: Calcium Ions Tune the Zinc-Sequestering Properties and Antimicrobial Activity of Human S100A12

Human S100A12 is a host-defense protein expressed and released by neutrophils that contributes to innate immunity. Apo S100A12 is a 21-kDa antiparallel homodimer that harbors two Ca(II)-binding EF-hand domains per subunit and exhibits two His₃Asp motifs for chelating transition metal ions at the homodimer interface. In this Chapter, we present results from metal-binding studies and microbiology assays designed to ascertain whether Ca(II) ions modulate the Zn(II)-binding properties of S100A12 and further evaluate the antimicrobial properties of this protein. Our metal depletion studies reveal that Ca(II) ions enhance the ability of S100A12 to sequester Zn(II) from microbial growth media. We report that human S100A12 has antifungal activity against *Candida albicans*, *C. krusei*, *C. glabrata* and *C. tropicalis*, all of which cause human disease. This antifungal activity is Ca(II)-dependent and requires the His₃Asp metal-

binding sites. We expand upon prior studies of the antibacterial activity of S100A12 and report Ca(II)-dependent and strain-selective behavior. S100A12 exhibited *in vitro* growth inhibitory activity against *Listeria monocytogenes*. In contrast, S100A12 had negligible effect on the growth of *Escherichia coli* K-12 and *Pseudomonas aeruginosa* PAO1. Loss of functional ZnuABC, a high-affinity Zn(II) import system, increased the susceptibility of *E. coli* and *P. aeruginosa* to S100A12, indicating that S100A12 deprives these mutant strains of Zn(II). To evaluate the Zn(II)-binding sites of S100A12 in solution, we present studies using Co(II) as a spectroscopic probe and chromophoric small-molecule chelators in Zn(II) competition titrations. We confirm that S100A12 binds Zn(II) with a 2:1 stoichiometry, and our data indicate sub-nanomolar binding affinity. Taken together, these data support a model whereby S100A12 uses Ca(II) ions to tune its Zn(II)-chelating properties and antimicrobial activity.

Chapter 3: Biochemical and Functional Evaluation of the Intramolecular Disulfide Bonds in the Zinc-Chelating Antimicrobial Protein Human S100A7 (Psoriasin)

Human S100A7 (psoriasin) is a metal-chelating protein expressed by epithelial cells. It is a 22-kDa homodimer with two EF-hand domains per subunit, and two transition-metal-binding His₃Asp sites at the dimer interface. Each subunit contains two cysteine residues that can exist as free thiols (S100A7_{red}) or as an intramolecular disulfide bond (S100A7_{ox}). In this Chapter, we examine the disulfide bond redox behavior, the Zn(II)-binding properties, and the antibacterial activity of S100A7, as well as the effect of Ca(II) ions on these properties. In agreement with prior work (Hein *et al. Proc. Natl. Acad. Sci. U. S. A.* **2013**, *112*, 13039-13044), we show that apo S100A7_{ox} is a substrate for the mammalian thioredoxin system; however, negligible reduction of the disulfide bond is observed for Ca(II)- and Zn(II)-bound S100A7_{ox}. Furthermore, metal binding depresses the midpoint potential of the disulfide bond. S100A7_{ox} and S100A7_{red} each coordinate two equivalents of Zn(II) with sub-nanomolar affinity in the absence and presence of Ca(II) ions,

and the cysteine thiolates in S100A7_{red} do not form a third high-affinity Zn(II) site. These results refute a prior model implicating the Cys thiolates of S100A7_{red} in high-affinity Zn(II) binding (Hein *et al. Proc. Natl. Acad. Sci. U. S. A.* **2013**, *112*, 13039-13044). S100A7_{ox} and the disulfide-null variants show comparable Zn(II)-depletion profiles; however, only S100A7_{ox} exhibits antibacterial activity against several bacterial species. Metal substitution experiments suggest that the disulfide bonds in S100A7 may enhance metal sequestration by the His₃Asp sites and thereby confer growth inhibitory properties to S100A7_{ox}.

Chapter 4: Investigation of the Bactericidal Properties of the Host-Defense Protein Human Calprotectin

Human calprotectin (CP) is accepted to inhibit bacterial growth by withholding metals through a process termed nutritional immunity. In this Chapter, we investigate an alternate, bactericidal activity of this protein. We show that CP is an effective AMP with enhanced activity at acidic pH, and that CP is resistant to high salt, but that binding of divalent metals Ca(II) and Zn(II) results in an attenuation of the activity of CP. We employ phase-contrast microscopy to image the cell morphology phenotypes caused by CP and employ a Live-Dead stain to show that the phenotypes are associated with cell wall permeabilization. Furthermore, fluorescence imaging studies reveal that CP causes leakage of periplasmic GFP indicating that CP affects the periplasmic integrity of *E. coli* cells. Next, we expand on the scope of the bactericidal activity of CP and argue that it can be considered a broad-spectrum AMP against Gram-negative strains. The underlying molecular details for this interaction are currently unclear, but we postulate that it may be mediated by electrostatic interactions between CP and the negatively-charged LPS moieties found on the outer-membrane of Gram-negative strains, or other cell-surface lipoproteins.

Chapter 5: Investigation of the Bactericidal Properties of Four Human S100 Proteins: Calprotectin, S100A7, S100A15, and S100A12

CP (calprotectin), S100A7 (psoriasin), S100A15 (koebnerisin), and S100A12 (calgranulin C) are members of the S100 family of human host-defense proteins. These S100 proteins are interesting candidate antimicrobial peptides (AMPs) due to their high helical character, overall cationic charge, relatively small size, and localization patterns. In this Chapter, we further probe the scope of the bactericidal activities of S100A7, S100A15, and S100A12. We investigate the chemical and environmental factors that affect their antimicrobial properties, and employ microscopy studies to characterize their killing activities. The S100 proteins were found to have enhanced killing properties under acidic conditions (pH 5.1) in the absence of added NaCl and Ca(II) when tested against bacterial cultures in mid-log phase of growth. CP, S100A7, and S100A15 were found to be active against three Gram-negative strains tested, suggesting that they can be broad-spectrum AMPs against Gram-negative strains. Microscopy studies of *Escherichia coli* reveal aberrant cell morphology phenotypes caused by CP, S100A7, and S100A15, while S100A12 was found to be inactive with a lack of observable phenotypes.

Appendix A: Preparation of the Oxidized and Reduced Forms of Psoriasin (S100A7)

S100A7 possesses two Cys residues that generate two redox isoforms of the protein. In the oxidized form (S100A7_{ox}), Cys47 and Cys96 form an intramolecular disulfide bond, whereas these residues exist as free thiols in the reduced form (S100A7_{red}). In this Appendix, we provide a step-by-step protocol for the purification of S100A7_{ox} and S100A7_{red} that affords each protein in high yield and purity. In this procedure, S100A7 is expressed in *Escherichia coli* BL21(DE3), and the homodimer is obtained following ammonium sulfate precipitation, folding, and column chromatography. Treatment of S100A7 with 1,4-dithiothreitol (DTT) affords S100A7_{red}. A Cu(II)-catalyzed oxidation reaction is employed to obtain S100A7_{ox}. An RP-HPLC method that allows

for baseline separation of S100A7_{ox} and S100A7_{red} is provided, as well as a biochemical Zn(II)-binding assay that can be employed to evaluate the functional integrity of S100A7.

Appendix B: S100A12 and Pra1: Competition for Zn(II) at the Host-Pathogen Interface

The ability of fungal pathogens to acquire essential nutrients from their hosts is a fundamental aspect of infection. The fungal pathogen *Candida albicans* is a member of the commensal microbiota and colonizes the skin, intestinal, oral, and genital mucosae. In most individuals, *C. albicans* is a lifelong commensal; however, it can become virulent and cause life-threatening systemic infections, particularly in immunocompromised individuals. *C. albicans* secretes a scavenger protein, Pra1, which sequesters Zn(II) from the host environment. Subsequently, Pra1 re-associates with the fungus through a high-affinity Zn(II) transporter, Zrt1, and delivers Zn(II) into the cell. Pra1 expression is upregulated at infection sites and under conditions of Zn(II) starvation. Our work in Chapter 2 showed that S100A12 has antifungal activity against *Candida* spp., and acts by depriving these pathogens of Zn(II). In this Appendix, we show through qRT-PCR that Pra1 and Zrt1 are upregulated when *C. albicans* is incubated with S100A12. Upregulation of Zap1, the transcription factor of Zrt1 and Zrt2, a low-affinity Zn(II) transporter, is also observed upon treatment of the cultures with S100A12. We show that the *C. albicans* *PRA1*^{-/-} and *ZRT1*^{-/-} single knockout strains are more susceptible to S100A12 treatment compared to the WT strain, further supporting the notion that S100A12 sequesters Zn(II). Moreover, these data provide evidence for competition between Pra1 and S100A12, and suggest that these two players may compete for Zn(II) at sites of infections.

À ma petite maman, Charlotte, et Lucy

Acknowledgments

My time at MIT has been both my most intellectually challenging and rewarding experience so far. Five years ago, I made the decision to enroll into the Chemistry PhD program at MIT because I wanted to become a better bench scientist, a more critical thinker, and I wanted to improve my writing and presentation skills. I have grown immensely as a scientist and as an adult since then, and I am grateful for what I learnt from MIT and the Nolan lab.

I am truthfully grateful for having had Prof. Liz Nolan as my mentor. She has been an incredibly thoughtful mentor to me since the day I started as a summer undergraduate in the summer of 2012. I learnt from Liz how to be a good mentor, how to teach, explain, be flexible, and care. I am also thankful to Liz for having taught me how to be more professional and organized. I learnt the importance of being on time and planning ahead. I look back at my time at MIT, and know that the reason why I was happy here is because I managed to remain productive in lab, while at the same time still making time to go for runs, maintain my friendships with my non-MIT friends, and enjoy what Boston has to give. As one of Liz's favorite meeting saying goes: "...with proper time management, it is possible...". Lastly, I want to thank Liz for having always been strict and understanding when needed, always fair and never judgmental; she saw me make so many faux-pas, but didn't treat differently the next day.

I would like to thank my thesis chair, Prof. Brad Pentelute; His positive attitude and cheerfulness made me smile whenever I ran into him in the hallway. I would also like to thank Prof. Cathy Drennan for serving as my thesis committee member. The thought-provoking questions she asked during my orals really helped me think more critically about my research projects. Thank you to all my chemistry teachers who instilled into me the love of Chemistry: Madame Poorahoo, Mr Deojee, Professor Jamieson, and Professor Linck. Professor Linck, thank you for having taught me how to properly conduct research, and always challenging to me to think about science (and life) outside of the box. I also want to thank all the people I have collaborated

with over the last few years on my research projects; Aleth Gaillard contributed to our published work on S100A12, Dr. Megan Brophy initiated our study on S100A7 and taught me how to purify and handle S100A7. I am indebted to Professor Dean Wilcox and Dr. Michael J. Stevenson for teaching us the fundamentals of ITC, and for allowing us to use their ITC instruments and lab space for days at a time. I am also grateful for all the incredible undergraduates I got to mentor and work with on various projects: Hope Flaxman, Grayson Rodriguez, Steven Lee, Eleane Lema, and Rebekah Costello.

My time at MIT wouldn't have been the same without the people here. I have had such great mentors and friends in the form of senior graduate students. Thank you Meg for having been such a great mentor, and now an even greater friend; Phoom for being so sassy but always here to go get bubble tea and talk about science and life; Jules for all your help brainstorming about our projects, for listening to me complain about everything, and above all for having such a great sense of humor; Emily for your willingness to always help; Toshiki and Haritha for training me and giving me good advice related to my research projects. I also want to thank all the past and present postdocs I overlapped with for being a reassuring and knowledgeable presence in lab: Tim, Fabien, Julie, Simona, Claire, Wilma, Tomer, Artur, and Aaron. I joined the lab as a first year with Rose and Anmol who were great labmates to have around. Rose- we made it! I am glad that we were together throughout these 5 years. Thank you to the folks down the hallway for your constant positive attitude: Chris, Louis, and Azade. I feel fortunate that I have been able to share my exciting and less exciting results with all of you, get your feedback on my papers and presentations, and I hope that I was helpful to you too in a way or another.

I cannot imagine my time at MIT without my friends. I'd like to start with my favorite crowd: Alba, Aleth, Christine, Kristin, Spencer, Javier, Lukas, Lucas, and Sahin. Thank you for all the weekend trips, hikes, dinners, beach dates, and friendsgiving dinners. I cannot wait to see where we will be in another five years. Alba and Aleth- I am so grateful to be surrounded by such strong, ambitious, and smart women. I cannot thank you enough for all valuable life advice I got from you

during our dates. I of course have to thank my Smith crowd: Brooke, Ruth, Sarah, Gigi, Emily, Avery, Sharon, Paula, Becky, Julia, Sheona, and Elliana. I am so glad that we're still going strong after five years! A special shout-out to Brooke and Ruth for being incredibly funny, reliable, and loving friends. A second shout-out to Brooke because she always falls for my tricks, and because I am amazed by how honest and vulnerable we can be with each other. Eliza, I respect you so much as a person and as a scientist. Thank you for always believing in me. Ashley, you will always be my favorite first-year. Thank you for being so loving and caring. Olivia, just writing your name makes me laugh. You're my little ball of fresh breath and sunshine. Stop being a diva and get that album out! I also cannot imagine my time at MIT without all the running I did, which kept me sane. I will never get tired of the view of the Charles river that takes my breath away with every season. I went from running 5Ks to marathons, and along those years had the honor to run with so many friends; Kristin, Christine, Niki, Eliza, Sarah, Brooke, Emily, Martin, and Eddy. Thank you for sharing with me one of the things I love doing the most in life: running.

Thank you to the people who have a very special place in my heart. Martin, thank you for being my person, and making everything just easier and better. Za, you are my soulmate (since elementary school!) and I don't understand how we manage to stay in sync despite living so far apart, but somehow we do, and I can't wait to see you so soon! Nim, you are a true inspiration to me, and I am amazed by your resilience and ability to love unconditionally. Nikkita and Vie, thank you for your friendship and so many memories since high school!

I also want to thank my big and beautifully-chaotic-at-times family for being so supportive, and always giving me a good laugh. *Loin des yeux, mais près du cœur*. Titive, Vero, and Patchouk. Thank you for raising me, looking after me, tolerating me, and always being here when I made mistake and needed a hand to hold to get back up. That's exactly what Mamie and Papie taught you about family, and they would be so proud of you! Scarl, thank for your unconditional love, all those little gestures that made a difference, and for providing me with a home away from home. To my loves: Wawa, Soson, Jay, Eva, Greg, and Derek; I will always be here for you. Ma

petite Nastou, I only have one wise piece of advice for you, which is really all you need because you're so on top of everything: "Riiiiiiiise Maurice!". David thank you for being my big brother. I admire your honesty and your ability to put up with my sister. My nieces Charlotte and Lucy are my little bits of sunshine, and even though one of you talks too much and the other one doesn't talk at all, I want you to know that I will always be here if you need to talk, vent, or cry.

I feel incredibly lucky to have grown up with three siblings: Veven, Ticia, and Stay. This bond we have is so special and unbreakable. I will not write about you individually because we are and have always been better as a team. I am sad that we don't get to see each other much, but whenever we do, it amazes me how organic we are....until the next fight! And the next day, it's like it never happened, and we go back to laughing, talking, and arguing again. We all have very different personalities and goals in life, but I truly respect every single one of you. All this brings me to the most important person in my life: ma petite maman. I am so thankful that you raised us and instilled into us such strong moral values. You always prioritized our education, and single-handedly sent all of us to college. I cannot even begin to understand how to managed to keep our family together despite everything you went through. You are so strong, and loving, and understanding, and your unconditional love has made us this amazing team that we are. Thank you maman.

Human subtlety will never devise an invention more beautiful, more simple, or more direct than does Nature—because in her inventions, nothing is lacking—and nothing is superfluous...
Leonardo da Vinci

Table of Contents

Abstract.....	3
Dedication.....	9
Acknowledgments.....	10
Table of Contents.....	14
List of Figures.....	22
List of Tables.....	28
Abbreviations.....	32
Chapter 1: A Molecular Investigation of the Antimicrobial Functions of the Human S100 Host-Defense Proteins	34
1. 1. Innate Immunity.....	35
1. 2. Antimicrobial Host-Defense Peptides (HDPs)	36
1. 3. Human S100 Proteins are Antimicrobial HDPs.....	38
1. 3. 1. Microbiostatic Properties of S100 Proteins through Zn(II) Sequestration.....	42
1. 3. 2. Microbicidal Properties of S100 Proteins through Membrane Interactions.....	44
1. 4. Calprotectin.....	44
1. 4. 1. Zn(II)-Sequestering Properties of CP.....	45
1. 4. 2. Microbicidal Properties of CP.....	50
1. 5. S100A12 (calgranulin C).....	51
1. 5. 1. Zn(II)-Sequestering Properties of S100A12....	51
1. 5. 2. Microbicidal Properties of S100A12.	53
1. 6. S100A7 (psoriasin)... ..	54

1. 6. 1. Zn(II)-Sequestering Properties of S100A7.....	55
1. 6. 2. Microbicidal Properties of S100A7.....	57
1. 7. S100A15 (koebnerisin).....	57
1. 8. Outlook.....	58
1. 9. Summary of Thesis.....	59
1. 10. References.....	62
Chapter 2: Calcium Ions Tune the Zinc-Sequestering Properties and Antimicrobial Activity of Human S100A12	78
2. 1. Contributions	79
2. 2. Introduction	79
2. 3. Experimental Section.....	83
2. 3. 1. Design of the Synthetic Genes for S100A12.....	83
2. 3. 2. Materials and General Methods.....	83
2. 3. 3. Cloning, Mutagenesis, Overexpression and Purification of S100A12 and S100A12 Δ His ₃ Asp and CP-Ser.....	85
2. 3. 4. Protein Characterization.....	87
2. 3. 5. Metal Analysis (ICP-MS).....	88
2. 3. 6. Western Blot of S100A12-Treated Medium (YPD).....	89
2. 3. 7. Antifungal Activity Assays.....	89
2. 3. 8. Antibacterial Activity Assays.....	91
2. 3. 9. Antimicrobial Activity Assays with Zinc Preincubation.....	92
2. 3. 10. Optical Absorption and Fluorescence Spectroscopy.....	92
2. 3. 11. Zinc Competition with S100A12 and Zincon.....	93
2. 3. 12. Zinc Competition with S100A12 and MF2.....	93

2. 3. 13. Zinc Competition with S100A12 and FZ3.....	93
2. 4. Results and Discussion.....	94
2. 4. 1. Protein Characterization.....	94
2. 4. 2. Human S100A12 Depletes Zn(II) from Microbial Growth Medium.....	97
2. 4. 3. Human S100A2 Exhibits Calcium-Dependent Antifungal Activity.....	104
2. 4. 4. The His ₃ Asp Motifs Are Essential for Antifungal Activity.....	107
2. 4. 5. Human S100A12 Exhibits Strain-Specific Antibacterial Activity.....	108
2. 4. 6. Bacteria with Defective Zinc Acquisition Machinery Are Susceptible to S100A12.....	109
2. 4. 7. Human S100A12 Is a High-Affinity Zinc Chelator.....	112
2. 5. Summary and Outlook.....	118
2. 6. Acknowledgements.....	120
2. 7. References.....	121
Chapter 3: Biochemical and Functional Evaluation of the Intramolecular Disulfide Bonds in the Zinc-Chelating Antimicrobial Protein Human S100A7 (Psoriasin)	129
3. 1. Contributions	130
3. 2. Introduction	130
3. 3. Experimental Section.....	134
3. 3. 1. Design of the Synthetic Genes for Human S100A7 Variants.....	134
3. 3. 2. Materials and General Methods.....	135
3. 3. 3. Purification of S100A7 _{red} , S100A7 _{ox} and Variants.....	139
3. 3. 4. Thioredoxin Activity Assays.....	140
3. 3. 5. Midpoint Potential (E_m) Determination.....	141
3. 3. 6. Nernst Equation Derivation.....	143

3. 3. 7. Logistic Equation Derivation.....	144
3. 3. 8. Aerobic Reduction of S100A7 _{ox} by DTT, GSH, and TCP.....	144
3. 3. 9. Zn(II) Competition Titrations with S100A7 and Zincon.....	144
3. 3. 10. Zinc Competition Assays with S100A7 and FZ3.....	145
3. 3. 11. Zinc Competition Titrations with S100A7 and ZP4	145
3. 3. 12. Co(II) Binding Titrations and Metal Substitution Assays.....	146
3. 3. 13. Metal Analysis (ICP-MS).....	147
3. 3. 14. Antibacterial Activity Assays	147
3. 4. Results and Discussion.....	149
3. 4. 1. Preparation of S100A7 and Variants	149
3. 4. 2. The Thioredoxin System Reduces Apo S100A7 _{ox}	159
3. 4. 3. Ca(II) Ions Depress the Midpoint Potential of S100A7.....	163
3. 4. 4. Both S100A7 _{ox} and S100A7 _{red} Have Two High-Affinity Zn(II)-binding Sites.....	169
3. 4. 5. Both S100A7 _{ox} and S100A7 _{red} Bind Zn(II) with Sub-Nanomolar Affinity.....	170
3. 4. 6. Human S100A7 Selectively Depletes Zn(II) From Bacterial Growth Medium.....	179
3. 4. 7. Evidence for a Contribution of the Intramolecular Disulfide Bonds to Antibacterial Activity.....	187
3. 4. 8. The Redox State of Human S100A7 Influences Metal Displacement at the His ₃ Asp Sites.....	192
3. 5. Summary and Outlook.....	196
3. 6. Acknowledgements.....	198
3. 7. References.....	199

Chapter 4: Investigation of the Bactericidal Properties of the Host-Defense Protein Human Calprotectin	206
4. 1. Introduction	207
4. 2. Experimental Section.....	211
4. 2. 1. Materials and General Methods.....	211
4. 2. 2. Protein Purification and Characterization.....	211
4. 2. 3. Preparation and Characterization of Fluorescein CP (FL-CP).....	212
4. 2. 4. Metal Analysis (ICP-MS).....	214
4. 2. 5. Membrane Permeabilization Assays.....	215
4. 2. 6. Assay and Imaging Conditions for Phase-contrast and Fluorescence Microscopy.....	220
4. 2. 7. Image Analysis for Phase-Contrast and Fluorescence Microscopy Image Analysis.....	222
4. 2. 8. Characterization of CP Variants from the Broth-Microdilution Assay Supernatant.....	222
4. 2. 9. Statistical Analyses.....	222
4. 3. Results and Discussion.....	222
4. 3. 1. CP is an <i>E. coli</i> -cidal Factor.....	222
4. 3. 2. The Bactericidal Activity of CP is Independent of Metal Sequestration.....	225
4. 3. 3. Divalent Metals Attenuate the <i>E. coli</i> -cidal Activity of CP.....	227
4. 3. 4. CP Induces Concentration-dependent Morphological Changes in <i>E.</i> <i>coli</i>	230
4. 3. 5. CP Binds and Permeabilizes the Bacterial Membrane.....	236
4. 3. 6. CP Treatment Causes Leakage of Periplasmic GFP.....	238

4. 3. 7. Synthesis and Characterization of Fluorescein-CP-Ser (FL-CP).....	240
4. 3. 8. FL-CP Localizes on the Bacterial Cell Surface of <i>E. coli</i>	242
4. 2. 9. CP Exhibits Broad-Spectrum Bactericidal Activity against Gram-negative Strains.....	244
4. 3. 10. The Transition Metal-binding Sites of CP Contribute to its Function as an AMP.....	248
4. 4. Summary and Outlook.....	252
4. 5. Acknowledgements.....	254
4. 6. References.....	255
Chapter 5: Investigation of the Bactericidal Properties of Four Human S100 Proteins: Calprotectin, S100A7, S100A15, and S100A12	264
5. 1. Introduction	265
5. 2. Experimental Section.....	269
5. 2. 1. Materials and General Methods.....	269
5. 2. 2. Purification of CP, S100A7, S100A15, and S100A12.....	270
5. 3. Results and Discussion.....	270
5. 3. 1. The <i>E. coli</i> -cidal Activity of the S100 Proteins are pH-Dependent.....	270
5. 3. 2. The <i>E. coli</i> -cidal Activity of the S100 Proteins are Concentration-Dependent.....	272
5. 3. 3. Ionic Strength and Salinity Affect the <i>E. coli</i> -cidal Activities of the S100 Proteins.....	274
5. 3. 4. Growth Stage of <i>E. coli</i> Cultures Affects the Activities of the S100 Proteins.....	278
5. 3. 5. The S100 Proteins Compromise the Bacterial Membrane of <i>E. coli</i> ...	279
5. 3. 6. The S100 Proteins Induce Morphological Changes in <i>E. coli</i>	283

5. 3. 7. The S100 Proteins Affect the Cell-Length Distribution of <i>E. coli</i>	285
5. 3. 8. The S100 Proteins Display Broad-Spectrum Bactericidal Activity against Gram-negative Strains.....	287
5. 4. Summary and Outlook.....	290
5. 5. Acknowledgements.....	291
5. 6. References.....	291
Appendix A: Preparation of the Oxidized and Reduced Forms of Psoriasin (S100A7)	301
A. 1. Introduction	302
A. 2. Materials.....	303
A. 2. 1. Commercial Materials and Reagents Preparations.....	303
A. 2. 2. Zincon Preparation.....	305
A. 2. 3. Buffer for Protein Purification.....	305
A. 2. 4. Equipment for Protein Purification.....	306
A. 2. 5. Equipment for Optical Absorption Spectroscopy.....	306
A. 3. Methods.....	306
A. 3. 1. Design of the synthetic gene for S100A7.....	306
A. 3. 2. Sub-cloning of the Human S100A7 Gene.....	307
A. 3. 3. Purification of Human S100A7.....	307
A. 3. 4. Zinc Competition Titration between S100A7 and Zincon.....	312
A. 4. Biochemical Characterization of human S100A7.....	313
A. 5. Notes.....	314
A. 6. Figures and Tables.....	317
A. 7. Acknowledgments.....	322
A. 8. References.....	322

Appendix B: S100A12 and Pra1: Competition for Zn(II) at the Host-Pathogen Interface	325
B. 1. Introduction	325
B. 2. Experimental Section.....	328
B. 2. 1. Antifungal Assays with S100A12.....	328
B. 2. 2. Extraction of RNA and Synthesis of cDNA from <i>C. albicans</i>	
Cultures Treated with S100A12.....	329
B. 2. 3. Quantitative Real-time PCR.....	330
B. 3. Results and Discussion.....	331
B. 4. Summary and Outlook.....	336
B. 5. References.....	336
Biographical Note.....	339
Curriculum Vitae.....	340

List of Figures

Chapter 1

Figure 1. 1. Schematic representing the select roles of antimicrobial HDPs.....	37
Figure 1. 2. Sequence alignment of human S100A8, S100A9, S100A7, S100A12, and S100A15.....	39
Figure 1. 3. Crystal structures of human CP, S100A12, S100A7, and S100A15.....	40
Figure 1. 4. Extracellular roles of CP, S100A12, and S100A7 in Zn sequestration....	43
Figure 1. 5. Comparison of the primary amino acid sequence of calcitrimin, human S100A12, and porcine S100A12.....	53

Chapter 2

Figure 2. 1. Crystal structures of metal-bound human S100A12 and amino acid sequence alignment.....	81
Figure 2. 2. SDS-PAGE purity gels S100A12 and S100A12 Δ His ₃ Asp.....	95
Figure 2. 3. Circular dichroism of purified S100A12 and S100A12 Δ His ₃ Asp.....	96
Figure 2. 4. Analytical SEC chromatograms of S100A12 and S100A12 Δ His ₃ Asp....	96
Figure 2. 5. Western blot of retentate from metal-depletion experiment with S100A12.....	98
Figure 2. 6. Metal depletion profile of S100A12-treated bacterial growth media.....	100
Figure 2. 7. Growth curves of <i>C. albicans</i> SC5314.....	105
Figure 2. 8. Antifungal activity of S100A12 against <i>Candida</i> species.....	106
Figure 2. 9. Effect of His ₃ Asp motifs on the Antifungal activity of S100A12.....	107
Figure 2. 10. Antibacterial activity of S100A12 against a panel of pathogens.....	109
Figure 2. 11. Antibacterial activity of S100A12 against <i>E. coli</i> K-12 and Δ znuA.....	111
Figure 2. 12. Antibacterial activity of S100A12 against <i>P. aeruginosa</i>	111

Figure 2. 13. Optical absorption spectra of S100A12 titrated with Co(II).....	113
Figure 2. 14. Plot of absorbance at 550 nm vs equivalents of Co(II) added for titration of S100A12 with Co(II)	114
Figure 2. 15. Optical absorption spectra showing displacement of Co(II) from Zn(II)-bound S100A12.....	115
Figure 2. 16. Zincon titration with S100A12 and S100A12 Δ His ₃ Asp.....	116
Figure 2. 17. MF2 titration with S100A12 and S100A12 Δ His ₃ Asp.....	116
Figure 2. 18. FZ3 competition with S100A12 and S100A12 Δ His ₃ Asp.....	117

Chapter 3

Figure 3. 1. Crystal structure of human S100A7 and amino sequence alignment of S100A7 and select S100 proteins.....	132
Figure 3. 2. Analytical HPLC traces for the purification of S100A7 and S100A7 Δ	151
Figure 3. 3. SDS-PAGE purity gel of purified S100A7.....	155
Figure 3. 4. HPLC chromatograms of S100A7.....	156
Figure 3. 5. CD spectra of S100A7.....	157
Figure 3. 6. Analytical SEC of S100A7.....	158
Figure 3. 7. Analytical HPLC traces for the enzymatic activity assays with Trx/TrxR and S100A7.....	159
Figure 3. 8. Analytical HPLC traces showing air oxidation of S100A7 _{red} over time....	162
Figure 3. 9. Analytical HPLC traces showing the reduction of HD5 _{ox} by Trx/TrxR in the presence of Ca(II).....	162
Figure 3. 10. Analytical HPLC traces showing the reduction of HD5 _{ox} by Trx/TrxR in the presence of Zn(II)-bound S100A7 _{ox}	163

Figure 3. 11. Midpoint potential plots for S100A7 in the absence and presence of Ca(II).....	165
Figure 3. 12. Plot showing the equilibration time for S100A7 in GSH/GSSH buffer...	165
Figure 3. 13. Analytical HPLC showing the speciation of S100A7 after 96 h for the midpoint potential experiments.....	166
Figure 3. 14. Midpoint potential data fitted to a logistic function.....	167
Figure 3. 15. HPLC traces showing the reduction of S100A7 by GSH, DTT, and TCEP.....	168
Figure 3. 16. Competition experiments between S100A7 and Zincon for Zn(II).....	170
Figure 3. 17. Competition experiments between S100A7 and FZ3 for Zn(II).....	171
Figure 3. 18. Competition experiments between S100A7 and ZP4 for Zn(II).....	172
Figure 3. 19. ZP4 competition titration against S100A7 _{ox} fitted to different binding sites models.....	173
Figure 3. 20. ZP4 competition titration against S100A7 _{red} fitted to different binding sites models.....	174
Figure 3. 21. ZP4 competition titration against S100A7-Ser fitted to different binding sites models.....	175
Figure 3. 22. ZP4 competition titration against S100A7-Ala fitted to different binding sites models.....	176
Figure 3. 23. Simulated Zn(II) competition curves for ZP4 and S100A7.....	178
Figure 3. 24. Metal depletion profile of S100A7 in Tris:TSB.....	181
Figure 3. 25. Antibacterial activity of S100A7 against <i>E. coli</i> K-12 and $\Delta znuA$	188
Figure 3. 26. Analytical traces showing the redox speciation of S100A7 during and after the AMA assays.....	189
Figure 3. 27. Antibacterial activity of S100A7 against a panel of pathogens.....	190

Figure 3. 28. Microdilution antimicrobial activity assay of S100A7 _{ox} and <i>E. coli</i>	192
Figure 3. 29. Co(II)-binding titrations with S100A7 variants without Ca(II)	193
Figure 3. 30. Co(II)-binding titrations with S100A7 variants with added Ca(II)	193
Figure 3. 31. Optical absorption spectra showing the substitution of Co(II) for Zn(II) at the His ₃ Asp sites of S100A7.....	195
 Chapter 4	
Figure 4. 1. Crystal structure of human calprotectin.....	208
Figure 4. 2. Schematic of the wash, resuspension, and dilution steps of <i>E. coli</i> 25922 cultures for the membrane permeabilization assays.....	216
Figure 4. 3. Bactericidal activity of CP against <i>E. coli</i>	224
Figure 4. 4. Effect of NaCl concentration on the <i>E. coli</i> -cidal activity of CP.....	225
Figure 4. 5. Effect of Ca(II) concentration on the <i>E. coli</i> -cidal activity of CP.....	228
Figure 4. 6. Effect of divalent metal-binding on the <i>E. coli</i> -cidal activity of CP.....	230
Figure 4. 7. Effect of CP on <i>E. coli</i> cell morphology.....	231
Figure 4. 8. Effect of CP concentration on <i>E. coli</i> cells.....	231
Figure 4. 9. CP induces aberrant cell morphology phenotypes in <i>E. coli</i>	232
Figure 4. 10. Quantification of the CP-induced CP morphology phenotypes in <i>E. coli</i>	233
Figure 4. 11. Time-lapse imaging of select untreated <i>E. coli</i> cells.....	235
Figure 4. 12. Time-lapse imaging of select CP-treated <i>E. coli</i> cells.....	236
Figure 4. 13. Live-Dead staining of CP-treated <i>E. coli</i> cells.....	237
Figure 4. 14. Treatment of <i>E. coli</i> peri-GFP with CP.....	239
Figure 4. 15. Treatment of <i>E. coli</i> cyto-GFP with CP.....	240
Figure 4. 16. Characterization of FL-CP.....	241

Figure 4. 17. Treatment of <i>E. coli</i> peri-GFP with FL-CP.....	243
Figure 4. 18. Bactericidal activity of CP proteins against a panel of bacterial strains.....	246
Figure 4. 19. Effect of CP-treatment on the morphology and membrane integrity on a panel of bacterial strains.....	247
Figure 4. 20. Structure-activity assay of CP against <i>E. coli</i>	250
Figure 4. 21. Circular dichroism spectra of CP recovered from the culture supernatant of <i>E. coli</i> cells.....	251
Figure 4. 22. SDS-PAGE gel of culture supernatant of CP-treated <i>E. coli</i>	252
 Chapter 5	
Figure 5. 1. Crystal structures and charge electrostatics of CP, S100A7, S100A15, and S100A12.....	267
Figure 5. 2. Effect of pH on the <i>E. coli</i> -cidal activity of the S100 proteins.....	272
Figure 5. 3. Effect of protein concentration on the activity of the S100 proteins.....	273
Figure 5. 4. Effect of NaCl concentration on the <i>E. coli</i> -cidal activity of the S100 proteins.....	275
Figure 5. 5. Effect of Ca(II) concentration on the <i>E. coli</i> -cidal activity of S100 proteins.....	277
Figure 5. 6. Effect of <i>E. coli</i> growth stage on the activity of the S100 proteins.....	278
Figure 5. 7. Effect of CFU on the activity of the S100 proteins.....	280
Figure 5. 8. The S100 proteins affect the cell wall integrity of <i>E. coli</i> ATCC 25922...	282
Figure 5. 9. Effect of S100 treatment on <i>E. coli</i> ATCC 25922 cell wall integrity.....	283
Figure 5. 10. S100A7 causes distinct morphological changes to <i>E. coli</i> cells.....	284
Figure 5. 11. S100A15 causes distinct morphological treatment on <i>E. coli</i> cells.....	284

Figure 5. 12. Cell length profile upon S100 treatment.....	286
Figure 5. 13. Cell length average of untreated and S100-treated cells.....	287
Figure 5. 14. Antibacterial activities of the S100 proteins against a panel of bacterial strains.....	289
 Appendix A	
Figure A. 1. Expression of S100A7 visualized by SDS-PAGE gel.....	317
Figure A. 2. Elution profile of S100A7 from the MonoQ column.....	318
Figure A. 3. Elution profile of S100A7 from the S75 column.....	319
Figure A. 4. Analytical HPLC traces showing S100A7 over the course of the purification and Cu(II)-catalyzed oxidation.....	320
Figure A. 5. SDS-PAGE purity gel and analytical HPLC traces of S100A7 _{ox} and S100A7 _{red}	321
Figure A. 6. Competition experiments between S100A7 and Zincon for Zn(II).....	322
 Appendix B	
Figure B. 1. Schematic of Zn(II) competition between <i>C. albicans</i> and S100A12 at the host-pathogen interface.....	327
Figure B. 2. Antifungal activity of S100A12 against <i>C. albicans</i> WT, <i>PRA1</i> ^{-/-} , and <i>ZRT1</i> ^{-/-}	332
Figure B. 3. qRT-PCR data of <i>C. albicans</i> WT, <i>PRA1</i> ^{-/-} and <i>ZRT1</i> ^{-/-} treated with S100A12.....	335

List of Tables

Chapter 1

Table 1. 1. Location of human CP, S100A12, S100A7, and S100A15 in humans.....	42
Table 1. 2. Reported apparent dissociation constant values for human S100 proteins.....	47

Chapter 2

Table 2. 1. Molecular weights and extinction coefficients for S100A12 monomers...	87
Table 2. 2. Strains and growth conditions.....	90
Table 2. 3. Mass spectrometric analysis of S100A12 and S100A12 Δ His ₃ Asp.....	95
Table 2. 4. Analytical SEC elution volumes and calculated molecular weights.....	97
Table 2. 5. Metal analysis of untreated Tris:YPD medium.....	101
Table 2. 6. Metal analysis of Tris:YPD medium treated with 62.5 μ g/mL of S100A12.....	101
Table 2. 7. Metal analysis of Tris:YPD medium treated with 125 μ g/mL of S100A12	101
Table 2. 8. Metal analysis of Tris:YPD medium treated with 250 μ g/mL of S100A12	102
Table 2. 9. Metal analysis of Tris:YPD medium treated with 250 μ g/mL of S100A12 Δ His ₃ Asp.....	102
Table 2. 10. Metal analysis of untreated Tris:TSB medium.....	102
Table 2. 11. Metal analysis of Tris:TSB medium treated with 62.5 μ g/mL of S100A12.....	103
Table 2. 12. Metal analysis of Tris:TSB medium treated with 125 μ g/mL of S100A12.....	103

Table 2. 13. Metal analysis of Tris:TSB medium treated with 250 $\mu\text{g}/\text{mL}$ of S100A12.....	103
Table 2. 14. Metal analysis of Tris:TSB medium treated with 250 $\mu\text{g}/\text{mL}$ of S100A12 $\Delta\text{His}_3\text{Asp}$	104
 Chapter 3	
Table 3. 1. Strains and growth conditions employed in this work.....	148
Table 3. 2. Extinction coefficients for S100A7 monomers.....	150
Table 3. 4. Characterization of S100A7 and variants.....	153
Table 3. 5. Metal analysis (ICP-MS) of S100A7 from representative protein purifications.....	154
Table 3. 6. Analytical SEC elution volumes and calculated molecular weights.....	158
Table 3. 7. Fits for apparent $K_{d,\text{Zn}}$ values from ZP4 competition titrations with S100A7 variants.....	177
Table 3. 8. Metal Analysis of untreated Tris:TSB.....	182
Table 3. 9. Metal Analysis of Tris:TSB medium treated with 31.25 $\mu\text{g}/\text{mL}$ of S100A7 _{ox}	182
Table 3. 10. Metal Analysis of Tris:TSB medium treated with 62.5 $\mu\text{g}/\text{mL}$ of S100A7 _{ox}	182
Table 3. 11 Metal Analysis of Tris:TSB medium treated with 125 $\mu\text{g}/\text{mL}$ of S100A7 _{ox}	183
Table 3. 12. Metal Analysis of Tris:TSB medium treated with 250 $\mu\text{g}/\text{mL}$ of S100A7 _{ox}	183

Table 3. 13. Metal Analysis of Tris:TSB medium treated with 500 µg/mL of S100A7 _{ox}	183
Table 3. 14. Metal Analysis of Tris:TSB medium treated with 31.25 µg/mL of S100A7-Ser.....	184
Table 3. 15. Metal Analysis of Tris:TSB medium treated with 62.5 µg/mL of S100A7-Ser.....	184
Table 3. 16 Metal Analysis of Tris:TSB medium treated with 125 µg/mL of S100A7-Ser.....	194
Table 3. 17. Metal Analysis of Tris:TSB medium treated with 250 µg/mL of S100A7-Ser.....	185
Table 3. 18. Metal Analysis of Tris:TSB medium treated with 500 µg/mL of S100A7-Ser.....	185
Table 3. 19. Metal Analysis of Tris:TSB medium treated with 31.25 µg/mL of S100A7-Ala.....	185
Table 3. 20. Metal Analysis of Tris:TSB medium treated with 62.5 µg/mL of S100A7-Ala.....	186
Table 3. 21. Metal Analysis of Tris:TSB medium treated with 125 µg/mL of S100A7-Ala.....	186
Table 3. 22 Metal Analysis of Tris:TSB medium treated with 250 µg/mL of S100A7-Ala.....	186
Table 3. 23. Metal Analysis of Tris:TSB medium treated with 500 µg/mL of S100A7-Ala.....	187

Chapter 4

Table 4. 1. Protein nomenclature and extinction coefficients.....	212
Table 4. 2. Quantum yield determination of FL-CP.....	214
Table 4. 3. Strains and growth conditions.....	220
Table 4. 4. Metal analysis of MES and phosphate buffers in the absence and presence of 40 μ M CP-Ser.....	227

Chapter 5

Table 5. 1. Protein extinction coefficient.....	269
Table 5. 2. Purification protocols for S100 proteins.....	270

Appendix A

Table A.1. Characterization of S100A7.....	317
---	-----

Appendix B

Table B. 1. List and sequences of primers used for qRT-PCR analysis.....	330
Table B. 2. <i>C. albicans</i> genes monitored through qRT-PCR and their functions.....	334

Abbreviations

AEC	anion-exchange chromatography
AMA	antimicrobial activity
AMP	antimicrobial peptide
ATCC	American Type Culture Collection
BHI	brain heart infusion
CD	circular dichroism
CI	confidence interval
CP	calprotectin
CP-Ser	calprotectin with both Cys at positions S100A8(C3) and S100A9(C42) mutated to Ser residues
Cys	cysteine
Da	dalton
DMSO	dimethyl sulfoxide
DTT	1,4-dithiothreitol
DTDP	4,4'-dithiodipyridine
EDTA	ethylenediaminetetraacetic acid
ESI	electrospray ionization
FZ3	fluoazin-3
HDP	Host-defense peptide
His	histidine
GSH	reduced glutathione
GSSG	oxidized glutathione
Glu	glutamate
HD5 _{ox}	oxidized human defensin 5
HEPES	4-(2-hydroxyethyl)-1-piperazineethanesulfonic acid
HPLC	high performance liquid chromatography
ICP-MS	inductively coupled plasma-mass spectrometry
K _d	dissociation constant
LB	Luria Bertani
LC-MS	liquid chromatography mass spectrometry
LPS	lipopolysaccharide
MDR	multidrug resistant
MIC	minimal inhibitory concentration
MF2	magfura-2
MWCO	molecular weight cutoff
MeCN	acetonitrile
MES	2-ethanesulfonic acid
MRS	De Man Rogosa and Sharpe
NADH	nicotinamide adenine dinucleotide
NIH	National Institute of Health
OD ₆₀₀	optical density at wavelength of 600 nm
PDB	protein databank
qPCR	quantitative polymerase chain reaction
rpm	rotation per minute
SDM	standard deviation of the mean
SEC	size-exclusion chromatography
S100A7 _{ox}	oxidized S100A7 with Cys47–Cys96 disulfide bond
S100A7 _{red}	reduced S100A7 with Cys47 and Cys96 as free thiols

S100A7-Ser	S100A7(C47S)(C96S) homodimer
S100A7-Ala	S100A7(C47A)(C96A) homodimers
S100A7 Δ_{ox}	S100A7(H18A)(H87A)(H91A)(D25A) oxidized with Cys47–Cys96 disulfide bond
S100A12	wildtype S100A12
S100A12 Δ	S100A12(H15A)(D25A)(H85A)(H89A)
S100A15 _{ox}	oxidized S100A15 with Cys47–Cys96 disulfide bond
S100A15 _{red}	reduced S100A15 with Cys47 and Cys96 as free thiols
S100A15-Ser	S100A15(C47S)(C96S) homodimers
S100A15(G24D)	S100A15(G24D) homodimers
TFA	trifluoroacetic acid
Tris	tris(hydroxymethyl)aminomethane
TCEP	tris(2-carboxyethyl)phosphine hydrochloride
TSB	tryptic soy broth
Trx	thioredoxin
TrxR	thioredoxin reductase
UTI	urinary tract infection
YPD	yeast extract-peptone dextrose
ZP4	zinpyr-4

Chapter 1: A Molecular Investigation of the Antimicrobial Functions of the Human S100 Host-Defense Proteins

This Chapter is adapted from *Biochemistry* **2018**, 57 (11), 1673-1680.

1. 1. Innate Immunity

The human host, along with other vertebrates, continually defends itself against invasion by potentially harmful microbes using both the innate and adaptive branches of the immune system. The innate immune system is the first line of defense against colonization by pathogenic microorganisms and is activated within hours post-infection.¹⁻³ The innate immune response, which is generally considered to be non-specific, triggers a generic response to all pathogens that it recognizes. The innate response is composed of initial recognition mechanisms that are either constitutive or rapidly inducible, and can distinguish or target structural and functional features associated with different classes of microorganisms.

In healthy, unwounded individuals, the most common sites of initial encounter with microbes are epithelial surfaces: the skin, the moist surfaces of the eyes, nose, airways and the lungs, the mouth, the digestive tract, the urinary tract, and the reproductive systems. Important components of innate immunity therefore include the barrier function of the skin, the reduced pH of the stomach, and chemical defenses such as the release of host-defense peptides and proteins (HDPs).¹⁻³ HDPs have important roles in the body's response to infection and inflammation, and mediate a broad range of activities. For instance, HDPs are involved in wound healing and the maintenance of the microbiota. HDPs can also influence multiple signaling pathways that are involved in inflammation and immunity, and can function as antimicrobial agents by preventing microbial proliferation through metabolic disruption (Figure 1. 1).⁴ A subgroup of antimicrobial HDPs exert microbicidal activity against pathogens, which is why they were traditionally referred to as antimicrobial peptides (AMPs) (Figure 1. 1). Therefore, we refer to peptides and proteins as HDPs except when discussing their microbicidal properties, in which case they are referred to as AMPs.

The innate and antimicrobial properties of epithelial surfaces were first reported by Elie Metchnikoff. He published a series of experiments describing the intracellular digestion of Coelenterata (coral animals, true jellies, sea anemones, sea pens, etc...) by two types of cells

with phagocytic activities.⁵ In a seminal experiment carried out in 1883, Metchnikoff described migratory cells of mesodermal origin “programmed” to attack foreign material, and challenged them with a thorn to trigger attachment to foreign insult.⁶ He named these cells “phagocytes” (from the Greek “phago”, meaning “to devour”, and “cytos”, meaning “cell”) and called the process “phagocytosis”. Together with his prior observations of nutrient uptake by the same cells, he extended his theory and connected the concepts of nutritional activity and host-defense against insults, including insults of microbial origins.⁷⁻⁸ Following Laschtsenko’s observation of hen egg white having antibacterial properties,⁹ Fleming characterized the first antimicrobial peptide: lysozyme.¹⁰ He reported that various physiological fluids of the human host contain lysozyme and showed that lysozyme can cause lysis of a panel of bacterial species. He also showed that lysozyme was abundantly present in phagocytes, thus connecting the antimicrobial properties of phagocytes to a key HDP, lysozyme.¹⁰

1. 2. Antimicrobial Host-Defense Peptides (HDPs)

Antimicrobial HDPs generally contain several hydrophobic amino acid residues that promote the formation of amphipathic secondary structures, allowing them to interact simultaneously with membrane-associated lipids and the surrounding aqueous environment. Generally speaking, 50% or more of their amino acids are cationic (+2 to +9 charge) due to an abundance of Lys and Arg residues, allowing them to interact with negatively charged bacterial membranes.¹¹ AMPs can be broadly classified on the basis of the secondary structures they can adopt in membrane-like environments, of which four classes exist: (1) α -helical (e.g. LL-37 in humans), (2) β -sheet stabilized through disulfide bridges (e. g. defensins), (3) looped (e. g. insect thanatin), and (4) extended peptides with a predominance of one or two amino acid residues (e.g. PR-39 found in pigs).¹¹⁻¹²

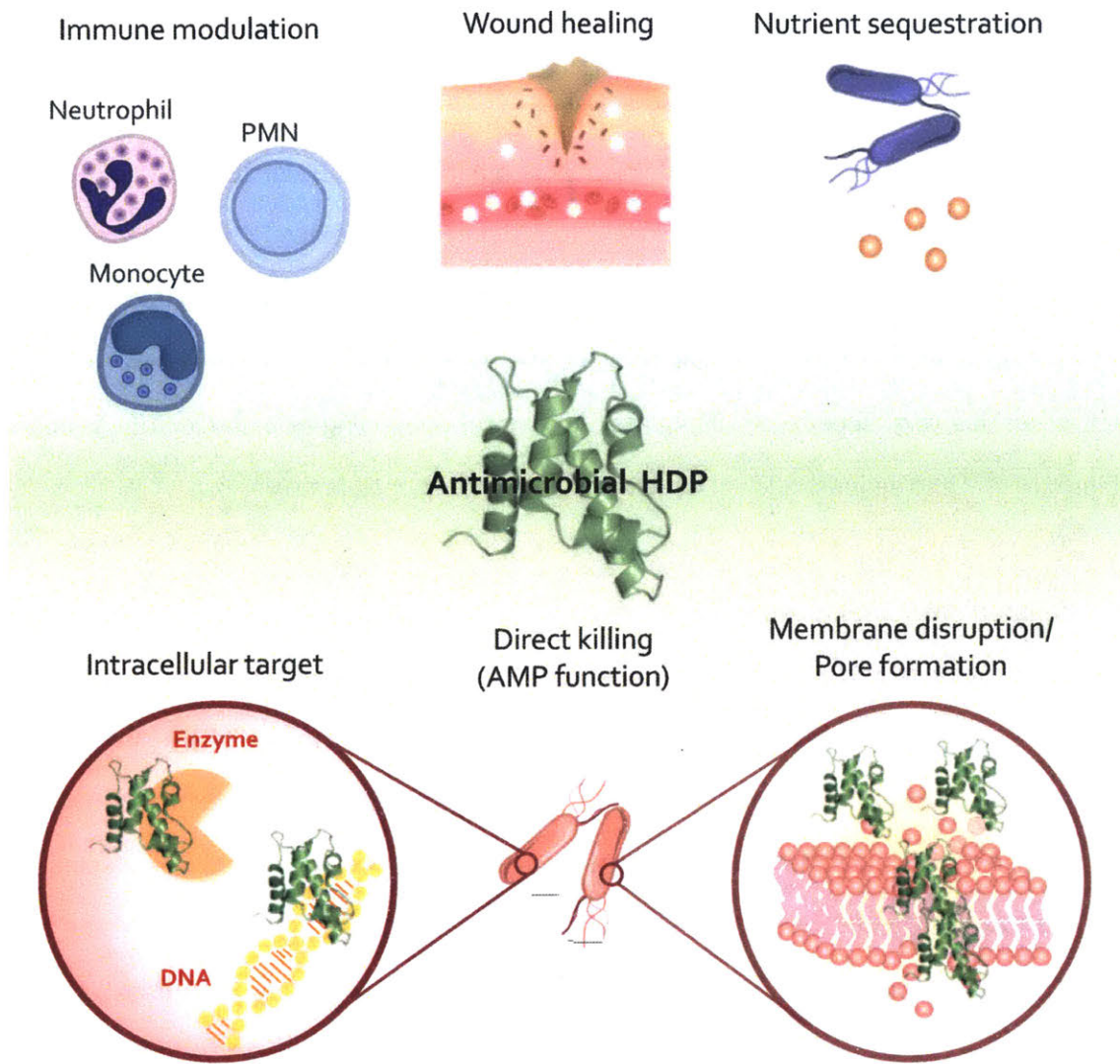


Figure 1. 1. Schematic representing select roles of antimicrobial HDPs in the innate response. Amongst many other functions, antimicrobial HDPs are involved in immune modulation, wound healing, and nutrient sequestration. A subtype of antimicrobial HDPs, termed AMPs, are involved in direct killing of pathogens through various mechanisms, including penetration into cells to interfere with DNA/ RNA or inhibit key metabolic enzymes, or membrane disruption.

It is worth noting that antimicrobial activity was originally considered to be the primary function of HDPs.¹³⁻¹⁴ Over the years, a large body of evidence has emerged, indicating that modulation of cellular function is an important role that HDPs play in preventing microbial invasion.^{12-13,15} These immunomodulatory effects include: (1) neutralization of the induction of proinflammatory cytokines by LPS/endotoxin and other microbial signatures, (2) leucocyte recruitment, (3) chemokine and cytokine production, (4) increased wound healing, (5) angiogenesis, (6) immune cell activation, and (7) promotion of enhanced and/or polarized adaptive responses.^{12-13,15} Other antimicrobial mechanisms of HDPs include generation of highly reactive species (e.g. superoxide dismutase),¹⁶ physical entrapping of pathogens (e.g. human defensin 6),¹⁷⁻¹⁹ and sequestration of essential nutrients (e. g. lactoferrin).²⁰⁻²¹

1. 3. Human S100 Proteins are Antimicrobial HDPs

A multitude of HDPs are secreted by various host cells. They include some members of a family of small proteins called S100 proteins, which are the emphasis of this thesis work. Specifically, we focus on four S100 HDPs: calprotectin (CP, S100A8/S100A9 oligomer, calgranulin A/B oligomer, MRP8/MRP14), S100A12 (calgranulin C), S100A7 (psoriasin), and S100A15 (koebnerisin) (Figures 1. 2 and 1. 3).

Human S100 proteins have been associated with a variety of intracellular and extracellular processes, including cytoskeletal interactions, protein phosphorylation, membrane trafficking, calcium homeostasis, cell growth and migration, regulation of the cell cycle and transcription factors, tissue development and repair, cell migration, chemotaxis, and innate and adaptive immune responses.²²⁻²⁴ During infection, certain S100 proteins act as damage-associated molecular patterns (DAMPs), interacting with pattern recognition receptors and the receptor for advanced glycation end products (RAGE) to modulate inflammatory responses.²⁵⁻²⁹ Furthermore, S100 proteins exhibit antimicrobial properties and thus play a key role in host defense at the host-pathogen interface. Two antimicrobial mechanisms have been reported for

select S100 proteins: (i) metal-limitation³⁰⁻⁴² and (ii) membrane disruption.⁴³⁻⁴⁶ While metal limitation is generally regarded as a microbiostatic process, membrane disruption is considered microbicidal.

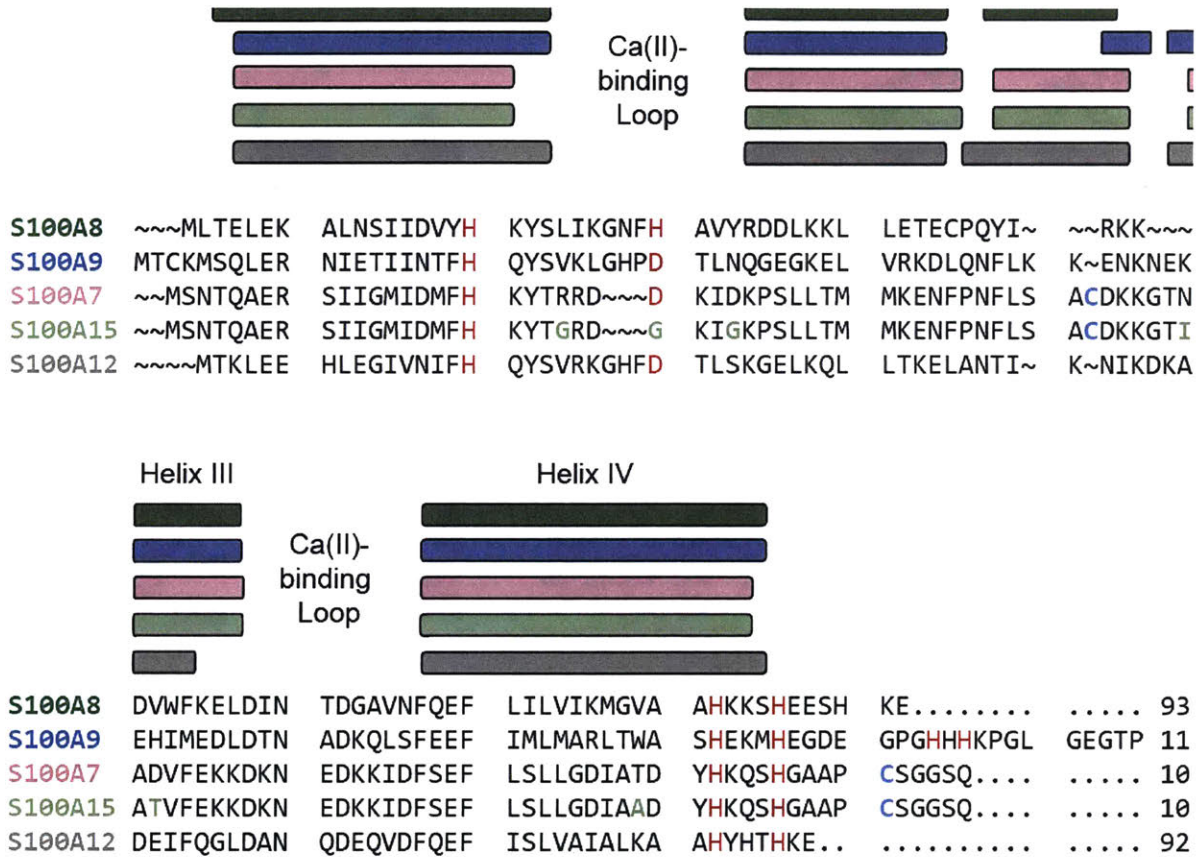


Figure 1. 2. Sequence alignment of human S100A8, S100A9, S100A7, S100A15, and S100A12. Secondary structural elements are presented above the alignment. The transition-metal-binding residues are presented in red, and Cys47 and Cys96 of S100A7 and S100A15 are highlighted in blue.

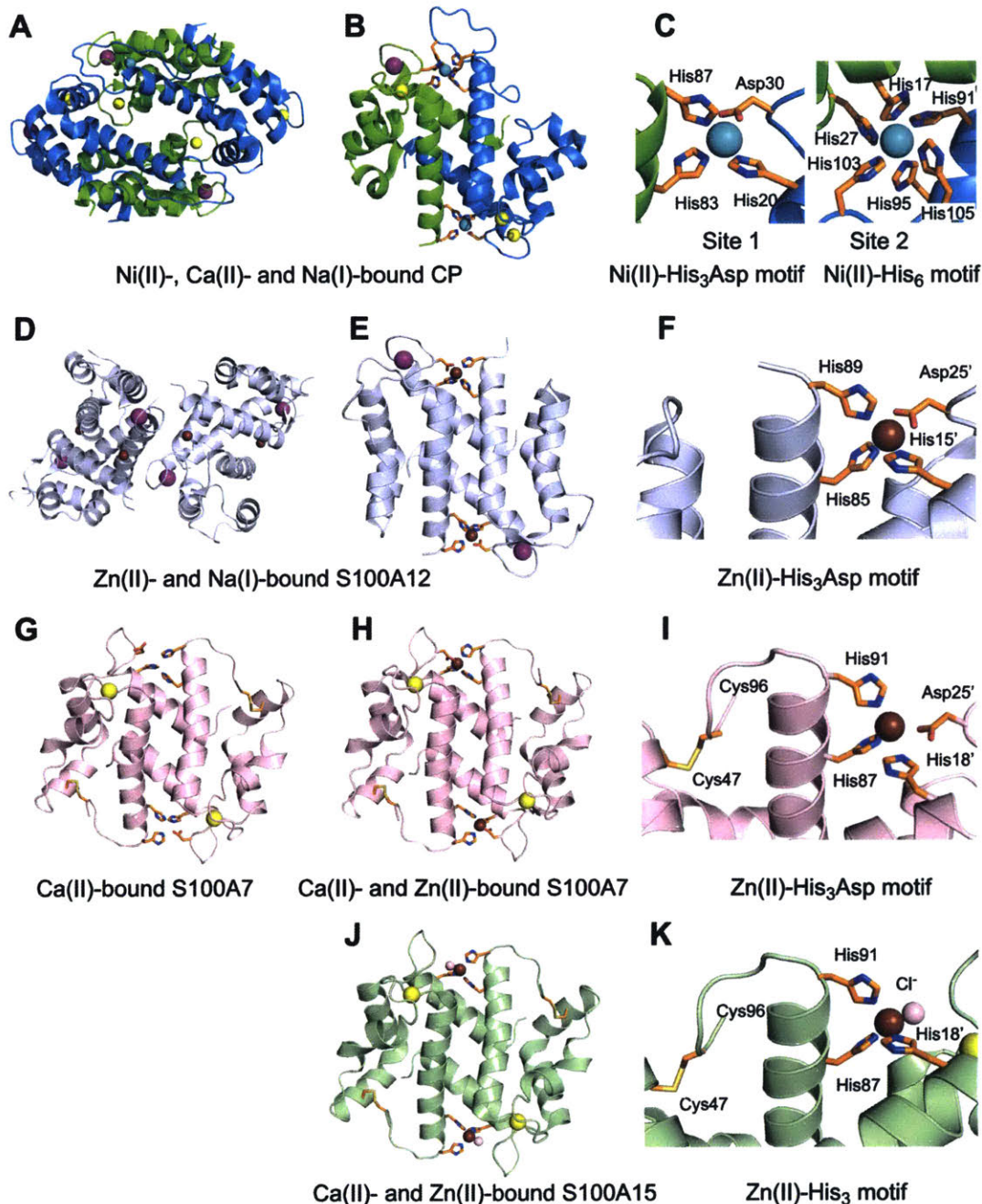


Figure 1.3. Crystal structures of human CP, S100A12, S100A7, and S100A15. (A, B) Structure of Ni(II)-, Ca(II)- and Na(I)-bound CP tetramer and dimer (PDB 5W1F). (C) Zoom-in view showing the His₃Asp (Site 1) and His₆ (Site 2) motifs of CP (PDB 5W1F). (D, E) Structure of Zn(II)- and Na(I)-bound S100A12 tetramer and dimer (PDB 2WC8). (F) Zoom-in view showing the His₃Asp motif of S100A12 (PDB 2WC8). (G) Ca(II)-bound structure of S100A7 dimer (PDB 3PSR). (H) Zn(II)- and Ca(II)-bound structure of S100A7 dimer (PDB 2PSR). (I) Zoom-in view showing the His₃Asp motif of S100A7 (PDB 2PSR). (J) Ca(II)- and Zn(II)-bound structure of S100A15 dimer (PDB 4AQL). (K) Zoom-in view showing the His₃ motif of S100A15 (PDB 4AQL). Zn(II), Ni(II), Ca(II), Na(I), and Cl⁻ ions are shown as brown, teal, yellow, purple, and pink spheres respectively.

The human S100 protein family of host-defense peptides includes 21 relatively small, α -helical, Ca(II)-binding polypeptides (Figure 1. 2).^{23,47} Human S100 proteins have conserved EF-hand domains for Ca(II) binding and diverse C-terminal and hinge regions.⁴⁷⁻⁴⁸ Each S100 polypeptide contains two EF-hands where the C-terminal EF-hand is described as “canonical” and the N-terminal EF-hand is described as “non-canonical.” This nomenclature originates from a comparison of S100 EF-hands to those of calmodulin. The “canonical” EF-hand domains are calmodulin-like and afford heptadentate coordination spheres for Ca(II). The “non-canonical” EF-hands provide fewer donor atoms and bind Ca(II) with lower coordination number and reduced affinity.⁴⁷ Like the EF-hand domains of calmodulin, each S100 EF-hand region assumes a helix-loop-helix motif, and binds Ca(II) via main-chain oxygen atoms and carboxylate side chains (Figure 1. 3).

Another structural hallmark of S100 proteins is a propensity to self-associate and form non-covalent oligomers. The homo- and heterodimers are each typified by a stable four-helix domain with a hydrophobic core.¹³⁻¹⁵ A comparison of the structures of CP, S100A12, S100A7, and S100A15 highlights some additional similarities (Figure 1. 2). For instance, each hetero- or homodimer exhibits two transition-metal-binding sites that are independent from the Ca(II)-binding sites. The transition-metal-binding sites form at the homo- or heterodimer interface and are composed of metal-binding residues from each subunit (Figure 1. 3). Despite similar overall structural features, CP, S100A12, S100A7, and S100A15 possess different expression patterns; Table 1. 1 lists examples of the cell types and organ systems where each of these proteins has been observed. Furthermore, differences in their metal-binding properties also account for distinct antimicrobial profiles and modes of action.

Table 1. 1. Location of human CP, S100A12, S100A7, and S100A15 in humans

S100 protein	Detected in	Ref
CP (S100A8/S100A9, Calgranulin A/B)	Neutrophils and monocytes Keratinocytes Female reproductive tract Cardiovascular system Gut epithelium	49-54
S100A12 (Calgranulin C)	Neutrophils and monocytes Psoriatic skin and keratinocytes	25, 54-61
S100A7 (psoriasis)	Abnormal keratinocytes Invasive squamous cell carcinoma Female reproductive tract Cerebrospinal fluids (bacterial meningitis, Alzheimer's disease) Microglial and meningeal cells (brain)	43, 45-46, 62-69
S100A15 (koebnerisin)	Basal keratinocytes Psoriatic skin Astrocytes and meningeal cells (brain)	65, 70-71

The location where the S100 proteins are detected can be deceptive. In some cases, the inflammation condition may prompt the immune cells to migrate to specific tissues and S100 proteins can be found at these inflammatory locations.

1. 3. 1. Microbiostatic Properties of S100 Proteins through Zn(II)-Sequestration.

Zn(II) is a ubiquitous d-block metal ion that performs structural, catalytic, and signaling roles in biology.⁷²⁻⁷³ In the context of the host/microbe interaction and infectious disease, invading microbial pathogens must obtain this essential metal nutrient from the host to colonize and promote virulence.⁷⁴⁻⁷⁵ The mammalian innate immune system, which provides a first line of defense against pathogenic invaders, employs one of two opposing strategies to modulate Zn(II) levels at infection sites and thereby inhibit the growth of pathogens: Zn(II) limitation and Zn(II) intoxication.⁷⁵⁻⁷⁶ The former phenomenon is a component of the metal-withholding innate immune response, and process is often termed “nutritional immunity”.^{20,77-78} In response to Zn(II) limitation and in an attempt to fulfill their nutritional requirements, pathogens express high-affinity Zn(II)-

uptake systems to acquire Zn(II) from the host environment.^{75-76,79-80} Thus, a tug-of-war for a limited supply of metal nutrient occurs at the host/pathogen interface, and the outcome of this competition impacts the progression of infection (Figure 1. 4). Zn(II)-sequestering HDPs are important contributors to this host/microbe interaction and, in humans, include CP, S100A7, S100A15, and S100A12. To the best of our knowledge, there are no extensive studies documenting the Zn(II)-binding and antimicrobial properties of S100A15, the presence of a Zn(II)-binding site in a crystal structure of S100A15 provides a foundation for addressing its Zn(II)-binding properties (Figures 1. 2 and 1. 3).⁸¹⁻⁸³

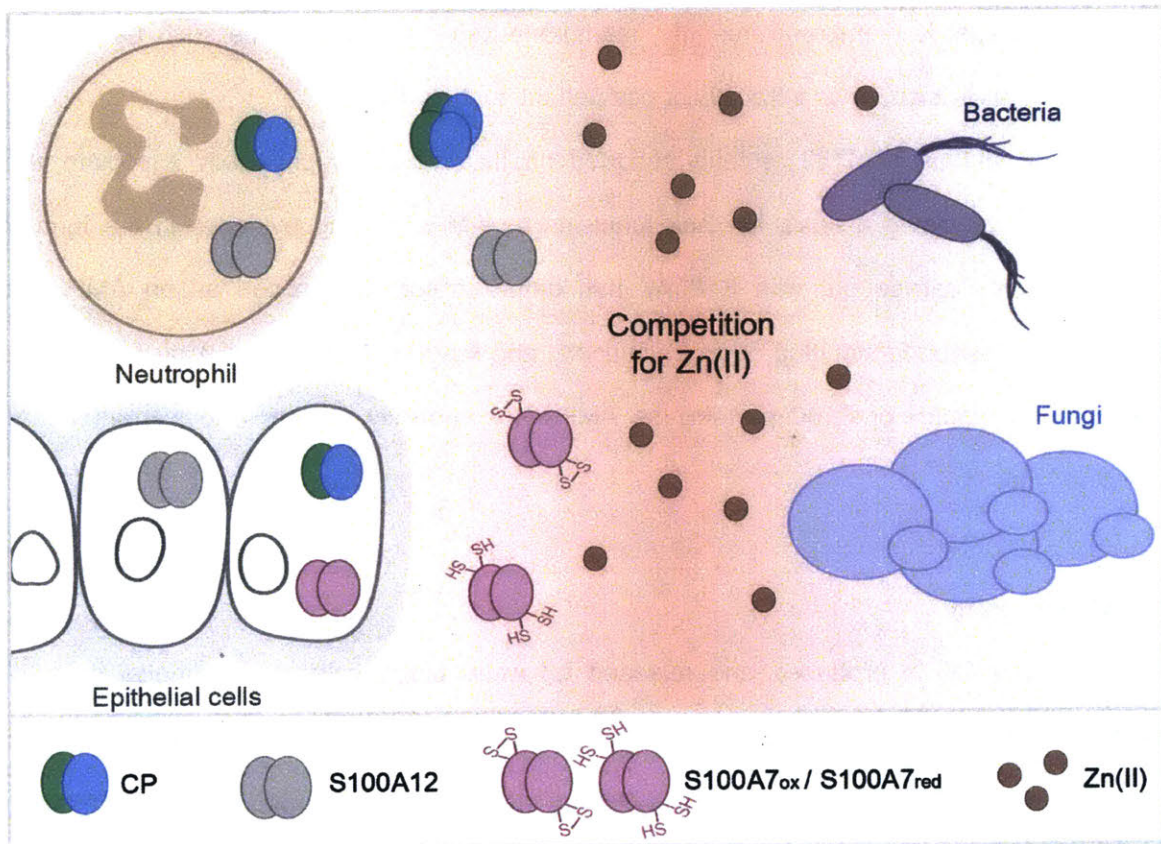


Figure 1. 4. Extracellular roles of CP, S100A12, and S100A7 in Zn(II) sequestration. CP is released from neutrophils and epithelial cells, S100A12 is released from neutrophils, and S100A7 is released from epithelial cells. These proteins compete with microbes for bioavailable Zn(II) in the extracellular space. S100A15 is excluded from this scenario since its role as a Zn(II)-sequestering protein has not been established.

1. 3. 2. Microbicidal Properties of S100 Proteins through Membrane Interactions.

The production of peptides and proteins exerting microbicidal activity is considered to be the most ancient mechanism of immunity. AMPs can direct antimicrobial activity against all categories of microbes, including viruses, archaea, bacteria and fungi, as well as against multicellular parasites.^{11,13} AMPs are thought to act by inhibiting microbial proliferation within the host through membrane or metabolic disruption,⁸⁴⁻⁸⁵ and their synthesis and secretion can be constitutive or inducible by microbial products or pro-inflammatory cytokines. Many AMPs target more than one type of microbe and use multiple mechanisms to achieve microbial killing. The antibacterial mechanisms of AMPs can be broadly divided into three categories based on whether the primary target is membrane integrity, membrane-dependent processes such as cell wall biosynthesis or division, or an intracellular component such as DNA.

Early studies of S100 proteins reported on their ability to physically associate with parasites,⁸⁶⁻⁸⁷ providing a basis for their functions as AMPs. Strong evidence in the form of solution studies carried out with S100A7 has demonstrated its function as an AMP, and contributed to an understanding of its bactericidal and fungicidal properties. Molecular details regarding the role(s) of S100 proteins as AMPs are currently unclear and warrant further investigations.

1. 4. Calprotectin

Human CP is produced and released by white blood cells and epithelial cells.^{88,89} Neutrophils constitutively express CP, which constitutes $\approx 40\%$ of total cytoplasmic protein in these immune cells. Monocytes and macrophages also express this protein.⁹⁰⁻⁹¹ Apo CP exists as a heterodimer of S100A8 (α , 10.8 kDa) and S100A9 (β , 13.2 kDa). Coordination of Ca(II) ions at the EF-hand domains, or a divalent transition metal ion at the His₆ site, causes two heterodimers to self-associate and form a $\alpha_2\beta_2$ heterotetramer.^{36,92-95} CP exhibits broad-spectrum

antimicrobial activity, and early studies identified a link between its growth inhibitory activity and Zn(II).⁹⁶⁻¹⁰⁰ Additional investigations have (i) defined how CP contributes to Zn(II) sequestration,^{30,37} (ii) examined how select microbial pathogens respond to Zn(II) limitation imposed by CP,¹⁰¹⁻¹⁰⁵ and (iii) uncovered that CP can withhold additional divalent first-row transition metals, including Mn(II),¹⁰⁶⁻¹⁰⁸ Fe(II),³³ Ni(II),³⁸ and Cu.⁴² More recent work has demonstrated that CP can also act through a mechanism that does not involve withholding of Mn or Zn from microbes, and instead requires a physical interaction between CP and microbes.¹⁰⁹

1. 4. 1. Zn(II)-Sequestering Properties of CP.

Among the Zn(II)-chelating S100 proteins, CP is unique because of its heterooligomeric (S100A8/S100A9) composition. This structural attribute affords four different EF-hand domains and two transition metal-binding sites with different amino acid compositions per heterodimer (Figure 1. 3A–C). Moreover, S100A9 is the longest human S100 polypeptide and it exhibits a C-terminal extension or “tail” that we define as residues 96-114 (Figures 1. 2 and 1. 3). These unusual features define the coordination chemistry of CP and its remarkable metal-sequestering ability. The transition-metal-binding sites are located at the S100A8/S100A9 heterodimer interface and are commonly referred to as site 1 and site 2. Site 1 is a His₃Asp motif composed of His83 and His87 from S100A8, and His20 and Asp30 from S100A9 (Figure 1. 3C). Site 2 is a biologically unprecedented His₆ motif defined by His17 and His27 from S100A8, and His91, His95, His103, and His105 from S100A9 (Figure 1. 3C).^{31,33-34,37-38,41} His103 and His105 are located in the flexible C-terminal tail of the S100A9 subunit. Both sites coordinate Zn(II) with high affinity and provide a 2:1 Zn(II):CP heterodimer stoichiometry, as described further below. Because no crystallographic or solution structure of Zn(II)-bound CP has been reported to date, current understanding of Zn(II) chelation by CP is based on results from solution studies.

A recent investigation established that the Zn(II) ion coordinated at site 2 is ligated by the six residues of the His₆ motif.³⁷ Prior to this work, it was unclear whether His103 and His105 of

the S100A9 C-terminal tail contribute to Zn(II) binding at this site. During investigations of the protease stability of CP, a serendipitous observation provided compelling evidence for the existence of an unprecedented Zn(II)-His₆ site. Whereas proteinase K cleaved the S100A9 polypeptide of Ca(II)-bound CP after His104, addition of 2 equivalents of Zn(II) protected this cleavage site.³⁶ When the CP variants His103Ala and His105Ala were examined, proteinase K cleaved the S100A9 subunit of the Zn(II)-free and Zn(II)-bound protein after His104, suggesting that both His103 and His105 are involved in coordinating Zn(II) at site 2. This notion was supported by X-ray absorption spectroscopy of the Zn(II)-bound Δ His₃Asp variant of CP, which has the four residues of the His₃Asp site mutated to Ala residues. The X-ray absorption near-edge structure (XANES) region of the spectrum indicated that the Zn(II) ion is coordinated in a six-coordinate geometry, and the extended X-ray absorption fine structure (EXAFS) region was consistent with Zn(II) in a His₆ coordination environment.³⁷ This result is consistent with studies of Mn(II), Fe(II) and Ni(II) coordination at this site; the promiscuous His₆ motif allows CP to compete with microbes for multiple divalent first-row transition metal ions.^{31,33,38,41} The coordination number of Zn(II) bound at the His₃Asp site is currently unclear and a topic for future investigation. In particular, whether the Asp residue is mono- or bidentate is unknown.

A variety of experiments have been performed to ascertain the Zn(II)-binding affinities of sites 1 and 2, including direct Zn(II)-binding titrations monitored by isothermal titration calorimetry (ITC) and Zn(II) competition titrations (Table 1. 2). In the latter experiments, a fluorescent small-molecule Zn(II) sensor of known Zn(II)-binding affinity (apparent dissociation constant value, $K_{d,Zn(II)}$) and CP are allowed to compete for Zn(II), and the fluorescence observed from the sensor provides a quantitative measure of the relative affinities of the two competitors. Because CP also binds Ca(II) ions, titrations with Ca(II)-insensitive Zn(II) sensors are important for interrogating the effect of Ca(II) ions on Zn(II) binding. In early work, the Ca(II)-insensitive sensor Zinpyr- 4 (ZP4, $K_{d,Zn(II)} = 650$ pM, pH 7.0)¹¹⁰ revealed that Ca(II) ions modulate the Zn(II) affinities of both sites 1 and 2 (Table 1. 2).³⁷ In particular, ZP4 showed that Ca(II)-bound CP coordinates Zn(II) with higher

affinity than the Ca(II)-free form. This discovery provided the foundation for the current model where the Ca(II) ion concentrations in the cytoplasm and extracellular space modulate the functional properties of CP (*vide infra*).³⁰

Table 1. 2. Reported apparent dissociation constant values ($K_{d,Zn(II)}$) for human S100 proteins.

Protein	$K_{d,Zn(II)}$	Method	Buffer conditions	Ref.
CP	1.4 nM 5.6 nM	ITC ^a	20 mM Tris, 100 mM NaCl, pH 7.5 stoichiometric Ca(II) ^{b, c}	107
CP-Ser ^d	133 ± 58 pM 185 ± 219 nM ≤ 10 pM ≤ 240 pM	Competition ^e	75 mM HEPES, 100 mM NaCl, pH 7.5 75 mM HEPES, 100 mM NaCl, pH 7.5, 2 mM Ca(II)	30
	90 ± 366 fM 0.9 ± 1 pM	Competition ^f	75 mM HEPES, 100 mM NaCl, pH 7.0 50 equivalents Ca(II)	37
CP ΔHis ₃ Asp variant ^g	3.4 ± 1.2 nM	ITC ^a	20 mM HEPES, 100 mM NaCl, pH 7.5 Stoichiometric Ca(II) ^b	41
CP ΔHis ₄ Variant ^h	8.2 ± 1.5 nM	ITC ^a	20 mM HEPES, 100 mM NaCl, pH 7.5 Stoichiometric Ca(II) ^b	41
CP-Ser H103A/H104A/H105A variant	4 ± 0.8 pM 22 ± 3 pM	Competition ^f	75 mM HEPES, 100 mM NaCl, pH 7.0 50 equivalents Ca(II)	37
S100A12	16 μM 83 μM	Tyr fluorescence	25 mM Tris-HCl, pH 7.4 ^c	29
S100A12	≤ 9 nM	Competition ⁱ	75 mM HEPES, 100 mM NaCl, pH 7.0	35 Chapter 2
S100A7	100 μM	Equilibrium dialysis	20 mM Tris, 150 mM KCl, pH 7.4 ^c	111 Chapter 3
S100A7 _{ox}	430 ± 13 pM	Competition ^e	75 mM HEPES, 100 mM NaCl, pH 7.0	39 Chapter 3

	580 ± 40 pM	Competition ^e	75 mM HEPES, 100 mM NaCl, pH 7.0 100 equivalents Ca(II)	39 Chapter 3
S100A7 _{red}	660 ± 56 pM	Competition ^e	75 mM HEPES, 100 mM NaCl, pH 7.0	39 Chapter 3
	420 ± 41 pM	Competition ^e	75 mM HEPES, 100 mM NaCl, pH 7.0 100 equivalents Ca(II)	39 Chapter 3
S100A7-Ser ^j	700 ± 58 pM	Competition ^e	75 mM HEPES, 100 mM NaCl, pH 7.0	39 Chapter 3
	370 ± 11 pM	Competition ^e	75 mM HEPES, 100 mM NaCl, pH 7.0 100 equivalents Ca(II)	39 Chapter 3
S100A7-Ala ^k	500 ± 69 pM	Competition ^e	75 mM HEPES, 100 mM NaCl, pH 7.0	39 Chapter 3
	490 ± 21 pM	Competition ^e	75 mM HEPES, 100 mM NaCl, pH 7.0 100 equivalents Ca(II)	39 Chapter 3

^aIsothermal titration calorimetry (ITC) experiments were performed at 30 °C. Stoichiometric Zn(II) binding was observed. ^bThe definition of stoichiometric Ca(II) relative to the CP concentration was not specified. ^cMetal-buffer equilibrium is a variable when Tris buffer is employed for studies of Zn(II) binding because Tris binds Zn(II) with $K_{d,Zn} = 10^{-4}$ M.¹¹² ^dCP contains two native Cys residues that were mutated to Ser for these metal-binding studies. CP-Ser is a S100A8(C42S)/S100A9(C3S) variant. ^eCP-Ser outcompetes ZP4 in the presence of Ca(II), and the $K_{d,Zn(II)}$ values were reported as upper limits. ^fCompetition experiments were performed with Zinpyr-4 (ZP4) at 25 °C. ^gCompetition experiments were performed with HNBO-DPA at 25 °C. These titrations were complicated by outcompetition and error. The fM $K_{d,Zn(II)}$ value is considered to be an upper limit and the pM $K_{d,Zn(II)}$ value is considered to be an estimate. The values were not assigned to particular sites. ^hA variant of CP that only contains the His₆ site. ⁱA variant of CP that only contains the His₃Asp site. ^jCompetition experiments were performed with FluoZin-3 (FZ3) at 25 °C. ^kA S100A7(C47S)(C96S) variant. ^lA S100A7(C47A)(C96A) variant. To determine the $K_{d,Zn(II)}$ values from competition experiments, the averaged data were fit to a two-site model where $K_{d1} \neq K_{d2}$ and $K_{d1} = K_{d2}$ for CP and S100A7, respectively.

One limitation of the ZP4 competition experiments was that CP outcompeted ZP4 for Zn(II) in the presence of excess Ca(II) ions; thus, only upper limits to the Zn(II) affinities could be determined from this method. Later, a new fluorescent Ca(II)-insensitive Zn(II) sensor named HNBO-DPA that binds Zn(II) with higher affinity than ZP4 was reported (HNBO-DPA $K_{d,Zn(II)} = 12$ pM, pH 7.0).¹¹³ Competition experiments performed with HNBO-DPA provided a new set of $K_{d,Zn(II)}$

values of Ca(II)-bound CP, and indicated that Ca(II)-insensitive Zn(II) sensors with greater Zn(II) affinity are needed because one Zn(II)-binding site out-competed HNBO-DPA for Zn(II) (Table 1).³⁷ Moreover, Zn(II) competition titrations with HNBO-DPA and a variant of CP that has no His residues in the S100A9 C-terminal tail (His103Ala/His104Ala/His105Ala variant) provided two additional important insights: (i) the tail His residues of CP contribute to high-affinity Zn(II) binding at the His₆ site and (ii) perturbation of the His₆ site lowered the Zn(II) affinity of the His₃Asp site. The latter observation provided the first hint of allostery between sites 1 and 2.³⁷ Further defining the Zn(II)-binding affinities, assessing the binding order, and deciphering crosstalk between the His₃Asp and His₆ sites are avenues that warrant continued investigation. In summary, the $K_{d,Zn(II)}$ values determined for CP to date are consistent with its role as a Zn(II)-sequestering HDP. Indeed, recent work demonstrated that both sites 1 and 2 of CP sequester Zn(II) from microbes and thereby contribute to its growth inhibitory properties.³⁷

As noted above, one major finding from the initial Zn(II) competition studies with ZP4 was that the presence of excess Ca(II) ions enhances the Zn(II) affinities of both sites 1 and 2.³⁰ This work, as well as subsequent studies of how CP coordinates other divalent transition metals,^{32-33,108} indicated that CP morphs into its high-affinity, metal-sequestering form in the extracellular milieu where Ca(II) concentrations are orders of magnitude higher than those found in the cytoplasm of resting cells (e.g. 10-100 nM versus ≈2 mM). The molecular basis for how Ca(II) complexation enhances the Zn(II) affinities requires elucidation. Ca(II) binding causes formation of S100A8/S100A9 tetramers⁹²⁻⁹⁴ and enhances the proteolytic stability of the protein,³⁶ which suggests that changes in conformation or dynamics may be at work. These observations also suggest that CP is predominantly a heterodimer when stored in the cytoplasm and forms heterotetramers in the extracellular space (Figure 1. 4). In agreement with the notion that Ca(II) ions enhance metal sequestration, several studies have shown that the presence of Ca(II) ions enhances the ability of CP to deplete transition metals from microbial growth medium and its antimicrobial activity.^{30,33,37,106,114}

1. 4. 2. Microbicidal Properties of CP.

Early work with CP documented its ability to physically interact with microbes, implicating CP in direct host-pathogen interactions.^{87,105,115-117,109} Indeed, these studies found CP to interact with cell wall-associated bacterial proteins,^{105,115} the cell wall of adult worms,⁸⁷ and select bacterial species.^{109,115} Immunohistochemistry results revealed that CP localized with macrophages within nodules containing *Onchocerca volvulus*, which is a filarial nematode that causes onchocerciasis.⁸⁷ In these studies, CP displayed a staining pattern that extended beyond the margins of the cell nodule, and was found on the surface of the worm.⁸⁷ The results from this study suggested that CP may either (i) kill the worms through direct physical interaction, (ii) inhibit their growth through an unknown mechanism, or (iii) act as a chemotactic signal to recruit host cells.

Recently, work by the Culotta lab reported that CP interacts with *Borrelia burgdorferi*, a bacterial pathogen that is the causative agent of Lyme disease.¹⁰⁹ *B. burgdorferi* cells exposed to CP ceased to grow, and interestingly, an increase rather than a decrease in intracellular and extracellular Mn and Zn levels was observed. Instead, they noted that CP inhibits *B. burgdorferi* growth through a mechanism that requires physical association of CP with the bacteria, as evidenced by the presence of CP in *B. burgdorferi* whole cell lysates. Investigations into the roles that metal-binding plays in the activity of CP suggested that both transition metal-binding sites contribute to the activity of CP towards *B. burgdorferi*; indeed, the authors observed that mutation of either the His₃Asp or His₄ site of CP attenuated the activity of CP, and that mutation of both sites rendered this CP variant inactive. Altogether, these findings demonstrated that CP exerts antimicrobial function on *B. burgdorferi* through a mechanism that does not involve metal-withholding. Instead, CP is thought to physically interact with *B. burgdorferi* and cause hypotonic stress.^{109,115}

1. 5. S100A12 (calgranulin C)

Human S100A12 (10.5 kDa) is also produced and released by neutrophils.⁵⁶⁻⁵⁷ This protein is abundant, at least based on studies of porcine neutrophils, where it was found to constitute up to 8% of total cytoplasmic protein.⁵⁵ Other white blood cells including monocytes, macrophages and eosinophils, as well as epithelial cells, also express S100A12.^{25,58,118-121} It is a 21-kDa homodimer that self-associates into tetramers and hexamers in the presence of metal ions.^{28-29, 122-124} Early studies implicated S100A12 as an anti-parasitic factor,^{86,125} and subsequent studies have demonstrated that S100A12 participates in Zn(II)-mediated nutritional immunity.^{35,126}

1. 5. 1. Zn(II)-Sequestering Properties of S100A12.

The human S100A12 homodimer houses two His₃Asp sites at the dimer interface that are composed of residues His15 and Asp25 of one subunit, and His85' and His89' of the other subunit (Figure 1. 3. D-F). Five crystal structures of S100A12 have been reported to date, including a structure of the Zn(II)-bound protein.^{28-29,122-124} In this structure, each Zn(II) ion is coordinated at a His₃Asp site in a distorted tetrahedral geometry, affording a 2:1 Zn(II):S100A12 stoichiometry.²⁹ On the basis of crystallographic and solution studies, S100A12 exhibits complex oligomerization behavior.^{28-29,122-124} For instance, Zn(II) binding causes two S100A12 dimers to self-associate into tetramers, and coordination of both Ca(II) and Zn(II) results in the formation of hexamers.^{29,122}

The crystal structure of Zn(II)-bound S100A12 provided a foundation for recent solution studies addressing its Zn(II)-chelating properties. Zn(II) competition experiments with a series of small-molecule Zn(II) sensors, including the fluorescent Zn(II) sensor FZ3 ($K_{d,Zn(II)} = 9$ nM, pH 7.4),¹²⁷ established that human S100A12 binds Zn(II) with subnanomolar affinity (Table 1).³⁵ These results are reminiscent of early studies of porcine S100A12, which reported that this orthologue binds Zn(II) tightly ($K_{d,Zn(II)} = 10$ nM),⁵⁵ and refute a prior study that employed intrinsic protein emission to study human S100A12 and reported $K_{d,Zn(II)}$ values of >10 μ M for each site.²⁹ Although further work is required to determine the $K_{d,Zn(II)}$ values of S100A12 and determine how

Ca(II) ions affect Zn(II) binding, the current data are consistent with the notion that S100A12 functions as a Zn(II)-sequestering protein. Moreover, results from several other experiments indicate that Ca(II)-bound S100A12 has higher Zn(II) affinity than the apo protein. For instance, selective Zn(II) depletion from microbial growth medium by S100A12 was enhanced when the medium was supplemented with ≈ 2 mM Ca(II).³⁵ Moreover, the antimicrobial activity of S100A12 is enhanced in the presence of excess Ca(II) ions.³⁵ These observations support the notion that Ca(II) ions modulate the functional properties of S100A12 such that its Zn(II)-sequestering ability is enhanced in the extracellular space.

Indeed, several recent reports provide compelling evidence that S100A12 functions as a Zn(II)-withholding protein. One investigation revealed that S100A12 is more prevalent within *Helicobacter pylori*-infected gastric tissue compared to healthy tissue, and S100A12 was shown to inhibit the growth of *H. pylori* through a Zn(II)-reversible sequestration mechanism.¹²⁶ We also identified S100A12 as an antifungal agent that displays Ca(II)-dependent growth inhibitory activity against *Candida* spp (Chapter 2).³⁵ The antifungal activity of S100A12 was lost when the protein was pre-incubated with 2 equivalents of Zn(II), supporting a Zn(II)-starvation mode of action.

Although both S100A12 and CP sequester Zn(II) and appear to have similar Ca(II) dependence, there are marked differences in the antimicrobial profiles of these proteins. S100A12 exhibits a relatively narrow spectrum of antimicrobial activity, whereas CP provides growth inhibition against a variety of bacterial and fungal pathogens.^{30,35,37} The metal-sequestration profiles of CP and S100A12 provide one explanation for this difference. CP is functionally versatile because of its ability to sequester multiple first-row transition metals that are essential nutrients at the His₆ site, whereas S100A12 (and the His₃Asp site of CP) is more selective and sequesters Zn(II) but not Mn(II), Fe(II) and Ni(II).³⁵ Thus, it appears that microbes that are more sensitive to Zn(II) deprivation are more susceptible to S100A12.

Because neutrophils produce and release S100A12 and CP, it is likely that these two proteins act together in the extracellular space. Metal substitution experiments with CP indicate

that the His₆ site binds a divalent transition metal rapidly and with slow exchange, and that it will entrap the metal it encounters first.³³ Given that Zn(II) is ubiquitous and relatively abundant, we propose that Zn(II) sequestration by S100A12 may boost the ability of CP to capture other nutrient metals like Fe(II), Mn(II), and Ni(II) at the His₆ site.³⁵ Most studies consider S100A12 and CP independently, and investigating these two proteins together may improve our understanding of metal sequestration by the host innate immune system.

1. 5. 2. Microbicidal Properties of S100A12.

Early studies implicated S100A12 as an anti-parasitic factor, when it was isolated from *Onchocerca volvulus* extracts obtained from tissues of onchocerciasis patients. However, to the best of our knowledge, there are no published studies documenting the microbicidal properties of S100A12.

Calcitermin	VAIALKAAHY <u>HTHKE</u>
Human S100A12	***** ...VAIALKAAHY <u>HTHKE</u>
Porcine S100A12	* <u>VT</u> DVLI <u>TA</u> HDNI <u>HKE</u> *

Figure 1. 5. Comparison of primary amino acid sequence of calcitermin, human S100A12, and porcine S100A12. Calcitermin is 100% identical to human S100A12, and 47% identical to porcine S100A12. Identical residues are highlighted with asterisks, and underlined residues indicate the Zn(II)-binding consensus sequence (HXXXH)

Interestingly, a peptide named calcitermin, which is a putative 15-residue C-terminal cleavage fragment of S100A12, was isolated from human nasal airways (Figure 1. 5).¹²⁸ Calcitermin was found to possess microbicidal activity against *Candida albicans*, *Escherichia coli*, *Listeria monocytogenes*, and *Pseudomonas aeruginosa* at pH 5.4, but not at pH 7.4. On the basis of the primary amino acid sequence of calcitermin, it is reasonable to assume that the three His residues of calcitermin become protonated at acidic pH. Thus, the concomitant increase in positive charge on calcitermin may enhance the peptide's interaction with the negatively charged groups on the bacterial cell walls. Furthermore, increasing the ionic strength and/or salinity of the

buffer in which the killing assays were carried out attenuated the activity of calcitermin, reminiscent of results obtained with another class of His-containing AMPs: clavanins.¹²⁹ The effect that Zn(II)-binding has on the microbicidal activity of calcitermin is not conclusive. The killing assays with calcitermin were performed with excess Zn(II) compared to calcitermin. Since the stoichiometry of Zn(II)-binding to calcitermin was not ascertained and the experiments were carried out at acidic pH, it is possible that the excess unbound Zn(II) was toxic and partially accounted for the killing activity reported with the “Zn(II)-bound” form of calcitermin.¹³⁰ The killing activity of a fragment of S100A12 is reminiscent of a “propeptide strategy” employed to modulate the activity of other HDPs, such as human defensin 6 (HD6).¹⁷⁻¹⁹ Hence, it is possible that proteolytic cleavage of S100A12 by the host or microbes generates a potent S100A12-derived AMP. This mechanism is appealing as it would allow for spatial and temporal control of the growth inhibitory and killing properties of S100A12.

1. 6. S100A7 (psoriasin)

Human S100A7 (psoriasin) is a 22-kDa homodimer that is expressed by epithelial cells and secreted into the upper epithelia.^{111,131-133} In contrast to CP and S100A12, higher-order oligomers of S100A7 have not been observed. S100A7 has been identified as a bactericidal factor of the skin,¹³⁴ tongue,⁶⁴ and female genital tract.¹³⁵ S100A7 is a well-established *E. coli*-cidal factor, and recent studies reported that S100A7 possesses antifungal activity.⁴⁶ To date, three different mechanisms of action have been proposed for the host-defense function of S100A7 involving (i) Zn(II) sequestration,^{39,134} (ii) membrane permeabilization,^{44,136} and (iii) barrier function.¹³⁷ The third model for S100A7 in host-defense focuses on its ability to adhere to *E. coli* and keratinocytes, and the occurrence of cross-linked S100A7 species in human wounds.¹³⁸ This model proposes that S100A7 functions as a solid-phase component of the physical barrier that protects the epithelium from microbial invasion.¹³⁸

1. 6. 1. Zn(II)-Sequestering Properties of S100A7.

The human S100A7 homodimer contains two His₃Asp motifs at the dimer interface.^{111,131-133} These Zn(II)-binding sites are composed of His87 and His91 from one monomer, and His18' and Asp25' from the other monomer (Figures 1. 2 and 1.3G–I).¹³²⁻¹³³ Two crystal structures of Zn(II)-bound S100A7 have been reported and both show that a 2:1 Zn(II):S100A7 stoichiometry with each Zn(II) ion coordinated at a His₃Asp site in a distorted tetrahedral geometry.¹³³

S100A7 has several unusual structural attributes. Its N-terminal EF-hand is truncated; thus, the loop is three residues shorter than the corresponding loops of S100A12 and CP (Figure 1. 2). The N-terminal EF hand also contains a Ser residue at position 30. This position corresponds to an Asp/Glu residue that binds Ca(II) in S100A12, S100A8, and S100A9 (Figure 1. 2). Another striking structural feature of S100A7 is that each polypeptide contains two Cys residues, Cys47 and Cys96, which can form an intramolecular disulfide bond (Figures 1. 2 and 1.3G–I).¹³²⁻¹³³ As a result, the S100A7 homodimer can exist in the reduced form (S100A7_{red}) with four free Cys thiulates or in the oxidized form (S100A7_{ox}) with two intramolecular disulfide bonds. Moreover, the Cys47–Cys96 disulfide bond is in close proximity to the Zn(II)-binding motifs; Cys96 is separated from the Zn(II)-coordinating residue His91 by a Gly-Ala-Ala-Pro loop. These structural features motivated examination of the effects of disulfide bond formation and Ca(II) ions on the Zn(II)-binding properties and antibacterial activity of S100A7.³⁹ Investigation of the disulfide redox behavior of S100A7 revealed that (i) the midpoint potential of S100A7 falls in the physiological range; (ii) Ca(II) binding depresses the midpoint potential by 40 mV from -255 mV for the apo protein to -298 mV for the Ca(II)-bound protein at pH 7.0; (iii) Zn(II) coordination appears to further depress the midpoint potential such that the value cannot be determined using standard redox buffer systems, (iv) apo S100A7_{ox} is a substrate for the mammalian thioredoxin system (Trx/TrxR), and (v) metal-bound S100A7_{ox} is not readily reduced by Trx/TrxR.³⁹ Taken together, these observations indicated that both S100A7_{ox} and S100A7_{red} can exist under physiological conditions, and that metal-bound S100A7 is more likely to be in the oxidized form. The former conclusion

agrees with prior *ex vivo* analyses that reported the isolation of S100A7_{ox} and S100A7_{red} from skin samples.^{46,139}

Zn(II) competition experiments demonstrated that S100A7_{ox} and S100A7_{red} each coordinate two equivalents of Zn(II) with sub-nanomolar affinity in the absence and presence of Ca(II) ions (Table 1. 1), and that the cysteine thiolates in S100A7_{red} do not form a third high-affinity Zn(II) site.³⁹ This work provided revision to a previously reported $K_{d,Zn(II)}$ value for S100A7 of 100 μ M.¹¹¹ The results also refuted a prior hypothesis that a third high-affinity Zn(II)-binding site created by the Cys thiolates conferred antifungal activity to S100A7_{red}.⁴⁶ Moreover, Zn(II) competition titrations with ZP4¹¹⁰ revealed similar $K_{d,Zn(II)}$ values for S100A7_{ox} and S100A7_{red} in both the absence and presence of excess Ca(II) ions (Table 1. 1). These results indicated that (i) the redox state of the Cys residues in S100A7 has a negligible effect on the apparent $K_{d,Zn(II)}$ value obtained using ZP4, and (ii) apo- and Ca(II)-bound S100A7 have similar Zn(II) affinities. The latter observation indicates that S100A7 does not share the same Ca(II) dependence as CP and S100A12.

Although the Zn(II) competition studies described above revealed negligible difference in Zn(II) affinities of S100A7_{red} and S100A7_{ox}, several other lines of experimental evidence indicated that S100A7_{ox} is more effective at Zn(II) sequestration than S100A7_{red}. For instance, experiments that probed metal exchange at the His₃Asp sites showed distinct metal substitution rates of S100A7_{ox} compared to S100A7_{red}. Moreover, investigations of antibacterial activity indicated that S100A7_{ox} is more active than S100A7_{red}.³⁹ In total, these results suggest that S100A7 can exist in a variety of forms depending on the redox environment and presence of divalent cations like Ca(II) and Zn(II). Moreover, it appears that S100A7 uses redox cues to tune its Zn(II)-sequestering ability and antibacterial activity (Figure 1. 4), and that S100A7_{ox} may be a more important contributor to Zn(II)-withholding in the extracellular space than S100A7_{red}. We expect that further biophysical studies designed to elucidate how disulfide-bond formation and reduction affects the protein scaffold and Zn(II) coordination at the His₃Asp sites will be informative.

1. 6. 2. Microbicidal Properties of S100A7.

S100A7 was first isolated from keratinocytes of psoriatic skin lesions in 1996.^{111,131} Seminal studies reported that S100A7 has Zn(II)-mediated antibacterial activity against *Escherichia coli*, and later investigations revealed antifungal activity against filamentous fungi, including the dermatophyte *Trichophyton rubrum* and *Aspergillus fumigatus*. These studies implicated S100A7 as having direct killing properties, a mode of action further supported by a recent report, indicating that S100A7 can damage the cell membrane of *Bacillus megaterium*.⁴⁴ Subsequently, the frog orthologue of S100A7, which lacks the Zn(II)-binding sites of human S100A7, was shown to compromise the membrane of *B. megaterium* and *Bacillus subtilis* at acidic pH.¹⁴⁰ There are a few studies that have established S100A7 as an *E. coli*-cidal factor. However, a molecular understanding of which structural features of S100A7 account for its microbicidal activity is unclear, and remain an avenue for future work.

1. 7. S100A15 (koebnerisin)

Human S100A15 (koebnerisin) is a 23-kDa homodimer that was first isolated from psoriatic lesions in 2003.⁷⁰ While most S100 proteins share moderate sequence identity,⁴⁰ S100A15 is interesting as a comparison to S100A7. S100A15 and S100A7 share 93% sequence homology and are co-expressed in epithelial cells (Figure 1. 2). Intriguingly, S100A15 and S100A7 display divergent functions, and expression profiles differ during inflammation and infection.⁸² Furthermore, S100A15 houses a His₃ motif instead of the canonical His₃Asp motif observed in the other S100s, including S100A7.⁸³ The scope of antimicrobial activity of S100A15 is not established, and prior work has suggested that S100A15 may exhibit antibacterial activity against *E. coli*; however, its mechanism of action remains elusive.⁸¹ We are not aware of prior work documenting S100A15 as an AMP. However, on the basis of studies reporting the microbicidal properties of S100A7, and the high sequence identity that S100A15 and S100A7 share, we postulate that S100A15 may possess bactericidal properties.

1. 8. Outlook

Over the past decade, our understanding of how the host and pathogen compete for Zn(II) and other essential metal nutrients has markedly advanced, and S100 proteins have emerged as key players in the metal-withholding innate immune response. The remarkable coordination chemistry exhibited by human CP, S100A12, and S100A7 provides new examples of how metal-binding properties can be tuned by environmental cues. Studies of Zn(II) chelation by CP revealed that Ca(II) binding enhances the Zn(II) affinity of this protein, and provided a paradigm for considering how Ca(II) ions affect its ability to sequester other metal nutrients as well as its antimicrobial activity. Subsequent investigations of Zn(II) sequestration by S100A12 and S100A7 built upon this work and afforded some similarities as well as striking differences, highlighting that metal-sequestering S100 proteins must be evaluated on a case-by-case basis. Similar to CP, current work indicates that Ca(II) ions modulate the Zn(II)-binding affinity of S100A12 and that this protein has the capacity to sequester Zn(II) in the extracellular space. S100A7, in contrast, appears to tune its Zn(II)-sequestering capacity through intramolecular disulfide-bond redox chemistry. Curiously, the disulfide bonds of S100A7 are more difficult to reduce when the protein is Ca(II) bound, which suggests an indirect modulatory effect of Ca(II) ions on the Zn(II)-binding properties of this protein. Taken together, a compelling picture emerges where CP, S100A12 and S100A7 are exquisitely designed to limit Zn(II) availability in the extracellular space.

Based on early studies of CP, S100A12, and S100A7 that implicate these proteins as having microbicidal functions, and motivated by the structural similarities between CP, S100A7, S100A15, and S100A12, we have investigated the bactericidal properties of these S100 proteins. The results from our studies indicate that these S100 proteins possess similar patterns of behavior; for instance, the proteins are generally more active at acidic vs neutral pH. Common to other AMPs, the proteins lose bactericidal activity at high ionic strength and salinity, likely due to charge neutralization of bacterial cell membranes. Interestingly, CP was found to be the most potent AMP amongst this group of S100 proteins, followed by S100A7 and S100A15. S100A12 showed

negligible bactericidal activity under all conditions tested. Microscopy studies revealed that CP, S100A7, and S100A15 can damage bacterial cell membranes as evidenced by live-dead staining assays, and the extent of membrane disruption observed by microscopy was consistent with the activities of the proteins determined by solution studies. These results provide a basis for future work to investigate the mode of action of S100s as AMPs. Furthermore, it will be informative to ascertain whether these bactericidal activities are physiologically relevant.

In closing, 100 proteins are a noteworthy example of the multifunctionality of HDPs, and warrant further investigation into their antimicrobial modes of action. However, a detailed understanding of how their microbiostatic and microbicidal functions are intertwined and modulated under (patho)physiological conditions are questions that remain to be addressed.

1. 9. Summary of Thesis

The goal of this dissertation is to understand the antimicrobial functions of a subset of S100 proteins, namely CP, S100A12, S100A7, and S100A15. We have developed robust purification and analytical methods that allow us to purify and work with various forms of the proteins, which we employ throughout this work. We have shown that the functions of these S100 proteins are beautifully complex, and are modulated by external chemical and environmental factors such as metal and salt levels, pH, and redox environment. We hope that the fundamental insights obtained from this work contribute to a better understanding of host-pathogen interactions, and set the stage for future studies investigating the multiple antimicrobial functions of these proteins.

In Chapter 2, we present results from metal-binding studies and antimicrobial assays that elucidate the role that Ca(II) ions play in modulating the Zn(II)-binding and antimicrobial properties of S100A12, and evaluate the scope of its antimicrobial activity. We carry out metal-depletion studies to demonstrate that S100A12 specifically depletes Zn from bacterial and fungal growth medium in a concentration- and Ca(II)-dependent manner. Motivated by the results from the

metal-depletion experiments, we assess the antifungal activity of S100A12 and demonstrate that it has potent activity against *Candida albicans*, *C. krusei*, *C. glabrata* and *C. tropicalis*, all of which cause human disease. We further expand on the scope of the antimicrobial properties of S100A12 by screening a series of bacterial pathogens, and show that S100A12 exerts strain-dependent antibacterial activity. We report that the antimicrobial activity of S100A12 is Ca(II)-dependent, a result that is consistent with the mechanism of action of its S100 counterpart, CP, and requires the presence of the apo His₃Asp motifs, consistent with a mechanism of Zn(II)-mediated growth inhibition. Lastly, we evaluate the Zn(II)-binding properties of S100A12 and confirm that S100A12 binds Zn(II) with a 2:1 stoichiometry with sub-nanomolar affinity binding. These findings are consistent with its role as an extracellular Zn(II)-sequestering protein. Taken together, these data support a model whereby S100A12 uses Ca(II) ions to tune its Zn(II)-chelating properties and antimicrobial activity, and effectively turn on these functions in the Ca(II)-rich environment of the extracellular space.

In Chapter 3, we examine the disulfide redox bond behavior and coordination chemistry of S100A7. We determine the midpoint potential of the disulfide bond formed by Cys47 and Cys96 of S100A7. We argue that both forms of the protein are physiologically relevant and that the oxidized form of S100A7 is likely the predominant species existing in the extracellular space. Zn(II) competition experiments demonstrate that S100A7_{ox} and S100A7_{red} each coordinate two equivalents of Zn(II) with sub-nanomolar affinity and that, unlike CP and S100A12, Ca(II) ions have negligible effect on the Zn(II)-binding affinity of S100A7. The results from our metal-binding studies with S100A7 provide a revision on its reported $K_{d,Zn(II)}$, and refute a previous hypothesis that a third high-affinity Zn(II)-binding site created by the Cys thiolates confers antifungal activity to S100A7_{red}. By carrying out antimicrobial studies, we show that S100A7_{ox} is a more potent antimicrobial agent compared to S100A7_{red}, and that unlike CP and S100A12, the antimicrobial properties of S100A7 are not directly modulated by Ca(II) levels. Altogether, we report a model whereby the local redox environment of S100A7 tunes its Zn(II)-sequestration capacity through

intramolecular disulfide-bond redox chemistry, and that Ca(II) ions exert an indirect modulatory effect on the Zn(II)-binding properties of this protein.

In Chapter 4, we carry out solution and microscopy studies to investigate the bactericidal properties of CP. We show that CP displays bactericidal activity against *E.coli* with enhanced activity at acidic pH, and that this activity is independent of metal sequestration. To the contrary, we report that divalent metal-binding by CP attenuates its *E. coli*-cidal activity. CP compromises the cell membrane of *E. coli* cells and causes aberrant cell morphology phenotypes that include cell distortion, cell wall protrusion, and cell lysis, and are all associated with cell membrane permeabilization. Time-lapse imaging studies reveal that *E. coli* cells exhibit cell surface roughness and distortion within 5-10 min of exposure to CP, protrusions appear later, and cell lysis is the last step that results into cell death. Additionally, we employ *E. coli* cells expressing GFP in the cytoplasm or the periplasm to show that CP causes leakage of periplasmic GFP, but not cytoplasmic GFP, suggesting that CP affects the periplasmic content of *E. coli* cells. Altogether, we propose that the function of CP as an AMP could point to one of its intracellular functions, where levels of Ca(II) and transition metal ions are low. This putative function could help prevent colonization by intracellular pathogens within host cells, as well as during macrophage engulfment of pathogens.

In Chapter 5, we carry out a systematic screening to characterize the physiological conditions under which CP, S100A7, S100A15, and S100A12 display the higher bactericidal activity. As a starting point, we screen the *E. coli*-cidal properties of the S100 proteins at varying salt, metal, and pH, and find that the proteins are effective bactericidal factors under acidic conditions, and remain active at salt levels that are physiologically relevant. We observed that Ca(II) supplementation attenuates the *E. coli*-cidal activities of the proteins to varying extents and we propose that these trends may be related to differences in the Ca(II)-binding properties of S100 proteins. Microscopy studies reveal that similarly to CP, S100A7 and S100A15 can compromise the bacterial cell membrane of *E. coli* cells, and induce aberrant cell morphology

phenotypes. In this work, we further expand upon the scope of the bactericidal properties of the proteins, and the results indicate that a select group of S100 proteins can be categorized AMPs against Gram-negative strains. Lastly, we postulate that their mode of action involves binding to the anionic LPS moieties on the cell outer-membrane of Gram-negative strains.

1. 10. References

1. Parkin, J.; Cohen, B., An overview of the immune system. *Lancet* **2001**, *357*, 1777-1789.
2. Medzhitov, R., Toll-like receptors and innate immunity. *Nat. Rev. Immunol.* **2001**, *1*, 135-145.
3. Ganz, T., The role of antimicrobial peptides in innate immunity. *Integr. Compt. Biol.* **2003**, *43*, 300-304.
4. Hancock, R. E. W.; Haney, E. F.; Gill, E. E., The immunology of host defence peptides: beyond antimicrobial activity. *Nat. Rev. Immunol.* **2016**, *16*, 321-334.
5. Metschnikoff, E., Über die intracelluläre verdauung bei coelenteraten. *Zool. Anz.* **1880**, *3*, 261-263.
6. Metschnikoff, E., Untersuchungen über die intracelluläre verdauung bei wirbellosen Theiren *Arb. Zool. Inst. Univ. wien. u. Zool. Stat. Triest* **1884**, *5*, 141-168.
7. Metschnikoff, E., Ueber die pathologische bedeutung der intracellularen Verdauung. *Fortschr. Med.* **1884**, *2*, 558-569.
8. Metschnikoff, E., *E. Allg. Wein. med. Ztg.* **1884**, *27/29*, 307-332.
9. Laschtschenko, P., Über die keimtötende und entwicklungshemmende Wirkung Hühnereiweiß" [On the germ-killing and growth-inhibiting effect chicken egg albumin]. *Z. Hyg. InfektKrankh* **1909**, *64*, 419-427.
10. Fleming, A., On a remarkable bacteriolytic element found in tissues and secretions. *Proc. R. Soc. B.* **1922**, *93* (653), 306-317.

11. Jenssen, H.; Hamill, P.; Hancock, R. E. W., Peptide antimicrobial agents. *Clin. Microbiol. Rev.* **2006**, *19*, 491-511.
12. Yeung, A. T. Y.; Gellatly, S. L.; Hancock, R. E. W., Multifunctional cationic host defence peptides and their clinical applications. *Cell. Mol. Life Sci.* **2011**, *68*, 2161-2176.
13. Afacan, N. J.; Yeung, A. T. Y.; Pena, O. M.; Hancock, R. E. W., Therapeutic potential of host defense peptides in antibiotic resistant infections. *Curr. Pharma. Design* **2012**, *18*, 807-819.
14. Nijnik, A.; Hancock, R. E. W., Host defence peptides: antimicrobial and immunomodulatory activity and potential applications for tackling antibiotic-resistant infections. *Emerg. Health. Threats* **2009**, *2*, e1.
15. Gallo, R. L.; Nizet, V., Endogenous production of antimicrobial peptides in innate immunity and human disease. *Curr. Allergy. Asthma* **2003**, *3*, 402-409.
16. Besold, A. N.; Culbertson, E. M.; Culotta, V. C., The Ying and Yang of copper during infection. *J. Biol. Inorg. Chem* **2016**, *21* (2), 137-144.
17. Chairatana, P.; Nolan, E. M., Molecular basis for self-assembly of a human host-defense peptide that entraps bacterial pathogens. *J. Am. Chem. Soc.* **2014**, *136*, 13267-13276.
18. Chairatana, P.; Nolan, E. M., Human α -Defensin 6: A small peptide that self-assembles and protects the host by entangling microbes. *Acc. Chem. Res.* **2017**, *50*, 960-967.
19. Chu, H.; Pazgier, M.; Jung, G.; Nuccio, S.-P.; Castillo, P. A.; deJong, M. F.; Winter, M. G.; Winter, S. E.; Wehkamp, J.; Shen, B.; Salzman, N. H.; Underwood, M. A.; Tsolis, R. M.; Young, G. M.; Lu, W.; Lehrer, R. I.; Baumler, A. J.; Bevins, C. L., Human α -defensin 6 promotes mucosal innate immunity through self-assembled peptide nanonets. *Science* **2012**, *337*, 477-481.
20. Weinberg, E. D., Nutritional immunity: Host's attempt to withhold iron from microbial invaders. *J. Am. Med. Assoc.* **1975**, *231* (1), 39-41.
21. Farnaud, S.; Evans, R. W., Lactoferrin - a multifunctional protein with antimicrobial properties. *Mol. Immunol.* **2003**, *40*, 395-405.

22. Donato, R., Functional roles of S100 proteins, calcium-binding proteins of the EF-hand type. *Biochim. Biophys. Acta* **1999**, (1450), 191-231.
23. Donato, R.; Canon, B. R.; Sorci, G.; Riuzzi, F.; Hsu, K.; Weber, D. J.; Geczy, C. L., Functions of S100 proteins. *Curr. Mol. Med.* **2013**, *13*, 24-57.
24. Goyette, J.; Geczy, C. L., Inflammation-associated S100 proteins: new mechanisms that regulate function. *Amino Acids* **2011**, *41* (4), 821-42.
25. Foell, D.; Kucharzik, T.; Kraft, M.; Vogl, T.; Sorg, C.; Domschke, W.; Roth, J., Neutrophil derived human S100A12 (EN-RAGE) is strongly expressed during chronic active inflammatory bowel disease. *Gut* **2003**, *52*, 847-853.
26. Foell, D.; Wittkowski, H.; Vogl, T.; Roth, J., S100 proteins expressed in phagocytes: a novel group of damage-associated molecular pattern molecules. *J. Leukoc. Biol.* **2007**, *81*, 28-37.
27. Leclerc, E.; Fritz, G.; Vetter, S. W.; Heizmann, C. W., Binding of S100 proteins to RAGE: an update. *Biochim. Biophys. Acta* **2009**, *1793*, 993-1007.
28. Moroz, O. V.; Antson, A. A.; Dodson, E. J.; Burrell, H. J.; Grist, S. J.; Lloyd, R. M.; Maitland, N. J.; Dodson, G. G.; Wilson, K. S.; Lukanidin, E.; Bronstein, I. B., The structure of S100A12 in a hexameric form and its proposed role in receptor signalling. *Acta Crystallogr. D Biol. Crystallogr.* **2002**, *58*, 407-413.
29. Moroz, O. V.; Burkitt, W.; Wittkowski, H.; He, W.; Ianoul, A.; Novitskaya, V.; Xie, J.; Polyakova, O.; Lednev, I. K.; Shekhtman, A.; Derrick, P. J.; Bjoerk, P.; Foell, D.; Bronstein, I. B., Both Ca^{2+} and Zn^{2+} are essential for S100A12 protein oligomerization and function. *BMC Biochem.* **2009**, *10*, 11.
30. Brophy, M. B.; Hayden, J. A.; Nolan, E. M., Calcium ion gradients modulate the zinc affinity and antibacterial activity of human calprotectin. *J. Am. Chem. Soc.* **2012**, *134* (43), 18089-18100.

31. Brophy, M. B.; Nakashige, T. G.; Gaillard, A.; Nolan, E. M., Contributions of the S100A9 C-terminal tail to high-affinity Mn(II) chelation by the host-defense protein human calprotectin. *J. Am. Chem. Soc.* **2013**, *135* (47), 17804-17817.
32. Hayden, J. A.; Brophy, M. B.; Cunden, L. S.; Nolan, E. M., High-affinity manganese coordination by human calprotectin is calcium-dependent and requires the histidine-rich site formed at the dimer interface. *J. Am. Chem. Soc.* **2013**, *135* (2), 775-787.
33. Nakashige, T. G.; Zhang, B.; Krebs, C.; Nolan, E. M., Human calprotectin is an iron-sequestering host-defense protein. *Nat. Chem. Biol.* **2015**, *11* (10), 765-771.
34. Gagnon, D. M.; Brophy, M. B.; Bowman, S. E.; Stich, T. A.; Drennan, C. L.; Britt, R. D.; Nolan, E. M., Manganese binding properties of human calprotectin under conditions of high and low calcium: X-ray crystallographic and advanced electron paramagnetic resonance spectroscopic analysis. *J. Am. Chem. Soc.* **2015**, *137* (8), 3004-3016.
35. Cunden, L. S.; Gaillard, A.; Nolan, E. M., Calcium ions tune the zinc-sequestering properties and antimicrobial activity of human S100A12. *Chem. Sci.* **2016**, *7* (2), 1338-1348.
36. Stephan, J. R.; Nolan, E. M., Calcium-induced tetramerization and zinc chelation shield human calprotectin from degradation by host and bacterial extracellular proteases. *Chem. Sci.* **2016**, *7* (3), 1962-1975.
37. Nakashige, T. G.; Stephan, J. R.; Cunden, L. S.; Brophy, M. B.; Wommack, A. J.; Keegan, B. C.; Shearer, J. M.; Nolan, E. M., The hexahistidine motif of host-defense protein human calprotectin contributes to zinc withholding and its functional versatility. *J. Am. Chem. Soc.* **2016**, *138* (37), 12243-12251.
38. Nakashige, T. G.; Zygiel, E. M.; Drennan, C. L.; Nolan, E. M., Nickel sequestration by the host-defense protein human calprotectin. *J. Am. Chem. Soc.* **2017**, *139* (26), 8828-8836.
39. Cunden, L. S.; Brophy, M. B.; Rodriguez, G. E.; Flaxman, H. A.; Nolan, E. M., Biochemical and functional evaluation of the intramolecular disulfide bonds in the zinc-chelating antimicrobial protein human S100A7 (Psoriasin). *Biochemistry* **2017**, *56*, 5726-5738.

40. Cunden, L. S.; Nolan, E. M., Bioinorganic explorations of Zn(II) sequestration by human S100 host-defense proteins. *Biochemistry* **2018**, *57* (11), 1673-1680.
41. Damo, S. M.; Kehli-Fie, T. E.; Sugitani, N.; Holt, M. E.; Rathi, S.; Murphy, W. J.; Zhang, Y.; Betz, C.; Hench, L.; Fritz, G.; Skaar, E. P.; Chazin, W. J., Molecular basis for manganese sequestration by calprotectin and roles in the innate immune response to invading bacterial pathogens. *Proc. Natl. Acad. Sci. U. S. A.* **2013**, *110* (10), 3841-3846.
42. Besold, A. N.; Gilston, B. A.; Radin, J. N.; Ramsoomair, C.; Culbertson, E. M.; Li, C. X.; Cormack, B. P.; Chazin, W. J.; Kehli-Fie, T. E.; Culotta, V. C., The role of calprotectin in withholding zinc and copper from *Candida albicans*. *Infect. Immun.* **2017**, *86* (2), e00779-17.
43. Mildner, M.; Gmeiner, R.; Abtin, A.; Sam, C.; Glaser, R.; Schroder, J. M.; Mlitz, V.; Stichenwirth, M.; Pammer, J.; Geusau, A.; Tschachler, E., The antimicrobial peptide psoriasin is the major component of vaginal fluids which show strong antimicrobial activities. *J. Invest. Dermatol.* **2007**, *127*, S119-S119.
44. Michalek, M.; Gelhaus, C.; Hecht, O.; Podschun, R.; Schroder, J. M.; Leippe, M.; Grotzinger, J., The human antimicrobial protein psoriasin acts by permeabilization of bacterial membranes. *Dev. Comp. Immunol.* **2009**, *33* (6), 740-746.
45. Mildner, M.; Abtin, A.; Gmeiner, R.; Sam, C.; Glaser, R.; Schroder, J. M.; Mlitz, V.; Stichenwirth, M.; Pammer, J.; Geusau, A.; Tschachler, E., Psoriasin (S100A7) is a major antimicrobial component of the female genital tract. *Mucosal Immunol.* **2010**, *127*, 602-609.
46. Hein, K. Z.; Takahashi, H.; Tsumori, T.; Yasui, Y.; Nanjoh, Y.; Toga, T.; Wu, Z.; Grötzinger, J.; Jung, S.; Wehkamp, J.; Schroeder, B. O.; Schroeder, J. M.; Morita, E., Disulphide-reduced psoriasin is a human apoptosis-inducing broad-spectrum fungicide. *Proc. Natl. Acad. Sci. U. S. A.* **2015**, *112* (42), 13039-13044.
47. Gifford, J. L.; Walsh, M. P.; Vogel, H. J., Structures and metal-ion-binding properties of the Ca²⁺-binding helix-loop-helix EF-hand motifs. *Biochem. J.* **2007**, *405* (2), 199-221.

48. Vogl, T.; Leukert, N.; Barczyk, K.; Strupat, K.; Roth, J., Biophysical characterization of S100A8 and S100A9 in the absence and presence of divalent cations. *Biochim. Biophys. Acta* **2006**, 1763 (11), 1298-1306.
49. Donato, R., Functional roles of S100 proteins, calcium-binding proteins of the EF-hand type. *Biochim. Biophys. Acta* **1999**, 1450, 191-231.
50. Zaia, A. A.; Sappington, K. J.; Nisapakultorn, K.; Chazin, W. J.; Dietrich, E. A.; Ross, K. F.; Herzberg, M. C., Subversion of antimicrobial calprotectin (S100A8/S100A9 complex) in the cytoplasm of TR146 epithelial cells after invasion by *Listeria monocytogenes*. *Mucosal Immunol.* **2009**, (2), 43-53.
51. Cole, A. M., Innate host defense of human vaginal and cervical mucosae. *Curr. Top. Microbiol. Immunol.* **2006**, 306, 199-230.
52. Valore, E. V.; Park, C. H.; Igreti, S. L.; Ganz, T., Antimicrobial components of vaginal fluid. *Am. J. Obstet. Gynecol.* **2002**, 187, 561-568.
53. Hein, M.; Valore, E. V.; Helmig, R. B.; Uldbjerg, N.; Ganz, T., Antimicrobial factors in the cervical mucus plug. *Am. J. Obstet. Gynecol.* **2002**, 187, 137-144.
54. Leach, S. T.; Yang, Z.; Messina, I.; Song, C.; Geczy, C. L.; Cunningham, A. M.; Day, A. S., Serum and mucosal S100 proteins, calprotectin (S100A8/S100A9) and S100A12, are elevated at diagnosis in children with inflammatory bowel disease. *Scand. J. Gastroenterol.* **2007**, 42, 1321-1331.
55. Dell'Angelica, E. C.; Schleicher, C. H.; Santomé, J. A., Primary structure and binding properties of calgranulin C, a novel S100-like calcium-binding protein from pig granulocytes. *J. Biol. Chem.* **1994**, 269 (46), 28929-28936.
56. Guignard, F.; Mael, J.; Markert, M., Identification and characterization of a novel human neutrophil protein related to the S100 family. *Biochem. J.* **1995**, 309 395-401.
57. Ilg, E. C.; Troxler, H.; Bürgisser, D. M.; Kuster, T.; Markert, M.; Guignard, F.; Hunziker, P.; Birchler, N.; Heizmann, C. W., Amino acid sequence determination of human S100A12 (P6,

- calgranulin C, CGRP, CAAF1) by tandem mass spectrometry. *Biochem. Biophys. Res. Commun.* **1996**, 225 (1), 146-150.
58. Foell, D.; Hernández-Rodríguez, J.; Sánchez, M.; Vogl, T.; Cid, M. C.; Roth, J., Early recruitment of phagocytes contributes to the vascular inflammation of giant cell arteritis. *J. Pathol.* **2004**, 204 (3), 311-316.
59. Goyette, J.; Yan, W. X.; Yamen, E.; Chung, Y. M.; Lim, S. Y.; Hsu, K.; Rahimi, F.; Di Girolamo, N.; Song, C.; Jessup, W.; Kockx, M.; Bobryshev, Y. V.; Freedman, S. B.; Geczy, C. L., Pleiotropic roles of S100A12 in coronary atherosclerotic plaque formation and rupture. *J. Immunol.* **2009**, 183, 593-603.
60. Yang, Z.; Tao, T.; Raftery, M. J.; Youssef, P.; Di Girolamo, N.; Geczy, C. L., Proinflammatory properties of the human S100 protein S100A12. *J. Leukoc. Biol.* **2001**, 69, 986-994.
61. Gaddy, J. A.; Radin, J. N.; Cullen, T. W.; Chazin, W. J.; Skaar, E. P.; Trent, M. S.; Algood, H. M., *Helicobacter pylori* resists the antimicrobial activity of calprotectin via lipid A modification and associated biofilm formation. *MBio* **2015**, 6 (6), e01349-15.
62. Madsen, P.; Rasmussen, H. H.; Leffers, H.; Honoré, B.; Dejgaard, K.; Olsen, E.; Kiil, J.; Walbum, E.; Andersen, A. H.; Basse, B.; et al., Molecular cloning, occurrence, and expression of a novel partially secreted protein "psoriasin" that is highly up-regulated in psoriatic skin. *J. Invest. Dermatol.* **1991**, 97 (4), 701-712.
63. Tan, J. Q.; Vorum, H.; Larsen, C. G.; Madsen, P.; Rasmussen, H. H.; Gesser, B.; Etzerodt, M.; Honore, B.; Celis, J. E.; Thestrup-Pedersen, K., Psoriasin: A novel chemotactic protein. *J. Invest. Dermatol.* **1996**, 107 (1), 5-10.
64. Meyer, J. E.; Harder, J.; Sipos, B.; Maune, S.; Klöppel, G.; Bartels, J.; Schröder, J. M.; Gläser, R., Psoriasin (S100A7) is a principal antimicrobial peptide of the human tongue. *Mucosal Immunol.* **2008**, 1 (3), 239-243.

65. Jansen, S.; Podschun, R.; Leib, S. L.; Grötzinger, J.; Oestern, S.; Michalek, M.; Pufe, T.; Brandenburg, L.-O., Expression and function of psoriasin (S100A7) and Koebnerisin (S100A15) in the brain. *Infect. Immun.* **2013**, *81* 1788-1797.
66. Semprini, S.; Capon, F.; Tacconelli, A.; Giardina, E.; Orecchia, A.; Mingarelli, R.; Gobello, T.; Zambruno, G.; Botta, A.; Fabrizi, G.; Novelli, G. H., Evidence for differential S100 gene over-expression in psoriatic patients from genetically heterogeneous pedigrees. *Hum. Genet.* **2002**, *111*, 310-313.
67. Broome, A.; Ryan, D.; Eckert, R. L. J., S100 protein subcellular localization during epidermal differentiation and psoriasis. *Histochem. Cytochem.* **2003**, *51*, 675-685.
68. Alowami, S.; Qing, G.; Emberley, E.; Snell, L.; Watson, P. H., Psoriasin (S100A7) expression is altered during skin tumorigenesis. *BMC Dermatol.* **2003**, (3), 1.
69. Qin, W.; Ho, L.; Wang, J.; Peskind, E.; Pasinetti, G. M., S100A7, a novel Alzheimer's disease biomarker with non-amyloidogenic alpha-secretase activity acts via selective promotion of ADAM-10. *PLoS One* **2009**, *4*, e4183.
70. Wolf, R.; Mirmohammadsadegh, A.; Walz, M.; Lysa, B.; Tarter, U.; Remus, R.; Hengge, U.; Michel, G.; Ruzicka, T., Molecular cloning and characterization of alternatively spliced mRNA isoforms from psoriatic skin encoding a novel member of the S100 family. *FASEB* **2003**, 1-22.
71. Wolf, R.; Ruzicka, T.; Yuspa, S. H., Novel S100A7 (psoriasin)/S100A15 (koebnerisin) subfamily: highly homologous but distinct in regulation and function. *Amino Acids* **2011**, *41*, 789-796.
72. Vallee, B. L.; Falchuk, K. H., The biochemical basis of zinc physiology. *Physiol. Rev.* **1993**, *73* (1), 79-118.
73. Andreini, C.; Banci, L.; Bertini, I.; Rosato, A., Zinc through the three domains of life. *J. Proteome Res.* **2006**, *5*, 3173-3178.
74. Wilson, D., An evolutionary perspective on zinc uptake by human fungal pathogens. *Metallomics* **2015**, *7* (6), 979-985.

75. Capdevila, D. A.; Wang, J.; Giedroc, D. P., Bacterial strategies to maintain zinc metallostasis at the host-pathogen interface. *J. Biol. Chem.* **2016**, *291* (40), 20858-20868.
76. Braymer, J. J.; Giedroc, D. P., Recent developments in copper and zinc homeostasis in bacterial pathogens. *Curr. Opin. Chem. Biol.* **2014**, *19*, 59-66.
77. Hood, M. I.; Skaar, E. P., Nutritional immunity: transition metals at the pathogen-host interface. *Nat. Rev. Microbiol.* **2012**, *10* (8), 525-537.
78. Zackular, J. P.; Chazin, W. J.; Skaar, E. P., Nutritional immunity: S100 proteins at the host-pathogen interface. *J. Biol. Chem.* **2015**, *290* (31), 18991-18998.
79. Hantke, K., Bacterial zinc uptake and regulators. *Curr. Opin. Microbiol.* **2005**, *8* (2), 196-202.
80. Jung, W. H., The zinc transport systems and their regulation in pathogenic fungi. *Mycobiology* **2015**, *43* (3), 179-183.
81. Büchau, A. S.; Mohamed, H.; Kukova, G.; Lewerenz, V.; Kellermann, S.; Würthner, J. U.; Wolf, R.; Walz, M.; Gallo, R. L.; Ruzicka, T., S100A15, an antimicrobial protein of the skin: regulation by *E. coli* through Toll-Like Receptor 4. *J. Invest. Dermatol.* **2007**, *127* (11), 2596-2604.
82. Wolf, R.; Ruzicka, T.; Yuspa, S. H., Novel S100A7 (psoriasin)/S100A15 (koebnerisin) subfamily: highly homologous but distinct in regulation and function. *Amino acids* **2011**, *41* (4), 789-796.
83. Murray, J. I.; Tonkin, M. L.; Whiting, A. L.; Peng, F.; Farnell, B.; Cullen, J. T.; Hof, F.; Boulange, M. J., Structural characterization of S100A15 reveals a novel zinc coordination site among S100 proteins and altered surface chemistry with functional implications for receptor binding. *MBC Struc. Biol.* **2012**, (12:16).
84. Dale, B. A.; Fredericks, L. P., Antimicrobial peptides in the oral environment: expression and function in health and disease. *Curr. Issues. Mol. Biol.* **2005**, *7*, 119-133.

85. Harder, J.; Meyer-Hoffert, U.; Wehkamp, K.; Schwichtenberg, L.; Schröder, J. M., Differential gene induction of human beta-defensins (hBD-1, -2, -3, and -4) in keratinocytes is inhibited by retinoic acid. *J. Invest. Dermatol.* **2004**, *123*, 522-529.
86. Marti, T.; Erttmann, K. D.; Gallin, M. Y., Host-parasite interaction in human onchocerciasis: identification and sequence analysis of a novel human calgranulin. *Biochem. Biophys. Res. Commun.* **1996**, *221* (2), 454-458.
87. Edgeworth, J. D.; Abiose, A.; Jones, B. R., An immunohistochemical analysis of onchocercal nodules: evidence for an interaction between macrophage MRP8/MRP14 and adult *Clin. Exp. Immunol.* **1993**, *92*, 84-92.
88. Wilkinson, M. M.; Busuttill, A.; Hayward, C.; Brock, D. J. H.; Dorin, J. R.; Van Heyningen, V., Expression pattern of two cystic fibrosis-associated calcium-binding proteins in normal and abnormal tissues. *J. Cell Sci.* **1988**, *91*, 221-230.
89. Steinbakk, M.; Naess-Andresen, C.-F.; Fagerhol, M. K.; Lingaas, E.; Dale, I.; Brandtzaeg, P., Antimicrobial actions of calcium binding leukocyte L1 protein, caprotectin. *Lancet* **1990**, *336*, 763-765.
90. Teigelkamp, S.; Bharwaj, R. S.; Roth, J.; Meinardus-Harger, G.; Karas, M. S., C., Calcium-dependent complex assembly of the myeloid differentiation proteins MRP-8 and MRP-14. *J. Biol. Chem.* **1991**, *266* (20), 13462-13467.
91. Nacken, W.; Roth, J.; Sorg, C.; Kerkhoff, C., S100A9/S100A8: Myeloid representatives of the S100 protein family as prominent players in innate immunity. *Microsc. Res. Tech.* **2003**, *60* (6), 569-580.
92. Vogl, T.; Roth, J.; Sorg, C.; Hillenkamp, F.; Strupat, K., Calcium-induced noncovalently linked tetramers of MRP8 and MRP14 detected by ultraviolet matrix-assisted laser desorption/ionization mass spectrometry. *J. Am. Soc. Mass Spectrom.* **1999**, *10* (11), 1124-1130.

93. Strupat, K.; Rogniaux, H.; Van Dorsselaer, A.; Roth, J.; Vogl, T., Calcium-induced noncovalently linked tetramers of MRP8 and MRP14 are confirmed by electrospray ionization-mass analysis. *J. Am. Soc. Mass Spectrom.* **2000**, *11* (9), 780-788.
94. Leukert, N.; Vogl, T.; Strupat, K.; Reichelt, R.; Sorg, C.; Roth, J., Calcium-dependent tetramer formation of S100A8 and S100A9 is essential for biological activity. *J. Mol. Biol.* **2006**, *359* (4), 961-72.
95. Korndörfer, I. P.; Brueckner, F.; Skerra, A., The crystal structure of the human (S100A8/S100A9)₂ heterotetramer, calprotectin, illustrates how conformational changes of interacting α -helices can determine specific association of two EF-hand proteins. *J. Mol. Biol.* **2007**, *370* (5), 887-898.
96. Sohnle, P. G.; Collins-Lech, C.; Wiessner, J. H., The zinc-reversible antimicrobial activity of neutrophil lysates and abscess fluid supernatants. *J. Infect. Dis.* **1991**, *164* (1), 137-142.
97. Murthy, A. R. K.; Lehrer, R. I.; Harwig, S. S. L.; Miyasaki, K. T., In vitro candidastatic properties of the human neutrophil calprotectin complex. *J. Immunol.* **1993**, *151*, 6291-6301.
98. Miyasaki, K. T.; Bodeau, A. L.; Murthy, A. R. K.; Lehrer, R. I., In vitro antimicrobial activity of the human neutrophil cytosolic S-100 protein complex, calprotectin, against *Capnocytophaga sputigena*. *J. Dent. Res.* **1993**, *72*, 517-523.
99. Clohessy, P. A.; Golden, B. E., Calprotectin-mediated zinc chelation as a biostatic mechanism in host-defense. *Scand. J. Immunol.* **1995**, *42* (5), 551-556.
100. Clohessy, P. A.; Golden, B. E., His-X-X-X-His motif in S100 protein, calprotectin: Relation to microbiostatic activity. *J. Leukoc. Biol.* **1996**, *60* (5), 674.
101. Liu, J. Z.; Jellbauer, S.; Poe, A. J.; Ton, V.; Pesciaroli, M.; Kehl-Fie, T. E.; Restrepo, N. A.; Hosking, M. P.; Edwards, R. A.; Battistoni, A.; Pasquali, P.; Lane, T. E.; Chazin, W. J.; Vogl, T.; Roth, J.; Skaar, E. P.; Raffatellu, M., Zinc sequestration by the neutrophil protein calprotectin enhances *Salmonella* growth in the inflamed gut. *Cell Host Microbe* **2012**, *11* (3), 227-239.

102. Hood, M. I.; Mortensen, B. L.; Moore, J. L.; Zhang, Y.; Kehl-Fie, T. E.; Sugitani, N.; Chazin, W. J.; Caprioli, R. M.; Skaar, E. P., Identification of an *Acinetobacter baumannii* zinc acquisition system that facilitates resistance to calprotectin-mediated zinc sequestration. *PLoS Pathog.* **2012**, *8* (12), e1003068.
103. Mortensen, B. L.; Rathi, S.; Chazin, W. J.; Skaar, E. P., *Acinetobacter baumannii* response to host-mediated zinc limitation requires the transcriptional regulator Zur. *J. Bacteriol.* **2014**, *196* (14), 2616-2626.
104. Nairn, B. L.; Lonergan, Z. R.; Wang, J.; Braymer, J. J.; Zhang, Y.; Calcutt, M. W.; Lisher, J. P.; Gilston, B. A.; Chazin, W. J.; de Crécy-Lagard, V.; Giedroc, D. P.; Skaar, E. P., The response of *Acinetobacter baumannii* to zinc starvation. *Cell Host Microbe* **2016**, *19* (6), 826-836.
105. Stork, M.; Grijpstra, J.; Bos, M. P.; Torres, C. M.; Devos, N.; Poolman, J. T.; Chazin, W. J.; Tommassen, J., Zinc piracy as a mechanism of *Neisseria meningitidis* for evasion of nutritional immunity. *PLoS Pathog.* **2013**, *9* (10), e1003733.
106. Corbin, B. D.; Seeley, E. H.; Raab, A.; Feldmann, J.; Miller, M. R.; Torres, V. J.; Anderson, K. L.; Dattilo, B. M.; Dunman, P. M.; Gerads, R.; Caprioli, R. M.; Nacken, W.; Chazin, W. J.; Skaar, E. P., Metal chelation and inhibition of bacterial growth in tissue abscesses. *Science* **2008**, *319* (5865), 962-965.
107. Kehl-Fie, T. E.; Chitayat, S.; Hood, M. I.; Damo, S.; Restrepo, N.; Garcia, C.; Munro, K. A.; Chazin, W. J.; Skaar, E. P., Nutrient metal sequestration by calprotectin inhibits bacterial superoxide defense, enhancing neutrophil killing of *Staphylococcus aureus*. *Cell Host Microbe* **2011**, *10* (2), 158-164.
108. Hadley, R. C.; Gagnon, D. M.; Brophy, M. B.; Gu, Y.; Nakashige, T. G.; Britt, R. D.; Nolan, E. M., Biochemical and spectroscopic observation of Mn(II) sequestration from bacterial Mn(II) transport machinery by calprotectin. *J. Am. Chem. Soc.* **2018**, *140*, 110-113.

109. Besold, A. N.; Culbertson, E. M.; Nama, L.; Hobbs, R. P.; Boyko, A.; Maxwell, C. N.; Chazin, W. J.; Marques, A. R.; Culotta, A. C., Antimicrobial action of calprotectin that does not involve metal withholding. *Metallomics* **2018**, 10.1039/c8mt00133b.
110. Burdette, S. C.; Frederickson, C. J.; Bu, W. M.; Lippard, S. J., ZP4, an improved neuronal Zn²⁺ sensor of the Zinpyr family. *J. Am. Chem. Soc.* **2003**, 125 (7), 1778-1787.
111. Vorum, H.; Madsen, P.; Rasmussen, H. H.; Etzerodt, M.; Svendsen, I.; Celis, J. E.; Honore, B., Expression and divalent cation binding properties of the novel chemotactic inflammatory protein psoriasin. *Electrophoresis* **1996**, 17 (11), 1787-1796.
112. Gazaryan, I. G.; Krasnikov, B. F.; Ashby, G. A.; Thorneley, R. N. F.; Kristal, B. S.; Brown, A. M., Zinc is a potent inhibitor of thiol oxidoreductase activity and stimulates reactive oxygen species production by lipoamide dehydrogenase. *J. Biol. Chem.* **2002**, 277 (12), 10064-10072.
113. Kwon, J. E.; Lee, S.; You, Y.; Baek, K.-H.; Ohkubo, K.; Cho, J.; Fukuzumi, S.; Shin, I.; Park, S. Y.; Nam, W., Fluorescent zinc sensor with minimized proton-induced interferences: photophysical mechanism for fluorescence turn-on response and detection of endogenous free zinc ions. *Inorg. Chem.* **2012**, 51 (16), 8760-8774.
114. Sohnle, P. G.; Collins-Lech, C.; Wiessner, J. H., Antimicrobial activity of an abundant calcium-binding protein in the cytoplasm of human neutrophils. *J. Infect. Dis.* **1991**, 163, 187-192.
115. Akerström, B.; Bjorck, L., Bacterial surface protein L binds and inactivates neutrophil proteins S100A8/A9. *J. Immunol.* **2009**, (183), 4583-4592.
116. Basika, T.; Muñoz, N.; Casaravilla, C.; Irigoín, F.; Batthyány, C.; Bonilla, M.; Salinas, G.; Pacheco, J. P.; Roth, J.; Durán, R.; Díaz, A., Phagocyte-specific S100 proteins in the local response to the *Echinococcus granulosus* larva. *Parasitology* **2012**, 139, 271-283.
117. Jean, S.; Juneau, R. A.; Criss, A. K.; Cornelissen, C. N., *Neisseria gonorrhoeae* evades Calprotectin-mediated nutritional immunity and survives neutrophil extracellular traps by production of TdfH. *Infect. Immun.* **2016**, 84, 2982-2994.

118. Hitomi, J.; Kimura, T.; Kusumi, E.; Nakagawa, S.; Kuwabara, S.; Hatakeyama, K.; Yamaguchi, K., Novel S100 proteins in human esophageal epithelial cells: CAAF1 expression is associated with cell growth arrest. *Arch. Histol. Cytol.* **1998**, *61* (2), 163-178.
119. Yang, Z.; Tao, T.; Raftery, M. J.; Youssef, P.; Di Girolamo, N.; L., G. C., Proinflammatory properties of the human S100 protein S100A12. *J. Leukoc. Biol.* **2001**, *69*, 986-994.
120. Robinson, M. J.; Hogg, N., A comparison of human S100A12 with MRP-14 (S100A9). *Biochem. Biophys. Res. Commun.* **2000**, *275* (3), 865-870.
121. Yang, Z.; Yan, W. X.; Cai, H.; Tedla, N.; Armishaw, C.; Di Girolamo, N.; Wang, H. W.; Hampartzoumian, T.; Simpson, J. L.; Gibson, P. G.; Hunt, J.; Hart, P.; Hughes, J. M.; Perry, M. A.; Alewood, P. F.; Geczy, C. L., S100A12 provokes mast cell activation: a potential amplification pathway in asthma and innate immunity. *J. Allergy Clin. Immunol.* **2007**, *119* (1), 106-114.
122. Moroz, O. V.; Dodson, G. G.; Wilson, K. S.; Lukanidin, E.; Bronstein, I. B., Multiple structural states of S100A12: A key to its functional diversity. *Microsc. Res. Tech.* **2003**, *60* (6), 581-592.
123. Moroz, O. V.; Antson, A. A.; Grist, S. J.; Maitland, N. J.; Dodson, G. G.; Wilson, K. S.; Lukanidin, E.; Bronstein, I. B., Structure of the human S100A12-copper complex: implications for host-parasite defence. *Acta Crystallogr. D Biol. Crystallogr.* **2003**, *59*, 859-867.
124. Moroz, O. V.; Antson, A. A.; Murshudov, G. N.; Maitland, N. J.; Dodson, G. G.; Wilson, K. S.; Skibshøj, I.; Lukanidin, E. M.; Bronstein, I. B., The three-dimensional structure of human S100A12. *Acta Crystallogr. D Biol. Crystallogr.* **2001**, *57* (Pt 1), 20-29.
125. Gottsch, J. D.; Eisinger, S. W.; Liu, S. H.; Scott, A. L., Calgranulin C has filariacidal and filariastatic activity. *Infect. Immun.* **1999**, *67* (12), 6631-6636.
126. Haley, K. P.; Delgado, A. G.; Piazuolo, M. B.; Mortensen, B. L.; Correa, P.; Damo, S. M.; Chazin, W. J.; Skaar, E. P.; Gaddy, J. A., The human antimicrobial protein calgranulin C participates in control of *Helicobacter pylori* growth and regulation of virulence. *Infect. Immun.* **2015**, *83* (7), 2944-2956.

127. Krężel, A.; Maret, W., Dual nanomolar and picomolar Zn(II) binding properties of metallothionein. *J. Am. Chem. Soc.* **2007**, *129* (35), 10911-10921.
128. Cole, A. M.; Kim, Y.-H.; Tahk, S.; Hong, T.; Weis, P.; Waring, A. J.; Ganz, T., Calcitermin, a novel antimicrobial peptide isolated from human airway secretions. *FEBS Lett.* **2001**, *504*, 5-10.
129. Lee, H.; Cho, Y.; I., L. R., Effects of pH and salinity on the antimicrobial properties of clavansins. *Infect. Immun.* **1997**, *65* (7), 2898-2903.
130. McDevitt, C. A.; Ogunniyi, A. D.; Valkov, E.; Lawrence, M. C.; Kobe, B.; McEwan, A. G.; Paton, J. C., A molecular mechanism for bacterial susceptibility to zinc. *PLoS Pathog.* **2011**, *7* (11), e1002357.
131. Jinquan, T.; Vorum, H.; Larsen, C. G.; Madsen, P.; Rasmussen, H. H.; Gesser, B.; Etzerodt, M.; Honoré, B.; Celis, J. E.; Thestrup-Pedersen, K., Psoriasin: A novel chemotactic protein. *J. Invest. Dermatol.* **1996**, *107* (1), 5-10.
132. Brodersen, D. E.; Etzerodt, M.; Madsen, P.; Celis, J. E.; Thøgersen, H. C.; Nyborg, J.; Kjeldgaard, M., EF-hands at atomic resolution: the structure of human psoriasin (S100A7) solved by MAD phasing. *Structure* **1998**, *6* (4), 477-489.
133. Brodersen, D. E.; Nyborg, J.; Kjeldgaard, M., Zinc-binding site of an S100 protein revealed. Two crystal structures of Ca²⁺-bound human psoriasin (S100A7) in the Zn²⁺-loaded and Zn²⁺-free states. *Biochemistry* **1999**, *38* (6), 1695-1704.
134. Gläser, R.; Harder, J.; Lange, H.; Bartels, J.; Christophers, E.; Schröder, J.-M., Antimicrobial psoriasin (S100A7) protects human skin from *Escherichia coli* infection. *Nat. Immunol.* **2005**, *6* (1), 57-64.
135. Mildner, M.; Stichenwirth, M.; Abtin, A.; Eckhart, L.; Sam, C.; Gläser, R.; Schröder, J.-M.; Gmeiner, R.; Mlitz, V.; Pammer, J.; Geusau, A.; Tschachler, E., Psoriasin (S100A7) is a major *Escherichia coli*-cidal factor of the female genital tract. *Mucosal Immunol.* **2010**, *127*, 602-609.

136. Gläser, R.; Harder, J.; Lange, H.; Bartels, J.; Christophers, E.; Schroder, J. M., Antimicrobial psoriasin (S100A7) protects human skin from *Escherichia coli* infection. *Nat. Immunol.* **2005**, *6* (1), 57-64.
137. Lee, K. C.; Eckert, R. L., S100A7 (Psoriasin)–mechanism of antibacterial action in wounds. *J. Invest. Dermatol.* **2007**, *124* (4), 945-957.
139. Gläser, R.; Harder, J.; Bartels, J.; Christophers, E.; Schroder, J. M., Psoriasin (S100A7) is a major and potent *E. coli*-selective antimicrobial protein of healthy human skin. *J. Invest. Dermatol.* **2001**, *117* (3), 768-768.
140. Wiesner, J.; Vilcinskas, A., Antimicrobial peptides the ancient arm of the human immune system. *Virulence* **2010**, *1* (5), 440-464.

Chapter 2: Calcium Ions Tune the Zinc-Sequestering Properties and Antimicrobial Activity of Human S100A12

This Chapter is adapted from *Chem. Sci.* **2016**, 7 (2), 1338-1348.

2. 1. Contributions

Ms. Aleth Gaillard developed the initial overexpression and purification protocol for S100A12. She also carried out the Co(II) titrations presented in this Chapter.

2. 2. Introduction

Neutrophils are an important cellular component of the innate immune system.¹⁻² These white blood cells are recruited to sites of infection and release antimicrobial factors into the extracellular space that include reactive oxygen and nitrogen species, proteases, antimicrobial peptides and metal-chelating proteins. In this work, motivated by the need to further elucidate the interplay between neutrophils, metal homeostasis, and microbial pathogenesis, we combine chemistry and biology to investigate a Ca(II)- and Zn(II)-binding protein named S100A12 that is housed in the neutrophil cytoplasm and deployed at sites of infection.

S100A12 (also termed calgranulin C, P6, CGRP, CO-Ag, CAAF-1, EN-RAGE) was first isolated from porcine granulocytes in 1994 and subsequently identified in specimens from other mammals.³⁻⁹ In 1995, the serendipitous discovery of S100A12 in human neutrophils was reported;⁴ this work revealed that S100A12 constitutes ≈5% of total cytosolic proteins in resting neutrophils, and further investigations provided its amino acid sequence and gene structure.^{10,11} S100A12 is associated with the inflammatory response and a variety of human pathologies that include disorders of the gastrointestinal tract (e.g. Crohn's disease, ulcerative colitis),¹² type 2 diabetes,¹³ arthritis,¹⁴ Alzheimer's disease,¹⁵ and cystic fibrosis.¹⁶ S100A12 can interact with the receptor for advanced glycation end products (RAGE)^{17,18} and toll-like receptor 4 (TLR4).¹⁹ The latter interaction is implicated in S100A12 activation of proinflammatory signaling in human monocytes.

Moreover, S100A12 likely contributes to host defense against invading pathogens.^{9,20} Evidence for anti-parasitic activity was first suggested during studies of *Onchocerca volvulus* extracts obtained from tissues of onchocerciasis patients.⁹ These specimens were contaminated

with various neutrophil proteins, including S100A12. Subsequent investigations demonstrated that S100A12 possesses *in vitro* anti-parasitic activity against the parasite *Brugia malayi*.²¹ Recently, elevated S100A12 levels were observed in gastric biopsy samples from patients colonized with *Helicobacter pylori*.²⁰ Moreover, *in vitro* studies revealed that S100A12 has antibacterial activity against *H. pylori* and inhibits the activity of its Cag type-IV secretion system, both of which involve Zn(II) chelation by S100A12.²⁰ Taken together, these clinical and biological investigations indicate that S100A12 is an abundant and important player in human biology, and provide multiple avenues for further exploration at the molecular and physiological levels. From the perspective of metals in biology, understanding how S100A12 contributes to metal homeostasis in broad terms, and elucidating whether its metal-bound forms are relevant players in human health and disease, is of particular interest.

Human S100A12 (92-residues, 10.5 kDa monomer) is a member of the S100 family of Ca(II)-binding peptides that harbors two EF-hand domains and forms homooligomers. Five crystal structures of human S100A12 are available and provide insight into its oligomerization properties and coordination chemistry.²²⁻²⁵ The first crystal structure revealed a homodimer with four Ca(II) ions bound at the EF-hand domains.²² This structure also revealed two His₃Asp motifs formed at the homodimer interface, which are comprised of His15 and Asp25 of one subunit and His85 and His89 of the other subunit. The crystal structures of Cu(II)- and Ca(II)-bound S100A12 and Zn(II)-bound S100A12 established a 2:1 M(II):S100A12 homodimer stoichiometry (M = Cu, Zn) with each M(II) ion coordinated by a His₃Asp motif (Figure 2. 1).²⁴ Comparison of the available apo and holo structures shows that metal binding modulates the oligomerization properties of S100A12.²²⁻²⁵ For instance, apo S100A12 crystallized as a dimer whereas the Zn(II)-bound form crystallized as a tetramer.²⁵ Thereafter, solution studies showed that Zn(II) and Ca(II) binding to S100A12 provide varying oligomeric states that include dimers, tetramers and hexamers.²⁶ These studies exemplify the complex speciation of S100A12, and suggest a model whereby different forms afford functional diversity.²⁷

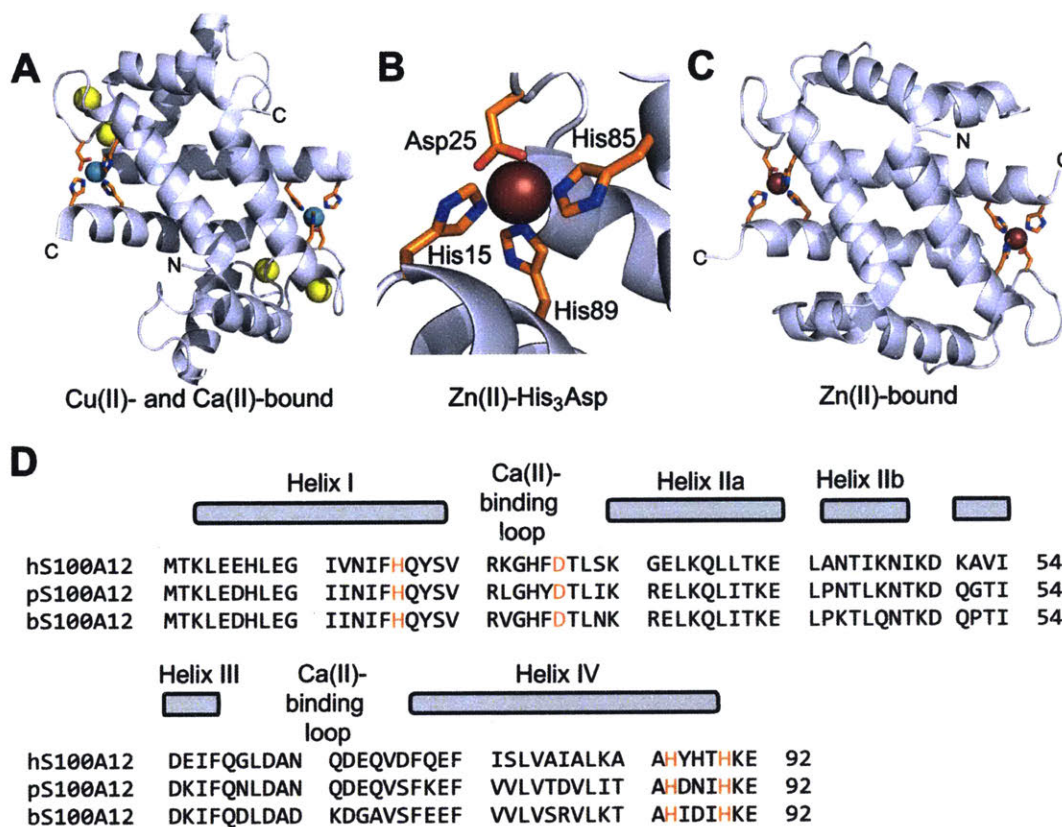


Figure 2. 1. Crystal structures of metal-bound human S100A12 and amino acid sequence alignment of S100A12 orthologues. (A) Structure of the Ca(II)- and Cu(II)-bound S100A12 homodimer. Cu(II) ions are shown as teal spheres, and Ca(II) ions as yellow spheres (PDB: 1ODB).²⁴ (B) View of the His₃Asp motif of S100A12 taken from the structure of the Zn(II)-bound form (PDB 2WCB).²⁵ The Zn(II) ion is shown as a brown sphere. (C) Structure of the Zn(II)-bound S100A12 homodimer. Zn(II) ions are shown as brown spheres (PDB: 2WCB).²⁵ (D) Sequence alignment of human, porcine, and bovine S100A12. The secondary structural elements presented above the alignment are for the human form. The transition-metal binding residues are presented in orange.

Beyond crystallographic characterization of the Cu(II)- and Zn(II)-bound forms, only limited information about how S100A12 coordinates Zn(II) and other first-row transition metal ions in solution is available, and some of the data appear contradictory. A seminal investigation of porcine S100A12 revealed stoichiometric Zn(II) binding ($K_d < 10$ nM), and found that Zn(II) coordination enhanced the affinity of this protein for Ca(II) by several orders of magnitude.³ More recently, a study of Zn(II) binding by human S100A12 reported K_d values for Zn(II) in the

micromolar range ($K_{d1} = 16 \mu\text{M}$, $K_{d2} = 83 \mu\text{M}$).²⁶ Given that the pig and human forms share 70% sequence identity and have conserved His₃Asp motifs, we had difficulty reconciling these data. Moreover, the study of human S100A12 in *H. pylori* infection supported a role for this protein in Zn(II) sequestration,²⁰ a function that requires formation of a high-affinity Zn(II) complex.

These observations indicate that re-evaluation of the Zn(II)-binding properties of human S100A12 is necessary. Moreover, S100A12 chelates both Ca(II) and Zn(II) at different sites (Figure 2. 1), and whether Ca(II) ions influence the Zn(II)-binding properties of S100A12 is unknown. In prior work, we discovered that human calprotectin uses Ca(II) to modulate its M(II)-binding (M = Mn, Fe, Zn) properties and exhibits enhanced M(II) affinities in the presence of high Ca(II) concentrations.²⁸⁻³⁰ We hypothesized that S100A12 may exhibit similar behavior given its accepted function as an extracellular Zn(II)-chelating protein.^{20,26} Many outstanding questions regarding the antimicrobial activity and host-defense function of S100A12 also remain. To the best of our knowledge, no extensive studies detailing the *in vitro* antimicrobial activity of S100A12 are available in the literature. This situation contrasts the wealth of data reported for other factors produced by human neutrophils, including calprotectin and the α -defensins.³¹⁻³² The limited *in vitro* data available for *Staphylococcus aureus* and *H. pylori* indicate that human S100A12 has strain-selective antibacterial activity and support its contribution to the host metal-withholding response.^{20,32}

In this work, we address these issues and examine the metal-binding properties and antimicrobial activity of human S100A12 under conditions of low and high Ca(II). In the presence of excess Ca(II), S100A12 readily sequesters Zn(II) from standard microbial growth media, exhibits growth inhibitory activity against a variety of pathogenic fungi, and provides antibacterial activity against the human gastrointestinal pathogen *Listeria monocytogenes*. Our data support a model where S100A12 responds to the local Ca(II) concentration to modulate its Zn(II)-

sequestering ability and antimicrobial activity, and effectively turn on these functions in the Ca(II)-rich environment of the extracellular space.

2. 3. Experimental Section

2. 3. 1. Design of the Synthetic Genes for Human S100A12- Δ His₃Asp

The synthetic gene for human S100A12(H15A)(D25A)(H85A)(H89A) was optimized for *E. coli* codon usage and ordered from DNA 2.0. A *Nde*I restriction site was placed at the 5' end. A stop codon and a *Xho*I restriction site were placed at the 3' end. This gene was received in the pJ201 vector from DNA 2.0. The gene was sub-cloned into the *Nde*I and *Xho*I sites of pET41a to afford pET41a-S100A12(H15A)-(D25A)(H85A)(H89A) for protein expression.

Nucleotide sequence for *Nde*I-S100A12(H15A(D25A)(H85A)(H89A)-STOP-*Xho*I

CATATGACGAAGCTGGAAGAACACTTGGAGGTATCGTGAACATTTTTGCCCAGTACTCCG
TTCGTAAGGGCCACTTTGCGACCCTGAGCAAGGGTGAGCTGAAACAGCTGCTGACCAAAG
AACTGGCGAATACCATTAAGAACATCAAGGACAAAGCAGTGATTGATGAGATTTCCAGGG
CCTGGACGCGAATCAAGATGAGCAAGTTGACTTCCAAGAGTTCATCAGCCTGGTCGCAATC
GCCTTGAAAGCGGCTGCGTATCATA CGGCAAAGAGTAACTCGAG

The restriction sites are underlined. The stop codon is in bold.

Amino acid sequence for S100A12(H15A(D25A)(H85A)(H89A)

MTKLEEHLEG IVNIF **A** QYSV RKGHF **A** TLSK GELKQLLTKE LANTI
KNIKD KAVIDEIFQG LDANQDEQVD FQEFISLVAI ALKAA **A** YHTA **A**
KE **Stop** LE

The residues of the restriction sites are underlined. The mutated residues are highlighted in yellow.

2. 3. 2. Materials and General Methods

All solvents and chemicals were obtained from commercial suppliers and used as received.

All aqueous solutions were prepared using Milli-Q water (18.2 M Ω •cm, 0.22- μ m filter).

Protein concentrations were routinely quantified by using the calculated extinction coefficients for the S100A12 homodimer (ProtParam, $\epsilon_{280} = 5960 \text{ M}^{-1} \text{ cm}^{-1}$). All protein

concentrations and reported stoichiometries are relative to the S100A12 homodimer (α_2).

For the microbiology assays, Luria-Bertani (LB) medium, Tryptic Soy Broth (TSB) medium, Yeast Peptone Dextrose (YPD) medium, deMan, Rogosa and Sharpe (MRS) medium, Brain Heart Infusion (BHI) medium, and agar plates were prepared with Milli-Q water. A Beckman Coulter DU 800 spectrophotometer thermostatted at 25 °C with a Peltier temperature controller or an Agilent 8453 diode-array spectrophotometer controlled with manufacturer-supplied software and thermostatted at 25 °C by a circulating water bath were employed for the OD₆₀₀ measurements of bacterial and fungal cultures.

For metal-binding experiments, HEPES buffer was prepared with Ultrol grade HEPES (free acid, Calbiochem) and TraceSELECT NaCl (Sigma). TraceSELECT aqueous NaOH (Sigma) was used to adjust the pH. To reduce metal-ion contamination, Teflon-coated or plastic spatulas were used to transfer buffer reagents, and buffers were treated with Chelex 100 resin (Bio-Rad, 10 g/L) by stirring in a polypropylene beaker for at least 1 h. The Chelex resin was removed by passing the buffer through a 0.22- μ m filter, and all buffers were stored in polypropylene containers. All metal-binding studies were conducted at pH 7.0 in 75 mM HEPES, 100 mM NaCl. A Tris buffer (1 mM Tris, pH 7.5) prepared from Tris base (J. T. Baker) was used for circular dichroism (CD) spectroscopy experiments. This buffer was treated with Chelex resin for 1 h (10 g/L), filtered through a 0.22- μ m filter, and the pH was readjusted to 7.0 with hydrochloric acid.

Cobalt stock solutions (100 mM) were prepared from 99.999% CoCl₂ hydrate (Sigma) and Milli-Q water, and zinc stock solutions (100 mM) were prepared from 99.999% anhydrous ZnCl₂ (Sigma) and Milli-Q water. The metal stock solutions were prepared in acid-washed volumetric glassware and transferred to sterile polypropylene tubes for long-term storage. The working solutions were prepared by diluting the stock solutions in Milli-Q water.

FluoZin-3 (FZ3) and Mag-Fura-2 (MF2) were purchased from Invitrogen. Zincon monosodium salt was purchased from Sigma-Aldrich. Stock solutions of Zincon (\approx 10 mM) were

prepared in anhydrous DMSO (Sigma), aliquoted into 50- μ L portions and stored at -20 °C. Stocks of FZ3 (\approx 2 mM), and MF2 (\approx 2 mM), were prepared in Chelexed-treated Milli-Q water, aliquoted into 50- μ L portions, and stored at -20 °C. Each aliquot was thawed only once, and experiments with these reagents were performed in the dark.

2. 3. 3. Cloning, Mutagenesis, Overexpression, and Purification of S100A12, S100A12 Δ His₃Asp, and CP-Ser

The pET41a-S100A12 expression plasmid was previously described.³³ A synthetic gene containing the *E. coli* optimized nucleotide sequence for human S100A12(H15A)(D25A)-(H85A)(H89A), hereafter S100A12 Δ His₃Asp, was obtained in the pJ201 vector from DNA 2.0 (see Design of the Synthetic Gene). The plasmid was subcloned into the *Nde*I and *Xho*I sites of pET41a using T4 DNA ligase. The plasmid identity was confirmed by DNA sequencing (MIT Biopolymers).

For protein expression, the pET41a-S100A12 and pET41a-S100A12(H15A)(D25A)-(H85A)(H89A) expression plasmids were transformed into chemically competent *E. coli* BL21(DE3) cells prepared following standard in-house protocols. Cultures from single colonies were grown to saturation in LB medium containing 50 μ g/mL kanamycin (37 °C with agitation, $t \approx$ 16-20 h), and freezer stocks were prepared by diluting the overnight cultures 1:1 (v/v) in 50% glycerol/water and stored at -80 °C.

The reconstitution and purification of human S100A12 and S100A12 Δ His₃Asp were performed following a modified published protocol.³³ For larger-scale protein preparations, the purification protocol was modified to avoid pressure limit issues with the ÄKTA Purifier FPLC system (GE Life Sciences). The complete modified protocol is detailed below.

Frozen cell pellets (\approx 3 g from a 2-L culture) were thawed on ice for \approx 20 min and resuspended in 10 mL/g of lysis buffer (50 mM Tris pH 8.0, 100 mM NaCl, 1 mM EDTA, 1 mM

PMSF, 0.5% Triton X-100). The resulting suspension was sonicated on ice using a Branson sonicator (40% amplitude for 2.5 min, 30 sec on / 10 sec off), and the crude lysate was clarified by centrifugation (13,000 rpm, 10 min, 4 °C). The supernatant was poured into a beaker on ice. The insoluble cell pellet was resuspended in lysis buffer (30 mL), and the sonication, centrifugation, and resuspension steps were repeated twice. The supernatant from the three rounds of lysis and centrifugation were combined, and transferred to the 4 °C cold room. For cell pellets from a 2-L culture, the volume of the supernatant was typically 100 mL. To remove contaminating protein in the soluble lysate, ammonium sulfate (37.5 g for 100 mL of lysate) was slowly added over the course of 20 min with constant stirring to provide a 60% ammonium sulfate solution, and precipitation of protein was observed. S100A12 is soluble in up to 80% ammonium sulfate and therefore remains in solution. The 60% ammonium sulfate mixture was allowed to stir for an additional 1 h, and the insoluble contaminating protein fraction was pelleted by centrifugation (13,000 rpm, 10 min, 4 °C). After centrifugation, a greasy layer of precipitate remained suspended and was carefully removed using a spatula. The supernatant was dialyzed (3500 MWCO, Spectropor3) against 2 x 4 L of 20 mM HEPES, pH 8.0 at 4 °C for at least 12 h each prior to further purification.

A thin layer of precipitate formed in the dialysis tubing, and the dialysate was centrifuged (13 000 rpm, 10 min, 4 °C). The supernatant was passed through a 0.45- μ m syringe filter and loaded onto a 150-mL Superloop (GE Lifesciences). Chromatographic purification of S100A12 was conducted using an ÄKTA Purifier FPLC system (GE Life Sciences) housed in a 4 °C cold room. Homodimeric S100A12 was first purified by anion-exchange chromatography using a MonoQ 10/100 GL column. A gradient of 0–10 % B over 8 column volumes (Eluent A, 20 mM HEPES, pH 8.0; Eluent B, 20 mM HEPES, 1 M NaCl, pH 8.0) was employed. This step allowed for separation of homodimeric S100A12 from higher oligomeric and aggregated species of S100A12. Fractions containing S100A12 (as determined by SDS-PAGE, 15% Tris-HCl gel) were pooled, concentrated to \approx 10 mL, and purified by size-exclusion chromatography (SEC) using a

HiLoad 26/600 S75 pg column (GE Lifesciences). For purified protein that was used in metal-binding experiments, the running buffer of the SEC was 20 mM HEPES, 100 mM NaCl, pH 8.0. For protein that was employed in microbiology assays, the running buffer was 20 mM Tris, 100 mM NaCl, pH 7.5. Fractions containing S100A12 were pooled and dialyzed against 1 L of the appropriate buffer (20 mM HEPES, 100 mM NaCl, pH 8.0, or 20 mM Tris, 100mM NaCl, pH 7.5) containing \approx 10 g Chelex resin (Bio-Rad) at 4 °C for \approx 12 h. The protein was concentrated using a 10K MWCO Amicon spin concentrator (3750 rpm, 4 °C). The concentration of S100A12 was determined using its calculated extinction coefficient (ϵ_{280}) (Table 2. 1.). S100A12 was then aliquoted into sterile microcentrifuge tubes in 100- μ L portions, flash frozen in liquid N₂, and stored at -80 °C. This procedure was performed using cell pellets from 2-L cultures to afford yields of \approx 100-170 mg.

Table 2. 1. Molecular weights and extinction coefficients for S100A12 monomers.

Protein	Molecular Weight (Da) ^a	ϵ_{280} (M ⁻¹ cm ⁻¹) ^b
S100A12	10575.0	2980
S100A12 Δ His ₃ Asp	10332.8	2980

^a Molecular weights were calculated by using the ProtParam tool available on the ExPASy server (<http://web.expasy.org/protparam>). These values include the N-terminal Met residue. No *m/z* corresponding to loss of the N-terminal Met residue was observed. ^b Extinction coefficients (280 nm) were calculated by using the ProtParam tool.

2. 3. 4. Protein Characterization

S100A12 and S100A12 Δ His₃Asp were characterized by SDS-PAGE, mass spectrometry, analytical size exclusion chromatography, and circular dichroism (CD) spectroscopy as described for calprotectin.¹

2. 3. 5. *Metal Analysis (ICP-MS)*

To remove contaminating metals from materials used in these experiments, 5-mL centrifuge tubes (Argos Technologies Inc.) were washed with 3% HNO₃ (Sigma) and allowed to air-dry, and 4-mL spin concentrators (10K MWCO, Amicon) were washed with EDTA (300 μM in water, 1x) and Milli-Q water (3x), and allowed to dry overnight.

For these studies, two types of growth media were analyzed. The Tris:YPD medium was composed of a 32:68 (v:v) ratio of YPD and AMA buffer (20 mM Tris-HCl, 100 mM NaCl, pH 7.5). The Tris:TSB medium was composed of a 32:68 (v:v) ratio of TSB and AMA buffer.

For the metal-depletion experiments, 2.5 mL of AMA medium (either Tris:TSB or Tris:YPD) were transferred to the washed 5-mL centrifuge tubes. Protein samples were buffer exchanged into AMA buffer using 0.5-mL 10 MWCO Amicon spin concentrators, and diluted to final concentrations of 62.5, 125, 250, and 500 μg/mL in the AMA medium. Untreated AMA medium containing no protein and the S100A12-treated media samples were incubated for 20 h (30 °C, 150 rpm). The samples were filtered using the 4-mL Amicon spin concentrators. The flow through was collected and acidified to 3% HNO₃ by addition of 70% HNO₃. Samples were analyzed at either the Microanalysis Laboratory at the University of Illinois at Urbana-Champaign (UIUC) (one set of samples for Tris:YPD incubated with S100A12) or the Center for Environmental Health Sciences (CEHS) Core Facility at MIT (all other samples). At UIUC, the concentrations of Mn, Co, Ni, Cu, and Zn were quantified by inductively coupled plasma-mass spectrometry (ICP-MS), and the metal concentrations of Mg, Ca, and Fe were quantified by inductively coupled plasma-optical emission spectroscopy (ICP-OES). For samples analyzed at MIT, the concentrations of Mg, Ca, Fe, Mn, Co, Ni, Cu, and Zn were quantified by an Agilent 7900 ICP-MS used in Helium mode outfitted with integrated autosampler (I-AS). An internal standard of erbium or terbium (Agilent) was used to control for sample effects, and the concentrations of analyte were calibrated using standards prepared by serial dilution of the Agilent Environmental Calibration Standard mix. All

experiments were performed at least three times with four different starting stocks of media. The mean and SEM values are reported.

2. 3. 6. *Western Blot of S100A12-treated medium (YPD)*

To ensure that the S100A12 present during treatment of growth medium did not pass through the spin filter, western blot analysis was performed on the retentate and flow through obtained from each sample following the spin-filtration step. Sodium dodecyl sulfate-PAGE (SDS-PAGE) was performed on a 15% glycine gel. The proteins were transferred to a nitrocellulose membrane following the manufacturer's procedure (BioRad). S100A12 was blotted with a 1:1000 dilution of monoclonal mouse IgG2b to human S100A12/EN-RAGE (161205) (R&D Systems). The antibody was blotted with a 1:10,000 dilution of infrared dye-labeled goat anti-mouse IgG (LI-COR Biosciences), and the blot was visualized using a LI-COR Odyssey Scanner.

2. 3. 7. *Antifungal Activity Assays*

The growth inhibitory activity of S100A12 against *Candida albicans* SC5314, *C. glabrata* ATCC 200918, *C. krusei* ATCC 200917, and *C. tropicalis* ATCC MYA-3404 was investigated by following previously published protocols for culturing these organisms.³⁴ Fungal strain stocks were stored at -80 °C in YPD medium containing 25% glycerol. Overnight cultures were inoculated into 10 mL of YPD in a 250-mL baffled flask from single colonies on agar plates and grown overnight (37 °C, 150 rpm, t ≈20 h) on a rotating wheel. The overnight cultures were then diluted 1:50 to a final volume of 10 mL in a 250-mL baffled flask and allowed to grow to mid-log phase at an OD₆₀₀ ≈ 1 (t ≈3.5 h). The cultures at mid-log phase were diluted 1:500 into Tris:YPD medium (32:68 (v:v) ratio of YPD and AMA buffer (20 mM Tris-HCl, 100 mM NaCl, pH 7.5)), and 90 μL of the dilution added to a well containing 10 μL of the 10x protein stock in 96-well plates (Corning, Inc.). For samples containing a Ca(II) supplement, the Tris buffer was supplemented with 3 mM Ca(II). Each

condition was repeated in three wells to obtain an average value for each time point for each trial. To avoid evaporation, the plate was covered with a wet paper towel and wrapped with Saran wrap. The plate was then incubated in an incubator-shaker (37 °C, 150 rpm, t ≈30 h). The growth was monitored by OD₆₀₀ at regular intervals using a Synergy HT plate reader (BioTek). To resuspend cultures that formed clumping at the bottom of the wells, the plates were shaken vigorously prior to OD₆₀₀ measurement. Each set of experiments was performed at least three times with at least two different protein and medium stocks. The mean and SEM are reported.

Table 2.2. Strains and growth conditions employed in this work

Strain	Source	Culture conditions ^a
<i>Candida albicans</i> SC5314	Linquist Lab (Whitehead)	Tris:YPD (32:68 v/v), 37 °C, 150 rpm
<i>Candida glabrata</i> ATCC 200918	ATCC	Tris:YPD (32:68 v/v), 37 °C, 150 rpm
<i>Candida krusei</i> ATCC 200917	ATCC	Tris:YPD (32:68 v/v), 37 °C, 150 rpm
<i>Candida tropicalis</i> ATCC MYA-3404	ATCC	Tris:YPD ((32:68 v/v), 37 °C, 150 rpm
<i>Escherichia coli</i> K-12	Keio Collection	Tris:TSB (32:68 v/v), 37 °C, 150 rpm
<i>Escherichia coli</i> K-12 Δ znuA	Keio Collection	Tris:TSB (32:68 v/v), 37 °C, 150 rpm
<i>Lactobacillus plantarum</i> WCSF1	ATCC	Tris:MRS (32:68 v/v). 30 °C, 150 rpm
<i>Listeria monocytogenes</i> ATCC 19115	ATCC	Tris:BHI (32:68 v/v), 30 °C, 150 rpm
<i>Pseudomonas aeruginosa</i> PAO1	Manoil Laboratory ^b	Tris:TSB (32:68 v/v), 37 °C, 150 rpm
<i>Pseudomonas aeruginosa</i> PAO1 Δ znuA	Manoil Laboratory ^b	Tris:TSB (32:68 v/v), 37 °C, 150 rpm
<i>Staphylococcus aureus</i> ATCC 25923	ATCC	Tris:TSB -dextrose, 37 °C, 150 rpm

^a TSB-dextrose and BHI were obtained from Becton Dickinson (BD). YPD was prepared in-house. All medium contained dextrose. These are the culture conditions employed for the antimicrobial activity assays. ^b University of Washington (Seattle, WA).

2. 3. 8. Antibacterial Activity Assays

The growth inhibitory activity of S100A12 against bacterial strains was investigated by following previously published protocols.^{28,30} Bacterial strain stocks were stored at -80 °C in media containing 25% glycerol. AMA medium (Tris:TSB) was prepared using sterile technique. TSB was used for *S. aureus* ATCC 25923, *E. coli* K-12, and *P. aeruginosa* PAO1, MRS was used for *L. plantarum* WCSF1, and BHI was used for *L. monocytogenes* ATCC 19115. Overnight cultures were inoculated into 5 mL of growth medium in a culture tube (TSB, MRS, or BHI) from single colonies from agar plates (TSB, MRS, BHI) and grown overnight (37 °C, t ≈16 h) on a rotating wheel. The overnight cultures were then diluted 1:100 in a 5-mL culture tube and allowed to grow to mid-log phase at an OD₆₀₀ ~ 0.6 (t ≈2 - 4.5 h).

The assays performed with *L. plantarum* and *L. monocytogenes* were modified as follows. *L. plantarum* cultures were grown at 30 °C, 150 rpm in MRS medium, and modified AMA medium composed of MRS medium and Tris buffer (20 mM Tris-HCl, 100 mM NaCl, pH 7.5) (Tris:MRS 32:68 (v:v)) was used. *L. monocytogenes* cultures were grown at 30 °C, 150 rpm in BHI medium, and modified AMA medium composed of BHI medium and Tris buffer (Tris:BHI 32:68 (v:v)) was used. The AMA medium for *S. aureus*, *E. coli*, and *P. aeruginosa* was composed of TSB medium and Tris buffer (Tris:TSB 32:68 (v:v)). The cultures at mid-log phase were diluted 1:500 into the corresponding AMA medium, and 90 µL of the dilution added to a well containing 10 µL of the 10x protein stock. For samples containing a Ca(II) supplement, the Tris buffer was supplemented with 3 mM Ca(II). Each condition was repeated in three wells to obtain an average value for each time point for each trial. The plate was covered with a wet paper towel and wrapped with Saran wrap. The plate was then allowed to incubate in an incubator-shaker (37 °C, 150 rpm, t ≈20 h). The growth was monitored by OD₆₀₀ at regular intervals using a plate reader. Each set of experiments was performed at least three times with at least two different protein and media stocks. The mean and SEM are reported.

2. 3. 9. Antimicrobial Activity Assays with Zinc Preincubation

The Zn(II) preincubation assays with *C. albicans* were performed following analogous protocols for studying the effects Mn(II) and Fe(II) addition to calprotectin.^{30, 33} Overnight cultures were inoculated with 10 mL of YPD in a 250-mL baffled flask from single colonies on agar plates, and grown overnight on an incubator-shaker (37 °C, 150 rpm, t ≈20 h). The overnight cultures were then diluted 1:50 in a 250-mL baffled flask and allowed to reach an OD₆₀₀ ≈1.0 after ≈3.5 h, corresponding to its mid-log phase. To prevent precipitation of protein (125 µg/mL) upon addition of 2 equiv. of Zn(II), the dilution factors were adjusted in this experiment. The mid-log phase cultures were diluted 1:56 into AMA medium (Tris:YPD containing a 2 mM Ca(II) supplement), and 10 µL of the dilution added to a well containing 90 µL of 1.1x of protein prepared in the same AMA medium, preincubated with two equivalents of Zn(II). The 96-well plate was covered with a wet paper towel, wrapped with Saran wrap, and allowed to incubate in an incubator-shaker (37 °C , 150 rpm, t ≈30 h). Fungal growth was monitored by OD₆₀₀ at regular intervals using a plate reader. To resuspend cultures that formed clumping at the bottom of the wells, the plates were shaken vigorously prior to OD₆₀₀ measurement. Each set of experiments was performed at least three times with at least two different protein and media stocks. The mean and SEM are reported.

2. 3. 10. Optical Absorption and Fluorescence Spectroscopy

Optical absorption spectra were collected on a Beckman Coulter DU 800 spectrophotometer thermostatted at 25 °C with a Peltier temperature controller. Fluorescence spectra were collected on a Photon Technologies International QuantaMaster 40 fluorimeter outfitted with a continuous xenon source for excitation, autocalibrated QuadraScopic monochromators, a multimode PMT detector, and a circulating water bath maintained at 25 °C. This instrument was controlled by the FelixGX software package. Quartz cuvettes with 1-cm path lengths (Starna) were employed for all optical absorption measurements. Due to the large number

of cuvettes needed for the experiments with FZ3, poly(methyl methacrylate) (PMMA) cuvettes (Fisher Scientific) were employed for the fluorescence experiments with this Zn(II) sensor. All optical absorption and fluorescence spectroscopic experiments were performed at least in triplicate.

2. 3. 11. Zinc Competition with S100A12 and Zincon

A 2-mL solution containing 10 μM S100A12 or S100A12 $\Delta\text{His}_3\text{Asp}$ and 20 μM Zincon was prepared in a quartz cuvette (75 mM HEPES, 100 mM NaCl, pH 7.0). The solution was titrated with 0–4.5 equivalents of Zn(II) (1 μL of a 2 mM Zn(II) solution per addition) at room temperature. The samples were allowed to equilibrate for 2 min after each Zn(II) addition, and the optical absorption spectra were collected from 200 to 800 nm. The absorbance at 621 nm was plotted versus the $[\text{Zn(II)}] / [\text{S100A12}]$ ratio. Zincon has reported $K_{d,\text{Zn}}$ values of 12.6 and 5.8 μM .^{35, 36}

2. 3. 12. Zinc Competition with S100A12 and MF2

A 2-mL solution containing 10 μM S100A12 or S100A12 $\Delta\text{His}_3\text{Asp}$ and 10 μM MF2 was prepared in a quartz cuvette (75 mM HEPES, 100mM NaCl, pH 7.0) and titrated with 0–4 equivalents of Zn(II) (1 μL of a 2 mM ZnCl_2 aqueous solution per addition) at room temperature. The samples were allowed to equilibrate for 2 min after each Zn(II) addition, and the optical absorption spectra were collected from 200 to 800 nm. The absorbance increase at 325 nm and decrease at 366 nm were plotted versus the $[\text{Zn(II)}] / [\text{S100A12}]$ ratio. Reported $K_{d,\text{Zn}}$ values of MF-2 are 20 and 36 nM.^{37, 38}

2. 3. 13. Zinc Competition with S100A12 and FZ3

Solutions (1 mL) containing FZ3 (2 μM) and S100A12 (2 μM) or S100A12 $\Delta\text{His}_3\text{Asp}$ (2 μM) were prepared in PMMA cuvettes (75 mM HEPES, 100 mM NaCl, pH 7.0). Each solution was

mixed gently and incubated for 1 h in the dark at room temperature. The emission spectrum of each solution was then recorded. One equivalent of Zn(II) was subsequently added to each sample, and the solutions were gently mixed and incubated for 2.5 h in the dark at room temperature. The emission spectrum of each solution was then recorded. The samples were excited at 494 nm, and the emission was monitored from 500–650 nm (-Zn(II) samples) or 507–650 nm (+Zn(II) samples). Emission spectra from a representative trial are presented. The apparent $K_{d,Zn}$ of FZ3 is 9 nM.³⁹

2. 4. Results and Discussion

2. 4. 1. Protein Characterization

The purity and integrity of S100A12 and S100A12 Δ His₃Asp were characterized by SDS-PAGE gel (Figure 2. 2), mass spectrometry (Table 2. 3), CD (Figure 2. 3), and analytical size-exclusion chromatography (SEC) (Figure 2. 4, Table 2. 4). A single band was observed on the SDS-PAGE gel of S100A12 and S100A12 Δ His₃Asp, confirming the purity of the preparations. The bands are consistent with the molecular weights of the monomers of 10.5 and 10.3 kDa for S100A12 and S100A12 Δ His₃Asp respectively (Figure 2. 2). ESI-MS afforded the expected mass for each protein (Figure 2. 3). Furthermore, the CD spectra showed local minima at 208 and 220 nm, confirming the expected α -helical secondary structure, and the shape of the spectra are consistent with prior reports for other S100 proteins.^{28, 29} Lastly, Analytical SEC demonstrated that S100A12 and S100A12 Δ His₃Asp have elution volumes of 12.4 and 12.1 mL respectively, corresponding to homodimeric species (Figure 2.4, Table 2. 4). A shift towards a lower elution was observed upon addition of Ca(II) (Figure 2. 4, Table 2. 4) indicative of slight conformational changes upon Ca(II) binding.

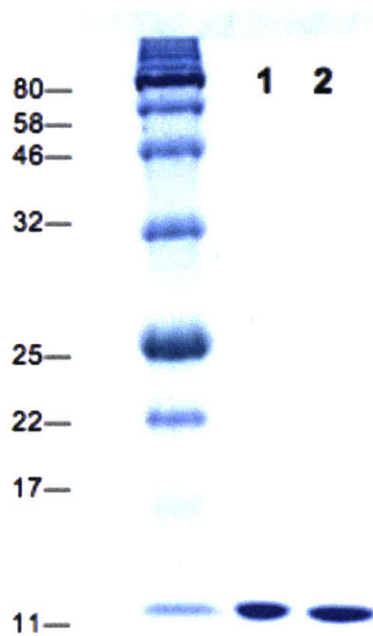


Figure 2. 2. SDS-PAGE (15% acrylamide Tris-HCl, glycine gel) visualized with Coomassie Blue of purified S100A12 (lane 1) and Δ His₃Asp (lane 2) used in this study. The ladder is P7712S from New England BioLabs.

Table 2. 3. Mass spectrometric analysis of S100A12 and S100A12 Δ His₃Asp.

Protein	Calculated Mass (Da)	Observed Mass (Da)
S100A12	10575.0 (monomer)	10575.6 (monomer)
	21150.0 (dimer)	21150.2 (dimer)
S100A12 Δ His ₃ Asp	10332.8 (monomer)	10332.8 (monomer)
	20665.6 (dimer)	20665.9 (dimer)

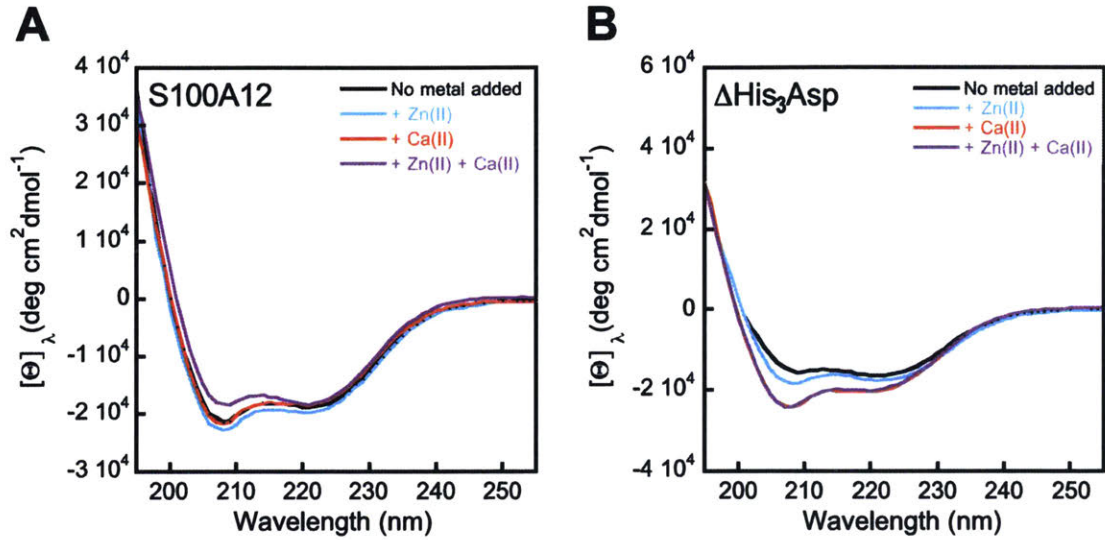


Figure 2. 3. Circular dichroism spectra of 10 μM S100A12 (A) and S100A12 $\Delta\text{His}_3\text{Asp}$ (B) in the absence and presence of divalent cations (1 mM Tris-HCl, pH 7.0, T = 25 $^\circ\text{C}$). Black trace, without metal addition; blue trace, in the presence of 20 μM Zn(II); red trace, in the presence of 2 mM Ca(II); purple trace, in the presence of 20 μM Zn(II) and 2 mM Ca(II).

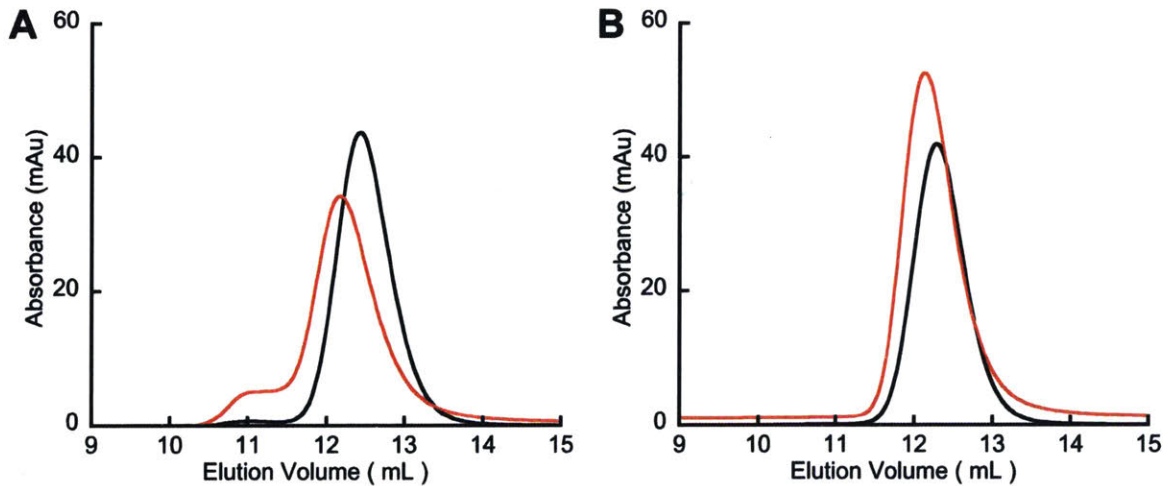


Figure 2. 4. Analytical SEC chromatograms of 30 μM S100A12 (A) and 30 μM S100A12 $\Delta\text{His}_3\text{Asp}$ (B) in the absence (black) and presence (red) of 2 mM Ca(II) in the sample and running buffer (75 mM HEPES, 100mM NaCl, pH 7.0).

Table 2. 4. Analytical SEC elution volumes and calculated molecular weights.^a

	Ca(II)	Elution Volume (mL)	Calculated Molecular Weight (kDa)
S100A12	-	12.4	24.2
S100A12	+	12.2	26.4
Δ His ₃ Asp	-	12.1	27.6
Δ His ₃ Asp	+	12.3	25.8

^a Each sample contained 30 μ M protein (75 mM HEPES, 100 mM NaCl, pH 7.0). The +Ca(II) samples contained 1.2 mM (40 equiv.) Ca(II) in the sample and running buffer. The experiments were performed at 4 °C.

2. 4. 2. Human S100A12 Depletes Zn(II) from Microbial Growth Medium

To probe which metal ions S100A12 sequesters from microbial growth medium, we conducted a series of metal depletion experiments. We treated standard growth media employed for *in vitro* antifungal (YPD-based medium) or antibacterial (TSB-based medium) activity assays with varying concentrations of S100A12 (0 – 250 μ g/mL, t = 20 h, T = 30 °C). Following treatment of the medium with S100A12, we employed spin filtration to separate the protein from the treated medium. Western blot analyses confirmed that S100A12 remains in the retentate and does not leak into the flow-through, thus confirming that the flow-through only contained metals that were not bound by S100A12 (Figure 2. 5). We quantified the amount of unbound metal in the treated medium by inductively coupled plasma-mass spectrometry (ICP-MS). Because the protein and treated medium were separated by spin filtration, this procedure does not afford an equilibrium measurement because the metal concentrations in the filtered sample are not precisely the “free” metal concentrations in a solution at equilibrium. Nevertheless, it provides an assessment of which metal ions can be sequestered by S100A12 in complex samples. To determine whether the presence of Ca(II) influences metal sequestration, we prepared and analyzed samples with and without a \approx 2-mM Ca(II) supplement.



Figure 2. 5. Western blot of the retentate and flow through obtained from S100A12-treated Tris:YPD medium. Medium without S100A12 treatment retentate (lane 2), medium without S100A12 treatment flow through (lane 4), Medium treated with 250 $\mu\text{g/mL}$ S100A12 -Ca(II) retentate (lane 6), Medium treated with 250 $\mu\text{g/mL}$ S100A12 -Ca(II) flow through (lane 8), medium treated with 250 $\mu\text{g/mL}$ S100A12 +Ca(II) retentate, (lane 11), medium treated with 250 $\mu\text{g/mL}$ S100A12 +Ca(II) flow through (lane 13). No sample was loaded in the other lanes (lanes 1, 3, 5, 7, 9, 10, and 12). The ladder is P7712S from New England BioLabs.

The Tris:YPD medium employed for antifungal activity assays (*vide infra*) contains relatively high concentrations of Fe ($\approx 3.5 \mu\text{M}$) and Zn ($\approx 7 \mu\text{M}$), and lower concentrations of Mn ($\approx 100 \text{ nM}$), Co ($\approx 130 \text{ nM}$), Ni ($\approx 100 \text{ nM}$) and Cu ($\approx 150 \text{ nM}$) (Figure 2. 6A, Table 2. 5). With the exception of Zn, S100A12 treatment had negligible effect on the concentrations of the first-row transition metals present in the Tris:YPD medium. Zinc depletion occurred, and the extent of Zn depletion depended on the concentration of S100A12 and whether the medium was supplemented with Ca(II). The Ca(II) effect was most obvious at 62.5 and 125 $\mu\text{g/mL}$ S100A12. For instance, at 125 $\mu\text{g/mL}$ S100A12, the Zn concentration in the treated medium decreased by a factor of ≈ 3 (-Ca) or ≈ 10 (+Ca).

The Tris:TSB medium employed for antibacterial activity assays (*vide infra*) also contains relatively high concentrations of Fe ($\approx 3 \mu\text{M}$) and Zn ($\approx 5 \mu\text{M}$), and the other first-row transition

metals are markedly less abundant (Figure 2. 6B, Table 2. 10). S100A12 treatment resulted in Ca(II)-dependent depletion of Zn, but not the other transition metals, from this medium. The Ca(II) effect was most pronounced at 62.5 $\mu\text{g}/\text{mL}$ S100A12 where negligible Zn(II) depletion occurs in the absence of the Ca(II) supplement and ≈ 4 -fold reduction in total Zn occurs in the presence of Ca(II). To confirm that the His₃Asp sites are essential for Zn(II) depletion, we treated Tris:YPD and Tris:TSB with S100A12 $\Delta\text{His}_3\text{Asp}$ (250 $\mu\text{g}/\text{mL}$), a variant that harbors the point mutations H15A, D25A, H85A, and H89A. This variant cannot bind metal ions at the His₃Asp sites because the four metal-chelating residues are replaced by non-coordinating alanine moieties. No metal depletion was observed for the $\Delta\text{His}_3\text{Asp}$ variant in either Tris:YPD or Tris:TSB (Figure 2. 6). These results demonstrate that the His₃Asp sites are essential for Zn(II) depletion from microbial growth media, as expected based on the Zn(II)-S100A12 crystal structure.²⁵

These metal depletion results illuminate three key points about the metal-sequestering properties of S100A12: (i) S100A12 binds Zn(II) with sufficient affinity to deplete it from growth medium; (ii) S100A12 appears to select for Zn(II) over other first-row transition metal ions, at least under these experimental conditions; and (iii) S100A12 uses Ca(II) ions to modulate its Zn(II)-binding properties, and the presence of Ca(II) results in more effective Zn(II) depletion from the medium. Moreover, the Tris:TSB metal-depletion profile of S100A12 is markedly different from that of calprotectin, a metal-sequestering S100 family member that harbors two different sites for transition metal ions (His₃Asp and His₄/His₆) and reduces the levels of Mn, Fe, Ni, Cu, and Zn from this medium.³⁰ The apparent Zn(II) selectivity of S100A12 is consistent with prior solution studies of this protein, which provided no evidence for the formation high-affinity Mn(II)-S100A12 and Fe(II)-S100A12 complexes in the absence or presence of Ca(II).^{30, 33} The selective Zn(II) depletion is also reminiscent of studies of a ΔHis_4 variant of calprotectin that only harbors an interfacial His₃Asp site for chelating transition metals. This variant only depleted Zn(II) from Tris:TSB mixtures.³⁰

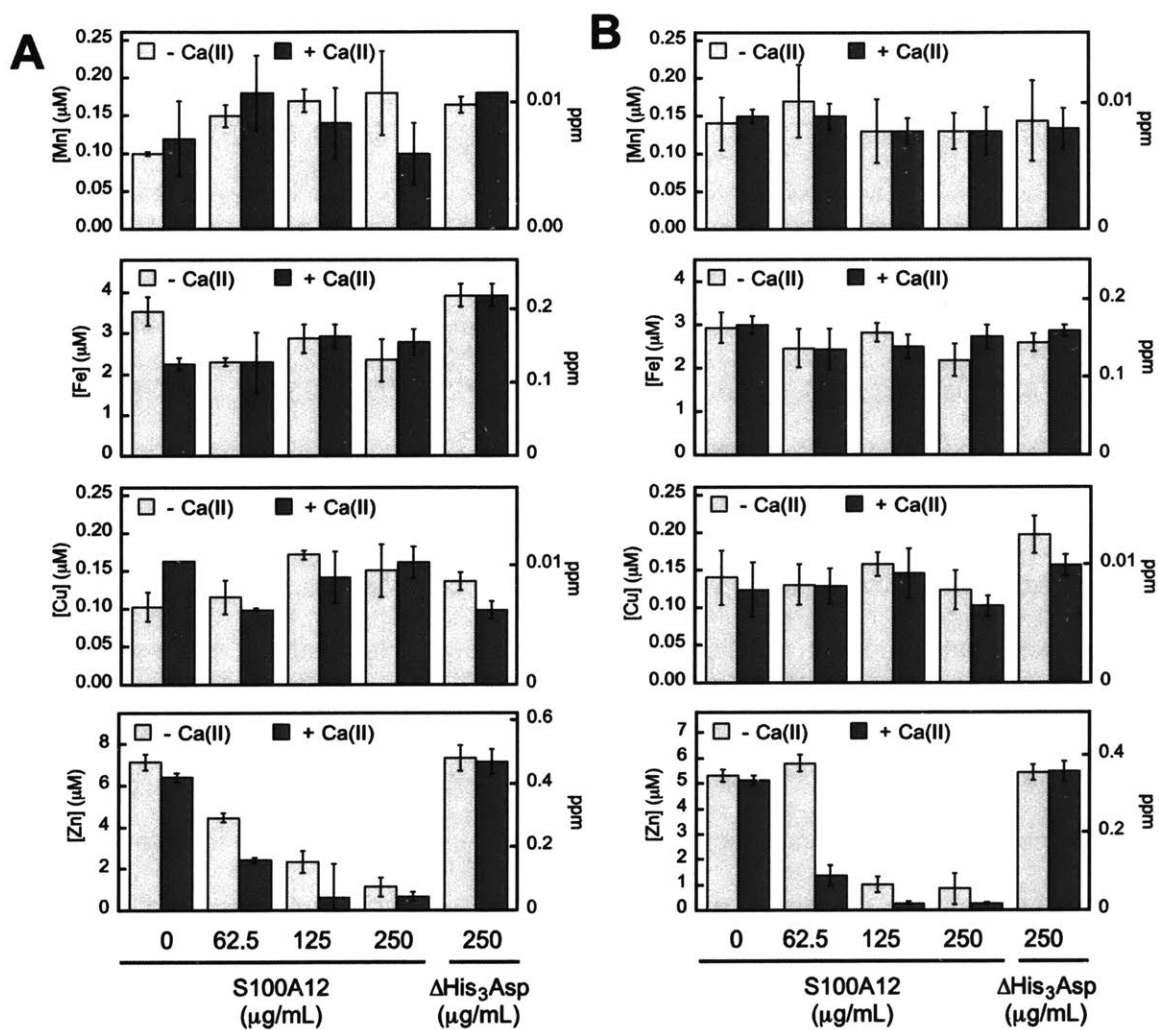


Figure 2. 6. S100A12 depletes Zn(II) from microbial growth media. (A) Metal analysis of Tris:YPD medium treated with 0–250 $\mu\text{g/mL}$ S100A12 or 250 $\mu\text{g/mL}$ S100A12 $\Delta\text{His}_3\text{Asp}$. (B) Metal analysis of Tris:TSB medium treated with 0–250 $\mu\text{g/mL}$ S100A12 or 250 $\mu\text{g/mL}$ S100A12 $\Delta\text{His}_3\text{Asp}$. The experiments were conducted in the absence (light gray bars) and presence (dark gray bars) of a $\approx 2\text{-mM}$ Ca(II) supplement (mean \pm SEM, $n \geq 3$).

Table 2. 5. Metal analysis of untreated Tris:YPD medium in the absence and presence of a 2-mM Ca(II) supplement (mean \pm SEM, $n = 4$).

Element	-Ca(II), ppm	-Ca(II), μ M	+Ca(II), ppm	+Ca(II), μ M
Mg	3.3 \pm 0.2	135 \pm 8	3.1 \pm 0.2	130 \pm 8
Ca	3.7 \pm 0.2	92 \pm 5	70 \pm 15	1800 \pm 400
Mn	0.009 \pm 0.001	0.100 \pm 0.002	0.006 \pm 0.002	0.12 \pm 0.05
Fe	0.20 \pm 0.02	3.5 \pm 0.4	0.126 \pm 0.007	2.3 \pm 0.2
Co	0.009 \pm 0.001	0.14 \pm 0.02	0.007 \pm 0.001	0.11 \pm 0.01
Ni	0.005 \pm 0.003	0.09 \pm 0.02	0.008 \pm 0.001	0.13 \pm 0.03
Cu	0.008 \pm 0.002	0.14 \pm 0.02	0.009 \pm 0.001	0.163 \pm 0.001
Zn	0.47 \pm 0.02	7.2 \pm 0.4	0.42 \pm 0.01	6.4 \pm 0.2

Table 2. 6. Metal analysis of Tris:YPD medium treated with 62.5 μ g/mL of S100A12 in the presence and absence of a 2-mM Ca(II) supplement (mean \pm SEM, $n = 4$).

Element	-Ca(II), ppm	-Ca(II), μ M	+Ca(II), ppm	+Ca(II), μ M
Mg	3.1 \pm 0.2	130 \pm 9	3.1 \pm 0.3	133 \pm 7
Ca	3.5 \pm 0.2	88 \pm 4	3.4 \pm 0.2	82 \pm 3
Mn	0.009 \pm 0.001	0.16 \pm 0.01	0.010 \pm 0.000	0.17 \pm 0.02
Fe	0.22 \pm 0.02	3.9 \pm 0.3	0.20 \pm 0.02	3.8 \pm 0.03
Co	0.001 \pm 0.000	0.17 \pm 0.000	0.01 \pm 0.004	0.17 \pm 0.004
Ni	0.003 \pm 0.003	0.06 \pm 0.06	0.0008 \pm 0.003	0.14 \pm 0.06
Cu	0.008 \pm 0.001	0.120 \pm 0.02	0.006 \pm 0.001	0.99 \pm 0.02
Zn	0.29 \pm 0.01	4.4 \pm 0.2	0.16 \pm 0.01	2.4 \pm 0.1

Table 2. 7. Metal analysis of Tris:YPD medium treated with 125 μ g/mL of S100A12 in the absence and presence of a 2-mM Ca(II) supplement (mean \pm SEM, $n = 4$).

Element	-Ca(II), ppm	-Ca(II), μ M	+Ca(II), ppm	+Ca(II), μ M
Mg	3.0 \pm 0.2	120 \pm 8	3.1 \pm 0.2	130 \pm 10
Ca	3.13 \pm 0.06	78 \pm 2	85 \pm 16	2100 \pm 400
Mn	0.008 \pm 0.001	0.15 \pm 0.01	0.013 \pm 0.002	0.23 \pm 0.04
Fe	0.129 \pm 0.006	2.3 \pm 0.1	0.13 \pm 0.04	2.3 \pm 0.7
Co	0.007 \pm 0.001	0.110 \pm 0.007	0.007 \pm 0.001	0.12 \pm 0.02
Ni	0.009 \pm 0.001	0.14 \pm 0.02	0.014 \pm 0.004	0.23 \pm 0.07
Cu	0.011 \pm 0.003	0.17 \pm 0.06	0.009 \pm 0.002	0.14 \pm 0.03
Zn	0.15 \pm 0.09	2.4 \pm 0.5	0.040 \pm 0.1	0.62 \pm 2

Table 2. 8. Metal analysis of Tris:YPD medium treated with 250 µg/mL of S100A12 in the presence and absence of a 2-mM Ca(II) supplement (mean ± SEM, *n* = 4).

Element	-Ca(II), ppm	-Ca(II), µM	+Ca(II), ppm	+Ca(II), µM
Mg	3.6 ± 0.4	150 ± 21	4.1 ± 0.8	170 ± 33
Ca	3.9 ± 0.6	100 ± 17	120 ± 11	2900 ± 300
Mn	0.009 ± 0.001	0.17 ± 0.02	0.008 ± 0.003	0.14 ± 0.05
Fe	0.16 ± 0.02	2.9 ± 0.4	0.16 ± 0.02	2.9 ± 0.3
Co	0.008 ± 0.001	0.14 ± 0.02	0.008 ± 0.001	0.14 ± 0.02
Ni	0.012 ± 0.002	0.20 ± 0.04	0.013 ± 0.005	0.21 ± 0.08
Cu	0.010 ± 0.002	0.15 ± 0.03	0.009 ± 0.003	0.12 ± 0.03
Zn	0.07 ± 0.03	1.1 ± 0.5	0.05 ± 0.01	0.7 ± 0.2

Table 2. 9. Metal analysis of Tris:YPD medium treated with 250 µg/mL of S100A12 ΔHis₃Asp in the absence and presence of a 2-mM Ca(II) supplement (mean ± SEM, *n* = 4).

Element	-Ca(II), ppm	-Ca(II), µM	+Ca(II), ppm	+Ca(II), µM
Mg	3.62 ± 0.06	148 ± 2	3.8 ± 0.2	158 ± 7
Ca	4.0 ± 0.1	100 ± 3	121 ± 4	3000 ± 80
Mn	0.007 ± 0.003	0.14 ± 0.05	0.007 ± 0.002	0.13 ± 0.02
Fe	0.14 ± 0.01	2.6 ± 0.2	0.160 ± 0.007	2.8 ± 0.1
Co	0.008 ± 0.000	0.040 ± 0.000	0.009 ± 0.000	0.043 ± 0.002
Ni	0.016 ± 0.000	0.271 ± 0.009	0.020 ± 0.000	0.313 ± 0.005
Cu	0.008 ± 0.000	0.13 ± 0.01	0.006 ± 0.000	0.09 ± 0.01
Zn	0.48 ± 0.06	7.3 ± 0.6	0.46 ± 0.06	7.2 ± 0.6

Table 2. 10. Metal analysis of untreated Tris:TSB medium in the absence and presence of a 2-mM Ca(II) supplement (mean ± SEM, *n* = 4).

Element	-Ca(II), ppm	-Ca(II), µM	+Ca(II), ppm	+Ca(II), µM
Mg	3.5 ± 0.2	140 ± 6	3.7 ± 0.2	150 ± 10
Ca	3.5 ± 0.1	90 ± 2	90 ± 12	2300 ± 300
Mn	0.01 ± 0.00	0.14 ± 0.01	0.006 ± 0.002	0.150 ± 0.009
Fe	0.16 ± 0.02	2.9 ± 0.3	0.17 ± 0.01	3.0 ± 0.2
Co	0.022 ± 0.001	0.037 ± 0.002	0.002 ± 0.000	0.04 ± 0.01
Ni	0.02 ± 0.00	0.28 ± 0.07	0.001 ± 0.000	0.211 ± 0.009
Cu	0.01 ± 0.00	0.14 ± 0.04	0.009 ± 0.002	0.12 ± 0.04
Zn	0.35 ± 0.02	5.3 ± 0.2	0.34 ± 0.01	5.1 ± 0.2

Table 2. 11. Metal analysis of Tris:TSB medium treated with 62.5 µg/mL of S100A12 in the absence and presence of a 2-mM Ca(II) supplement (mean ± SEM, *n* = 4).

Element	–Ca(II), ppm	–Ca(II), µM	+Ca(II), ppm	+Ca(II), µM
Mg	3.3 ± 0.2	140 ± 9	3.4 ± 0.3	140 ± 13
Ca	3.5 ± 0.2	90 ± 5	97 ± 7	2400 ± 200
Mn	0.009 ± 0.002	0.17 ± 0.05	0.008 ± 0.001	0.15 ± 0.02
Fe	0.14 ± 0.02	2.5 ± 0.4	0.14 ± 0.03	2.4 ± 0.5
Co	0.002 ± 0.000	0.037 ± 0.003	0.002 ± 0.000	0.033 ± 0.002
Ni	0.023 ± 0.002	0.39 ± 0.03	0.015 ± 0.001	0.26 ± 0.02
Cu	0.008 ± 0.002	0.13 ± 0.03	0.008 ± 0.002	0.13 ± 0.02
Zn	0.38 ± 0.02	5.8 ± 0.3	0.09 ± 0.02	1.4 ± 0.4

Table 2. 12. Metal analysis of Tris:TSB medium treated with 125 µg/mL of S100A12 in the absence and presence of a 2-mM Ca(II) supplement (mean ± SEM, *n* = 4).

Element	–Ca(II), ppm	–Ca(II), µM	+Ca(II), ppm	+Ca(II), µM
Mg	3.8 ± 0.3	160 ± 13	3.9 ± 0.3	160 ± 14
Ca	3.2 ± 0.2	80 ± 6	110 ± 20	2700 ± 400
Mn	0.007 ± 0.002	0.13 ± 0.04	0.007 ± 0.001	0.13 ± 0.02
Fe	0.16 ± 0.01	2.8 ± 0.2	0.14 ± 0.02	2.5 ± 0.03
Co	0.022 ± 0.000	0.040 ± 0.002	0.003 ± 0.000	0.047 ± 0.008
Ni	0.025 ± 0.009	0.4 ± 0.1	0.014 ± 0.001	0.24 ± 0.02
Cu	0.008 ± 0.001	0.13 ± 0.02	0.009 ± 0.002	0.15 ± 0.03
Zn	0.227 ± 0.02	3.5 ± 0.3	0.190 ± 0.004	0.29 ± 0.06

Table 2. 13. Metal analysis of Tris:TSB medium treated with 250 µg/mL of S100A12 in the absence and presence of a 2-mM Ca(II) supplement (mean ± SEM, *n* = 4).

Element	–Ca(II), ppm	–Ca(II), µM	+Ca(II), ppm	+Ca(II), µM
Mg	3.5 ± 0.3	150 ± 10	3.7 ± 0.4	150 ± 20
Ca	2.9 ± 0.3	73 ± 8	110 ± 10	2800 ± 300
Mn	0.007 ± 0.001	0.13 ± 0.02	0.007 ± 0.002	0.13 ± 0.03
Fe	0.12 ± 0.02	2.2 ± 0.4	0.15 ± 0.2	2.7 ± 0.3
Co	0.002 ± 0.000	0.027 ± 0.002	0.002 ± 0.000	0.035 ± 0.003
Ni	0.015 ± 0.002	0.26 ± 0.03	0.013 ± 0.001	0.224 ± 0.008
Cu	0.008 ± 0.002	0.12 ± 0.02	0.007 ± 0.001	0.10 ± 0.01
Zn	0.06 ± 0.04	0.9 ± 0.6	0.019 ± 0.003	0.29 ± 0.04

Table 2. 14. Metal analysis of Tris:TSB medium treated with 250 $\mu\text{g}/\text{mL}$ of S100A12 $\Delta\text{His}_3\text{Asp}$ in the absence and presence of a 2-mM Ca(II) supplement (mean \pm SEM, $n = 4$).

Element	-Ca(II), ppm	-Ca(II), μM	+Ca(II), ppm	+Ca(II), μM
Mg	3.62 ± 0.06	148 ± 2	3.8 ± 0.2	158 ± 7
Ca	4.0 ± 0.1	100 ± 3	121 ± 4	3000 ± 80
Mn	0.007 ± 0.003	0.14 ± 0.05	0.007 ± 0.002	0.13 ± 0.02
Fe	0.14 ± 0.01	2.6 ± 0.2	0.160 ± 0.007	2.8 ± 0.1
Co	0.002 ± 0.000	0.040 ± 0.000	0.003 ± 0.000	0.043 ± 0.002
Ni	0.016 ± 0.000	0.271 ± 0.009	0.020 ± 0.000	0.313 ± 0.005
Cu	0.012 ± 0.002	0.20 ± 0.02	0.010 ± 0.000	0.16 ± 0.01
Zn	0.36 ± 0.02	5.4 ± 0.3	0.36 ± 0.02	5.5 ± 0.3

2. 4. 3. Human S100A12 Exhibits Calcium-Dependent Antifungal Activity

Fungi have a significant Zn(II) requirement, and Zn(II) acquisition by fungal pathogens is important for virulence.^{34,40-45} We therefore questioned whether S100A12 exhibits antifungal activity that would result from its ability to bind Zn(II). To the best of our knowledge, an antifungal activity for S100A12 has not been reported. We evaluated the growth inhibitory activity of S100A12 against four *Candida* strains that cause human disease. *C. albicans* is a commensal organism of the human gastrointestinal tract and opportunistic human pathogen that can invade the mucosa and cause bloodstream infections.^{46,47} *C. krusei*, *C. glabrata*, and *C. tropicalis* are emerging human health threats, form biofilms, and exhibit resistance to antifungals such as the fluconazoles.⁴⁸⁻⁵⁰ When cultured in the Tris:YPD medium employed in the metal-depletion studies (Figure 2. 6), each fungal strain grew to an OD₆₀₀ value of ≈ 0.6 in the absence and presence of a ≈ 2 -mM Ca(II) supplement (Figure 2. 7). Addition of S100A12 (0 – 500 $\mu\text{g}/\text{mL}$) to *C. albicans* resulted in concentration-dependent growth inhibition, and this effect was enhanced when Ca(II) was present in the medium (Figure 2. 8A). The Ca(II) enhancement was most striking at 125 $\mu\text{g}/\text{mL}$ S100A12 where the OD₆₀₀ value decreased to ≈ 0.3 in the absence of Ca(II), and negligible *C. albicans* growth was observed when Ca(II) was included in the medium.

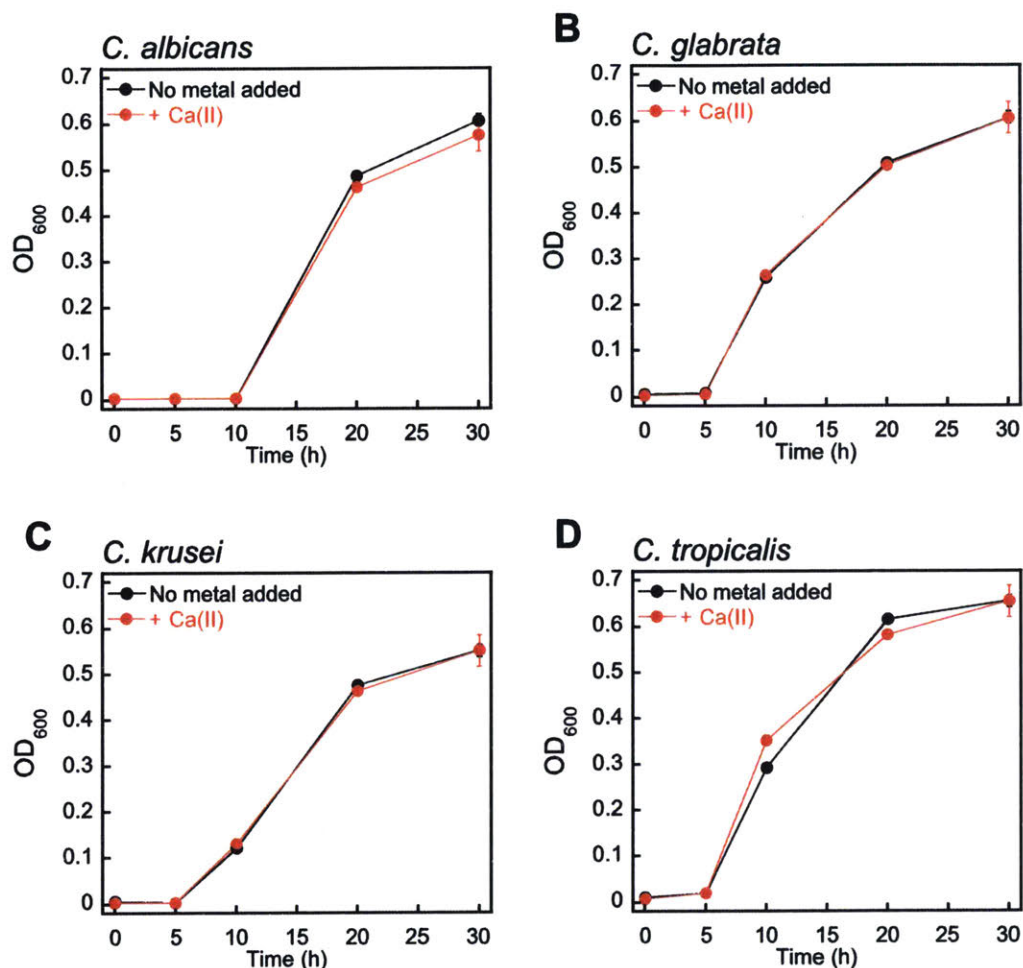


Figure 2. 7. Growth curves of *C. albicans* SC 5314 (A), *C. glabrata* ATCC 200918 (B), *C. krusei* ATCC 200917 (C) and *C. tropicalis* ATCC MYA-3404 (D) in the absence (black trace) and presence (red trace) of a 2-mM Ca(II) supplement (mean \pm SEM, $n = 3$).

S100A12 also displayed Ca(II)-dependent growth inhibitory activity against *C. krusei*, *C. glabrata*, and *C. tropicalis* (Figure 2. 8B-D). As observed for *C. albicans*, the presence of the Ca(II) supplement enhanced the antifungal activity of S100A12 against these three strains. Moreover, strain-to-strain variability in S100A12-mediated growth inhibition occurred in both the absence and presence of the Ca(II) supplement. In the absence of a Ca(II) supplement, *C. albicans* and *C. glabrata* were more susceptible to S100A12 than *C. krusei* and *C. tropicalis*. Indeed, neither

C. krusei nor *C. tropicalis* exhibited growth inhibition in the presence of 500 $\mu\text{g/mL}$ S100A12 when the Ca(II) supplement, was omitted, whereas *C. albicans* and *C. glabrata* growth was inhibited to varying degrees at this S100A12 concentration. Taken together, these data establish that (i) S100A12 exhibits *in vitro* antifungal activity against a number of *Candida* strains, (ii) enhanced fungal growth inhibition occurs under conditions of high Ca(II), and (iii) the susceptibility of *Candida* spp. to S100A12 is strain-dependent.

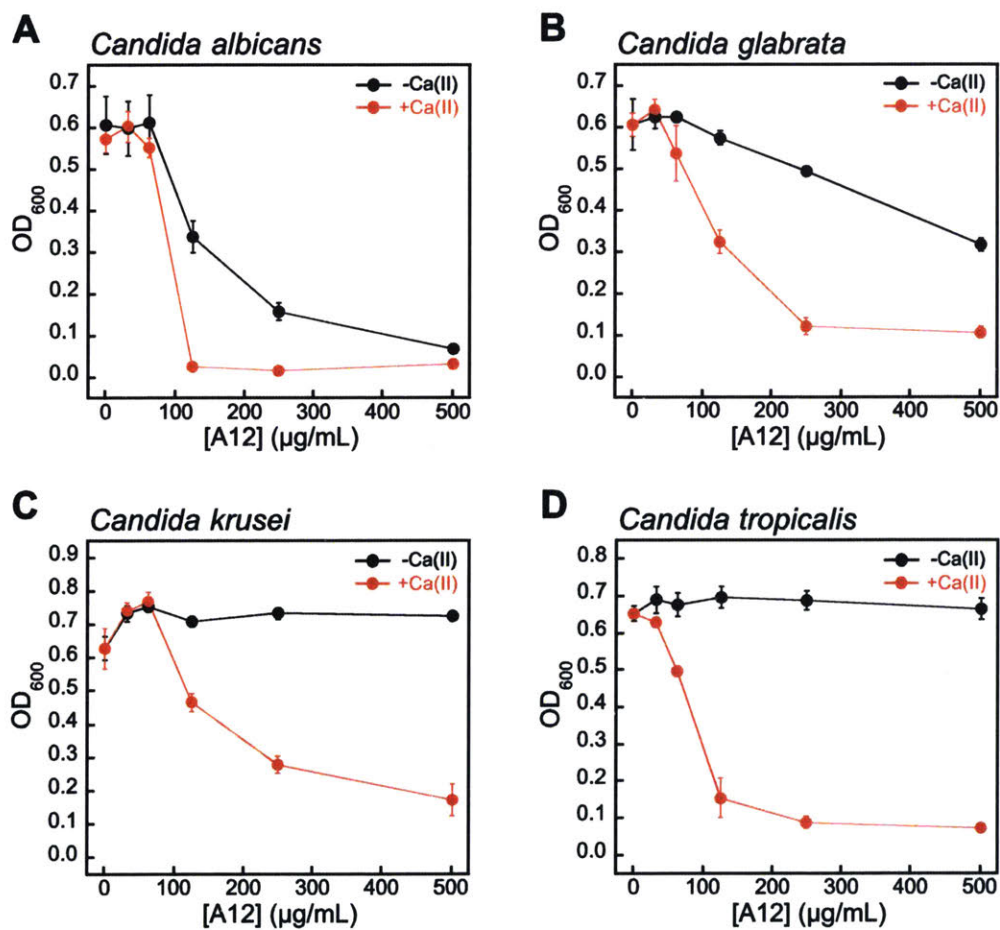


Figure 2. 8. Human S100A12 exhibits Ca(II)-dependent antifungal activity in mixed Tris:YPD medium. (A) *C. albicans* SC 5314, (B) *C. glabrata* ATCC 200918, (C) *krusei* ATCC 200917, and (D) *C. tropicalis* ATCC MYA-3404. Black, *Candida* spp. treated with S100A12 in the absence of a Ca(II) supplement. Red, *Candida* spp. treated with S100A12 in the presence of a $\approx 2\text{-mM}$ Ca(II) supplement. The OD₆₀₀ values were recorded at $t = 30$ h (mean \pm SEM, $n = 3$).

2. 4. 4. The His₃Asp Motifs Are Essential for Antifungal Activity

We reasoned that the Ca(II)-dependent antifungal activity of S100A12 results from Zn(II) sequestration. We performed two additional assays to test this hypothesis and evaluate the requirement of the His₃Asp sites for the antifungal activity against *C. albicans*. First, to determine whether the His₃Asp sites are essential, we compared the antifungal activity of S100A12 and the Δ His₃Asp variant (Figure 2. 9A). This assay revealed that S100A12 Δ His₃Asp (1 mg/mL, +Ca) has no effect on *C. albicans* growth relative to the untreated control. To confirm that the antifungal activity originates from apo His₃Asp sites of S100A12 and not a transition-metal-bound form, we pre-incubated S100A12 with two equivalents of Zn(II) to obtain Zn(II)-S100A12. Similar to the Δ His₃Asp variant, Zn(II)-S100A12 (125 μ g/mL, +Ca) did not inhibit *C. albicans* growth (Figure 2. 9B).

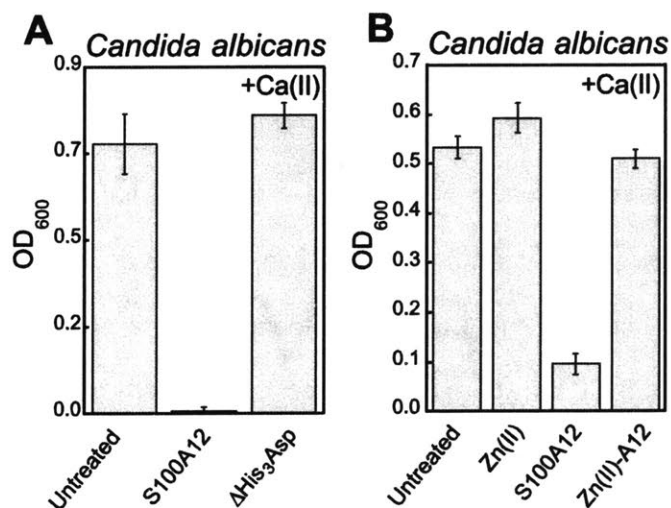


Figure 2. 9. The His₃Asp motifs of S100A12 are essential for antifungal activity against *C. albicans*. (A) Antifungal activity of 1000 μ g/mL S100A12 and S10012 Δ His₃Asp (t = 20 h, mean \pm SEM, n = 3). (B) Antifungal activity of 125 μ g/mL S100A12 and Zn(II)-S100A12 (t = 30 h, mean \pm SEM, n = 3). The Zn(II)-S100A12 sample was prepared by pre-incubating S100A12 with 2 equiv. of Zn(II) (11.9 μ M) prior to the assay. The bar labeled "Zn(II)" indicates the growth of a culture where 11.9 μ M Zn(II) was added to the Tris:YPD medium. For each assay, the Tris:YPD medium contained a \approx 2-mM Ca(II) supplement.

A comparison of the S100A12 concentrations (125 $\mu\text{g}/\text{mL}$, $\approx 5 \mu\text{M}$ S100A12 or $\approx 10 \mu\text{M}$ His₃Asp sites) required for maximum antifungal activity with the Zn(II) content ($\approx 7 \mu\text{M}$) in the Tris:YPD medium is informative. This comparison indicates that an excess of Zn(II)-binding sites relative to the Zn(II) content in the growth medium is required for S100A12 to exert its full growth inhibitory activity against *Candida* spp. under these assay conditions. The metal depletion studies indicated that 125 $\mu\text{g}/\text{mL}$ S100A12 reduces the Zn level in Tris:YPD to baseline ($\approx 620 \text{ nM}$) when Ca(II) is present in the medium. Taken together, these observations suggest that the *Candida* strains evaluated in this work compete with S100A12 for Zn(II) available in the growth medium.

2. 4. 5. Human S100A12 Exhibits Strain-Specific Antibacterial Activity

To further evaluate the *in vitro* antibacterial activity of human S100A12, we examined its growth inhibitory activity against a panel of five bacterial strains that included *E. coli* K-12, *Pseudomonas aeruginosa* PAO1, *S. aureus* ATCC 25923, *Listeria monocytogenes* ATCC 19115, and *Lactobacillus plantarum* WCSF1. Because a prior investigation reported that S100A12 lacked antibacterial activity against *S. aureus* Neuman,³² we screened for bacterial growth inhibition using a high concentration (1000 $\mu\text{g}/\text{mL}$) of S100A12 in Tris:TSB or Tris:MRS (for *L. plantarum* only) medium with or without a $\approx 2\text{-mM}$ Ca(II) supplement (Figure 2. 10). In agreement with prior work,³² we observed that S100A12 ($\pm\text{Ca}$) had no effect on *S. aureus* growth. Likewise, S100A12 afforded negligible growth inhibition for *E. coli* K-12 or *P. aeruginosa* PAO1. In contrast, cultures of *L. monocytogenes* and *L. plantarum* treated with S100A12 exhibited Ca(II)-dependent growth inhibition. Negligible growth of *L. monocytogenes* occurred, and the growth of *L. plantarum* was markedly attenuated, when the medium contained the Ca(II) supplement. On the basis of the metal depletion studies, we reason that the strains susceptible to S100A12 are more sensitive to Zn(II) deprivation. Future studies are required to address this notion on a strain-by-strain basis. We note that the inhibited growth of *L. plantarum* by S100A12 is in general agreement with our

prior work, which found that the His₃Asp site of calprotectin accounts for the full antibacterial activity against this strain *in vitro*.³⁰ Moreover, the negligible activity of S100A12 against *S. aureus* and *E. coli* is reminiscent of the calprotectin Δ His₄ variant, which only has a His₃Asp site at the S100A8/S100A9 interface and exhibits attenuated antibacterial activity against *S. aureus* and *E. coli* in mixed Tris:TSB medium.^{28, 32}

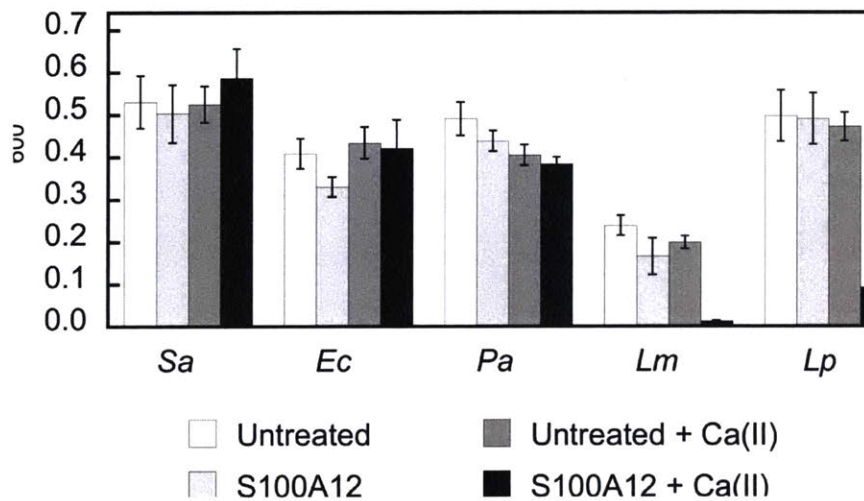


Figure 2. 10. Antibacterial activity of human S100A12 (1000 μ g/mL) against *S. aureus* ATCC 25923 (*Sa*), *E. coli* K-12 (*Ec*), *P. aeruginosa* PAO1 (*Pa*), *L. monocytogenes* ATCC 19115 (*Lm*), and *L. plantarum* WSCF1 (*Lp*) in the absence and presence of a \approx 2-mM Ca(II) supplement. The assays were performed in mixed Tris:TSB medium ($t = 20$ h, $T = 30$ °C).

2. 4. 6. Bacteria with Defective Zinc Acquisition Machinery Are Susceptible to S100A12

To evaluate whether bacterial strains with defective Zn(II) uptake machinery exhibit enhanced susceptibility to S100A12, we performed antibacterial activity assays with Δ *znuA* mutants of *E. coli* K-12 and *P. aeruginosa* PAO1 obtained from the Keio Collection⁵¹ and Seattle *Pseudomonas aeruginosa* PAO1 Transposon Mutant Library,⁵² respectively. ZnuABC is a high-affinity Zn(II) uptake system employed by Gram-negative bacteria.⁵³⁻⁵⁶ ZnuA is the periplasmic Zn(II)-binding protein that captures Zn(II) and delivers the ion to ZnuBC, which are located in the

inner membrane.⁵⁷ Bacterial strains with defective ZnuABC transport machinery are more susceptible to Zn(II) deprivation than their native counterparts.^{54,58} Indeed, S100A12 completely attenuated the growth of *E. coli* $\Delta znuA$ at 125 $\mu\text{g/mL}$ in both the absence and presence of a Ca(II) supplement (Figure 2. 11). *P. aeruginosa* $\Delta znuA$ also exhibited enhanced sensitivity to S100A12; however, the growth inhibition was only partial and required the presence of Ca(II) in the medium (Figure 2. 12). A similar observation was reported in studies examining the *in vitro* antimicrobial activity of calprotectin against *P. aeruginosa* PA14.⁵⁶ In this prior work, calprotectin did not provide complete growth inhibition of the wild-type strain or $\Delta znuA$ mutant, but the growth of the $\Delta znuA$ strain was impaired relative to the wild-type strain.⁵⁶ These results afforded a new hypothesis where *P. aeruginosa* PA14 has additional and as-yet undiscovered Zn(II) acquisition machinery that allows for Zn(II) uptake in the absence of ZnuA.⁵⁶ Subsequent investigations of *P. aeruginosa* PAO1 and a $\Delta znuA$ strain cultured under conditions of low Zn(II) revealed the expression of genes associated with additional import pathways associated with Zn(II) acquisition as well as up-regulation of genes that encode Zn(II)-independent proteins, which prokaryotes can employ in place of Zn(II)-containing proteins when Zn(II) is limited (e.g., Zn(II)-independent ribosomal proteins).⁵⁹ The current results with S100A12 are also consistent with these studies.

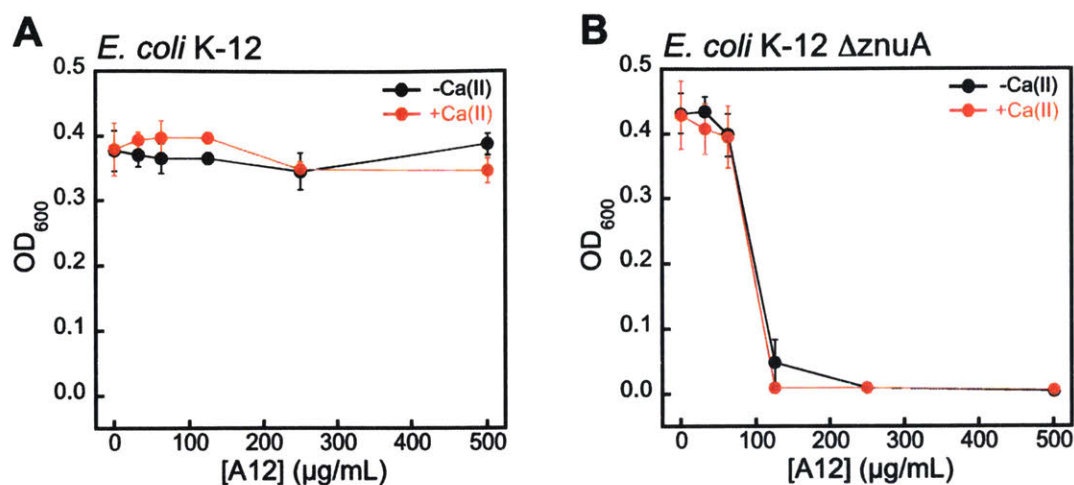


Figure 2. 11. S100A12 exhibits antibacterial activity against *E. coli* with defective Zn(II) uptake machinery in Tris:TSB medium. (A) Antibacterial activity of S100A12 against *Escherichia coli* K-12. (B) Antibacterial activity of S100A12 against *E. coli* K-12 ΔznuA. Black, *E. coli* treated with S100A12 in the absence of a Ca(II) supplement. Red, *E. coli* treated with S100A12 in the presence of ≈2 mM Ca(II). The OD₆₀₀ values were recorded at t = 20 h (mean ± SEM, n = 3).

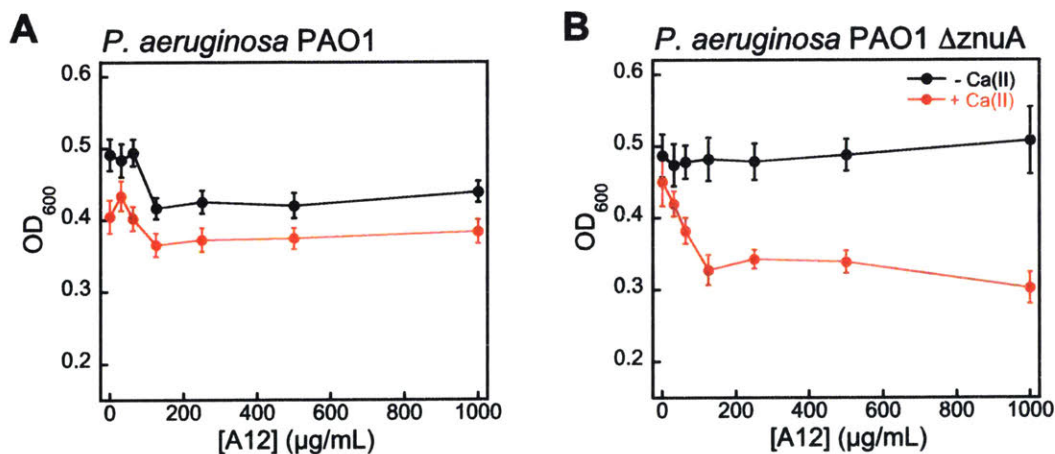


Figure 2. 12. *P. aeruginosa* PAO1* antimicrobial activity data for S100A12 in the absence (black) and presence (red) of a 3 mM Ca(II) supplement, t = 20 h (mean ± SEM, n = 3).

* The *znuA* gene is not annotated in the Seattle *Pseudomonas aeruginosa* PAO1 Mutant Library. The *znuA* gene was found by searching “znuA” at pseudomonas.com. Gene with locus tag PA5498 is annotated with the name “znuA.” BLAST analysis revealed that this gene is a homologue to other *znuA* genes. The Seattle *Pseudomonas aeruginosa* PAO1 Transposon Mutant Library was searched and five strains with a *znuA* mutation were found. One of these strains (mutant: phoAbp01q2A01, gene: PA5498) was employed in this study. The sequence of the ZnuA protein deduced from gene PA5498 for *P. aeruginosa* PAO1 was blasted against two proteins identified as ZnuA transporters (accession numbers EOT09947 and EOT14059) in *P. aeruginosa* PA14. ZnuA PA5498 was found to share 100% and 72% sequence homology with the

ZnuA proteins EOT09947 and EOT14059, respectively. A recent report also identified PA5498 as ZnuA.¹⁰

2. 4. 7. *Human S100A12 Is a High-Affinity Zinc Chelator*

The metal-depletion and antimicrobial activity assays presented in this work indicate that S100A12 coordinates Zn(II) with sufficient affinity to sequester the ion and that Ca(II) ions accentuate this function. Prior studies have examined the Zn(II)-binding properties of S100A12 in solution. In seminal characterization of porcine S100A12, metal-binding titrations that monitored the intrinsic fluorescence of S100A12 revealed stoichiometric Zn(II) binding ($K_{d,Zn} \leq 10$ nM).³ More recently, intrinsic fluorescence was employed to study Zn(II) chelation by human S100A12.²⁶ In this work, titration of human S100A12 with Zn(II) resulted in a gradual change in protein emission, and this titration curve was fit to afford $K_{d,Zn}$ values of 16 and 83 μ M for the two His₃Asp sites.²⁶ It was difficult for us to reconcile how the Zn(II) dissociation constants for these two orthologues could vary by several orders of magnitude, and our conclusions from the metal-depletion studies and antifungal activity assays are contradicting the prior study of the human orthologue. As a consequence, we decided to further evaluate the metal-binding properties of human S100A12 in solution using techniques we employed to characterize the Zn(II)-binding properties of calprotectin.²⁸

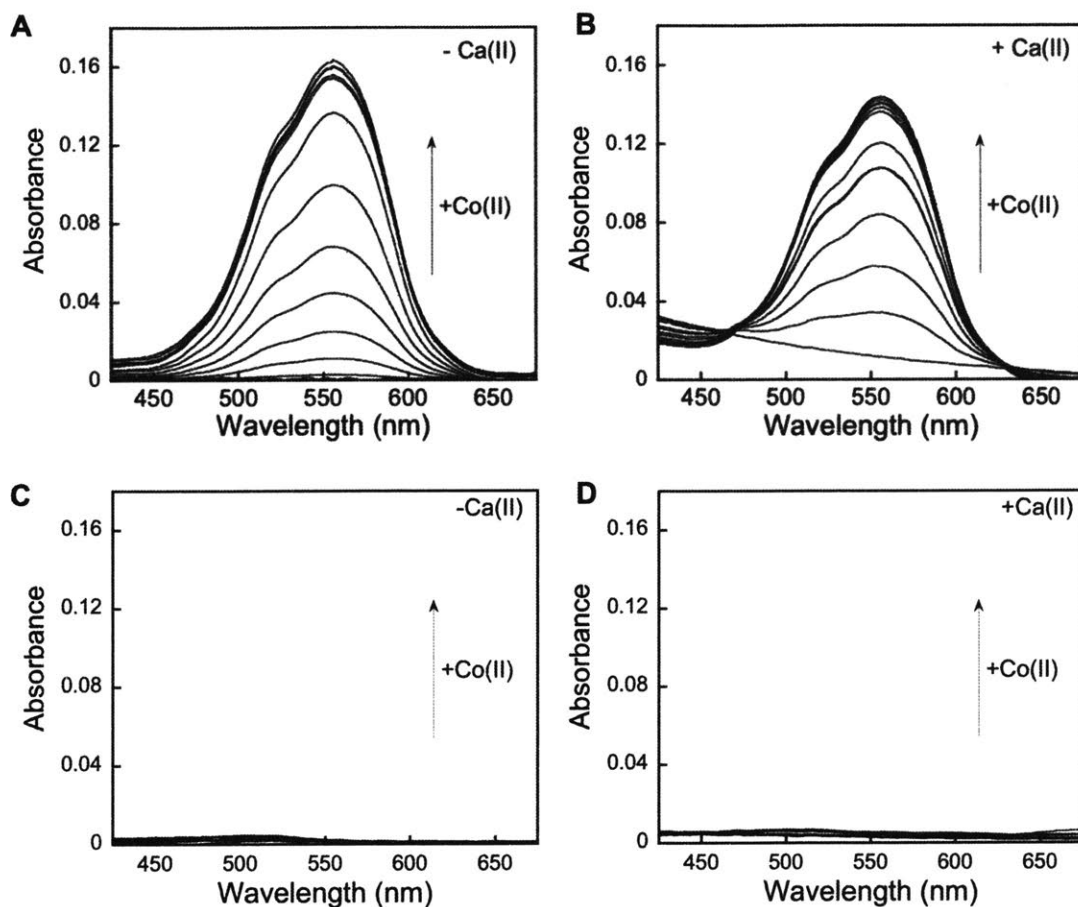


Figure 2. 13. Optical absorption spectra of S100A12 (200 μM) titrated with 0–4 equiv. of Co(II) at pH 7.0 (75 mM HEPES, 100 mM NaCl) and 25 $^{\circ}\text{C}$, in the absence (A) and presence (B) of 40 equiv. of Ca(II). Optical absorption spectra of S100A12 $\Delta\text{His}_3\text{Asp}$ (200 μM) titrated with 0–4 equiv. of Co(II) at pH 7.0 (75 mM HEPES, 100 mM NaCl) and 25 $^{\circ}\text{C}$, in the absence (C) and presence (D) of 40 equiv. of Ca(II).

We first employed Co(II) as a probe for the His₃Asp sites because it exhibits rich spectroscopic properties as a result of its $3d^7$ electronic configuration.⁶⁰ Addition of Co(II) to S100A12 caused the solution to change from colorless to pink (75 mM HEPES, 100 mM NaCl, pH 7.0), and the optical absorption spectrum of Co(II)-S100A12 exhibited ligand field transitions centered at 563 nm ($\epsilon = 820 \text{ M}^{-1}\text{cm}^{-1}$) (Figure 2. 13). This spectroscopic signature is reminiscent of four- or five-coordinate Co(II) species,⁶⁰ including Co(II)-calprotectin where the optical features

in the $d-d$ range are dominated by Co(II) bound at the His₃Asp site.²⁸ Moreover, Co(II)-binding titrations revealed that the intensity of this signal increased until two equivalents of Co(II) per S100A12 homodimer were added. The sharp inflection point indicates a 2:1 Co(II)/S100A12 stoichiometry (Figure 2. 14A), in agreement with two His₃Asp sites per homodimer. As expected, when the Co(II)-binding studies were repeated with the S100A12 Δ His₃Asp variant, no change in the absorbance spectrum due to Co(II) binding was observed (Figure 2. 13C, 13D, Figure 2. 14B). These results confirm that the His₃Asp motifs in S100A12 are required for transition-metal binding. The Co(II)-binding studies were performed in the absence and presence of excess Ca(II) and comparable spectra were obtained under both sets of conditions (Figure 2. 13, Figure 2. 14).

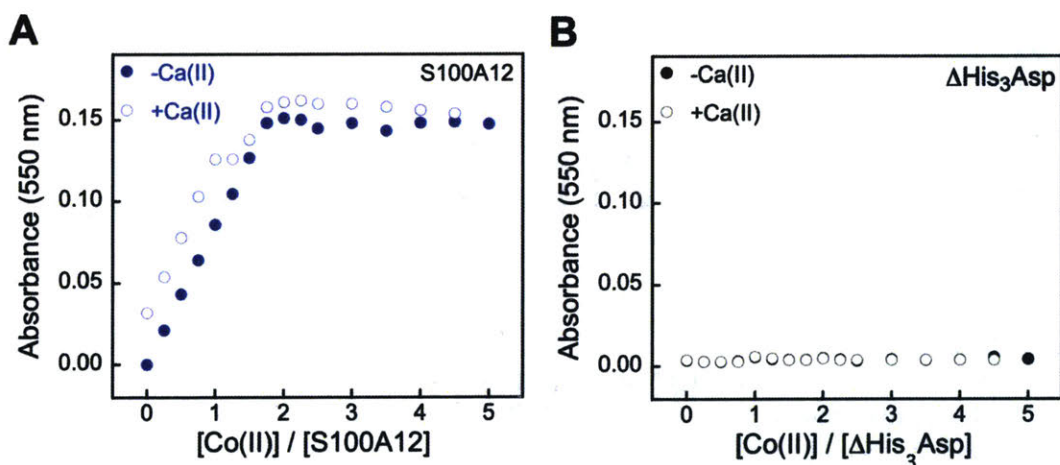


Figure 2. 14. (A) Plot of absorbance at 550 nm versus equivalents of Co(II) added for titration of S100A12 (200 μ M) in the absence and presence of 40 equiv. of Ca(II). (B) Plot of absorbance at 550 nm versus equivalents of Co(II) added for titration of Δ His₃Asp (200 μ M) in the absence and presence of 40 equiv. of Ca(II).

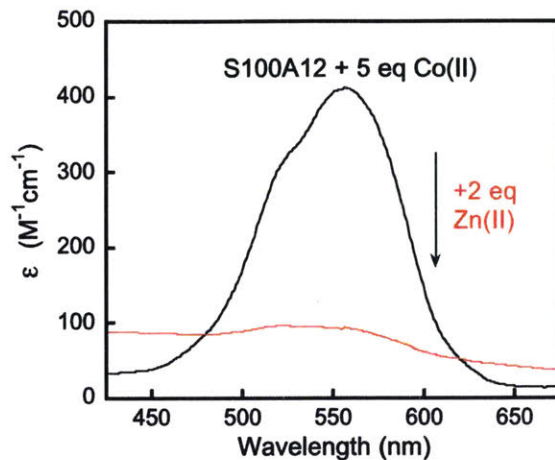


Figure 2. 15. Optical absorption spectra showing displacement of Co(II) from 200 μM S100A12 by Zn(II) addition at pH 7.0 (75 mM HEPES, 100 mM NaCl) and $T = 25^\circ\text{C}$. The increase in baseline with Zn(II) addition indicates the formation of some precipitate.

Addition of Zn(II) to Co(II)-S100A12 resulted in loss of the absorption feature (Figure 2. 15), which indicates that S100A12 binds Zn(II) with higher affinity than Co(II). This behavior is expected based on the Irving-Williams series.⁶¹ To confirm the Zn(II)-S100A12 stoichiometry and further investigate the Zn(II) affinity, we successfully competed S100A12 with three different chromophoric Zn(II) chelators. Zincon is a colorimetric Zn(II) indicator with a dissociation constant in the micromolar range ($K_{d,Zn} \approx 10 \mu\text{M}$).³⁵⁻³⁶ In both the absence and presence of excess Ca(II), no change in Zincon absorbance occurred until after two equivalents of Zn(II) per S100A12 homodimer were added, demonstrating that S100A12 outcompeted Zincon for Zn(II) (Figure 2. 16). These titrations confirmed the expected 2:1 Zn(II):S100A12 homodimer stoichiometry and indicated that S100A12 coordinates Zn(II) with sub-micromolar affinity. Next, we examined the competition of S100A12 with the fluorescent Zn(II) sensors MF2 ($K_{d,Zn} \approx 20 \text{nM}$)^{37,38} and FluoZin-3 ($K_{d,Zn} = 9 \text{nM}$).³⁹ These experiments were performed only in the absence of Ca(II) because both MF2 and FZ3 exhibit a fluorescence response to this divalent cation. S100A12 outcompeted MF2 (Figure 2. 17) as well as FZ3 (Figure 2. 18), suggesting that S100A12 coordinates two equivalents

of Zn(II) with low- or sub-nanomolar affinity in the absence of Ca(II). Taken together, the outcomes of these Zn(II) competition titrations are in general agreement with prior characterization of porcine S100A12 where stoichiometric Zn(II) binding ($K_{d,Zn} < 10$ nM) was observed,³ as well as the metal-depletion studies presented in this work.

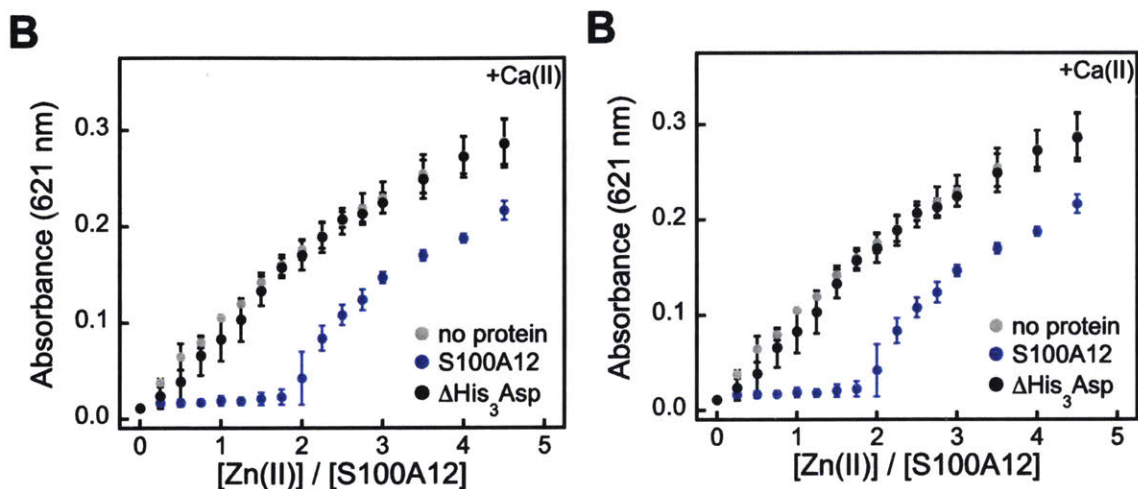


Figure 2. 16. Response of Zincon (20 μ M) to Zn(II) in the presence of S100A12 or Δ His₃Asp (10 μ M) and in the absence (A) and presence of 400 μ M Ca(II) (B) at pH 7.0 (75 mM HEPES, 100 mM NaCl) and 25 $^{\circ}$ C (mean \pm SDM, $n=3$). The Zn(II)-Zincon complex exhibits an absorbance maximum at 621 nm.

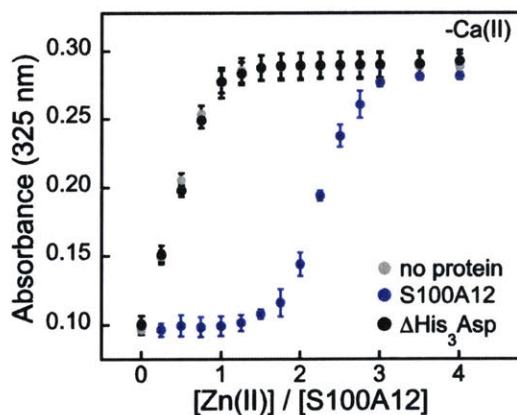


Figure 2. 17. S100A12 metal-binding titrations. Response of MF2 (10 μ M) to Zn(II) in the presence of S100A12 or Δ His₃Asp (10 μ M) at pH 7.0 (75 mM HEPES, 100 mM NaCl) and 25 $^{\circ}$ C (mean \pm SDM, $n=3$). The Zn(II)-MF2 complex absorbs at 325 nm.

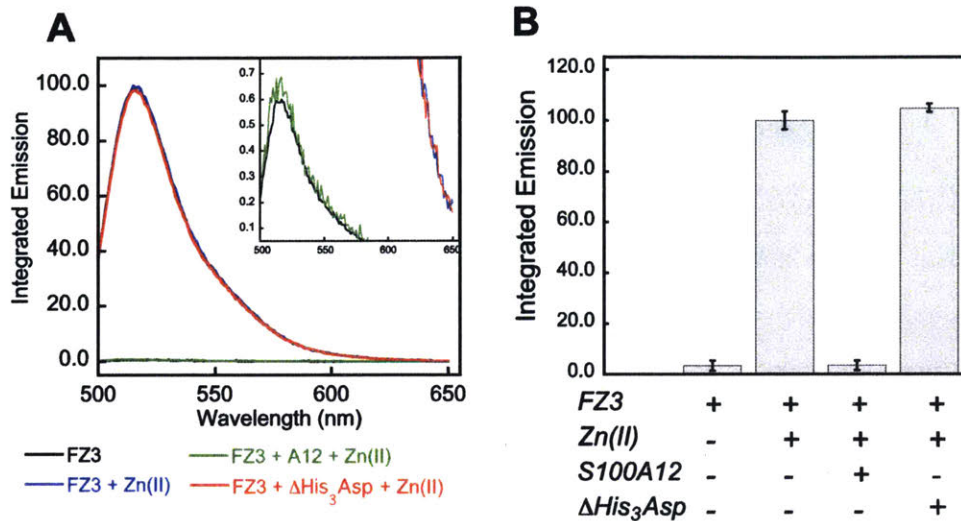


Figure 2. 18. S100A12 outcompetes FZ3 for Zn(II). Fluorescence response of 2 μ M FZ3 to 2 μ M Zn(II) in the presence of 2 μ M S100A12 or Δ His₃Asp at pH 7.0 (75 mM HEPES, 100 mM NaCl) and 25 °C. (A) An \approx 36-fold fluorescent enhancement is observed for FZ3 in the absence of protein (blue trace) and in the presence of Δ His₃Asp (red trace) upon addition of 1 equiv. of Zn(II). Negligible fluorescent response is observed for FZ3 in the presence of S100A12 (green trace) upon addition of 1 equiv. of Zn(II) (Inset: Expansion of the y-axis). (B) integrated emission values for the data presented in panel A and replicates. The maximum emission for FZ3 in the presence of 1 equiv. of Zn(II) was normalized to an integrated emission value of 100, and the remaining emission spectra were scaled accordingly (mean \pm SEM, $n=3$).

The metal depletion studies and antimicrobial activity assays indicate that the Zn(II)-binding properties of S100A12 are modulated by Ca(II) ions. In prior studies of the Zn(II)-binding properties of human calprotectin, we employed a Ca(II)-insensitive Zn(II) sensor named Zinpyr-4 (ZP4, $K_{d,Zn} = 650$ pM),⁶² and discovered that CP exhibits enhanced Zn(II) affinity in the presence of Ca(II).²⁸ We sought to employ the same strategy to further elucidate how Ca(II) modulates Zn(II) chelation by S100A12; however, our preliminary S100A12/ZP4 experiments were plagued by artifacts that precluded using ZP4 in a quantitative or reliable manner (data not shown). In particular, mixtures of ZP4, S100A12 and Zn(II) exhibited unstable emission. The origin of this confounding behavior is unclear, and various issues can arise when employing competitors in

metal-binding titrations.⁶³ We note that formation of the Zn(II)-S100A12 complex contributed to the problem because stable emission was observed for ZP4/S100A12/Zn(II) mixtures that contained the Δ His₃Asp variant. As a result, it is possible that (i) formation of ternary complexes involving Zn(II)-bound S100A12 and ZP4 occurred, and/or (ii) Zn(II)-dependent oligomerization of S100A12 causes ZP4 to associate with the protein. Regarding the latter scenario, the self-association properties of S100A12 are complex. Zinc binding is reported to cause the homodimer to self-associate and form tetramers and hexamers,²⁶ and the Zn(II)-S100A12 crystal structure revealed exposure of a hydrophobic patch with Zn(II) binding.²⁵ On the basis of the metal-depletion studies and antimicrobial activity assays, we expect that the presence of Ca(II) ions increases the binding affinity of S100A12 for Zn(II), as we discovered for calprotectin,²⁸ and as yet unidentified competitors or alternative methods are required to probe this notion further.

2. 5. Summary and Outlook

This work informs current understanding of how S100A12 contributes to metal homeostasis and innate immunity. We present the discovery that S100A12 uses Ca(II) ions to modulate its Zn(II)-sequestering properties and antimicrobial activity. We also report the discovery that S100A12 has *in vitro* antifungal activity. We hypothesize this activity results from the fungi succumbing to Zn(II) deprivation. These studies provide a guide for future investigations of human S100A12 in the contexts of the host/microbe interaction, metal homeostasis, and innate immunity.

S100A12 is co-packaged with its fellow metal-sequestering S100 protein calprotectin in the cytoplasm of human neutrophils, which indicates that the proteins are co-released at sites of infection and inflammation. Our current work illuminates similarities and differences between the metal-chelating properties of these two human S100 proteins. Both employ Ca(II) ions to tune the affinities for transition metal ions, which are bound at sites that form at the interface between two subunits. The heterooligomeric nature of calprotectin affords two different sites at the S100A8/S100A9 interface.⁶⁴ One site is a His₃Asp motif similar to the sites of S100A12, whereas

the other is an unusual histidine-rich motif. Like S100A12, the His₃Asp site of calprotectin binds Zn(II) with high affinity and has markedly lower affinity for Mn(II) and Fe(II).²⁸⁻³⁰ The histidine-rich motif was first identified as a His₄ motif in the crystal structure of Ca(II)-bound calprotectin and later determined to provide a hexahistidine coordination environment for Mn(II) and Fe(II).^{30,32-33} ⁶⁵ The histidine-rich site coordinates Mn(II), Fe(II) and Zn(II) with high affinity and the metal selectivity of this site (Mn(II) < Fe(II) < Zn(II)) is in agreement with the Irving-Williams series.⁶¹ We recently proposed that kinetics also contribute to metal sequestration at this site, enabling calprotectin to retain bound Mn(II) and Fe(II).³⁰ On the basis of the current studies, we now question whether Zn(II) chelation by S100A12 reduces the Zn(II) available for capture by calprotectin in the extracellular milieu and thereby boosts the ability of calprotectin to capture other nutrient metals like Mn(II) and Fe(II) at the His₆ site.

S100A12 is often described as a Cu(II)- and Zn(II)-chelating protein, as evidenced by crystallographic characterization (Figure 2. 1). The Tris:YPD and Tris:TSB growth medium employed in the metal depletion studies contains markedly greater levels of Zn ($\approx 5 \mu\text{M}$) relative to Cu ($\approx 100 \text{ nM}$), and we observed negligible depletion of Cu for either medium as a result of S100A12 treatment. This latter result may stem from the relative metal concentrations in the growth medium, and additional investigations are required to clarify the origin of this observation. In particular, investigations of Cu(II)-S100A12 are limited and the Cu(II) affinity of S100A12 is unknown, making further solution studies of copper binding to S100A12 an important avenue for future work. We note here that a proposal in which Cu-S100A12 generates reactive oxygen species and thereby affords anti-parasitic activity has been put forth.^{24,27} To the best of our knowledge, the reported experimental support for this proposal is insufficient and limited to the fact that S100A12 can bind Cu(II).

From the perspective of human S100A12 structure and function, the results presented in this work augment prior studies that evaluated the biophysical properties of this protein. The reported solution studies and crystallographic characterization of apo and metal-bound S100A12

delineate that the protein has the capacity to exist in many different states.²²⁻²⁷ This complex speciation may give S100A12 functional diversity that is important for cell signaling and the immune response.^{18,26,66} The data presented in this work that reveal S100A12 uses Ca(II) binding to its EF-hand domains to tune its Zn(II)-chelating properties at the His₃Asp sites add another dimension to this behavior. This observation is reminiscent of studies of porcine S100A12, which showed that the presence of Zn(II) increased the Ca(II) affinity by several orders of magnitude.³

Conditions of high Ca(II) enhance the Zn(II)-sequestering ability and antimicrobial activities of S100A12. These observations support a model whereby S100A12 responds to local Ca(II) concentrations to tune its Zn(II)-binding properties and are consistent with its function as an extracellular Zn(II)-chelating protein. The extracellular space contains Ca(II) ions at concentrations that are orders of magnitude greater than those found in the cytoplasm of resting cells.⁶⁷ We reason that the low Ca(II) levels in resting neutrophils allow S100A12 to maintain an apo state in the cytoplasm, and the high Ca(II) levels in the extracellular space allow S100A12 to sequester Zn(II) once it is deployed at a site of infection or inflammation. In prior work, we put forth the same model for the behavior of calprotectin. Whether this model is general for all S100 proteins that chelate transition metals at interfacial sites is a topic for future investigation.

2. 6. Acknowledgements

This work was supported by the NSF (CHE-1352132) and the NIH (1DP2OD007045). We thank Dr. M. B. Brophy and Mr. T. G. Nakashige for helpful discussions, Mr. T. G. Nakashige for identifying the *P. aeruginosa* $\Delta znuA$ mutant, Ms. H. Flaxman for preparing pET41a-S100A12(H15A)(D25A)(H85A)(H89A), Dr. B. Vincent and Prof. S. Lindquist for helpful advice about the fungal pathogens, Dr. Koli Taghizadeh for assistance with the ICP-MS instrumentation at MIT, and Mr. Rudiger Laufhutte for performing some of the ICP-MS analyses and the ICP- OES analyses at UIUC. The ICP-MS instrument is housed in the MIT Center for Environmental Health Sciences Bioanalytical Core supported by NIH grant P30-ES002109. The *E. coli* K-12 and $\Delta znuA$

strains were obtained from the Keio Collection.⁵¹ The *P. aeruginosa* PAO1 and $\Delta znuA$ strains were obtained from the Seattle *Pseudomonas aeruginosa* PAO1 Transposon Mutant Library.

2. 7. References

1. Nathan, C., Neutrophils and immunity: challenges and opportunities. *Nat. Rev. Immunol.* **2006**, 6 (3), 173-182.
2. Bardoel, B. W.; Kenny, E. F.; Sollberger, G.; Zychlinsky, A., The balancing act of neutrophils. *Cell Host Microbe* **2014**, 15 (5), 526-536.
3. Dell'Angelica, E. C.; Schleicher, C. H.; Santomé, J. A., Primary structure and binding properties of calgranulin C, a novel S100-like calcium-binding protein from pig granulocytes. *J. Biol. Chem.* **1994**, 269 (46), 28929-28936.
4. Guignard, F.; Mauel, J.; Markert, M., Identification and characterization of a novel human neutrophil protein related to the S100 family. *Biochem. J.* **1995**, 309 395-401.
5. Gottsch, J. D.; Liu, S. H.; Minkovitz, J. B.; Goodman, D. F.; Srinivasan, M.; Stark, W. J., Autoimmunity to a cornea-associated stromal antigen in patients with Mooren's ulcer. *Invest. Ophthalmol. Vis. Sci.* **1995**, 36 (8), 1541-1547.
6. Gottsch, J. D.; Liu, S. H., Cloning and expression of bovine corneal antigen cDNA. *Curr. Eye Res.* **1997**, 16 (12), 1239-1244.
7. Gottsch, J. D.; Stark, W. J.; Liu, S. H., Cloning and sequence analysis of human and bovine corneal antigen (CO-Ag) cDNA: identification of host-parasite protein calgranulin C. *Trans. Am. Ophthalmol. Soc.* **1997**, 95, 111-125; discussion 126-129.
8. Hitomi, J.; Yamaguchi, K.; Kikuchi, Y.; Kimura, T.; Maruyama, K.; Nagasaki, K., A novel calcium-binding protein in amniotic fluid, CAAF1: its molecular cloning and tissue distribution. *J. Cell Sci.* **1996**, 109 805-815.

9. Marti, T.; Erttmann, K. D.; Gallin, M. Y., Host-parasite interaction in human onchocerciasis: identification and sequence analysis of a novel human calgranulin. *Biochem. Biophys. Res. Commun.* **1996**, *221* (2), 454-458.
10. Yamamura, T.; Hitomi, J.; Nagasaki, K.; Suzuki, M.; Takahashi, E.; Saito, S.; Tsukada, T.; Yamaguchi, K., Human CAAF1 gene—molecular cloning, gene structure, and chromosome mapping. *Biochem. Biophys. Res. Commun.* **1996**, *221* (2), 356-360.
11. Ilg, E. C.; Troxler, H.; Burgisser, D. M.; Kuster, T.; Markert, M.; Guignard, F.; Hunziker, P.; Birchler, N.; Heizmann, C. W., Amino acid sequence determination of human S100A12 (P6, calgranulin C, CGRP, CAAF1) by tandem mass spectrometry. *Biochem. Biophys. Res. Commun.* **1996**, *225* (1), 146-150.
12. Foell, D.; Kucharzik, T.; Kraft, M.; Vogl, T.; Sorg, C.; Domschke, W.; Roth, J., Neutrophil derived human S100A12 (EN-RAGE) is strongly expressed during chronic active inflammatory bowel disease. *Gut* **2003**, *52* (6), 847-853.
13. Kosaki, A.; Hasegawa, T.; Kimura, T.; Iida, K.; Hitomi, J.; Matsubara, H.; Mori, Y.; Okigaki, M.; Toyoda, N.; Masaki, H.; Inoue-Shibata, M.; Nishikawa, M.; Iwasaka, T., Increased plasma S100A12 (EN-RAGE) levels in patients with type 2 diabetes. *J. Clin. Endocrinol. Metab.* **2004**, *89* (11), 5423-5428.
14. Rouleau, P.; Vandal, K.; Ryckman, C.; Poubelle, P. E.; Boivin, A.; Talbot, M.; Tessier, P. A., The calcium-binding protein S100A12 induces neutrophil adhesion, migration, and release from bone marrow in mouse at concentrations similar to those found in human inflammatory arthritis. *Clin. Immunol.* **2003**, *107* (1), 46-54.
15. Shepherd, C. E.; Goyette, J.; Utter, V.; Rahimi, F.; Yang, Z.; Geczy, C. L.; Halliday, G. M., Inflammatory S100A9 and S100A12 proteins in alzheimer's disease. *Neurobiol. Aging* **2006**, *27* (11), 1554-1563.
16. Foell, D.; Seeliger, S.; Vogl, T.; Koch, H.-G.; Maschek, H.; Harms, E.; Sorg, C.; Roth, J., Expression of S100A12 (EN-RAGE) in cystic fibrosis. *Thorax* **2003**, *58* (7), 613-617.

17. Hofmann, M. A.; Drury, S.; Fu, C.; Qu, W.; Taguchi, A.; Lu, Y.; Avila, C.; Kambham, N.; Bierhaus, A.; Nawroth, P.; Neurath, M. F.; Slattery, T.; Beach, D.; McClary, J.; Nagashima, M.; Morser, J.; Stern, D.; Schmidt, A. M., RAGE mediates a novel proinflammatory axis: a central cell surface receptor for S100/calgranulin polypeptides. *Cell* **1999**, *97* (7), 889-901.
18. Xie, J.; Burz, D. S.; He, W.; Bronstein, I. B.; Lednev, I.; Shekhtman, A., Hexameric calgranulin C (S100A12) binds to the receptor for advanced glycated end products (RAGE) using symmetric hydrophobic target-binding patches. *J. Biol. Chem.* **2007**, *282* (6), 4218-42131.
19. Foell, D.; Wittkowski, H.; Kessel, C.; Luken, A.; Weinlage, T.; Varga, G.; Vogl, T.; Wirth, T.; Viemann, D.; Bjork, P.; van Zoelen, M. A.; Gohar, F.; Srikrishna, G.; Kraft, M.; Roth, J., Proinflammatory S100A12 can activate human monocytes via Toll-like receptor 4. *Am. J. Respir. Crit. Care Med.* **2013**, *187* (12), 1324-1334.
20. Haley, K. P.; Delgado, A. G.; Piazuolo, M. B.; Mortensen, B. L.; Correa, P.; Damo, S. M.; Chazin, W. J.; Skaar, E. P.; Gaddy, J. A., The human antimicrobial protein calgranulin C participates in control of *Helicobacter pylori* growth and regulation of virulence. *Infect. Immun.* **2015**, *83* (7), 2944-2956.
21. Gottsch, J. D.; Eisinger, S. W.; Liu, S. H.; Scott, A. L., Calgranulin C has filariacidal and filariastatic activity. *Infect. Immun.* **1999**, *67* (12), 6631-6636.
22. Moroz, O. V.; Antson, A. A.; Murshudov, G. N.; Maitland, N. J.; Dodson, G. G.; Wilson, K. S.; Skibshoj, I.; Lukanidin, E. M.; Bronstein, I. B., The three-dimensional structure of human S100A12. *Acta Crystallogr. D Biol. Crystallogr.* **2001**, *57* (Pt 1), 20-29.
23. Moroz, O. V.; Antson, A. A.; Dodson, E. J.; Burrell, H. J.; Grist, S. J.; Lloyd, R. M.; Maitland, N. J.; Dodson, G. G.; Wilson, K. S.; Lukanidin, E.; Bronstein, I. B., The structure of S100A12 in a hexameric form and its proposed role in receptor signalling. *Acta Crystallogr. D Biol Crystallogr.* **2002**, *58* (Pt 3), 407-413.

24. Moroz, O. V.; Antson, A. A.; Grist, S. J.; Maitland, N. J.; Dodson, G. G.; Wilson, K. S.; Lukanidin, E.; Bronstein, I. B., Structure of the human S100A12-copper complex: implications for host-parasite defence. *Acta Crystallogr. D Biol. Crystallogr.* **2003**, *59* (Pt 5), 859-867.
25. Moroz, O. V.; Blagova, E. V.; Wilkinson, A. J.; Wilson, K. S.; Bronstein, I. B., The crystal structures of human S100A12 in apo form and in complex with zinc: new insights into S100A12 oligomerisation. *J. Mol. Biol.* **2009**, *391* (3), 536-551.
26. Moroz, O. V.; Burkitt, W.; Wittkowski, H.; He, W.; Ianoul, A.; Novitskaya, V.; Xie, J.; Polyakova, O.; Lednev, I. K.; Shekhtman, A.; Derrick, P. J.; Bjoerk, P.; Foell, D.; Bronstein, I. B., Both Ca^{2+} and Zn^{2+} are essential for S100A12 protein oligomerization and function. *BMC Biochem.* **2009**, *10*, 11.
27. Moroz, O. V.; Dodson, G. G.; Wilson, K. S.; Lukanidin, E.; Bronstein, I. B., Multiple structural states of S100A12: A key to its functional diversity. *Microsc. Res. Tech.* **2003**, *60* (6), 581-592.
28. Brophy, M. B.; Hayden, J. A.; Nolan, E. M., Calcium ion gradients modulate the zinc affinity and antibacterial activity of human calprotectin. *J. Am. Chem. Soc.* **2012**, *134* (43), 18089-18100.
29. Hayden, J. A.; Brophy, M. B.; Cunden, L. S.; Nolan, E. M., High-affinity manganese coordination by human calprotectin is calcium-dependent and requires the histidine-rich site formed at the dimer interface. *J. Am. Chem. Soc.* **2013**, *135* (2), 775-787.
30. Nakashige, T. G.; Zhang, B.; Krebs, C.; Nolan, E. M., Human calprotectin is an iron-sequestering host-defense protein. *Nat. Chem. Biol.* **2015**, *11*, 765-771.
31. Lehrer, R. I.; Lu, W., alpha-defensins in human innate immunity. *Immunol. Rev.* **2012**, *245* (1), 84-112.
32. Damo, S. M.; Kehl-Fie, T. E.; Sugitani, N.; Holt, M. E.; Rathi, S.; Murphy, W. J.; Zhang, Y. F.; Betz, C.; Hench, L.; Fritz, G.; Skaar, E. P.; Chazin, W. J., Molecular basis for manganese sequestration by calprotectin and roles in the innate immune response to invading bacterial pathogens. *Proc. Natl. Acad. Sci. U. S. A.* **2013**, *110* (10), 3841-3846.

33. Brophy, M. B.; Nakashige, T. G.; Gaillard, A.; Nolan, E. M., Contributions of the S100A9 C-terminal tail to high-affinity Mn(II) chelation by the host-defense protein human calprotectin. *J. Am. Chem. Soc.* **2013**, *135* (47), 17804-17817.
34. Citiulo, F.; Jacobsen, I. D.; Miramon, P.; Schild, L.; Brunke, S.; Zipfel, P.; Brock, M.; Hube, B.; Wilson, D., *Candida albicans* scavenges host zinc via Pra1 during endothelial invasion. *PLoS Pathog.* **2012**, *8* (6), e1002777.
35. Maret, W.; Vallee, B. L., Thiolate ligands in metallothionein confer redox activity on zinc clusters. *Proc. Natl. Acad. Sci. U. S. A.* **1998**, *95* (7), 3478-3482.
36. Talmard, C.; Bouzan, A.; Faller, P., Zinc binding to amyloid-beta: isothermal titration calorimetry and zn competition experiments with zn sensors. *Biochemistry* **2007**, *46* (47), 13658-13666.
37. Simons, T. J. B., Measurement of Free Zn²⁺ ion concentration with the fluorescent-probe Mag-Fura-2 (Furaptra). *J. Biochem. Biophys. Methods* **1993**, *27* (1), 25-37.
38. Golynskiy, M. V.; Gunderson, W. A.; Hendrich, M. P.; Cohen, S. M., Metal binding studies and EPR spectroscopy of the manganese transport regulator MntR. *Biochemistry* **2006**, *45* (51), 15359-15372.
39. Krężel, A.; Maret, W., Dual nanomolar and picomolar Zn(II) binding properties of metallothionein. *J. Am. Chem. Soc.* **2007**, *129* (35), 10911-10921.
40. MacPherson, S.; Larochele, M.; Turcotte, B., A fungal family of transcriptional regulators: the zinc cluster proteins. *Microbiol. Mol. Biol. Rev.* **2006**, *70* (3), 583-604.
41. Du, H.; Guan, G.; Xie, J.; Sun, Y.; Tong, Y.; Zhang, L.; Huang, G., Roles of *Candida albicans* Gat2, a GATA-type zinc finger transcription factor, in biofilm formation, filamentous growth and virulence. *PLoS One* **2012**, *7* (1), e29707.
42. Amich, J.; Calera, J. A., Zinc acquisition: a key aspect in *Aspergillus fumigatus* virulence. *Mycopathologia* **2014**, *178* (5-6), 379-385.

43. Klimova, N.; Yeung, R.; Kachurina, N.; Turcotte, B., Phenotypic analysis of a family of transcriptional regulators, the zinc cluster proteins, in the human fungal pathogen *Candida glabrata*. *G3* **2014**, *4* (5), 931-940.
44. Simm, C.; Luan, C.-H.; Weiss, E.; O'Halloran, T., High-throughput screen for identifying small molecules that target fungal zinc homeostasis. *PLoS One* **2011**, *6* (9), e25136.
45. Kim, M.-J.; Kil, M.; Jung, J.-H.; Kim, J., Roles of Zinc-responsive transcription factor Csr1 in filamentous growth of the pathogenic yeast *Candida albicans*. *J. Microbiol. Biotechnol.* **2008**, *18* (2), 242-247.
46. Perlot, J.; Choi, B.; Spellberg, B., Nosocomial fungal infections: epidemiology, diagnosis, and treatment. *Med. Mycol.* **2007**, *45* (4), 321-346.
47. Mavor, A. L.; Thewes, S.; Hube, B., Systemic fungal infections caused by *Candida* species: epidemiology, infection process and virulence attributes. *Curr. Drug Targets* **2005**, *6* (8), 863-874.
48. Yokoyama, K.; Biswas, S. K.; Miyaji, M.; Nishimura, K., Identification and phylogenetic relationship of the most common pathogenic *Candida* species inferred from mitochondrial cytochrome b gene sequences. *J. Clin. Microbiol.* **2000**, *38* (12), 4503-4510.
49. Finkel, J. S.; Mitchell, A. P., Genetic control of *Candida albicans* biofilm development. *Nat. Rev. Microbiol.* **2011**, *9* (2), 109-118.
50. Cottier, F.; Pavelka, N., Complexity and dynamics of host-fungal interactions. *Immunol. Res.* **2012**, *53* (1-3), 127-135.
51. Baba, T.; Ara, T.; Hasegawa, M.; Takai, Y.; Okumura, Y.; Baba, M.; Datsenko, K. A.; Tomita, M.; Wanner, B. L.; Mori, H., Construction of *Escherichia coli* K-12 in-frame, single-gene knockout mutants: the Keio collection. *Mol. Syst. Biol.* **2006**, *2*, 2006 0008.
52. Jacobs, M. A.; Alwood, A.; Thaipisuttikul, I.; Spencer, D.; Haugen, E.; Ernst, S.; Will, O.; Kaul, R.; Raymond, C.; Levy, R.; Chun-Rong, L.; Guenther, D.; Bovee, D.; Olson, M. V.; Manoil,

- C., Comprehensive transposon mutant library of *Pseudomonas aeruginosa*. *Proc. Natl. Acad. Sci. U. S. A.* **2003**, *100* (24), 14339-14344.
53. Patzer, S. I.; Hantke, K., The ZnuABC high-affinity zinc uptake system and its regulator Zur in *Escherichia coli*. *Mol. Microbiol.* **1998**, *28* (6), 1199-1210.
54. Ammendola, S.; Pasquali, P.; Pistoia, C.; Petrucci, P.; Petrarca, P.; Rotilio, G.; Battistoni, A., High-Affinity Zn²⁺ Uptake system ZnuABC is required for bacterial zinc homeostasis in intracellular environments and contributes to the virulence of salmonella enterica. *Infect. Immun.* **2007**, *75*, 5867-5876.
55. Davis, L. M.; Kakuda, T.; DiRita, V. J., A *Campylobacter jejuni* znuA orthologue is essential for growth in low-zinc environments and chick colonization. *J. Bacteriol.* **2009**, *191* (5), 1631-1640.
56. D'Orazio, M.; Mastropasqua, M. C.; Cerasi, M.; Pacello, F.; Consalvo, A.; Chirullo, B.; Mortensen, B.; Skaar, E. P.; Ciavardelli, D.; Pasquali, P.; Battistoni, A., The capability of *Pseudomonas aeruginosa* to recruit zinc under conditions of limited metal availability is affected by inactivation of the ZnuABC transporter. *Metallomics* **2015**, *7* (6), 1023-1035.
57. Yatsunyk, L. A.; Easton, J. A.; Kim, L. R.; Sugarbaker, S. A.; Bennett, B.; Breece, R. M.; Vorontsov, I. I.; Tierney, D. L.; Crowder, M. W.; Rosenzweig, A. C., Structure and metal binding properties of ZnuA, a periplasmic zinc transporter from *Escherichia coli*. *J. Biol. Inorg. Chem.* **2008**, *13* (2), 271-288.
58. Liu, J. Z.; Jellbauer, S.; Poe, A. J.; Ton, V.; Pesciaroli, M.; Kehl-Fie, T. E.; Restrepo, N. A.; Hosking, M. P.; Edwards, R. A.; Battistoni, A.; Pasquali, P.; Lane, T. E.; Chazin, W. J.; Vogl, T.; Roth, J.; Skaar, E. P.; Raffatellu, M., Zinc sequestration by the neutrophil protein calprotectin enhances Salmonella growth in the inflamed gut. *Cell Host Microbe* **2012**, *11* (3), 227-239.
59. Pederick, V. G.; Eijkelkamp, B. A.; Begg, S. L.; Ween, M. P.; McAllister, L. J.; Paton, J. C.; McDevitt, C. A., ZnuA and zinc homeostasis in *Pseudomonas aeruginosa*. *Sci. Rep.* **2015**, *5*, 13139.

60. Bertini, I.; Luchinat, C., High spin Co(II) as a probe for the investigation of metalloproteins. *Adv. Inorg. Biochem.* **1984**, *6*, 71-111.
61. Irving, I.; Williams, R. J. P., Irving Williams series. *Nature* **1948**, *162*, 746-747.
62. Burdette, S. C.; Frederickson, C. J.; Bu, W.; Lippard, S. J., ZP4, an improved neuronal Zn²⁺ sensor of the Zinpyr family. *J. Am. Chem. Soc.* **2003**, *125* (7), 1778-1787.
63. Xiao, Z.; Wedd, A. G., The challenges of determining metal-protein affinities. *Nat. Prod. Rep.* **2010**, *27* (5), 768-789.
64. Korndorfer, I. P.; Brueckner, F.; Skerra, A., The crystal structure of the human (S100A8/S100A9)₂ heterotetramer, calprotectin, illustrates how conformational changes of interacting alpha-helices can determine specific association of two EF-hand proteins. *J. Mol. Biol.* **2007**, *370* (5), 887-898.
65. Gagnon, D. M.; Brophy, M. B.; Bowman, S. E. J.; Stich, T. A.; Drennan, C. L.; Britt, R. D.; Nolan, E. M., Manganese binding properties of human calprotectin under conditions of high and low calcium: X-ray crystallographic and advanced electron paramagnetic resonance spectroscopic analysis. *J. Am. Chem. Soc.* **2015**, *137* (8), 3004-3016.
66. Zackular, J. P.; Chazin, W. J.; Skaar, E. P., Nutritional immunity: S100 proteins at the post-pathogen interface. *J. Biol. Chem.* **2015**, *290* (31), 18991-18998.
67. Williams, R. J. P., Calcium binding proteins in normal and transformed cells, Perugia, May 1996. *Cell Calcium* **1996**, *20* (1), 87-93.

Chapter 3: Biochemical and Functional Evaluation of the Intramolecular Disulfide Bonds in the Zinc-Chelating Antimicrobial Protein Human S100A7 (Psoriasin)

This Chapter is adapted from *Biochemistry* **2016**, 56 (43), 5726-5738.

3. 1. Contributions

Dr. Megan Brophy optimized the purification protocol for S100A7_{red}. Miss Hope Flaxman and Miss Grayson Rodriguez provided technical assistance with the purification of S100A7_{ox} and the Co(II) titrations respectively.

3. 2. Introduction

Epithelial surfaces are continuously exposed to a variety of microbial challenges and thus maintain a complex biochemical barrier that prevents infections and preserves the ensemble of microbes that constitute the normal microflora.¹ The production and release of multiple innate immune factors is one strategy employed by epithelial cells for barrier protection.^{2,3} Human S100A7 (psoriasin, Figure 3. 1) is a Ca(II)- and Zn(II)-chelating host-defense protein that is expressed by epithelial cells and secreted into the upper layers of the epithelium.⁴⁻⁷ It contributes to the innate immune response as well as cell differentiation, epidermal maturation, and epithelial tumorigenesis.^{6,8,9} S100A7 is recognized as an antimicrobial factor of the skin as well as the human tongue, esophagus and female genital tract.¹⁰⁻¹³ Several mechanisms for the antimicrobial activity of S100A7 have been proposed.^{10,12,14,15} Seminal studies reported that S100A7 has antibacterial activity against *Escherichia coli*, a microbe that rarely colonizes the skin and oral cavity.¹⁰

Later work revealed that S100A7_{red} and S100A7_{ox} have antifungal activity against filamentous fungi, including the dermatophyte *Trichophyton rubrum* and *Aspergillus fumigatus*.¹² These two investigations pointed to a role of the Zn(II)-binding sites of S100A7 in antimicrobial function,^{10, 12} and thus indicated a putative contribution to nutritional immunity, an innate immune response that limits nutrient metal availability to microbes.¹⁶⁻¹⁷ Furthermore, human S100A7 damages the cell membrane of *Bacillus megaterium*, suggesting an alternative model for its antimicrobial activity by membrane permeabilization.¹⁵ Along these lines, a putative frog orthologue of S100A7, which lacks the Zn(II)-binding sites of human S100A7, was shown to

damage the cell membranes of *B. megaterium* and *Bacillus subtilis*.¹⁸ A third model for S100A7 in host-defense focuses on its ability to adhere to *E. coli* and keratinocytes, and the occurrence of cross-linked S100A7 species in human wounds.¹⁴ This model proposes that S100A7 functions as a solid-phase component of the physical barrier that protects the epithelium from microbial invasion, as well as a soluble antimicrobial protein in wound fluids.¹⁴ Taken together, these studies suggest that the host-defense function S100A7 may be multi-faceted: the protein may exhibit different antimicrobial activity depending on the environmental milieu and microbe. Herein, we focus on the Zn(II)-chelating ability of human S100A7 and its putative contributions to the metal-withholding innate immune response.

Human S100A7 is a 22-kDa homodimer and member of the S100 family of Ca(II)-binding proteins (Figure 3. 1). Each S100A7 subunit (101-aa, 11-kDa) contains two EF-hand domains (Figure 3. 1D). The C-terminal EF-hand is “canonical” or calmodulin-like and binds Ca(II) in a 7-coordinate geometry.⁶ The “non-canonical” N-terminal EF-hand domain provides a lower coordination number and is a hallmark of S100 polypeptides.¹⁹ The N-terminal EF-hand of S100A7 is particularly noteworthy because its loop region is three residues shorter relative to those of other S100 polypeptides (e.g. S100A8, S100A9, S100A12), and it contains a Ser residue at position 30 (Figure 3. 1D). This residue aligns with a Glu/Asp residue in the other S100 polypeptides, a bidentate ligand that binds Ca(II) at the N-terminal EF-hand.^{6,20} In addition to the Ca(II) sites, the S100A7 homodimer harbors two His₃Asp motifs at the dimer interface. His87 and His91 of one monomer together with His18 and Asp25 of the second monomer form each His₃Asp site. Amino acid sequence alignment shows that these residues align with the metal-coordinating moieties of other human S100 polypeptides, including S100A12 and the calprotectin subunits S100A8 and S100A9 (Figure 3. 1D).

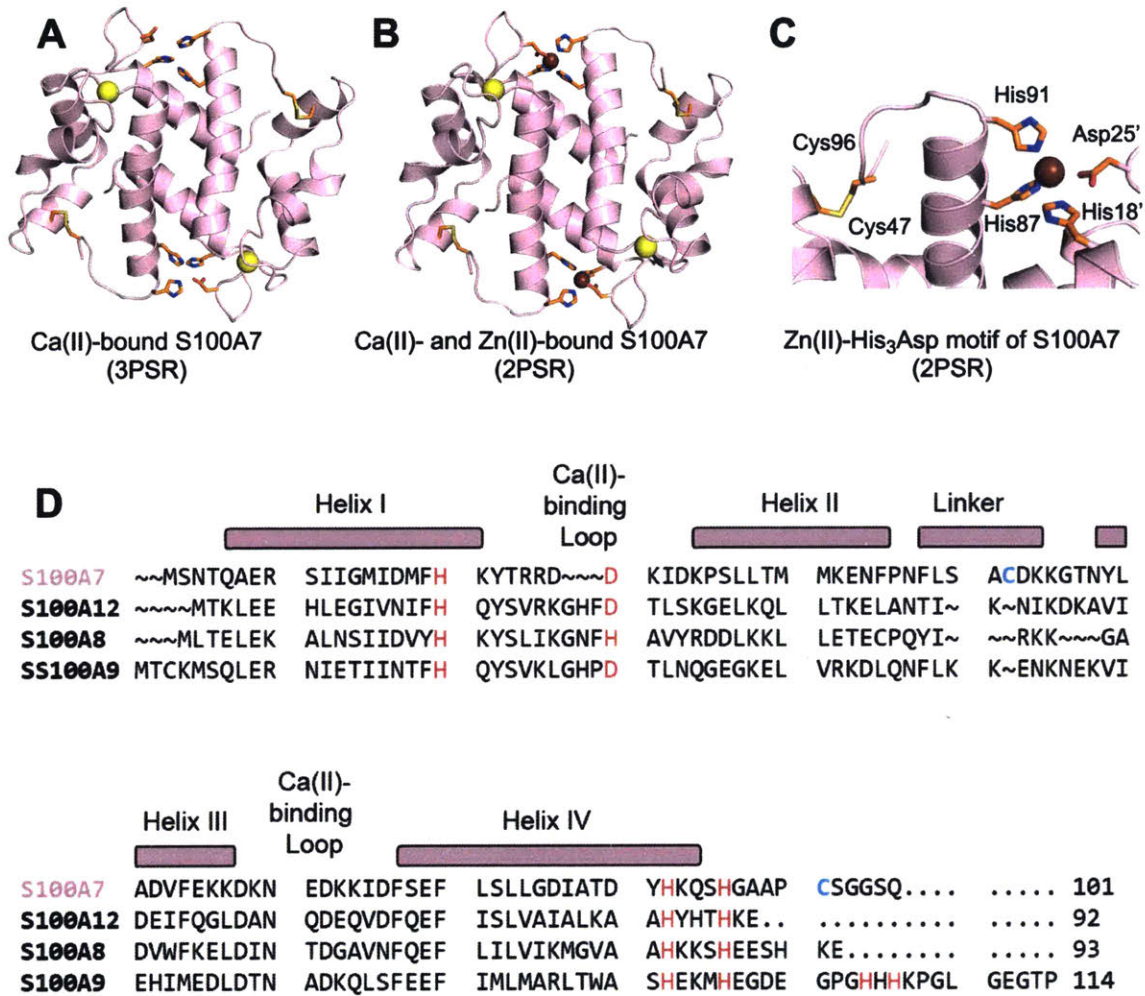


Figure 3. 1. Crystal structures of human S100A7 and amino acid sequence alignment of S100A7 and select human S100 polypeptides. (A) Structure of the Ca(II)-bound S100A7 homodimer (PDB 3PSR).⁶ (B) Structure of the Ca(II)- and Zn(II)-bound S100A7 homodimer (PDB 2PSR).⁶ (C) Zoom-in view showing the His₃Asp motif and Cys47–Cys96 disulfide. Ca(II) ions are shown as yellow spheres, and Zn(II) ions as brown spheres. (D) Sequence alignment of human S100A7, human S100A8, human S100A9, and human S100A12. The secondary structural elements presented above the alignment are for human S100A7. The transition-metal binding residues are presented in red, Ser30 is boxed in green, and Cys47 and Cys96 of S100A7 are highlighted in blue.

Crystal structures of Ca(II)-bound and Ca(II)- and Zn(II)-bound S100A7 provide snapshots of the Ca(II)- and Zn(II)-binding sites (Figure 3. 1A-C).⁶ These two structures were obtained using

≥ 20 equivalents of Ca(II) in the crystallization conditions, and the C-terminal EF-hands contain bound Ca(II) whereas the N-terminal EF-hands do not.⁶ The Ca(II)- and Zn(II)-bound S100A7 structure reveals a 2:1 Zn(II):S100A7 homodimer stoichiometry with a Zn(II) ion coordinated at each His₃Asp site in a distorted tetrahedral geometry (Figure 3. 1B, 3. 1C). Another striking structural feature of S100A7 is the presence of Cys47 and Cys96, two cysteine residues that can form an intramolecular disulfide bond in each subunit of the homodimer (Figure 3. 1C).^{6,20} Amino acid sequence comparisons show that the ability to form an intramolecular disulfide in each subunit differentiates S100A7 from S100A8, S100A9, and S100A12 (Figure 3. 1D). Intra- and intermolecular disulfide bond formation occurs for bovine S100B, a dimeric S100 protein abundant in the brain that exhibits two Cys residues per S100 subunit.²¹⁻²⁴ Notably, the Cys47–Cys96 disulfide bond of S100A7_{ox} is in close proximity to the Zn(II)-binding site (Figure 3. 1C). Indeed, Cys96 is separated from the Zn(II)-coordinating residue His91 by a Gly–Ala–Ala–Pro loop.

These observations highlight some fundamental questions pertaining to the disulfide bond redox chemistry, structure, and function of S100A7. In particular, do S100A7_{red} and S100A7_{ox} exhibit different biophysical and functional properties? Are both the oxidized and reduced forms physiologically significant? A recent analysis of extracts from lesional psoriasis scales identified S100A7_{red} as an antifungal component of this mixture, indicating that the reduced form can exist *in vivo*.¹² This discovery motivated evaluation of the antimicrobial activity of S100A7_{ox}, S100A7_{red} and the disulfide-null variant S100A7-Ala, and resulted in a new proposal that the redox states of the Cys residues in S100A7 modulate its functional properties.¹²

In this work, we address outstanding questions pertaining to the disulfide bond redox chemistry, Zn(II)-binding properties, and antibacterial activity of human S100A7. Because S100A7 is a Ca(II)-binding protein that is secreted from the cytoplasm, where Ca(II) levels are low (i.e. nanomolar), to the extracellular space where Ca(II) levels are high (i.e. ≈ 2 mM),^{25,26} we also consider the effects of Ca(II) ions on the behavior of this protein. To evaluate S100A7_{ox} and S100A7_{red}, we describe methods to prepare these two forms in high yield and purity following

recombinant protein expression in *E. coli*. Because reported solution studies describing the Zn(II)-binding properties of S100A7 are, to the best of our knowledge, limited to one equilibrium dialysis experiment,⁸ we probe its Zn(II)-binding stoichiometry and affinity, and investigate whether disulfide bond formation and Ca(II) ions affect Zn(II) binding. Towards deciphering the antibacterial activity of S100A7, we examine the metal-depletion profiles and growth inhibitory activity of S100A7_{ox} and the disulfide-null variants S100A7-Ser and S100A7-Ala. We also employ Co(II)/Zn(II) substitution experiments to examine metal exchange at the His₃Asp sites. Taken together, our data provide fundamental insights into the disulfide bond redox behavior and coordination chemistry of S100A7, and suggest that the disulfide bond may enhance Zn(II) sequestration by the His₃Asp sites.

3. 3. Experimental Section

3. 3. 1. Design of the Synthetic Genes for Human S100A7 Variants

The synthetic gene for human S100A7 was previously described.²⁷ Briefly, it was optimized for *E. coli* codon usage and ordered from DNA 2.0. A *Nde*I restriction site was placed at the 5' end. A stop codon and a *Xho*I restriction site were placed at the 3' end. This gene was received in the pJ201 vector from DNA 2.0. The gene was sub-cloned into the *Nde*I and *Xho*I sites of pET41a to afford pET41a-S100A7 for protein expression. Synthetic genes were designed in the same manner for the variants S100A7-Ser, S100A7-Ala, and S100A7 Δ His₃Asp. The *E. coli* optimized genes were sub-cloned into the *Nde*I and *Xho*I sites of pET41a.

1. For the S100A7-Ser variant

***E. coli* optimized nucleotide sequence for *Nde*I-S100A7(C47S)(C96S)-Stop-*Xho*I:**

CATATGAGCAACACCCAGGCAGAACGTAGCATTATTGGTATGATTGACATGTTTTCACAAATA
CACGCGTCGCGATGACAAAATCGATAAGCCGAGCCTGTTGACCATGATGAAAGAGAACTTT
CCGAATTTTCTGAGCGCGTCTGATAAGAAGGGTACGAACTACCTGGCTGATGTTTTCGAGA
AGAAAGACAAGAATGAGGATAAGAAAATCGACTTCTCGGAATTCCTGAGCCTGCTGGGCG
ACATCGCGACCGACTATCATAAACAGAGCCACGGCGCAGCCCCGTCCAGCGGTGGTAGC
CAATAACTCGAG

Translated sequence for NdeI-S100A7(C47S)(C96S)-Stop-XhoI:

MSNTQAERSI IGMIDMFHKY TRRDDKIDKP SLLTMMKENF PNFLSASDKK GTNYLADVFE
KKDKNEDKKI DFSEFLSLLG DIATDYHKQS HGAAPSSGGS Q Stop L E

2. For the S100A7-Ala variant

***E. coli* optimized nucleotide sequence for NdeI-S100A7(C47A)(C96A)-Stop-XhoI:**

CATATGAGCAACACCCAGGCAGAACGTAGCATTATTGGTATGATTGACATGTTTCACAAATA
CACGCGTCGCGATGACAAAATCGATAAGCCGAGCCTGTTGACCATGATGAAAGAGAACTTT
CCGAATTTTCTGAGCGCGGCGGATAAGAAGGGTACGAACTACCTGGCTGATGTTTTCGAG
AAGAAAGACAAGAATGAGGATAAGAAAATCGACTTCTCGGAATTCCTGAGCCTGCTGGGC
GACATCGCGACCGACTATCATAAACAGAGCCACGGCGCAGCCCCGGCGAGCGGTGGTAG
CCAATAACTCGAG

Translated sequence for NdeI-S100A7(C47A)(C96A)-Stop-XhoI:

MSNTQAERSI IGMIDMFHKY TRRDDKIDKP SLLTMMKENF PNFLSAAADKK GTNYLADVFE
KKDKNEDKKI DFSEFLSLLG DIATDYHKQS HGAAPASGGS Q Stop L E

3. For the S100A7 ΔHis₃Asp variant

***E. coli* optimized nucleotide sequence for NdeI-S100A7(H18A)(D25A)(H87A)(H91A)-Stop-XhoI:**

CATATGAGCAACACCCAGGCAGAACGTTCCATTATTGGTATGATTGATATGTTTGCGAAATA
CACCCGCCGTGACGCCAAGATCGATAAACCGAGCTTGCTGACGATGATGAAAGAGAACTT
CCCGAATTTCTGTCGGCTTGTGATAAGAAGGGCACGAACTATCTGGCAGACGTTTTCGAG
AAGAAAGACAAAATGAGGATAAGAAGATCGACTTTAGCGAATTTCTGAGCCTGCTGGGTG
ATATCGCGACCGACTACGCGAAACAGAGCGCCGGTGCGGCACCGTGCAGCGGCGGTTCT
CAATAACTCGAG

Translated sequence for NdeI- S100A7(H18A)(D25A)(H87A)(H91A)-Stop-XhoI:

MSNTQAERSI IGMIDMFAKY TRRDAKIDKP SLLTMMKENF PNFLSACDKK GTNYLADVFE
KKDKNEDKKI DFSEFLSLLG DIATDYAKQS AGAAPCSGGS Q Stop L E

For the nucleotide sequence, the restriction sites and stop codon are underlined and in bold, respectively.

For the amino acid sequence, the mutated residues are highlighted in yellow.

3. 3. 2. Materials and General Methods

All solvents and chemicals were obtained from commercial suppliers as detailed below and used as received. All aqueous solutions were prepared using Milli-Q water (18.2 MΩ•cm, 0.22-μm filter). Protein concentrations were routinely quantified by using the calculated extinction coefficients for the S100A7 homodimer (ProtParam: $\epsilon_{280} = 9190 \text{ M}^{-1}\text{cm}^{-1}$ for S100A7_{ox} and

S100A7 Δ_{ox} ; $\epsilon_{280} = 8940 \text{ M}^{-1}\text{cm}^{-1}$ for S100A7 $_{\text{red}}$, S100A7-Ser, S100A7-Ala, and S100A7 Δ_{red} ; Table 3. 1 includes ϵ_{280} values for the S100A7 monomers). All protein concentrations are for the S100A7 homodimer, and all reported stoichiometries are relative to the S100A7 homodimer.

Commercial materials, buffers, and solution preparations. Human thioredoxin (Sigma-Aldrich and Fisher Scientific) and rat liver thioredoxin reductase (Sigma-Aldrich) were stored according to manufacturer protocols, and used as received. NADPH reduced form tetrasodium salt was obtained from Tocris Bioscience; GSH from Sigma-Aldrich; GSSG from Alfa Aesar; guanidinium hydrochloride (GuHCl) from Sigma-Aldrich. Solutions of GuHCl were filtered through a 0.22- μm millipax filter and stored in glass bottles. Chelex resin was purchased from Bio-Rad.

For metal-binding experiments and redox studies, metal-binding buffer (75 mM HEPES, 100 mM NaCl, pH 7.0) was prepared with Ultrol grade HEPES (free acid, Calbiochem) and TraceSELECT NaCl (Sigma), and TraceSELECT aqueous NaOH (Sigma) was used to adjust the solution pH. To reduce metal-ion contamination, plastic spatulas were used to transfer buffer reagents. A Tris buffer (1 mM Tris-HCl, pH 7.5) prepared from Tris base (J. T. Baker) was used for circular dichroism (CD) spectroscopy experiments. For experiments requiring anaerobic conditions, the buffers were degassed for at least 1 h by Ar bubbling, and then transferred to an anaerobic glovebox (Vac Atmospheres, N₂ atmosphere) where they were equilibrated for at least 24 h before an experiment and subsequently stored in the glovebox.

Stock solutions of CoCl₂ (100 mM, 100 mL), CaCl₂ (1 M, 100 mL), and ZnCl₂ (100 mM, 100 mL) were prepared from 99.999% CoCl₂ (Sigma), CaCl₂ (Sigma), and ZnCl₂ (Sigma, anhydrous) respectively, and Milli-Q water. The metal stock solutions were prepared in acid-washed volumetric glassware and transferred to sterile polypropylene tubes for long-term storage. The working solutions were prepared by diluting the stock solutions in Milli-Q water.

For Zn(II) competition experiments, the competitors Zincon monosodium salt (Sigma-

Aldrich), FluoZin-3 (FZ3, Fisher Scientific), and Zinpyr-4 (ZP4, Strem Chemicals) were employed. Stock solutions (≈ 10 mM) of Zincon and ZP4 (≈ 2 mM) were prepared in anhydrous DMSO (Sigma), aliquoted into 50- μ L portions, and stored at -20 °C. Stocks of FZ3 (≈ 2 mM) were prepared in Milli-Q water, aliquoted into 10- μ L portions, and stored at -20 °C. Each aliquot was thawed only once, and experiments with these reagents were performed in the dark.

For the metal-depletion experiments and antibacterial activity assays, Tryptic Soy Broth (TSB) medium (Becton Dickinson), deMan, Rogosa, and Sharpe (MRS) medium (Becton Dickinson), and Brain Heart Infusion (BHI) medium (Becton Dickinson) were prepared with Milli-Q water.

HD5_{ox} preparation and handling. HD5_{ox} was prepared and stored as described in the literature.²⁸ The calculated extinction coefficient of $\epsilon_{278} = 3181 \text{ M}^{-1}\text{cm}^{-1}$ for HD5_{ox} was employed to determine peptide concentration.

Optical Absorption and Fluorescence Spectroscopy. Optical absorption spectra were collected on a Beckman Coulter DU 800 spectrophotometer thermostatted at 25 °C with a Peltier temperature controller. Quartz cuvettes with 1-cm path lengths (Starna) were employed for all optical absorption measurements. Fluorescence spectra were collected on a Photon Technologies International QuantaMaster 40 fluorimeter outfitted with a continuous xenon source for excitation, autocalibrated QuadraScopic monochromators, a multimode PMT detector, and a circulating water bath maintained at 25 °C. This instrument was controlled by the FelixGX software package. Either quartz (Starna) or PMMA (Fischer Scientific) cuvettes with 1-cm path lengths were employed for fluorescence measurements.

CD Spectroscopy. An Aviv Model 202 CD spectrometer was employed to collect CD spectra. Protein was buffer exchanged into 1 mM Tris-HCl, pH 7.5 and then transferred (10 μ M, 300 μ L) and transferred to a Hellma quartz cuvette (1-mm path length). The CD spectra were recorded from 195 to 260 nm at 1-nm intervals. Each measurement was averaged for 3 sec, and three independent scans were conducted. The averaged data are reported.

Analytical HPLC. Analytical HPLC was performed on an Agilent 1200 instrument equipped with a thermostatted autosampler set at 4 °C, a thermostatted column compartment set at 20 °C, and a multi-wavelength detector set at 220 and 280 nm (500 nm reference wavelength, 100 nm bandwidth). A Proto C4 column (5- μ m pore, 4.6 x 250 mm, Higgins Analytical Inc.) and a flow rate of 1 mL/min with a gradient of 35–50% B over 30 min was employed for all analytical HPLC experiments with S100A7. A Cliepus C18 column (5- μ m pore, 4.6 x 250 mm, Higgins, Inc.) and a flow rate of 1 mL/min with a gradient of 10–60% B over 25 min was employed all analytical HPLC experiments with HD5_{ox}. For all analytical HPLC, solvent A was 0.1% TFA/H₂O and solvent B was 0.1% TFA/MeCN.

LC-MS. An Agilent 1290 series LC system equipped with an Agilent 6230 TOF system housing Agilent Jetstream ESI source was employed to perform high-resolution mass spectrometry. An Agilent Poroshell 300SB-C18 column (5- μ m pore) was employed. Solvent A was 0.1% formic acid/H₂O. Solvent B was 0.1% formic acid/MeCN. Protein samples (10 μ M) were prepared in Milli-Q water and 1 μ L was injected for each analysis. Data was acquired by using the Agilent MassHunter Workstation Data Acquisition software and processed with the Agilent MassHunter Qualitative Analysis program. All ESI-MS spectra were acquired in positive ion mode.

Analytical SEC. Analytical SEC was conducted using an ÄKTA purification system with a Superdex 75 10/300 GL column (GE Healthcare Life Sciences) housed at 4 °C as previously described.²⁷

3. 3. 3. Purification of Human S100A7_{red}, S100A7_{ox} and Variants

The synthetic gene for human S100A7 and the pET-41a-S100A7 vector were previously described.²⁷ The synthetic genes containing the *E. coli* optimized nucleotide sequence for human S100A7-Ala, S100A7-Ser, and S100A7 Δ were sub-cloned into the *Nde*I and *Xho*I sites of pET41a by DNA 2.0. The identity of each plasmid was confirmed by DNA sequencing (MIT Biopolymers or Quintarabio). Each S100A7 protein was overexpressed in *E. coli* BL21(DE3) as previously described for human S100A7.²⁷ S100A7-Ser and S100A7-Ala were purified and stored using the original protocol reported for S100A7.²⁷ To obtain S100A7_{red} and S100A7_{ox}, as well as S100A7 Δ _{red} and S100A7 Δ _{ox}, the original purification protocol was also followed,²⁷ and additional steps were performed after the SEC step to fully reduce or fully oxidize the protein. In general, the protein purifications for the S100A7 variants were carried out starting from 2 L of *E. coli* cell culture.

For the purification of S100A7_{red} and S100A7 Δ _{red} from a 2-L culture, after the SEC step (75 mM HEPES, 100 mM NaCl, pH 7.0, or 20 mM Tris, 100 mM NaCl, pH 7.5), fractions containing S100A7 were pooled and transferred to a Spectropor3 3500 MWCO dialysis bag. The protein was dialyzed against 1 L of 75 mM HEPES, 1 mM DTT, 100 mM NaCl, pH 7.0 containing \approx 10 g Chelex resin at 4 °C for \approx 12 h. The dialysate was passed through a 0.45- μ m syringe filter to remove any contaminating Chelex resin. The protein was concentrated using an Amicon 10-kDa MWCO spin filter (3750 rpm, 4 °C) to $>$ 500 μ M, partitioned into sterile microcentrifuge tubes in 50- μ L aliquots, flash frozen in liquid nitrogen, and stored at -80 °C.

For the purification of S100A7_{ox} and S100A7 Δ _{ox}, the original S100A7 purification protocol was followed except that the SEC was performed using a Tris running buffer (20 mM Tris, 100 mM NaCl, pH 7.5). Fractions containing S100A7 were pooled and diluted to 20 μ M in 20 mM Tris,

100 mM NaCl, pH 7.5, and the solution was transferred to a 150-mL glass beaker. For the Cu(II)-catalyzed oxidation of S100A7_{ox}, three equivalents of Cu(II) ($\approx 90 \mu\text{L}$ from a 100-mM stock solution of CuCl_2) were added dropwise to the protein solution and the mixture was incubated at room temperature for 2 h with stirring. The oxidation state of the protein was confirmed by HPLC analysis. For the Cu(II)-catalyzed oxidation of S100A7 Δ , two equivalents of Cu(II) ($\approx 60 \mu\text{L}$ from a 100-mM stock solution of CuCl_2) were added dropwise to the protein solution, and the mixture was incubated at room temperature for 2 h with stirring. A precipitate formed, and the mixture was centrifuged (3750 rpm, 10 min, 4 °C) to remove the precipitate. The resulting solution containing soluble protein and copper was incubated overnight with stirring at room temperature. The oxidation state of the protein was confirmed by HPLC analysis. The resulting protein solution (S100A7_{ox} or S100A7 Δ_{ox}) was then transferred to a Spectropor3 3500 MWCO dialysis bag and dialyzed overnight against 1 L of 75 mM HEPES, 100 mM NaCl, pH 7.0 containing ≈ 10 g Chelex resin (Biorad), and 1 mM EDTA at 4 °C. The EDTA was subsequently removed by dialysis against 75 mM HEPES, 100 mM NaCl, pH 7.0 (2 x 4 L, ≈ 12 h per dialysis, 4 °C). The protein was then concentrated using an Amicon 10-kDa MWCO spin filter (3750 rpm, 4 °C) to $>500 \mu\text{M}$, partitioned into sterile microcentrifuge tubes in 50- μL aliquots, flash frozen in liquid nitrogen, and stored at -80 °C. The metal contents of the purified oxidized proteins were analyzed by ICP-MS and were found to contain ≈ 0.03 and ≈ 0.04 equivalents of Cu and Zn, respectively (Table 3. 3).

These procedures afforded protein yields that ranged from ≈ 30 -80 mg/L of cell culture. In general the yields were 50-80 mg/L of S100A7-Ser and S100A7-Ala, and 30-50 mg/L of S100A7_{ox}, S100A7_{red}, S100A7 Δ_{ox} , and S100A7 Δ_{red} . Protein aliquots were freeze-thawed only once. All experiments were performed with at least two independent batches of purified proteins. Tables S1-S3 and Figures S2-S5 detail the purity, identity, and basic biochemical characterization of these proteins.

3. 3. 4. Thioredoxin Activity Assays

Solutions (500 μL) containing 5 μM S100A7_{ox}, 1 μM human thioredoxin (Trx), 100 nM rat liver thioredoxin reductase (TrxR), and 1 mM NADPH in 75 mM HEPES, 100 mM NaCl, pH 7.0, were prepared and incubated at 37 °C. To initiate the reaction, Trx was added last. A 100- μL aliquot was collected at each time point ($t = 0, 15$ and 120 min), immediately quenched with 10 μL of 6% TFA, followed by the addition of 50 μL of 6 M GuHCl. The quenched samples were centrifuged (13 000 rpm x 5 min, 4 °C), and the resulting supernatants (120 μL aliquot) analyzed by HPLC. To investigate the effect of Ca(II) on the reduction of S100A7_{ox} by Trx/TrxR, these experiments were also performed in the presence of 2 mM Ca(II). To investigate the effect of Zn(II) on the reduction of S100A7_{ox} by Trx/TrxR, Zn(II) (1.9 equiv) was added to S100A7_{ox}, and the sample was incubated for at least 15 min prior to the start of the experiment. This Zn(II):S100A7 homodimer ratio was used to minimize the amount of unbound Zn(II) in the assay because Zn(II) inhibits the activity of Trx/TrxR.²⁹ Following optimization, each experiment was performed in duplicate and HPLC traces from one experiment are presented.

The peptide HD5_{ox}, which we study in an independent initiative, binds neither Ca(II) nor Zn(II) and is a substrate for Trx/TrxR.³⁰ We used Trx/TrxR-catalyzed reduction of HD5_{ox} to HD5_{red} in control assays to confirm that the presence of Ca(II) or Zn(II)-bound S100A7_{ox} did not cause enzyme inhibition. In a first set of assays, HD5_{ox} reduction in the absence and presence of 2 mM Ca(II) was monitored over time ($t = 0, 5, 10, 15$ and 120 min). This assay was conducted as described above using 10 μM HD5_{ox}. In a second set of assays, HD5_{ox} was co-incubated with Zn(II)-bound S100A7_{ox}, and HD5_{ox} reduction by Trx/TrxR was monitored over time ($t = 0, 5, 10, 15$ and 120 min). This assay was conducted as described above for the Zn(II):S100A7_{ox} experiment except that 10 μM HD5_{ox} was included in the assay mixture.

3. 3. 5. Midpoint Potential (E_m) Determination

These experiments were designed based on a reported procedure.³⁰ All redox buffers were prepared at room temperature in a glovebox, and the assays were performed in a glovebox. In order to prepare buffers of defined redox potentials, aqueous stock solutions of GSH and GSSG (10 mL, 10 mM) were prepared in the glovebox using volumetric flasks (75 mM HEPES, 100 mM NaCl, pH 7.0, \pm 2mM Ca(II)). Using these solutions, buffers with redox potentials spanning the -200 to -400 mV range were prepared in \approx 7-mV increments using GSH and GSSG ratios determined by the Nernst equation (75 mM HEPES, 100 mM NaCl, pH 7.0, \pm 2 mM Ca(II)). The midpoint potential (E_m) of S100A7 was determined by incubating S100A7_{ox} (10 μ M) in each redox buffer under anaerobic conditions at 37 °C. For the experiments with apo S100A7_{ox}, solutions of S100A7_{ox} (10 μ M, 200 μ L) were prepared in the appropriate redox buffers (-200 to -400 mV). The samples were prepared in a 96-well plate with each well containing a sample at a specified redox value. For experiments performed in the presence of 2 mM Ca(II), the samples were prepared by the same procedure except that the buffer contained 2 mM Ca(II). The plate was sealed, and incubated in a heat block at 37 °C anaerobically for \approx 96 h (4 days). Then, the samples were quenched with 10 μ L of 6% aqueous TFA. The quenched samples were removed from the glovebox, transferred to microcentrifuge tubes, and centrifuged (13 000 rpm x 5 min, 4 °C). The resulting supernatants (120 μ L aliquot) were analyzed by HPLC. The redox potential of the S100A7 disulfide bond was determined from the equilibrium between S100A7_{ox} and S100A7_{red} as quantified by HPLC (integration of peak areas). The E_m values were first estimated from the data plotted in Figure 3. 11 by determining the midpoint potential value that provides a 1:1 ratio of S100A7_{ox} and S100A7_{red}. We did not include the S100A7-glutathione disulfide adduct that formed (\approx 15.9 min retention time, Figure S11) in the calculation because this equilibrium is independent of the equilibrium between S100A7_{ox} and S100A7_{red}. We did not perform experiments starting from S100A7_{red} because, during trial assays, we observed marked formation of the protein-

glutathione adduct that accounted for up to 30% of the total protein and did not obtain reproducible results. Each experiment was performed at least three times, and errors are shown at SDM.

3. 3. 6. Nernst Equation Derivation

The midpoint potential (E_m) of S100A7 was determined by incubating S100A7_{ox} in buffers at defined redox potentials prepared using the reduced (GSH) and oxidized (GSSG) forms of glutathione as described above. The [GSH] / [GSSG] ratio needed for a specified redox potential value was calculated using the Nernst equation as follows:

$$E_{buffer} = E_m^o(GSH/GSSG) - \frac{RT}{nF} \ln \left(\frac{[GSH]^2}{[GSSG]} \right) \quad (\text{eq. 1})$$

where $E_m^o(GSH/GSSG)$ is the midpoint potential of the glutathione redox couple, R is the universal gas constant (8.314 JK⁻¹mol⁻¹), T is the temperature (310.2 K), n is the number of moles of electrons transferred (2 electrons per disulfide bond; $n = 2$ for glutathione and $n = 2$ per monomer of S100A7), and F is the Faraday constant (9.6485 x 10⁴ Cmol⁻¹). At pH 7.0, $E_m^o(GSH/GSSG)$ is -240 mV.³¹ Therefore, eq. 1 can be rewritten as follows:

$$E_{buffer} = -240 \text{ mV} - \frac{61.5}{2} \log \left(\frac{[GSH]^2}{[GSSG]} \right) \quad (\text{eq. 2})$$

Attempts to obtain E_m values of S100A7 in the absence and presence of Ca(II) by fitting the data to the Nernst Equation (eq. 3) resulted in poor fits as discussed in the main text.

$$E_m^o(S100A7_{red}/S100A7_{ox}) - \left(\frac{61.5}{2} \right) \log \left(\frac{S100A7_{red}}{S100A7_{ox}} \right) = -240 \text{ mV} - \frac{61.5}{2} \log \left(\frac{[GSH]^2}{[GSSG]} \right) \quad (\text{eq. 3})$$

3. 3. 7. Logistic Equation Derivation.

Data fitting showed that the midpoint data was not well fit using the Nernst equation because conversion to 100% of S100A7_{ox} could not be reached under the experimental conditions. We therefore employed a logistic function (eq. 4) and allowed the calculated maxima to vary during data fitting, which provided better fits for the midpoint potential determination of S100A7_{ox}.

$$F(x) = \%S100A7_{ox-max} / (1 + \exp(-k * (E_{buffer} - E_m^o(S100A7_{red}/S100A7_{ox})))) \quad (\text{eq. 4})$$

where $F(x)$ is percentage of S100A7_{ox} at a specified redox potential value (E_{buffer}), $\%S100A7_{ox-max}$ is the maximum percentage of S100A7_{ox} obtained, k is a variable that accounts for temperature, the universal gas constant, Faraday's constant, and moles of electrons transferred, and $E_m^o(S100A7_{red}/S100A7_{ox})$ is the midpoint potential of S100A7.

3. 3. 8. Aerobic Reduction of S100A7_{ox} by DTT, GSH, and TCEP

A 400- μ L sample containing 30 μ M of S100A7_{ox} (75 mM HEPES, 100 mM NaCl, pH 7.0) was allowed to incubate at room temperature in the presence of 1 mM DTT, GSH, or TCEP (4 μ L from a 100-mM stock solution). A 45- μ L aliquot was collected at each time point ($t = 0, 5, 10, 15, 30, 60,$ and 120 min), immediately quenched with a mixture of 5 μ L of 6% TFA and 100 μ L of 6 M GuHCl. The quenched samples were centrifuged (13 000 rpm x 5 min, 4 °C), and the resulting supernatants (120 μ L aliquot) analyzed by HPLC. For samples containing Zn(II), the protein was allowed to incubate with 2 equivalents of Zn(II) for 15 min minutes prior to the addition of the reducing agent. The reducing agents were prepared from powder stocks, and the pH of the solutions confirmed to be 7.0.

3. 3. 9. Zinc Competition Titrations with S100A7 and Zincon

A 2-mL solution containing S100A7 (10 μ M) and Zincon (20 μ M) was prepared in a quartz

cuvette (75 mM HEPES, 100 mM NaCl, pH 7.0, \pm 2 mM Ca(II)). The sample was titrated with Zn(II) in 2.5 μ M increments up to 50 μ M (1 μ L from a 5-mM Zn(II) stock solution per addition). The sample was equilibrated for 2 min before the optical absorption spectrum was collected. For the titration with S100A7_{red}, the thawed protein sample was immediately buffer-exchanged to remove contaminating DTT (3 x 5 min, 13 000 rpm), mixed with Zincon, and Zn(II) titrated in. We observed no air-oxidation of S100A7_{red} over the time course of the titration (\approx 20 min duration) as ascertained by analytical HPLC. The absorbance at 621 nm versus the [Zn(II)] / [S100A7] ratio was plotted. Each experiment was performed in triplicate and data from representative trials are presented.

3. 3. 10. Zinc Competition Assays with S100A7 and FZ3

A 1-mL solution containing FZ3 (2 μ M) and S100A7 (2 μ M) was prepared in a PMMA cuvette (75 mM HEPES, 100 mM NaCl, pH 7.0). The solution was mixed gently and incubated for 1 h in the dark at room temperature. The emission spectrum of the solution was then recorded. An aliquot of Zn(II) was subsequently added to the sample to a final concentration of 2 μ M, the solution was gently mixed, and incubated for 2.5 h in the dark at room temperature. The emission spectrum of the solution was then recorded. The sample was excited at 494 nm, and the emission was monitored from 505–650 nm and integrated over this range. Each experiment was performed in triplicate. The mean and SDM values are reported.

3. 3. 11. Zinc Competition Titrations with S100A7 and ZP4

Competition experiments with S100A7 and ZP4 were employed to determine the apparent dissociation constant values of S100A7 for Zn(II) at pH 7.0. ZP4 ($\epsilon_{506} = 61\,000\text{ M}^{-1}\text{cm}^{-1}$)³² was diluted to 2 μ M in a total volume of 2 mL (75 mM HEPES, 100 mM NaCl, pH 7.0, \pm 2 mM Ca(II)). After the optical absorption and emission spectra of the ZP4 solution were recorded, S100A7 was added to a final concentration of 5 μ M, and the optical absorption and emission spectra were

recorded again to check that they were unperturbed by addition of the protein sample. The ZP4/S100A7 mixture was titrated with Zn(II) in 0.5 μ M increments (1 μ L from a 1-mM Zn(II) stock solution), the emission spectrum was recorded from 505 to 650 nm ($\lambda_{\text{ex}} = 495$ nm), and integrated over this range. The samples were allowed to equilibrate for \approx 2 min between each Zn(II) addition. Normalized integrated emission versus the concentration of Zn(II) added was plotted, and the resulting titration curve was fit to one- and two-binding site models using the DynaFit software and a custom script previously described.³³ Each titration was performed in triplicate. The mean and SDM values are reported.

3. 3. 12. Co(II)-binding Titrations and Metal Substitution Assays

Protein samples (300 μ M, 400 μ L) were prepared in 75 mM HEPES, 100 mM NaCl, pH 7.0 and the absorption spectrum recorded. Co(II) was then added in 75- μ M increments (1 μ L from a 30-mM stock) and the solution was gently mixed. The optical absorption spectrum was recorded, and the extinction coefficient calculated from the protein concentration. Co(II)-binding titrations with S100A7_{red} were carried out aerobically, and protein was analyzed by HPLC before and after the titration to confirm that air oxidation of the disulfide bond did not occur during the experiment. For metal substitution experiments, a solution containing S100A7 (300 μ M) and Co(II) (1.2 mM, 4.0 equiv) was prepared (75 mM HEPES, 100 mM NaCl, pH 7.0) and the optical absorption spectrum recorded. Then, Zn(II) was added (1.2 mM, 4.0 equiv) from a 100-mM stock solution, and the optical absorption spectra were recorded over a 20-h time period. For metal substitution experiments with S100A7_{red}, the Co(II)-bound protein sample was prepared anaerobically in a septum-capped quartz cuvette in the glovebox. The sample was removed from the glovebox and the absorption spectrum was recorded. An aliquot of Zn(II) (1.2 mM, 4.0 equiv) was then added by syringe transfer, and the optical absorption spectra recorded. The protein was analyzed by HPLC before and after the displacement experiment to confirm that air oxidation of the disulfide

bond did not occur. Each Co(II)-binding titration and metal displacement experiment was performed at least in duplicate and data from representative trials are shown.

3. 3. 13. Metal Analysis (ICP-MS)

For the metal-depletion experiments, 1 mL of TSB:Tris (32:68 (v:v) ratio) was transferred to 5-mL centrifuge tubes (Argos). Protein samples were buffer-exchanged into AMA buffer (20 mM Tris-HCl, 100 mM NaCl, pH 7.5) using 0.5-mL 10 MWCO Amicon spin concentrators, and diluted to final concentrations of 31.25, 62.5, 125, 250, and 500 $\mu\text{g}/\text{mL}$ in the TSB:Tris medium. Untreated TSB:Tris containing no protein and the S100A7-treated samples were incubated for 20 h (30 °C, 150 rpm). The samples were spin filtered using the 4-mL Amicon spin concentrators (3750 rpm, 30 min). The flow through was collected (900 μL) and diluted 1:1 with 3% HNO_3 nitric acid. Samples were analyzed at the Center for Environmental Health Sciences (CEHS) Core Facility at MIT. The concentrations of Mg, Ca, Fe, Mn, Co, Ni, Cu, and Zn were quantified employing an Agilent 7900 ICP-MS used in Helium mode outfitted with integrated autosampler (I-AS). An internal standard of terbium (Agilent) was used to control for sample effects, and the concentrations of analyte were calibrated using standards prepared by serial dilution of the Agilent Environmental Calibration Standard mix. All experiments were performed three times with at least two different starting stocks of media and protein. The mean and SDM values are reported.

3. 3. 14. Antibacterial Activity Assays (AMA)

For these studies, TSB:Tris, MRS:Tris, and BHI:Tris AMA media were composed of 32:68 (v:v) ratio of TSB/MRS/BHI and AMA buffer (20 mM Tris-HCl, 100 mM NaCl, pH 7.5). The growth inhibitory activity of S100A7 against bacterial strains was investigated by following literature protocols.³³⁻³⁴ Bacterial strain stocks were stored at -80 °C in media containing 25% glycerol. AMA medium (TSB:Tris for *Escherichia coli*, *Staphylococcus aureus*, *Pseudomonas aeruginosa*;

MRS:Tris for *Lactobacillus plantarum*; and BHI:Tris for *Listeria monocytogenes*) was prepared using sterile technique (Table 3. 1). The growth medium (TSB:Tris for *E. coli*, *S. aureus*, *P. aeruginosa*; MRS:Tris for *L. plantarum*; and BHI:Tris for *L. monocytogenes*) was inoculated with a single colony and grown overnight (37 °C, t ≈ 16 h) on a rotating wheel. The overnight cultures were then diluted 1:100 in a culture tube containing 5 mL of medium and allowed to grow to mid-log phase at an OD₆₀₀ ≈ 0.6 (t ≈ 2 - 3 h). The cultures at mid-log phase were diluted 1:500 into AMA medium, and 90 μL of the dilution was added to a well containing 10 μL of 10x protein in AMA buffer in 96-well round-bottom plates (Corning, Inc.). For samples containing a ≈2-mM Ca(II) supplement, the Tris buffer was supplemented with 3 mM Ca(II). Each condition was repeated in three wells. The plate was covered with a wet paper towel and wrapped with Saran wrap. The plate was then allowed to incubate in an incubator-shaker (37 °C for *E. coli*, *S. aureus*, and *P. aeruginosa*; 30 °C for *L. plantarum* and *L. monocytogenes*, 150 rpm, t=20 h). Bacterial growth was monitored by OD₆₀₀ at regular intervals using a plate reader. Each set of experiments was performed at least three times with at least two different protein and media stocks. The mean and SDM are reported.

The microdilution AMA presented in Figure 3. 28 was performed according to a literature protocol.¹⁰

Table 3. 1. Strains and growth conditions employed in this work

Strain	Source	Culture conditions ^a
<i>E. coli</i> K-12	Keio Collection ⁴⁷	TSB/Tris (32:68 v/v), 37 °C, 150 rpm
<i>E. coli</i> K-12 Δ <i>znuA</i>	Keio Collection ⁴⁷	TSB/Tris (32:68 v/v), 37 °C, 150 rpm
<i>E. coli</i> 25922	ATCC	TSB/Tris (32:68 v/v), 37 °C, 150 rpm
<i>L. plantarum</i> WCSF1	ATCC	MRS/Tris (32:68 v/v). 30 °C, 150 rpm
<i>L. monocytogenes</i> ATCC 19115	ATCC	BHI/Tris (32:68 v/v), 30 °C, 150 rpm
<i>P. aeruginosa</i> PAO1	Manoil Laboratory ^b	TSB/Tris (32:68 v/v),

S. aureus ATCC 25923

ATCC

37 °C, 150 rpm

TSB/Tris (32:68 v/v),

37 °C, 150 rpm

^a All media contained dextrose. These are the culture conditions employed for the antimicrobial activity assays. ^b University of Washington (Seattle, WA).

3. 4. Results and Discussion

3. 4. 1. Preparation of S100A7 and Variants

We previously reported a procedure for obtaining apo human S100A7 in high yield following recombinant expression in *E. coli* BL21(DE3), column chromatography, and dialysis.²⁷ This procedure afforded S100A7 in high purity based on SDS-PAGE. Nevertheless, analytical HPLC revealed that this purification resulted in mixtures of S100A7_{red} and S100A7_{ox}, with the reduced species being predominant. Thus, for the current work, we established protocols that provide homogenous samples of S100A7_{red} and S100A7_{ox}. We also employed these general methods to obtain samples of S100A7 Δ _{red} and S100A7 Δ _{ox}, variants that lack the His₃Asp metal-binding sites because the four amino acids comprising the His₃Asp site (His18, Asp25, His87, and His91) site were replaced by non-coordinating Ala residues (Table 3. 2). These proteins serve as non-Zn(II)-binding controls.

We considered several approaches to obtain homogenous S100A7_{ox}. Starting from the S100A7_{red}/S100A7_{ox} mixture obtained from the original purification protocol, attempts to fully oxidize the protein on a preparative scale by air oxidation or by using redox buffers containing glutathione- or cysteine-based redox systems proved unsuccessful. In all instances, mixtures of S100A7_{red} and S100A7_{ox} were obtained. We subsequently evaluated a procedure involving Cu(II)-catalyzed oxidation of thiols to disulfides, which proved to be successful. Although an uncommon method in protein purification, the Cu(II)-catalyzed oxidation of thiols to form intra- and intermolecular disulfides in proteins has been reported for bovine oxyhemoglobin,^{35,36} human S100A8,³⁷ and bovine S100B.²³ Initial analytical-scale trials revealed that addition of Cu(II) to S100A7 under aerobic conditions resulted in nearly quantitative conversion to S100A7_{ox}.

Optimization of the procedure yielded homogenous S100A7_{ox} with negligible Cu contamination.

Table 3. 2. Extinction coefficients for S100A7 monomers

Protein	Description	ϵ_{280} (M ⁻¹ cm ⁻¹) ^a
S100A7 _{ox}	Oxidized; Cys47–Cys96 disulfide bond	4595
S100A7 Δ_{ox}	(H18A)(D25A)(H87A)(H91A) variant Oxidized; Cys47–Cys96 disulfide bond	4595
S100A7 _{red}	Reduced; Cys47 and Cys96 free thiols	4470
S100A7 Δ_{red}	(H18A)(D25A)(H87A)(H91A) variant Reduced; Cys47 and Cys96 free thiols	4470
S100A7-Ser	(C47S)(S96S) variant	4470
S100A7-Ala	(C47A)(S96A) variant	4470

^a Extinction coefficients (280 nm) were calculated by using the ProtParam tool available on the ExPASy server (<http://web.expasy.org/protparam>).

For the Cu(II)-catalyzed oxidation, we first purified S100A7 as previously described²⁷ except that we employed a Tris buffer (20 mM Tris, 100 mM NaCl, pH 7.5) in the final column purification by SEC. We selected a Tris buffer because precipitation occurred when the Cu(II)-catalyzed oxidation was carried out in the HEPES buffer that we routinely employ during S100 protein purification (75 mM HEPES, 100 mM NaCl, pH 7.0).^{27,38} We found that $\approx 100\%$ conversion to S100A7_{ox} could be achieved by incubating the protein with three equivalents of Cu(II) for 2 h at room temperature (Figure 3. 2A). Excess Cu(II) was employed in order to fully oxidize S100A7 because the two His₃Asp sites of S100A7 bind Cu(II). Following disulfide bond formation, the Cu was removed by extensive dialysis. ICP-MS of the resulting protein revealed ≈ 0.03 and ≈ 0.04 equivalents of contaminating Cu and Zn, respectively, per S100A7_{ox} homodimer (Table 3. 2).

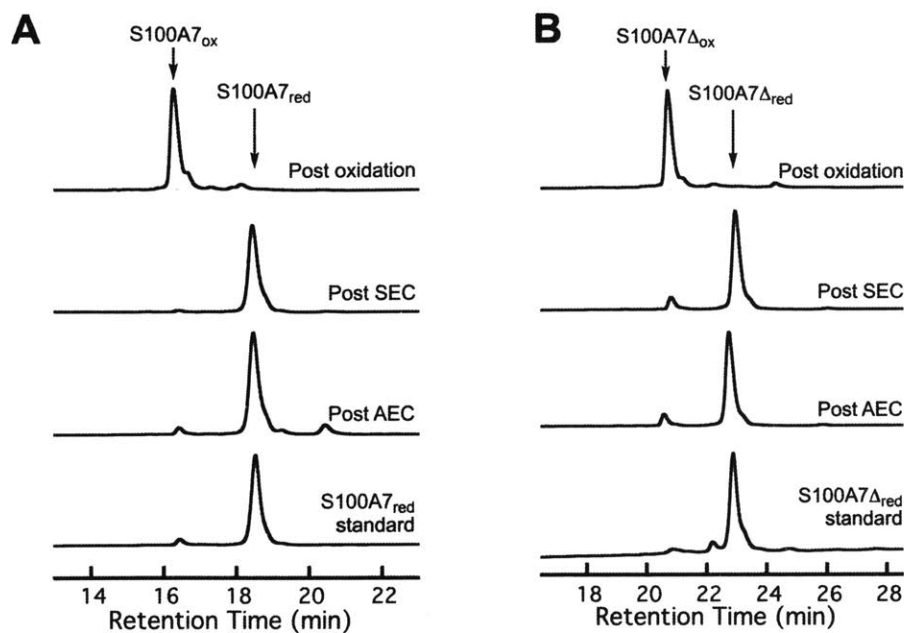


Figure 3. 2. Analytical HPLC traces (220 nm absorption) showing the speciation of 9 μ M S100A7 (A) and S100A7 Δ (B) after different steps of the protein purification and following Cu(II)-catalyzed oxidation. The protein purification involves purification of S100A7 and S100A7 Δ by AEC and SEC.²⁷ Each trace was normalized to a maximum peak absorbance of 1. The shoulder peak observed in the chromatograms of S100A7_{ox} and S100A7 Δ _{ox} corresponds to the isoform of S100A7 missing the N-terminal methionine.

We obtained S100A7 Δ _{ox} using the same procedure except that (i) two equivalents of Cu(II) were employed and (ii) a precipitate was removed by centrifugation after the 2-h incubation at room temperature, and the resulting soluble fraction was stirred overnight at room temperature, which yielded the completely oxidized protein (Figure 3. 2B).

We obtained homogenous S100A7_{red} and S100A7 Δ _{red} by simply dialyzing the S100A7 protein obtained from our reported procedure against Chelex resin in the presence of 1 mM DTT. We also prepared two disulfide-null variants, S100A7-Ser (S100A7(C47S)(C96S)) and S100A7-Ala (S100A7(C47A)(C96A)) using the original purification procedure.²⁷ These two variants serve as models for S100A7_{red} because they allow for studies to be performed under aerobic conditions in the absence of reducing agents. In addition, comparisons of S100A7_{red} to variants with

Cys→Ser/Ala substitutions allow monitoring for potential functions of the free thiolates in the native protein.

We obtained the S100A7 proteins in yields that ranged from 30-80 mg/L of culture. Each protein was characterized by SDS-PAGE, analytical HPLC, ESI-MS, thiol quantification, CD spectroscopy, analytical SEC, and ICP-MS. SDS-PAGE and analytical HPLC analysis revealed that all proteins were obtained in high purity (Figures 3. 3 and 3. 4), ESI-MS afforded the expected mass for each protein, and free thiol quantification using DTDP further verified the redox states of S100A7_{red} (≈ 4 free thiols per homodimer) and S100A7_{ox} (≈ 0 free thiol per homodimer) (Table 3. 4). The CD spectra showed local minima at 208 and 220 nm, confirming the expected α -helical secondary structure (Figure 3. 5). Analytical SEC demonstrated that each apo protein was isolated as a homodimer, and that each protein eluted as a homodimer in the presence of excess Ca(II) and Zn(II), indicating that metal binding does not cause a change in quaternary structure (Table 3. 5, Figure 3. 6). ICP-MS demonstrated low contaminating metal content in the purified proteins (Table 3. 4).

Table 3. 4. Characterization of S100A7 and variants

Protein	HPLC Retention Time (min)^a	Free thiol^b	Calculated Mass (Da)	Observed Mass (Da)
S100A7 _{ox}	16.4	0.11 ± 0.03	11 454.9	11 445.4 11 324.0 (-Met1)
S100A7 _{red}	18.4	4.16 ± 0.45	11 456.9	11 457.4 11 326.0 (-Met1)
S100A7-Ser	16.0	0.05 ± 0.01	11 424.8	11 425.5 11 294.2 (-Met1)
S100A7-Ala	16.7	0.04 ± 0.00	11 392.8	11 392.8 11 261.1 (-Met1)
S100A7 _{Δox}	21.0	0.14 ± 0.04	11 212.7	11 212.9 11 082.0 (-Met1)

^a The purified proteins are mixtures of full-length S100A7 and S100A7 lacking the N-terminal Met residue. In some chromatograms, partial separation of these two species is observed. The retention time is for the major species, which corresponds to the isoform containing the N-terminal Met residue. ^b Free thiol content determined by using the DTDP assay (mean ± SDM, *n* = 2).

Table 3. 5. Metal analysis (ICP-MS) of S100A7 from representative protein purifications

Metal	Protein (10 μ M)				
	S100A7 _{ox}	S100A7 _{red}	S100A7-Ser	S100A7-Ala	S100A7 Δ _{ox}
Mg (μ M)	1.525	1.844	0.825	1.236	0.702
(equiv)	0.153	0.184	0.083	0.124	0.070
Ca (μ M)	0.543	1.039	13.3	6.733	12.95
(equiv)	0.054	0.104	1.33	0.673	1.300
Mn (μ M)	0.040	0.052	0.009	0.022	0.0174
(equiv)	0.004	0.005	0.000	0.002	0.002
Fe (μ M)	0.379	0.486	0.086	0.965	0.0836
(equiv)	0.038	0.049	0.009	0.097	0.008
Co (μ M)	0.001	0.002	0.003	0.001	0.002
(equiv)	0.000	0.000	0.000	0.000	0.000
Ni (μ M)	0.314	0.324	0.077	0.205	0.065
(equiv)	0.031	0.03	0.008	0.021	0.007
Cu (μ M)	0.057	0.033	0.045	0.427	0.018
(equiv)	0.006	0.003	0.005	0.043	0.002
Zn (μ M)	0.416	0.383	0.602	0.604	0.030
(equiv)	0.042	0.038	0.06	0.060	0.003

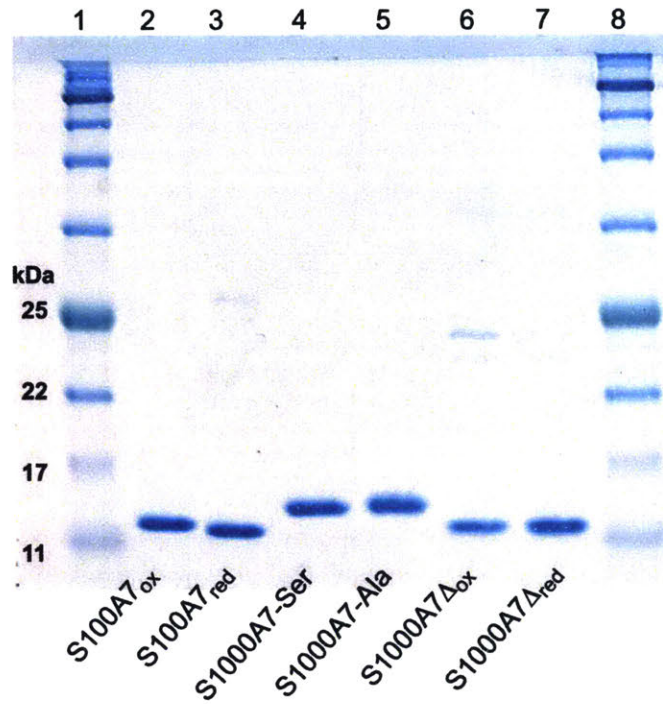


Figure 3. 3. SDS-PAGE purity gel (13% Tris-HCl, tricine gel) of the S100A7 variants employed in this work. Ladder: P7712s color prestained protein standard broad range (New England Biolabs). Ladder (lane 1), S100A7_{ox} (lane 2), S100A7_{red} (lane 3), S100A7-Ser (lane 4), S100A7-Ala (lane 5), S100A7 Δ _{ox} (lane 6), S100A7 Δ _{red} (lane 7), and ladder (lane 8).

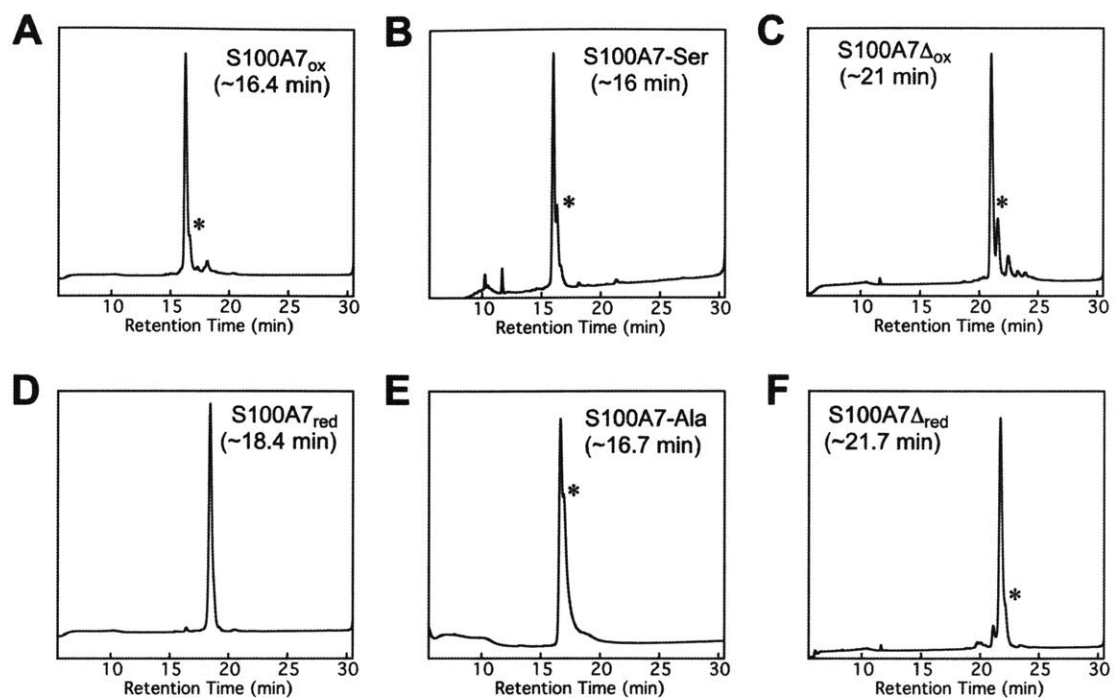


Figure 3. 4. HPLC chromatograms (220 nm absorption) of S100A7 variants: (A) S100A7_{ox}, (B) S100A7-Ser, (C) S100A7 Δ_{ox} , (D) S100A7_{red}, (E) S100A7-Ala, and (F) S100A7 Δ_{red} . Conditions: 9 μ M protein, 100 μ L injection volume. An asterisk (*) indicates the position of the isoform of S100A7 missing the N-terminal methionine.

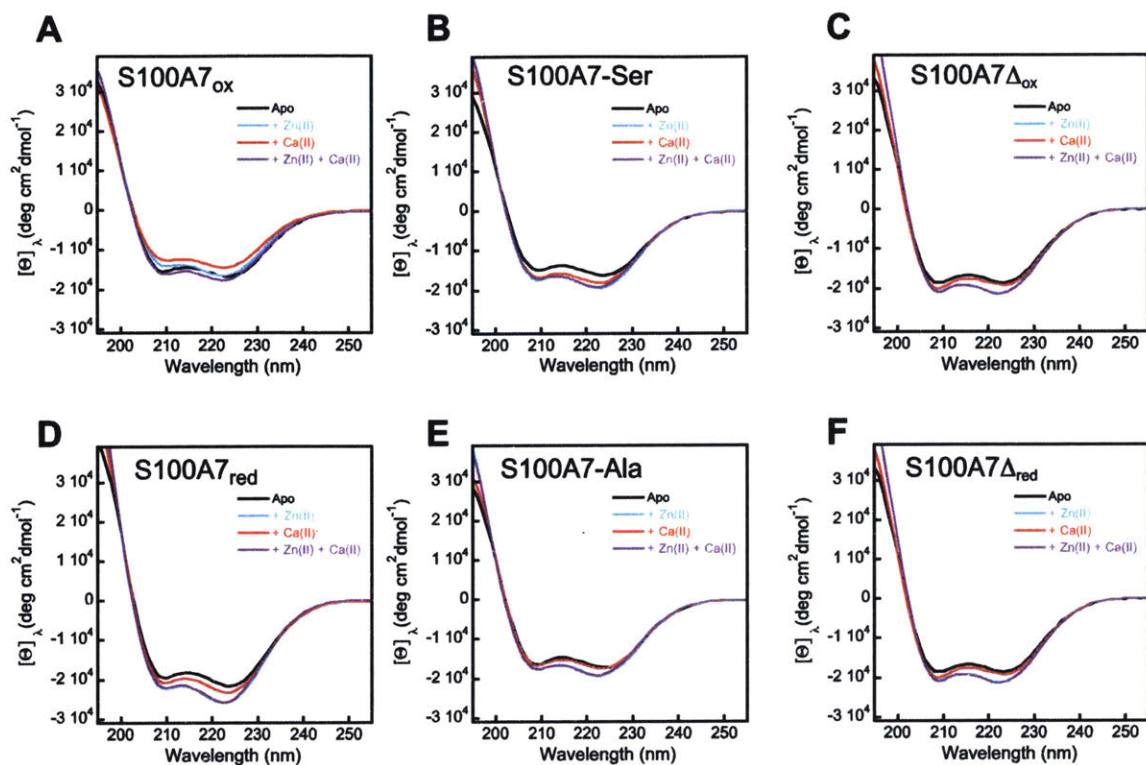


Figure 3. 5. CD spectra of 10 μM of (A) S100A7_{ox}, (B) S100A7-Ser, (C) S100A7 Δ_{ox} , (D) S100A7_{red}, (E) S100A7-Ala, and (F) S100A7 Δ_{red} in the absence and presence of divalent cations (1 mM Tris-HCl, pH 7.5, T = 25°C). Black trace, without metal addition; blue trace, in the presence of 20 μM Zn(II); red trace, in the presence of 2 mM Ca(II); purple trace, in the presence of 20 μM Zn(II) and 2 mM Ca(II).

Table 3. 6. Analytical SEC elution volumes and calculated molecular weights^a

Protein	Ca(II)	Elution Volume (mL)	Calculated Molecular Weight (kDa)
S100A7 _{ox}	-	12.7	24.2
S100A7 _{ox}	+	12.7	26.4
S100A7 _{red}	-	12.3	27.6
S100A7 _{red}	+	12.4	25.8
S100A7-Ser	-	12.0	22.1
S100A7-Ser	+	12.2	23.1
S100A7-Ala	-	11.9	21.4
S100A7-Ala	+	12.0	22.1

^a Each sample contained 30 μ M protein (75 mM HEPES, 100 mM NaCl, pH 7.0). The +Ca(II) samples contained 2 mM Ca(II) in the sample and running buffer. The experiments were performed at 4 °C.

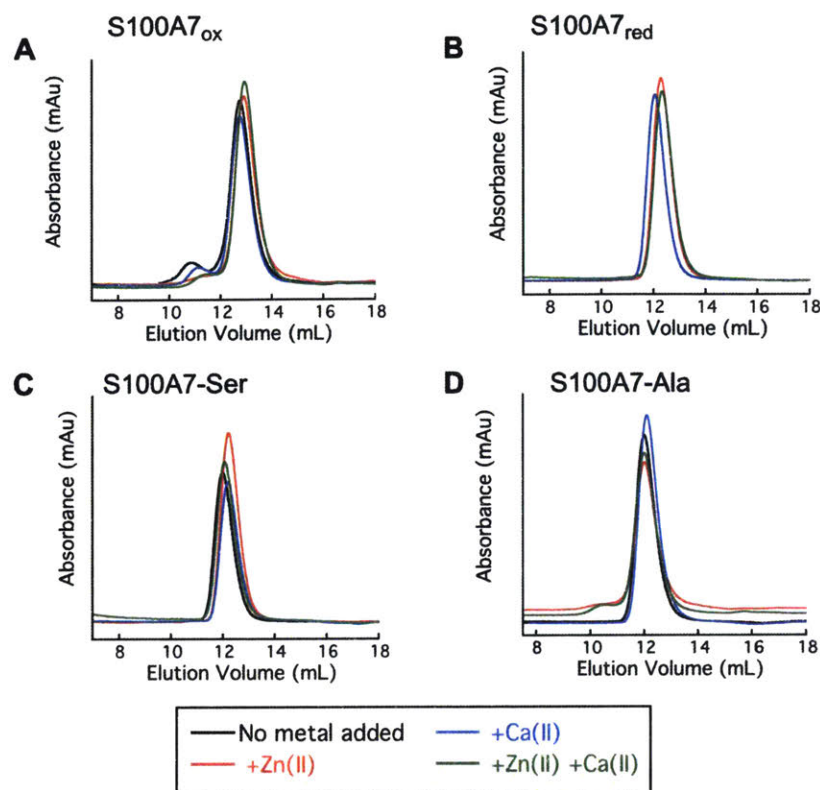


Figure 3. 6. Analytical size exclusion chromatography (SEC) of S100A7 (30 μ M, 300 μ L) in the absence and presence of divalent cations (75 mM HEPES, 100 mM NaCl, pH 7.0). (A) S100A7_{ox}, (B) S100A7_{red}, (C) S100A7-Ser, and (D) S100A7-Ala. For experiments containing Zn(II) and Ca(II), 2 equiv of Zn(II) were added to the samples, and 2 mM Ca(II) were added to the sample and running buffer. The absorbance was monitored at 280 nm.

3. 4. 2. The Thioredoxin System Reduces Apo S100A7_{ox}

In agreement with prior work,¹² we observed that apo S100A7_{ox} is a substrate for the mammalian thioredoxin system. Analytical HPLC of samples from enzymatic activity assays conducted at pH 7.0 containing apo S100A7_{ox}, human Trx, rat liver TrxR, and NADPH revealed loss of S100A7_{ox} (16.4 min, \pm Met1) and formation of S100A7_{red} (18.4 min, \pm Met1) (Figure 3. 7A). At the final 2-h time point, the reaction mixture predominantly contained S100A7_{red}. As expected, HPLC traces for the no-enzyme control showed no S100A7_{red} formation over this time period (Figure 3. 7E–H). This assay was performed aerobically, and it is possible that some background air oxidation of S100A7_{red} occurred over the 2-h time course, which would regenerate the substrate (Figure 3. 8).

Next, we examined the effect of Ca(II) on the Trx/TrxR-catalyzed reduction of the Cys47–Cys96 disulfide bond in S100A7_{ox}. When we included 2 mM Ca(II) in the assay buffer, we observed less formation of S100A7_{red}; integration of the peak areas revealed that the S100A7 mixtures contained only ≈12% and ≈22% S100A7_{red} at 15 and 120 min, respectively (Figure 3. 7B). Prior investigations demonstrated that Ca(II) does not affect the enzymatic activity of Trx/TrxR.²⁹ In order to corroborate these results, we performed Trx/TrxR activity assays using HD5_{ox}, a peptide with three disulfide bonds that does not coordinate Ca(II), as a substrate and observed comparable disulfide bond reduction in the absence and presence of 2 mM Ca(II) (Figure 3. 9). When we pre-incubated S100A7_{ox} with 1.9 equivalents of Zn(II) to form the Zn(II):S100A7_{ox} complex, negligible formation of S100A7_{red} in the absence or presence of Ca(II) occurred (Figures 3. 7C and 3. 7D). Because Zn(II) is an inhibitor of the thioredoxin system,²⁹ we designed a control assay to probe whether the Zn(II) included in this assay poisoned the enzyme. Using the same assay conditions, we spiked the reaction mixture with HD5_{ox}, a Trx/TrxR substrate that does not bind Zn(II). We observed comparable reduction of HD5_{ox} to HD5_{red} in the absence and presence of Zn(II)-S100A7_{ox}, indicating that the Zn(II) was bound to S100A7_{ox} and therefore did not inhibit the thioredoxin system (Figure 3. 10). Thus, Zn(II) binding to S100A7_{ox} prevents intramolecular disulfide bond reduction by Trx/TrxR.

Taken together, these data suggest that Ca(II) and Zn(II) depress the redox potential of the intramolecular disulfide bonds in S100A7_{ox}. An alternative scenario is that metal binding causes a change in protein structure or dynamics that precludes enzymatic access to the disulfide bonds. However, apo, Ca(II)-bound, Zn(II)-bound, and Ca(II)- and Zn(II)-bound S100A7_{ox} are homodimers and the Cys47–Cys96 disulfide bond is surface exposed in the crystal structures of S100A7 (Figure 3. 1), making us favor the former possibility.

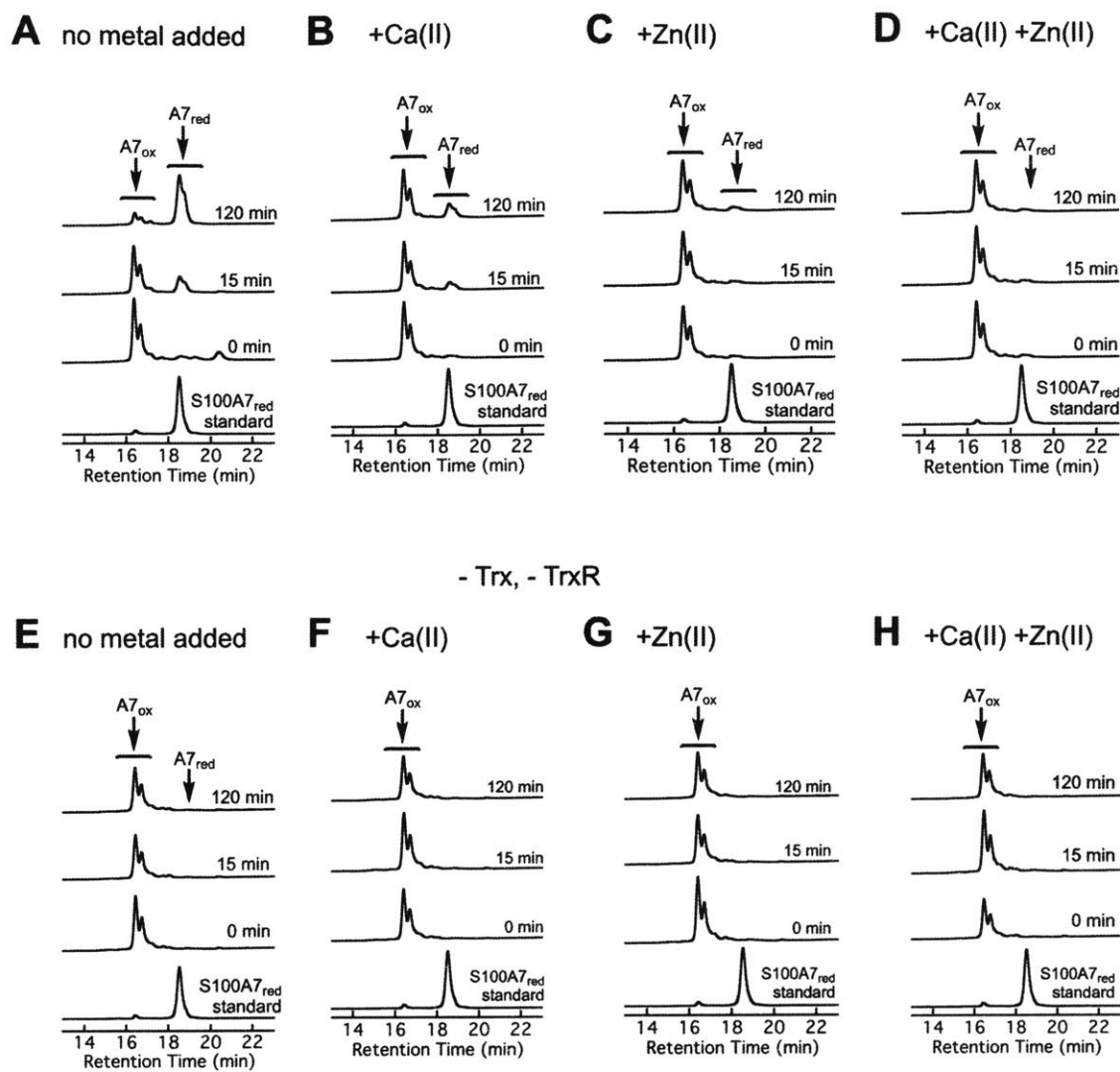


Figure 3. 7. Analytical HPLC traces (220 nm absorption) from enzymatic activity assays employing the mammalian thioredoxin system and S100A7_{ox} as a substrate. Conditions: 5 μ M S100A7_{ox}, 1 μ M human Trx, 0.1 μ M rat liver TrxR, and 1 mM NADPH (75 mM HEPES, 100 mM NaCl, pH 7.0, 37 $^{\circ}$ C) with (A) no metal added, (B) 2 mM Ca(II) added to the buffer, (C) 1.9 equiv of Zn(II) added, (D) 1.9 equiv of Zn(II) and 2 mM Ca(II) added to the buffer, (E) no metal added, no enzyme added, (F) 2 mM Ca(II) added to the buffer, no enzyme added, (G) 1.9 equiv of Zn(II) added, no enzyme added, and (H) 1.9 equiv of Zn(II) and 2 mM Ca(II) added to the buffer, no enzyme added. In each panel, the bottom chromatogram is a S100A7_{red} standard. The shoulder peaks observed in the chromatograms of S100A7_{ox} and S100A7_{red} correspond to S100A7 isoforms missing the N-terminal methionine.

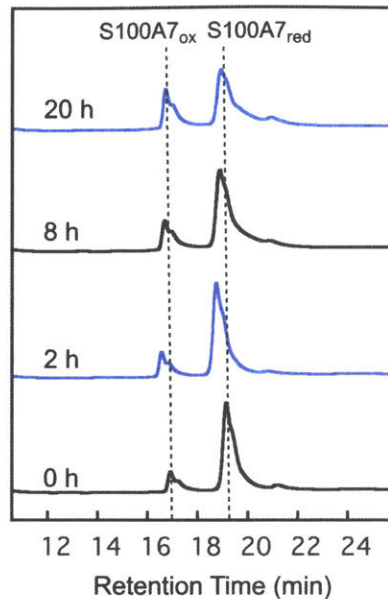


Figure 3. 8. Analytical HPLC (220 nm) showing air oxidation of S100A7_{red} over time (0, 2, 8, and 20 h). A 500- μ L aliquot of 30 μ M S100A7_{red} in 75 mM HEPES, 100 mM NaCl, pH 7.0 was incubated at room temperature, and 100- μ L aliquots were analyzed by HPLC at the specified timepoints. The shoulder peak observed corresponds to the isoform of S100A7 missing the N-terminal methionine.

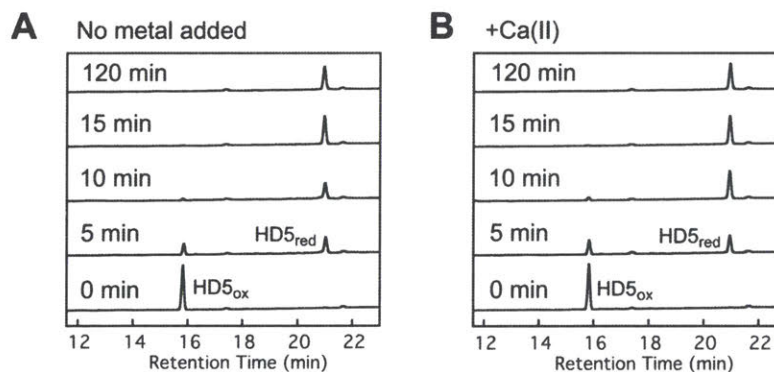


Figure 3. 9. Analytical HPLC traces (220 nm) monitoring the reduction of HD5_{ox} by Trx/TrxR in the (A) absence and (B) presence of 2 mM Ca(II). These assays served as controls for examining the effect of 2 mM Ca(II) on the activity of the thioredoxin system. Conditions: 10 μ M HD5_{ox}, 1 μ M human Trx, 0.1 μ M rat liver TrxR, 1 mM NADPH, \pm 2 mM Ca(II), 75 mM HEPES, 100 mM NaCl, pH 7.0.

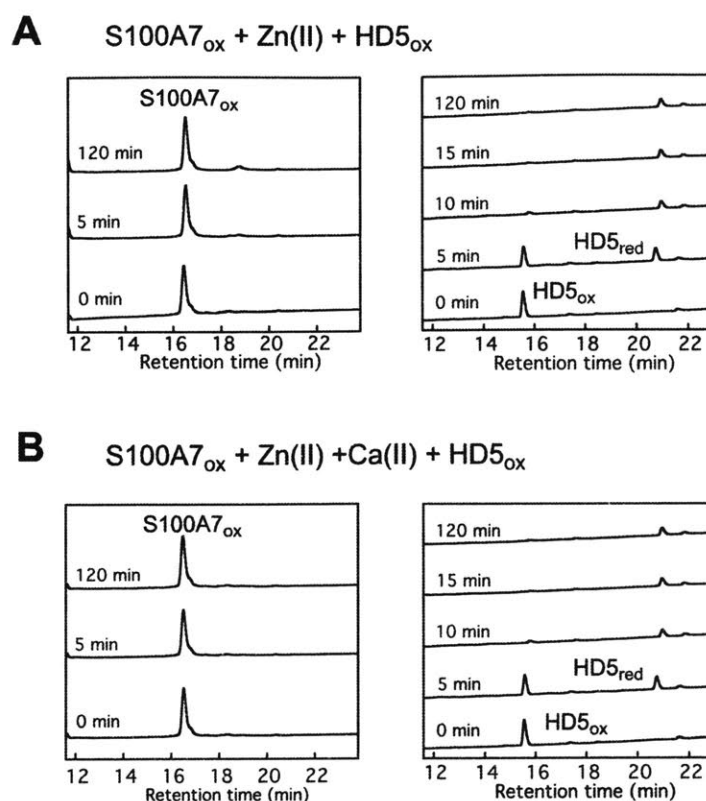


Figure 3. 10. Analytical HPLC traces (220 nm) monitoring the reduction of HD5_{ox} by Trx/TrxR in the presence of Zn(II)-bound S100A7_{ox} in the (A) absence and (B) presence of 2 mM added Ca(II). (1 mM NADPH in 75 mM HEPES, 100 mM NaCl, pH 7.0). These assays served as controls for examining the effect of Zn(II)-S100A7_{ox} on the activity of the thioredoxin system. Conditions: 10 μ M HD5_{ox}, 5 μ M S100A7_{ox}, 9.5 μ M Zn(II), 1 μ M human Trx, 0.1 μ M rat liver TrxR, 1 mM NADPH, \pm 2 mM Ca(II).

3. 4. 3. Ca(II) Ions Depress the Midpoint Potential of S100A7

In order to gain further insight into the redox behavior of S100A7, we determined the midpoint potential (E_m) of S100A7 at pH 7.0 in the absence and presence of 2 mM Ca(II) (Figure 3. 11). We incubated anaerobic solutions of S100A7_{ox} in glutathione-based buffers with defined redox potentials spanning the -400 to -200 mV range for 96 h at 37 °C. To demonstrate that redox equilibrium was reached, we verified that the protein speciation was unchanged at 96 h compared to earlier and later time points (Figure 3. 12). Analytical HPLC of the equilibrium mixtures revealed

varying ratios of peaks corresponding to S100A7_{ox} and S100A7_{red}, and an S100A7-glutathione adduct was also identified (Figure 3. 13). The E_m value of the S100A7 disulfide bond was determined from the equilibrium between S100A7_{ox} and S100A7_{red} as quantified by HPLC. It was first estimated by identifying the E_m value that provided a 1:1 ratio of S100A7_{ox} and S100A7_{red} (Figure 3. 11). This simple analysis yielded values of ca. -255 (-Ca) and -298 (+Ca) mV. Subsequent data fitting showed that the data were not well fit using the Nernst equation (Figures 3. 14B and 3.14D). This poor data fitting occurred because all samples contained mixtures of S100A7_{ox} and S100A7_{red} at equilibrium; the percentage of S100A7_{ox} in solution maximized at -200 mV where the mixtures contain \approx 93 and \approx 96% S100A7_{ox} for apo and Ca(II)-bound S100A7, respectively (Figure 3. 11). We therefore employed a logistic function and allowed the calculated maxima to vary during data fitting. In agreement with the simple by-the-eye analysis, this analysis provided E_m values of -255 (-Ca) and -298 (+Ca) mV (Figures 3. 14A and 3. 14C). These values fall within the range expected for disulfide-containing peptides and proteins.^{30,36,39,40} Of note, this work provides a foundation for future experiment that address how additional experimental conditions of physiological relevance, such as changes in ionic strength, affect the redox properties of S100A7.

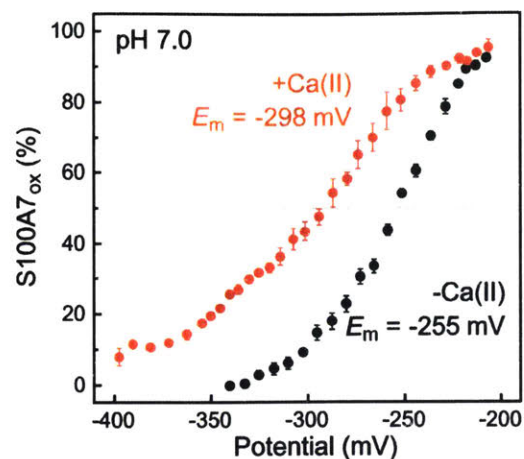


Figure 3. 11. Ca(II) depresses the midpoint potential of S100A7. Percentage of S100A7_{ox} at equilibrium following incubation of S100A7_{ox} (10 μ M) in buffers with defined redox potentials (75 mM HEPES, 100 mM NaCl, pH 7.0, 10 mM total [GSH] and [GSSG], \pm 2 mM Ca(II)) determined from integration of HPLC peaks (mean \pm SDM, $n = 3$). Black spheres: in the absence of Ca(II); red spheres: in the presence of 2 mM Ca(II).

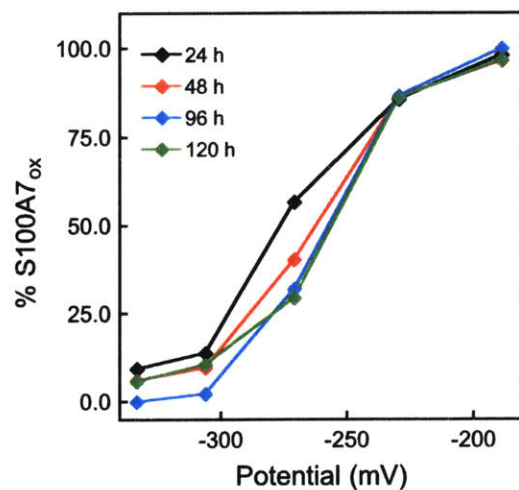


Figure 3. 12. Percentage of S100A7_{ox} at $t = 24, 48, 96,$ and 120 h after incubation of 10 μ M S100A7_{ox} in glutathione-based redox buffers with defined redox potentials (75 mM HEPES, 100 mM NaCl, pH 7.0), at 37 $^{\circ}$ C under anaerobic conditions.

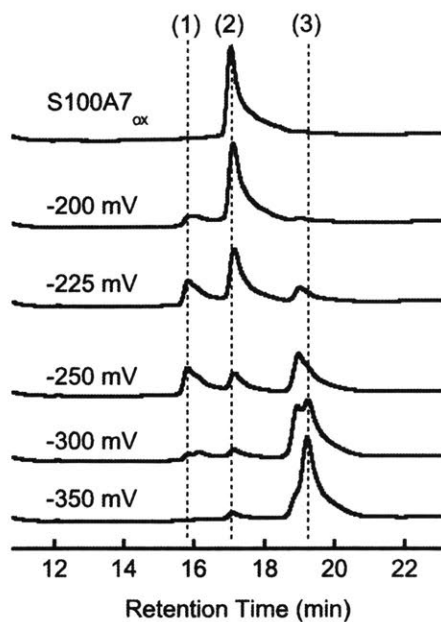


Figure 3. 13. Representative HPLC traces showing the speciation of S100A7 after a 96-h incubation of 10 μM S100A7_{ox} in glutathione-based redox buffers with defined redox potentials (75 mM HEPES, 100 mM NaCl, pH 7.0). Peak 1 corresponds to a glutathione-S100A7 mixed disulfide species, peak 2 corresponds to S100A7_{ox}, and peak 3 corresponds to S100A7_{red}. The identity of each peak was confirmed by LC-MS.

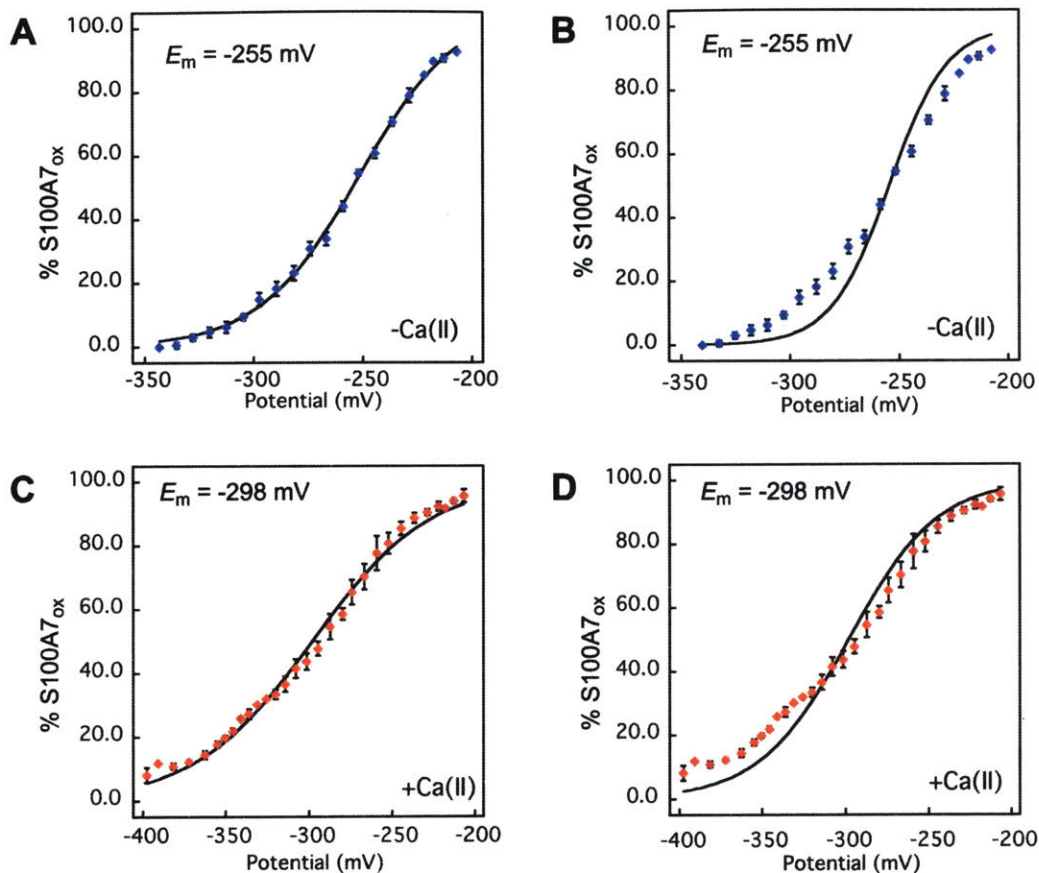


Figure 3. 14. Midpoint potential data presented in Figure 4 were fit to a logistic function (A and C) and the Nernst equation (B and D). This experiment was performed in the absence (A and B, blue markers) and in the presence of 2 mM Ca(II) (C and D, red markers). Derivations for the Nernst and Logistic functions are presented in sections 3. 1. 6 and 3. 1. 7, respectively.

Further investigations are required to elucidate the molecular basis for how Ca(II) coordination depresses the E_m value of S100A7 by ≈ 50 mV. Overlaying the Ca(II)-free²⁰ and Ca(II)-bound⁶ crystal structures suggests that Ca(II) binding by S100A7 does not cause a significant structural re-arrangement. However, in solution, Ca(II)-binding at the EF-hand domains — and specifically the C-terminal EF hand, which is in closest proximity to the disulfide bridge (Figure 3. 1D) — may affect protein dynamics such that intramolecular disulfide bond formation is favored. Ca(II) binding may also decrease entropy and cause the regions around Cys47 and Cys96 to become more rigid, and thus prearrange these residues for disulfide bond formation

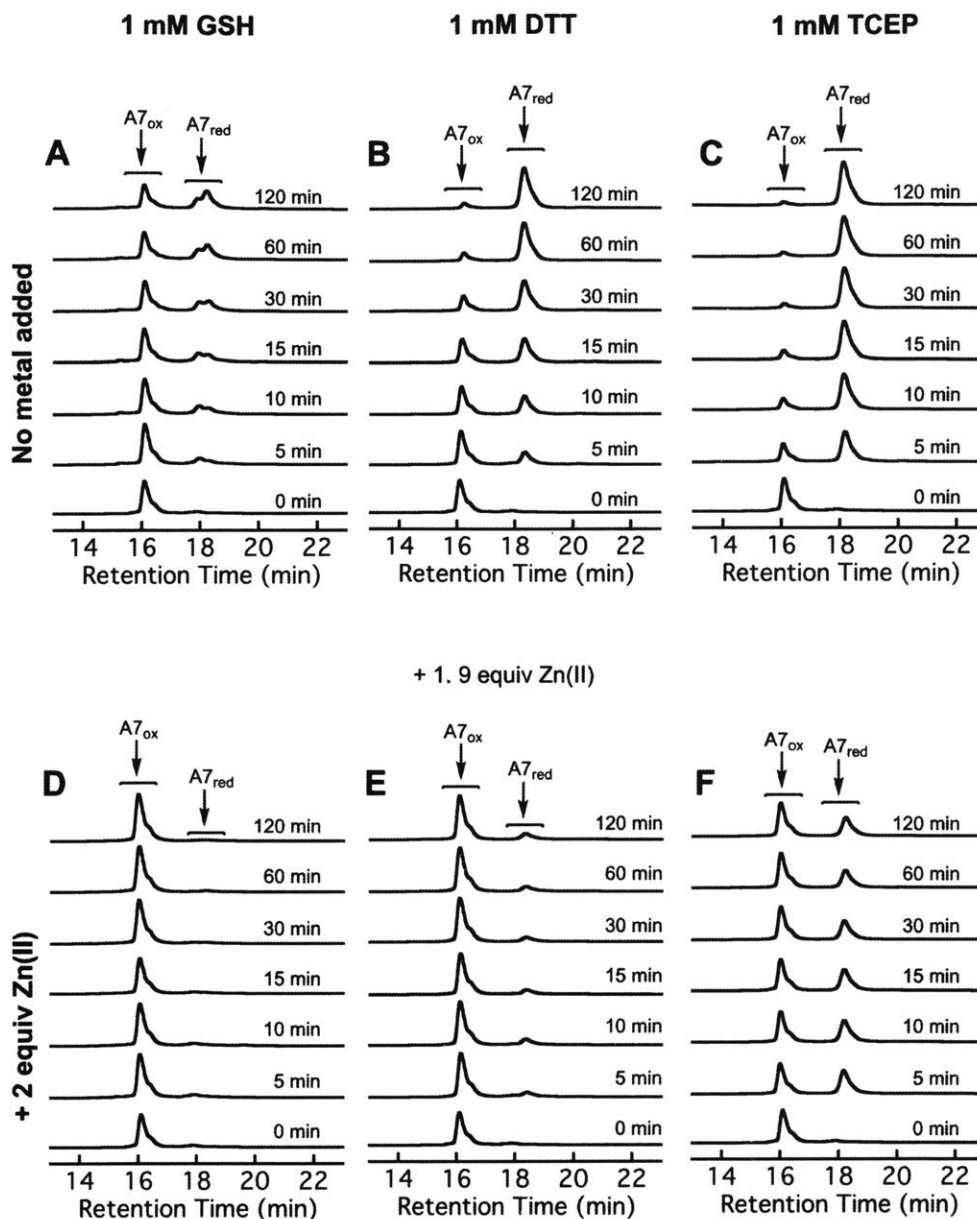


Figure 3. 15. Representative HPLC traces showing the reduction of S100A7_{ox} to S100A7_{red} in the absence (A-C) and presence (D-F) of Zn(II) following addition of 1 mM GSH, DTT or TCEP over time. Aliquots of 400 μ L of 30 μ M S100A7_{ox} in were allowed to incubate with 1 mM of a reducing agent at room temperature. Aliquots of 100 μ L were analyzed by HPLC at the specified timepoints (0, 5, 10, 15, 30, 60, and 120 min). For the Zn(II)-bound samples (D-F), S100A7_{ox} was pre-incubated with 1.9 equiv of Zn(II) (60 μ M) for 15 min prior to addition of the reducing agent.

We attempted to determine the midpoint potentials of Zn(II)- and Ca(II)- and Zn(II)-bound S100A7. These experiments were unsuccessful because we were unable to reduce Zn(II)-bound S100A7_{ox}, even under the most reducing conditions provided by the glutathione redox buffer system (-400 mV) (data not shown). We also observed that reduction of the disulfide bond in Zn(II)-bound S100A7_{ox} by addition of excess GSH, DTT or TCEP occurs less readily than for its apo counterpart (Figure 3. 15). Similar to the effect of Ca(II) ions on the E_m value of S100A7, Zn(II) coordination at the His₃Asp sites may stabilize or favor formation of the disulfide bridge.

3. 4. 4. Both S100A7_{ox} and S100A7_{red} Have Two High-Affinity Zn(II)-binding Sites

The crystal structure of Ca(II)- and Zn(II)-bound S100A7_{ox} shows a Zn(II):S100A7_{ox} homodimer stoichiometry of 2:1,⁶ which is expected because of the two His₃Asp sites per homodimer. Nevertheless, the Zn(II)-binding stoichiometry of S100A7_{red} has not been ascertained, and it was recently hypothesized that the free thiolates of Cys47 and Cys96 create a third high-affinity Zn(II) site in S100A7_{red}.¹² This notion originated from studies in which S100A7_{red} exhibited greater antimicrobial activity than S100A7_{ox} against the fungal pathogen *A. fumigatus*, which was attributed to more effective Zn(II)-sequestering activity by the reduced form.¹² To investigate the Zn(II)-binding stoichiometry of S100A7_{ox} and S100A7_{red} in solution, we performed Zn(II) competition experiments with each protein and the colorimetric Zn(II) indicator Zincon ($K_{d,Zn} \approx 10 \mu\text{M}$).⁴¹⁻⁴² These titrations revealed that S100A7_{ox} and S100A7_{red} outcompete Zincon for two equivalents of Zn(II) in both the absence and presence of 2 mM Ca(II) (Figures 3. 16), and that the free Cys residues in S100A7_{red} do not form a third high-affinity Zn(II) site.

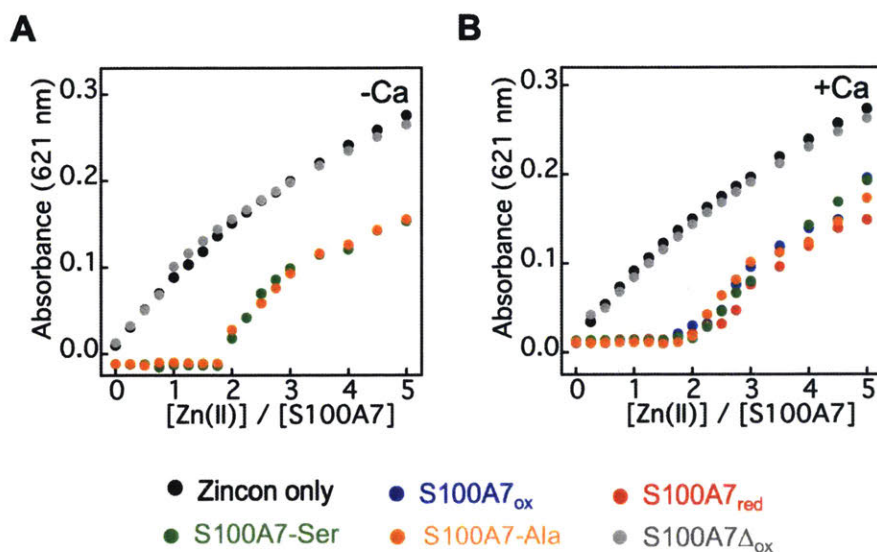


Figure 3. 16. Representative plot showing the response of 20 μM Zincon to Zn(II) in the presence of 10 μM S100A7 variants in 75 mM HEPES, 100 mM NaCl, pH 7.0, ± 2 mM Ca(II) at 25 $^{\circ}\text{C}$. (A) In the absence of Ca(II). (B) In the presence of Ca(II). The Zn(II)-Zincon complex exhibits an absorbance maximum at 621 nm.

3. 4. 5. Both S100A7_{ox} and S100A7_{red} Bind Zn(II) with Sub-Nanomolar Affinity

To further probe the Zn(II) affinity of S100A7, we performed additional competition titrations with S100A7_{ox}, S100A7_{red}, and the variants S100A7-Ser, S100A7-Ala, and S100A7 Δ_{ox} . We examined the competition between S100A7 and the turn-on fluorescent Zn(II) sensor FluoZin-3 (FZ3, apparent $K_{d,Zn} = 9$ nM).⁴³ Because FZ3 exhibits a fluorescent response to Ca(II), these titrations were performed in the absence of Ca(II). With the exception of S100A7 Δ_{ox} , negligible change in FZ3 emission was observed following addition of 2 μM Zn(II) to solutions containing 2 μM of FZ3 and 2 μM S100A7 (Figure 3. 17). This result indicates that S100A7 coordinates Zn(II) with higher affinity than FZ3. In contrast, fluorescent turn-on comparable to the FZ3-only control was observed in the presence of S100A7 Δ_{ox} , confirming the importance of the His₃Asp sites in Zn(II) coordination.

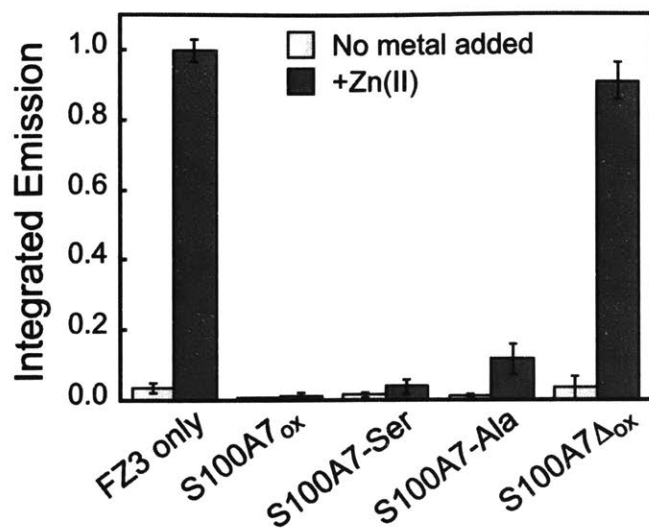


Figure 3. 17. S100A7 outcompetes FZ3 for Zn(II). Fluorescence response of 2 μ M FZ3 to 2 μ M Zn(II) in the absence and presence of 2 μ M S100A7_{ox}, S100A7-Ser, S100A7-Ala, or S100A7 Δ _{ox} at pH 7.0 (75 mM HEPES, 100 mM NaCl) and 25 °C. Integrated emission values were normalized to the maximum emission for FZ3 in the presence of 1 equiv. of Zn(II) (mean \pm SDM, $n = 3$).

We next conducted competition experiments by using a higher-affinity and Ca(II)-insensitive turn-on fluorescent Zn(II) sensor, Zinpyr-4 (ZP4, apparent $K_{d,Zn} = 650$ pM).³² In preliminary studies, we observed that ZP4 and the S100A7 proteins competed for Zn(II) in both the absence and presence of Ca(II). We therefore titrated Zn(II) into mixtures containing 5 μ M S100A7 and 2 μ M ZP4 (75 mM HEPES, 100 mM NaCl, pH 7.0) and fit the resulting data to obtain apparent $K_{d,Zn}$ values (Figures 3. 18–3. 22, Table 3. 7). Because S100A7 is a homodimer with two identical His₃Asp sites, we focus on a two-site binding model where $K_{d1} = K_{d2}$. Nevertheless, during our analyses, we also fit the data using a one-site model and a two-site binding model where $K_{d1} \neq K_{d2}$ for the purpose of comparison (Table 3. 5, Figures 3.19–3. 22). We also simulated fits using K_d values that are 2- to 10-fold lower and 2- to 10-fold higher than the values we ascertained; these simulations support the validity of the reported fits (Figure 3. 23).

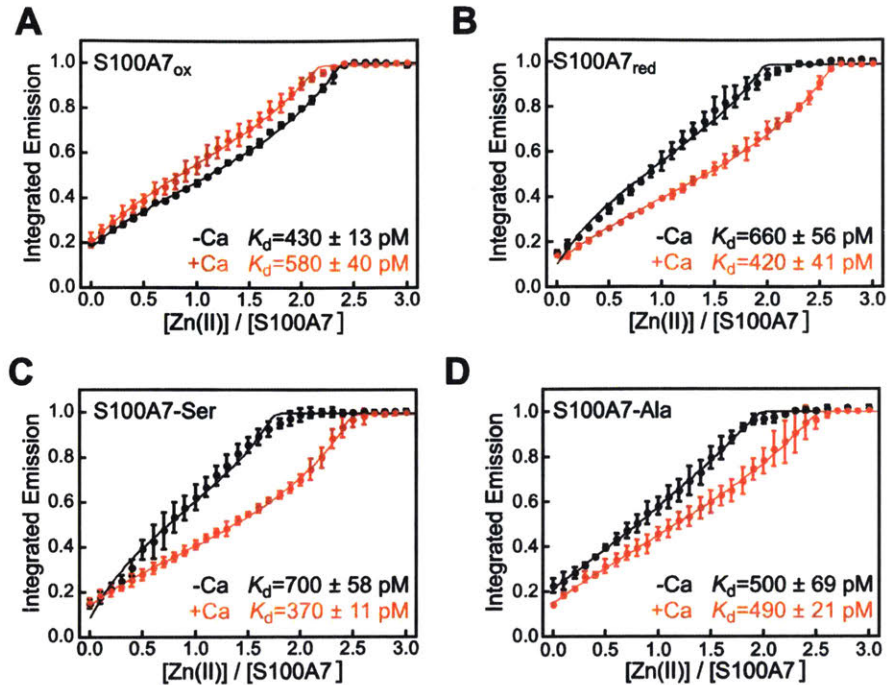


Figure 3. 18. Zn(II)-induced response of 2 μM ZP4 in the presence of 5 μM (A) S100A7_{ox}, (B) S100A7_{red}, (C) S100A7-Ser, and (D) S100A7-Ala at pH 7.0 (75 mM HEPES, 100 mM NaCl) at 25 $^{\circ}\text{C}$, in the absence (black circles) and presence (red circles) of 100 equiv of Ca(II). Excitation was provided at 495 nm and the emission spectra were integrated from 505–650 nm. The integrated emission was normalized to the maximum response (mean \pm SDM, $n = 3$). The data were fit to a two-sites binding model with $K_{d1} = K_{d2}$. The calculated apparent K_d values corresponding to the fits are listed in the bottom right of each plot.

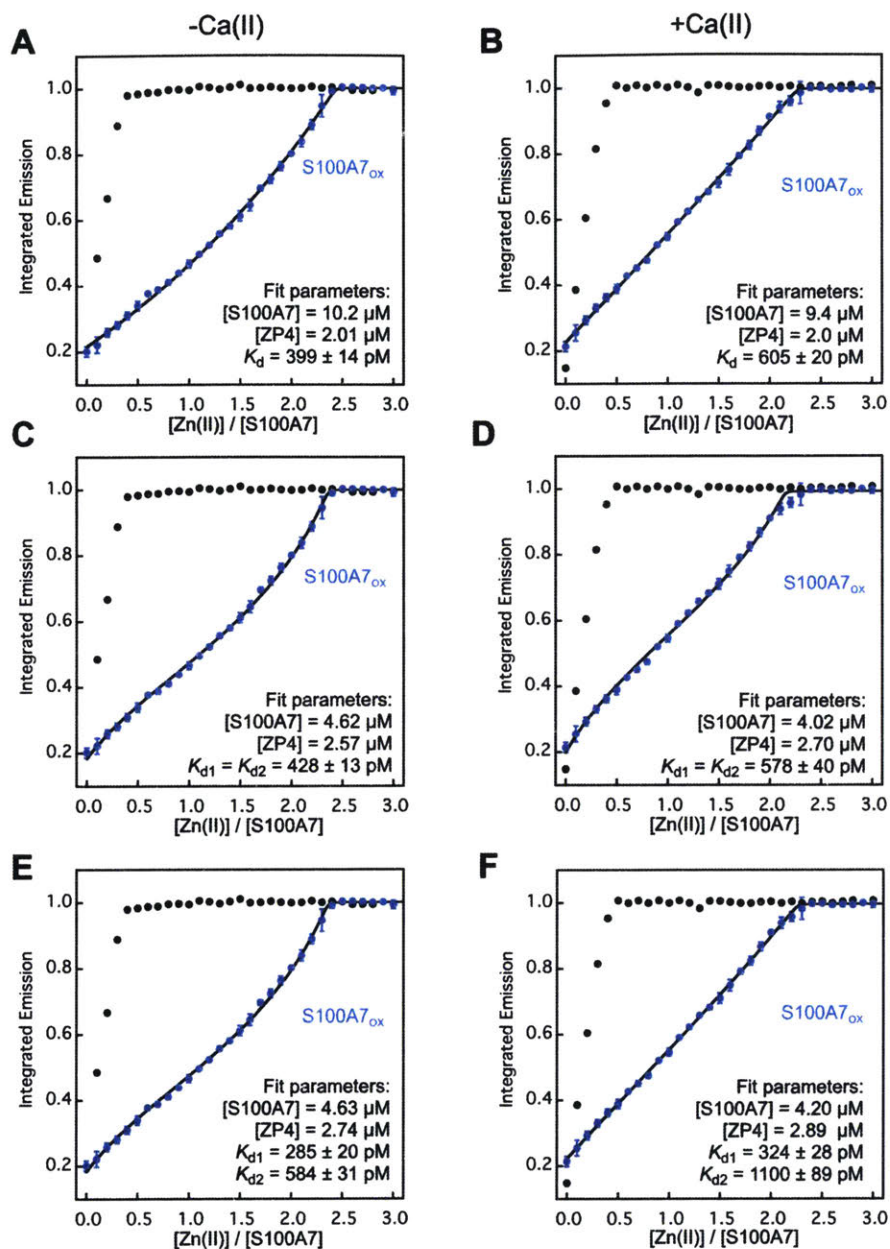


Figure 3. 19. Zn(II)-induced response of 2 μ M ZP4 in the presence of 5 μ M S100A7_{ox} at pH 7.0 (75 mM HEPES, 100 mM NaCl) at 25 $^{\circ}$ C, in the absence (left panels) and presence (right panels) of 100 equiv of Ca(II). The integrated emission was normalized to the maximum response (mean \pm SDM, n = 3). The data were fit to a one-site binding model (A and B), two-sites binding model with $K_{d1} = K_{d2}$ (C and D), or a two-sites binding model with $K_{d1} \neq K_{d2}$ (E and F). In each panel, the black and blue spheres correspond to the ZP4 only control and the ZP4 response in the presence of S100A7_{ox}, respectively. The calculated apparent K_d values corresponding to the fits and the fit parameters are listed in the bottom right of each plot.

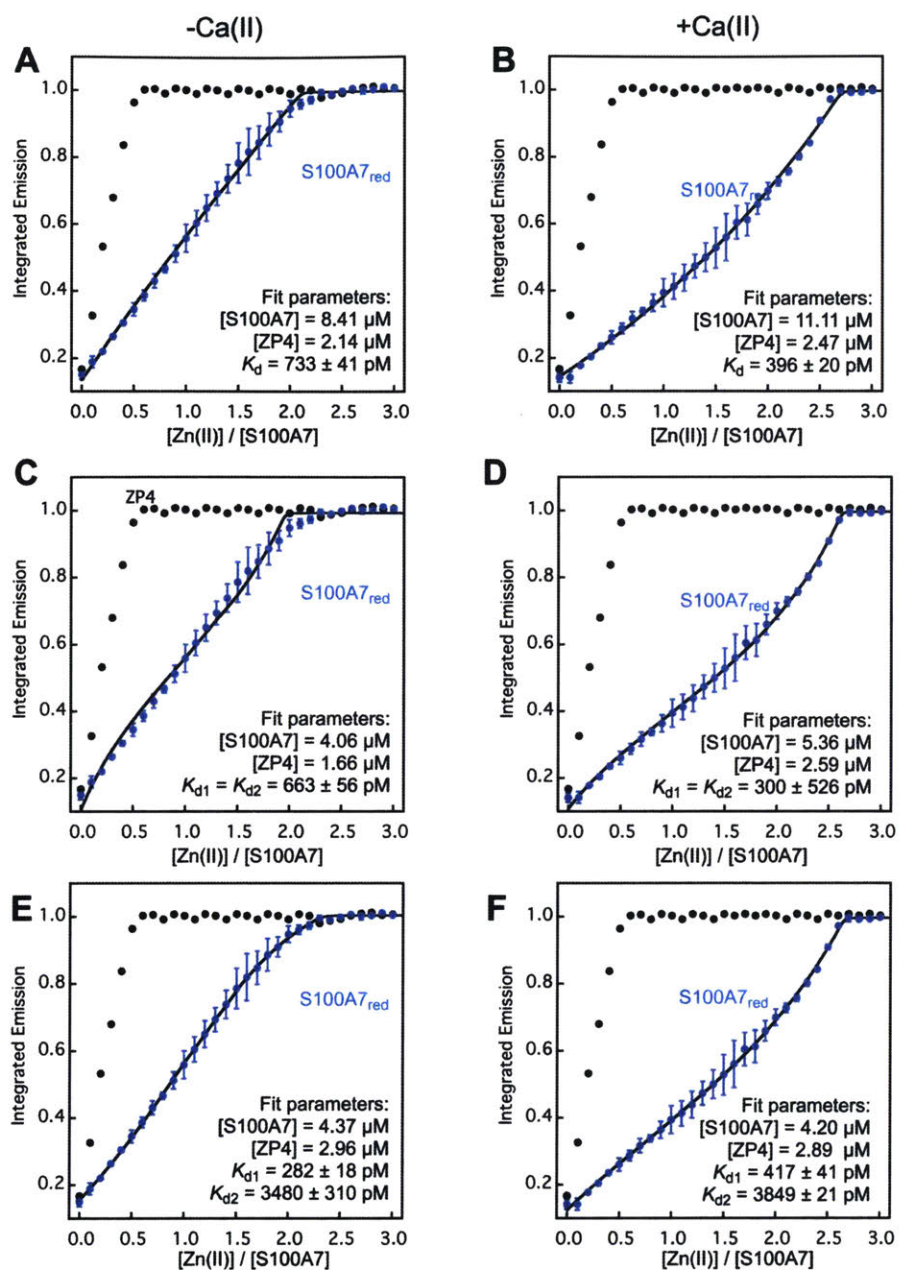


Figure 3. 20. Zn(II)-induced response of 2 μM ZP4 in the presence of 5 μM S100A7_{red} at pH 7.0 (75 mM HEPES, 100 mM NaCl) at 25 °C, in the absence (left panels) and presence (right panels) of 100 equiv of Ca(II). The integrated emission was normalized to the maximum response (mean \pm SDM, $n = 3$). The data were fit to a one-site binding model (A and B), two-sites binding model with $K_{d1} = K_{d2}$ (C and D), or a two-sites binding model with $K_{d1} \neq K_{d2}$ (E and F). In each panel, the black and blue spheres correspond to the ZP4 only control and the ZP4 response in the presence of S100A7_{red}, respectively. The calculated apparent K_d values corresponding to the fits and the fit parameters are listed in the bottom right of each plot.

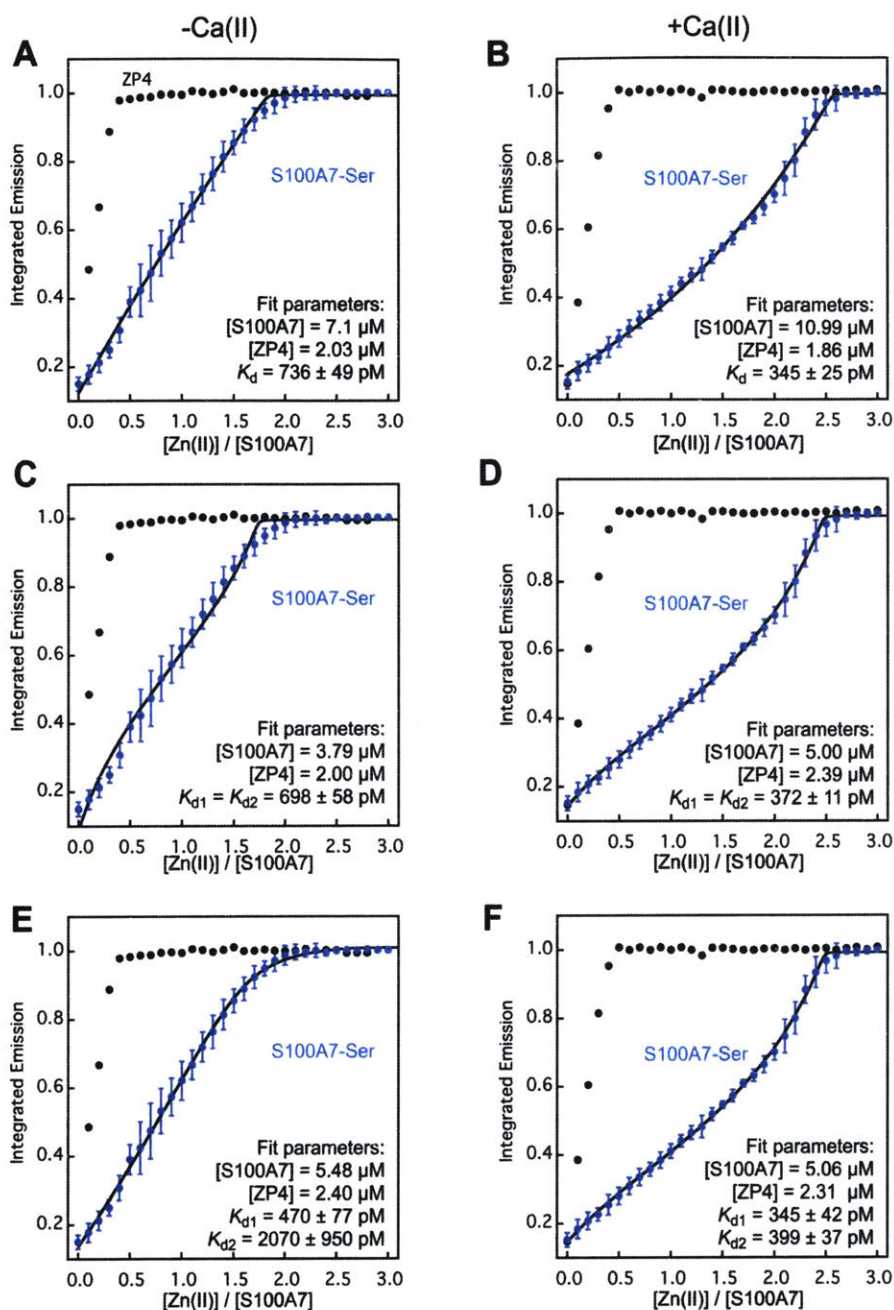


Figure 3. 21. Zn(II)-induced response of 2 μ M ZP4 in the presence of 5 μ M S100A7-Ser at pH 7.0 (75 mM HEPES, 100 mM NaCl) at 25 $^{\circ}$ C, in the absence (left panels) and presence (right panels) of 100 equiv of Ca(II). The integrated emission was normalized to the maximum response (mean \pm SDM, $n = 3$). The data were fit to a one-site binding model (A and B), two-sites binding model with $K_{d1} = K_{d2}$ (C and D), or a two-sites binding model with $K_{d1} \neq K_{d2}$ (E and F). In each panel, the black and blue spheres correspond to the ZP4 only control and the ZP4 response in the presence of S100A7-Ser, respectively. The calculated apparent K_d values corresponding to the fits and the optimized parameters are listed in the bottom right of each plot.

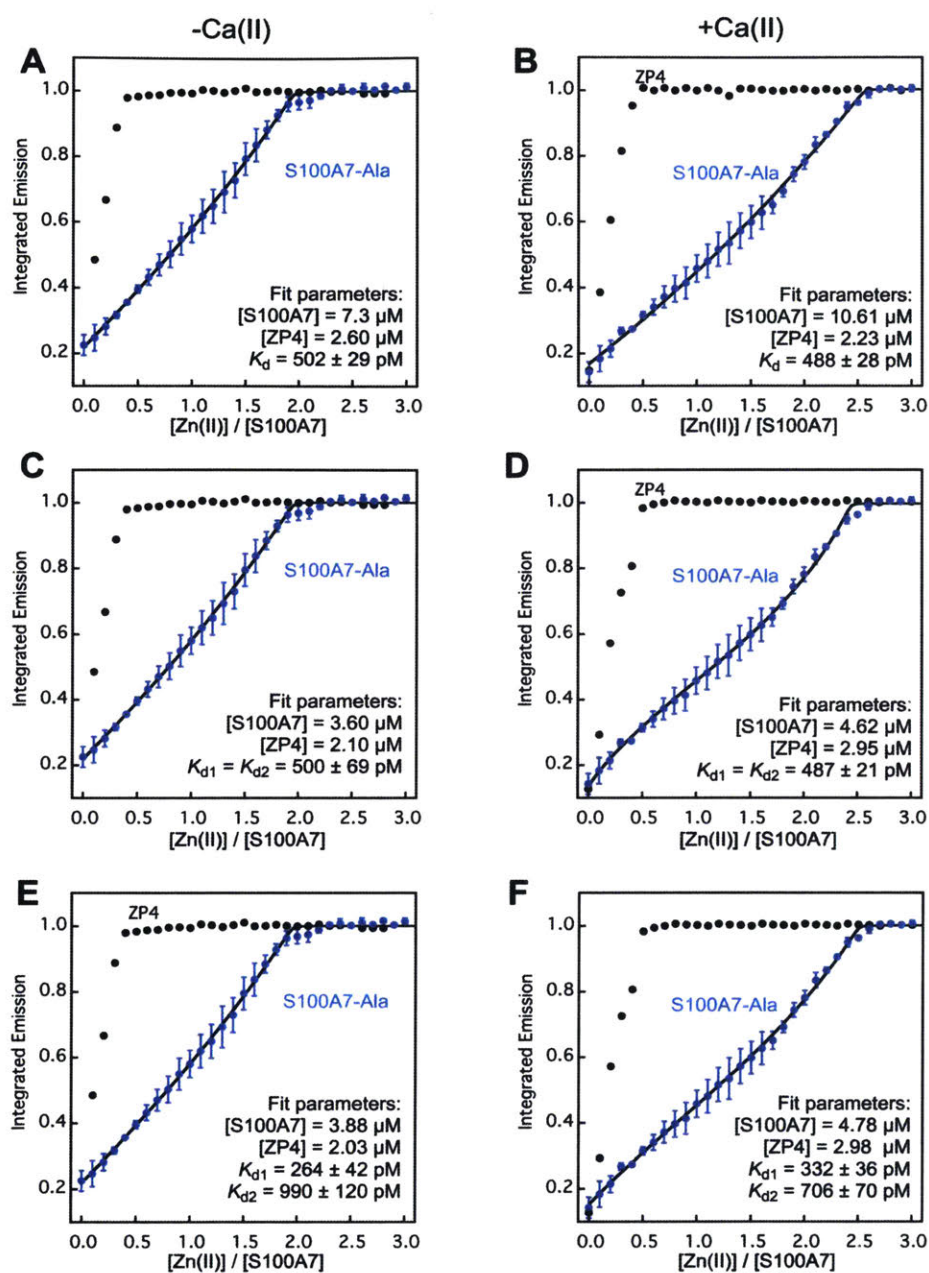


Figure 3. 22. Zn(II)-induced response of 2 μ M ZP4 in the presence of 5 μ M S100A7-Ala at pH 7.0 (75 mM HEPES, 100 mM NaCl) at 25 $^{\circ}$ C, in the absence (left panels) and presence (right panels) of 100 equiv of Ca(II). The integrated emission was normalized to the maximum response (mean \pm SDM, $n = 3$). The data were fit to a one-site binding model (A and B), two-sites binding model with $K_{d1} = K_{d2}$ (C and D), or a two-sites binding model with $K_{d1} \neq K_{d2}$ (E and F). In each panel, the black and blue spheres correspond to the ZP4 only control and the ZP4 response in the presence of S100A7-Ala, respectively. The calculated apparent K_d values corresponding to the fits and the fit parameters are listed in the bottom right of each plot.

Table 3. 7. Fits for apparent $K_{d,Zn}$ values from ZP4 competition titrations with S100A7 variants

Protein	Ca(II) ^a	Apparent $K_{d,Zn}$ (pM)		
		One site	Two sites $K_{d1} = K_{d2}$	Two sites $K_{d1} \neq K_{d2}$
S100A7 _{ox}	-	400 ± 14	430 ± 13	290 ± 20 580 ± 31
	+	605 ± 20	580 ± 40	320 ± 28 1100 ± 89
S100A7 _{red}	-	730 ± 41	660 ± 56	280 ± 18 3500 ± 310
	+	400 ± 20	420 ± 41	300 ± 26 570 ± 39
S100A7-Ser	-	740 ± 49	700 ± 58	470 ± 77 2070 ± 950
	+	350 ± 25	370 ± 11	350 ± 42 400 ± 37
S100A7-Ala	-	500 ± 29	500 ± 69	260 ± 42 990 ± 120
	+	490 ± 28	490 ± 21	330 ± 36 710 ± 70

^a For the +Ca(II) samples, 100 equiv of Ca(II) (500 μM) were added to the buffer. For the -Ca(II) samples, no Ca(II) was added to the buffer. Metal analysis (ICP-MS) showed the buffer employed in the -Ca(II) experiments contained less than 100 nM Ca.

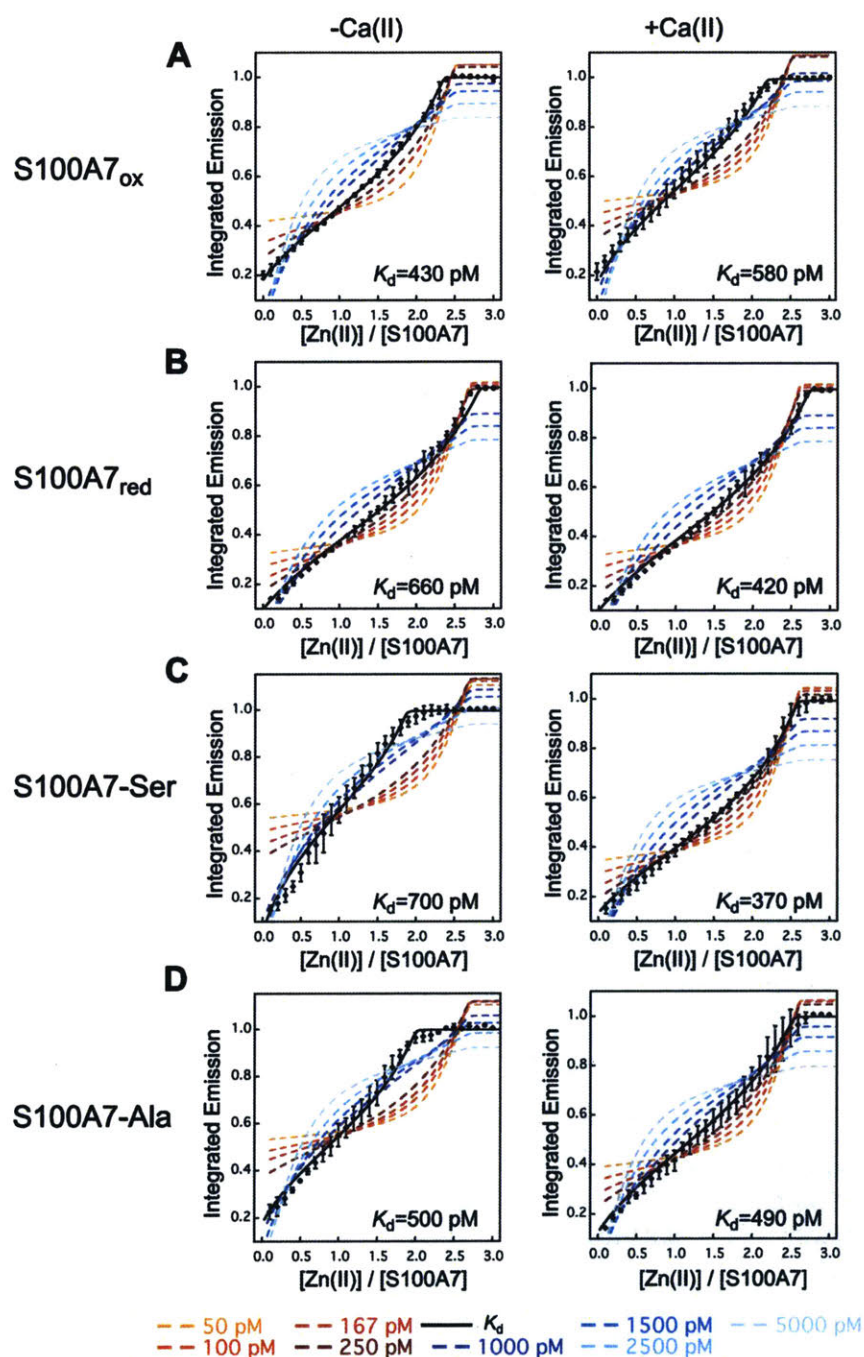


Figure 3. 23 Simulated Zn(II) competition curves for ZP4 and (A) S100A7_{ox}, (B) S100A7_{red}, (C) S100A7-Ser, and (D) S100A7-Ala in the absence and presence of 100 equiv Ca(II). Curves were simulated employing K_d values from 50 to 5000 pM. The data were fit to a two-sites binding model with $K_{d1} = K_{d2}$. For all plots, the data are the black circles (mean \pm SDM), and the reported fit is the black line. The colored dashed lines indicate the simulated curves.

The dataset obtained from the ZP4 competitions yields several noteworthy observations. For the four S100A7 species examined, the apparent $K_{d,Zn}$ values obtained from data fitting are all within one order of magnitude, ranging from 430-700 pM and 370-580 pM in the absence and presence of excess Ca(II) ions, respectively (Table 3. 7, Figure 3. 18). These results indicate that (i) the absence or presence of the Cys47–Cys96 disulfide bond in each S100A7 subunit has negligible impact on the apparent $K_{d,Zn}$ and (ii) the Ca(II)-free and Ca(II)-bound forms of S100A7 have similar Zn(II) affinities. We note that the titration curves for S100A7_{ox} obtained in the absence and presence of Ca(II) are similar and suggest that Ca(II) may slightly reduce the Zn(II)-binding affinity (Figure 3. 18A), whereas the corresponding titration curves for S100A7_{red}, S100A7-Ser, and S100A7-Ala show the opposite trend where the presence of Ca(II) ions shift the titration curve to the right, indicating slightly higher affinity binding (Figure 3. 18B–D). These comparisons also suggest that Ca(II) binding has greater influence on S100A7 when the Cys47–Cys96 disulfide bond is reduced or removed by site-directed mutagenesis. Although the Ca(II)-induced perturbations observed by ZP4 is small, and arguably not functionally significant, it appears that Ca(II) binding to S100A7 slightly enhances the Zn(II)-binding affinity when the Cys47–Cys96 disulfide bond is absent. The overall conclusion from this dataset – a minor effect of Ca(II) ions on the Zn(II)-binding affinities for S100A7 – differs from what is observed for calprotectin (S100A8/S100A9 oligomer). In general, the metal-binding affinities of calprotectin increase by at least several orders of magnitude in the presence of excess Ca(II) ions.³³⁻³⁴ Lastly, the results from the Zn(II) competition experiments and the apparent $K_{d,Zn}$ values obtained using ZP4 are contrary to the $K_{d,Zn}$ value of 100 μ M for S100A7 that was previously reported from equilibrium dialysis studies.⁸

3. 4. 6. Human S100A7 Selectively Depletes Zn(II) From Bacterial Growth Medium

With information about the Zn(II):S100A7 stoichiometries and support for high-affinity Zn(II) binding in hand, we performed a series of metal-depletion experiments to ascertain which metal(s)

is depleted from microbial growth media upon S100A7-treatment.⁴⁴ We treated TSB:Tris growth medium, which has been routinely employed in microbiology studies of related S100 proteins (e.g. calprotectin, S100A12),^{27,33-34,45-46} with S100A7 (0-500 $\mu\text{g/mL}$) for 20 h with shaking at 30 °C and then separated the protein from the treated medium by spin filtration. The concentrations of unbound Mn, Fe, Ni, Cu and Zn in the treated medium were determined by ICP-MS (Figure 3. 24). Because of the spin filtration step, which can disrupt a mixture at equilibrium, these experiments provide information about the metal ions that are likely to be sequestered by S100A7 rather than an equilibrium measurement.

The TSB:Tris medium prepared in our laboratory contains approximately 5 μM Zn, 3 μM Fe, 200 nM Mn, 600 nM Ni, and 150 nM Cu (Table 3. 8, Figure 3. 24). We observed that S100A7_{ox}, S100A7-Ser and S100A7-Ala depleted Zn from the medium in a concentration-dependent manner, whereas the concentrations of the other transition metal ions were largely unperturbed (Figures 3. 24, Tables 3. 8–3. 23). Moreover, the presence of a 2-mM Ca(II) supplement had negligible effect on the metal depletion profile of each protein. These results illuminate two key points: (i) the absence or presence of 2 mM Ca(II) and (ii) the presence or absence of the disulfide bond do not significantly impact the ability of S100A7 to deplete Zn from TSB:Tris medium. Both observations are reminiscent of the ZP4 competition experiments, which indicate similar apparent $K_{d,Zn}$ values for all proteins tested under conditions of low and high Ca(II) (Table 3. 7). In general, the metal-depletion profile of S100A7 is similar to that of S100A12, which selectively depletes Zn(II) from TSB:Tris medium.³⁴ However, one major difference is that the presence of excess Ca(II) ions enhances Zn(II) depletion by S100A12.

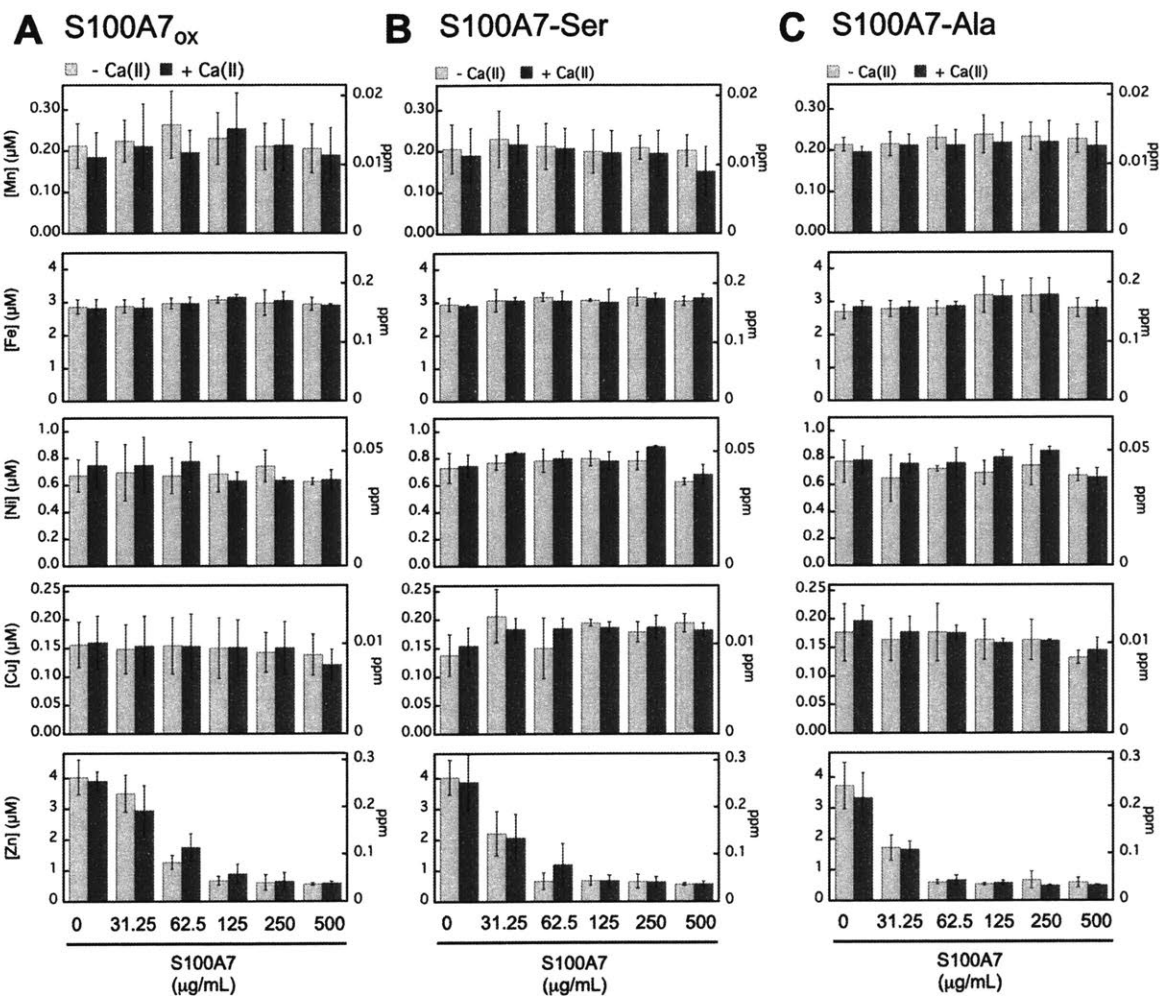


Figure 3. 24. S100A7 selectively depletes Zn(II) from TSB:Tris medium. Metal analysis of TSB:Tris medium treated with 0–500 $\mu\text{g mL}^{-1}$ of S100A7_{ox}, S100A7-Ser, and S100A7-Ala. Mn, Fe, Cu, and Zn depletion profiles are shown for S100A7_{ox} (A), S100A7-Ser (B), and S100A7-Ala (C). The experiments were conducted in the absence (light gray bars) and presence (dark gray bars) of a 2-mM Ca(II) supplement (mean \pm SDM, $n = 3$).

Table 3. 8. Metal Analysis of untreated Tris:TSB medium in the presence and absence of a 2-mM Ca(II) supplement (mean \pm SDM, $n = 3$)

Element	-Ca(II) (ppm)	-Ca(II) (μ M)	+Ca(II) (ppm)	+Ca(II) (μ M)
Mg	4300 \pm 400	180 \pm 17	4000 \pm 165	170 \pm 19
Ca	4100 \pm 95	102 \pm 2.4	9500 \pm 2600	2400 \pm 65
Mn	12 \pm 3.0	0.02 \pm 0.06	10 \pm 3.3	0.20 \pm 0.06
Fe	2.9 \pm 0.21	160 \pm 12	2.8 \pm 0.3	160 \pm 14
Co	2.8 \pm 0.31	0.050 \pm 0.006	2.5 \pm 0.23	0.040 \pm 0.004
Ni	39 \pm 6.9	0.67 \pm 0.12	434 \pm 10.3	0.750 \pm 0.18
Cu	0.16 \pm 0.039	10 \pm 2.5	0.16 \pm 0.05	10 \pm 2.9
Zn	260 \pm 37	4.0 \pm 0.56	260 \pm 20	3.9 \pm 0.30

Table 3. 9. Metal Analysis of Tris:TSB medium treated with 31.25 μ g/mL of S100A7_{ox} in the presence and absence of a 2-mM Ca(II) supplement (mean \pm SDM, $n = 3$)

Element	-Ca(II) (ppm)	-Ca(II) (μ M)	+Ca(II) (ppm)	+Ca(II) (μ M)
Mg	4400 \pm 400	180 \pm 18	4200 \pm 330	170 \pm 13
Ca	4300 \pm 230	110 \pm 6.1	10000 \pm 8500	2500 \pm 210
Mn	12 \pm 2.8	0.2 \pm 0.05	12 \pm 5.7	0.2 \pm 0.10
Fe	3.0 \pm 0.16	160 \pm 11	2.8 \pm 0.29	160 \pm 16
Co	2.8 \pm 0.29	0.050 \pm 0.005	2.7 \pm 0.41	0.050 \pm 0.007
Ni	40 \pm 12	0.7 \pm 0.21	44 \pm 12.2	0.70 \pm 0.21
Cu	0.150 \pm 0.043	9 \pm 2.7	0.15 \pm 0.052	10 \pm 3.3
Zn	230 \pm 39	3.5 \pm 0.60	190 \pm 54	2.9 \pm 0.83

Table 3. 10. Metal Analysis of Tris:TSB medium treated with 62.5 μ g/mL of S100A7_{ox} in the presence and absence of a 2-mM Ca(II) supplement (mean \pm SDM, $n = 3$)

Element	-Ca(II) (ppm)	-Ca(II) (μ M)	+Ca(II) (ppm)	+Ca(II) (μ M)
Mg	4300 \pm 160	178 \pm 7	4100 \pm 59	170 \pm 3
Ca	4200 \pm 200	106 \pm 5	10100 \pm 4500	2430 \pm 17
Mn	15 \pm 4.5	0.26 \pm 0.08	11 \pm 3.0	0.20 \pm 0.05
Fe	170 \pm 9	3.0 \pm 0.16	170 \pm 11	3.0 \pm 0.20
Co	2.8 \pm 0.17	0.047 \pm 0.003	2.6 \pm 0.23	0.04 \pm 0.004
Ni	39 \pm 7.7	0.7 \pm 0.13	46 \pm 8.4	0.8 \pm 0.14
Cu	0.15 \pm 0.05	10 \pm 3.1	0.15 \pm 0.056	10 \pm 3.6
Zn	82 \pm 15	1.3 \pm 0.22	110 \pm 29	1.8 \pm 0.44

Table 3. 11 Metal Analysis of Tris:TSB medium treated with 125 µg/mL of S100A7_{ox} in the presence and absence of a 2-mM Ca(II) supplement (mean ± SDM, *n* = 3)

Element	-Ca(II) (ppm)	-Ca(II) (µM)	+Ca(II) (ppm)	+Ca(II) (µM)
Mg	4200 ± 170	175 ± 7	4200 ± 250	175 ± 10
Ca	4300 ± 300	107 ± 8	97000 ± 680	2500 ± 110
Mn	13 ± 3.4	0.23 ± 0.06	14 ± 4.7	0. ± 0.10
Fe	172 ± 6	3.1 ± 0.10	176 ± 4	3.15 ± 0.07
Co	2.8 ± 0.17	0.049 ± 0.004	2.6 ± 0.23	0.049 ± 0.003
Ni	40 ± 7.7	0.7 ± 0.13	37 ± 3.7	0.63 ± 0.063
Cu	0.15 ± 0.034	10 ± 3.4	0.015 ± 0.048	10 ± 3.1
Zn	44 ± 9.4	0.7 ± 0.14	60 ± 20	0.9 ± 0.31

Table 3. 12. Metal Analysis of Tris:TSB medium treated with 250 µg/mL of S100A7_{ox} in the presence and absence of a 2-mM Ca(II) supplement (mean ± SDM, *n* = 3)

Element	-Ca(II) (ppm)	-Ca(II) (µM)	+Ca(II) (ppm)	+Ca(II) (µM)
Mg	4000 ± 170	170 ± 19	4200 ± 250	170 ± 2.5
Ca	4200 ± 200	110 ± 13	101000 ± 4500	2430 ± 17
Mn	12 ± 3.1	0.21 ± 0.06	12 ± 3.4	0.21 ± 0.06
Fe	170 ± 21	3.0 ± 0.38	170 ± 15	3.1 ± 0.26
Co	2.9 ± 0.22	0.049 ± 0.006	2.8 ± 0.17	0.049 ± 0.003
Ni	44 ± 6.9	0.7 ± 0.12	37 ± 1.1	0.63 ± 0.019
Cu	0.14 ± 0.034	9 ± 2.2	0.015 ± 0.046	10 ± 2.9
Zn	39 ± 16	0.6 ± 0.25	43 ± 18	0.6 ± 0.28

Table 3. 13. Metal Analysis of Tris:TSB medium treated with 500 µg/mL of S100A7_{ox} in the presence and absence of a 2-mM Ca(II) supplement (mean ± SDM, *n* = 3)

Element	-Ca(II) (ppm)	-Ca(II) (µM)	+Ca(II) (ppm)	+Ca(II) (µM)
Mg	4200 ± 460	166 ± 7	4000 ± 80	165 ± 4
Ca	4300 ± 530	2370 ± 65	9500 ± 6700	2400 ± 170
Mn	11 ± 3.2	0.21 ± 0.06	10 ± 3.6	0.19 ± 0.06
Fe	160 ± 11	2.9 ± 0.20	162 ± 2	2.91 ± 0.03
Co	2.5 ± 0.23	0.049 ± 0.004	2.8 ± 0.29	0.049 ± 0.008
Ni	37 ± 1.4	0.63 ± 0.024	38 ± 4.2	0.64 ± 0.072
Cu	0.14 ± 0.036	9 ± 2.3	0.12 ± 0.026	8 ± 1.7
Zn	36 ± 2.8	0.56 ± 0.04	38 ± 3.2	0.58 ± 0.05

Table 3. 14. Metal Analysis of Tris:TSB medium treated with 31.25 µg/mL of S100A7-Ser in the presence and absence of a 2-mM Ca(II) supplement (mean ± SDM, *n* = 3)

Element	-Ca(II) (ppm)	-Ca(II) (µM)	+Ca(II) (ppm)	+Ca(II) (µM)
Mg	4400 ± 550	180 ± 23	4100 ± 360	170 ± 15
Ca	4100 ± 360	102 ± 9.1	95000 ± 7400	2400 ± 190
Mn	11 ± 3.2	0.21 ± 0.058	10 ± 3.6	0.19 ± 0.065
Fe	160 ± 11	2.9 ± 0.20	162 ± 2	2.91 ± 0.03
Co	3.0 ± 0.21	0.051 ± 0.004	2.6 ± 0.38	0.044 ± 0.006
Ni	43 ± 6.5	0.73 ± 0.11	44 ± 4.9	0.75 ± 0.084
Cu	9 ± 2.3	0.14 ± 0.04	10 ± 2.0	0.15 ± 0.032
Zn	140 ± 47	2.2 ± 0.72	140 ± 50	2.1 ± 0.77

Table 3. 15. Metal Analysis of Tris:TSB medium treated with 62.5 µg/mL of S100A7-Ser in the presence and absence of a 2-mM Ca(II) supplement (mean ± SDM, *n* = 3)

Element	-Ca(II) (ppm)	-Ca(II) (µM)	+Ca(II) (ppm)	+Ca(II) (µM)
Mg	4400 ± 320	180 ± 13	4400 ± 250	180 ± 11
Ca	4000 ± 420	100 ± 10	104000 ± 5600	2600 ± 140
Mn	13 ± 3.8	0.22 ± 0.068	12 ± 2.6	0.22 ± 0.047
Fe	170 ± 19	3.1 ± 0.34	171 ± 6	3.1 ± 0.11
Co	2.94 ± 0.04	0.050 ± 0.001	2.9 ± 0.29	0.049 ± 0.005
Ni	45 ± 3.2	0.77 ± 0.054	49.3 ± 0.5	0.840 ± 0.007
Cu	13 ± 3.0	0.21 ± 0.047	12 ± 1.2	0.18 ± 0.019
Zn	40 ± 18	0.7 ± 0.27	80 ± 44	0.7 ± 0.18

Table 3. 16 Metal Analysis of Tris:TSB medium treated with 125 µg/mL of S100A7-Ser in the presence and absence of a 2-mM Ca(II) supplement (mean ± SDM, *n* = 3)

Element	-Ca(II) (ppm)	-Ca(II) (µM)	+Ca(II) (ppm)	+Ca(II) (µM)
Mg	4300 ± 420	180 ± 18	4300 ± 270	180 ± 11
Ca	4000 ± 280	100 ± 10	102000 ± 4300	2500 ± 110
Mn	12 ± 3.0	0.21 ± 0.06	11 ± 2.6	0.21 ± 0.048
Fe	177 ± 7	3.2 ± 0.13	170 ± 16	3.1 ± 0.29
Co	29.0 ± 0.27	0.05 ± 0.001	2.7 ± 0.18	0.045 ± 0.003
Ni	46 ± 5	0.78 ± 0.086	47 ± 3.3	0.80 ± 0.056
Cu	10 ± 3.4	0.15 ± 0.053	12 ± 1.2	0.18 ± 0.018
Zn	44 ± 9.9	0.7 ± 0.15	40 ± 12	0.67 ± 0.18

Table 3. 17. Metal Analysis of Tris:TSB medium treated with 250 µg/mL of S100A7-Ser in the presence and absence of a 2-mM Ca(II) supplement (mean ± SDM, *n* = 3)

Element	-Ca(II) (ppm)	-Ca(II) (µM)	+Ca(II) (ppm)	+Ca(II) (µM)
Mg	4300 ± 480	180 ± 18	4400 ± 270	180 ± 11
Ca	4200 ± 320	100 ± 7	104000 ± 4900	2600 ± 120
Mn	11 ± 2.9	0.20 ± 0.052	11 ± 2.9	0.20 ± 0.053
Fe	172 ± 2	3.07 ± 0.036	170 ± 22	3.0 ± 0.39
Co	3.0 ± 0.33	0.049 ± 0.005	2.9 ± 0.23	0.049 ± 0.004
Ni	47 ± 3.3	0.80 ± 0.06	46 ± 3.9	0.78 ± 0.066
Cu	12.4 ± 0.4	0.194 ± 0.005	12 ± 0.6	0.186 ± 0.009
Zn	40 ± 15	0.7 ± 0.23	40 ± 11	0.63 ± 0.16

Table 3. 18. Metal Analysis of Tris:TSB medium treated with 500 µg/mL of S100A7-Ser in the presence and absence of a 2-mM Ca(II) supplement (mean ± SDM, *n* = 3)

Element	-Ca(II) (ppm)	-Ca(II) (µM)	+Ca(II) (ppm)	+Ca(II) (µM)
Mg	4500 ± 550	180 ± 20	4300 ± 267	180 ± 11
Ca	4600 ± 720	105 ± 8	102000 ± 5100	2600 ± 130
Mn	11 ± 1.6	0.21 ± 0.028	11 ± 3.1	0.19 ± 0.056
Fe	180 ± 15	3.2 ± 0.26	174 ± 9	3.1 ± 0.16
Co	3.1 ± 0.38	0.050 ± 0.006	2.9 ± 0.20	0.049 ± 0.004
Ni	46 ± 4.1	0.78 ± 0.07	52.0 ± 0.34	0.886 ± 0.006
Cu	11 ± 1.1	0.18 ± 0.017	12 ± 1.3	0.19 ± 0.020
Zn	37 ± 2.9	0.56 ± 0.044	37 ± 5.5	0.57 ± 0.083

Table 3. 19. Metal Analysis of Tris:TSB medium treated with 31.25 µg/mL of S100A7-Ala in the presence and absence of a 2-mM Ca(II) supplement (mean ± SDM, *n* = 3)

Element	-Ca(II) (ppm)	-Ca(II) (µM)	+Ca(II) (ppm)	+Ca(II) (µM)
Mg	3700 ± 350	150 ± 14	4200 ± 600	180 ± 25
Ca	3600 ± 300	90 ± 7.5	94750 ± 480	2400 ± 325
Mn	12 ± 0.9	0.21 ± 0.017	10.8 ± 0.7	0.196 ± 0.011
Fe	150 ± 12	2.7 ± 0.21	159 ± 10	2.8 ± 0.17
Co	2.9 ± 0.23	0.049 ± 0.004	3.0 ± 0.28	0.051 ± 0.005
Ni	45 ± 9.3	0.7 ± 0.16	46 ± 6.0	0.8 ± 0.11
Cu	11 ± 3.2	0.18 ± 0.05	13 ± 1.7	0.20 ± 0.026
Zn	110 ± 26	1.7 ± 0.41	100 ± 17	1.7 ± 0.26

Table 3. 20. Metal Analysis of Tris:TSB medium treated with 62.5 µg/mL of S100A7-Ala in the presence and absence of a 2-mM Ca(II) supplement (mean ± SDM, *n* = 3)

Element	-Ca(II) (ppm)	-Ca(II) (µM)	+Ca(II) (ppm)	+Ca(II) (µM)
Mg	3900 ± 440	170 ± 19	4100 ± 140	170 ± 5.8
Ca	4000 ± 340	99 ± 8.4	96300 ± 830	400 ± 430
Mn	11.8 ± 0.9	0.22 ± 0.029	12 ± 1.4	0.21 ± 0.025
Fe	160 ± 14	2.8 ± 0.25	160 ± 9.5	2.8 ± 0.17
Co	3.0 ± 0.30	0.051 ± 0.005	2.9 ± 0.13	0.051 ± 0.005
Ni	40 ± 10	0.65 ± 0.17	44 ± 4.0	0.76 ± 0.068
Cu	10 ± 2.3	0.16 ± 0.037	11 ± 1.7	0.2 ± 0.27
Zn	38 ± 4.2	0.60 ± 0.066	42 ± 9.2	0.7 ± 0.15

Table 3. 21. Metal Analysis of Tris:TSB medium treated with 125 µg/mL of S100A7-Ala in the presence and absence of a 2-mM Ca(II) supplement (mean ± SDM, *n* = 3)

Element	-Ca(II) (ppm)	-Ca(II) (µM)	+Ca(II) (ppm)	+Ca(II) (µM)
Mg	4200 ± 640	170 ± 27	4100 ± 300	170 ± 12
Ca	37100 ± 680	90 ± 17	97000 ± 7300	2400 ± 180
Mn	13 ± 1.6	0.23 ± 0.029	12 ± 2.0	0.21 ± 0.036
Fe	160 ± 12	2.8 ± 0.21	160 ± 6.9	2.9 ± 0.122
Co	3.1 ± 0.36	0.053 ± 0.006	3.0 ± 0.25	0.051 ± 0.004
Ni	42 ± 1.2	0.72 ± 0.02	45 ± 6.4	0.8 ± 0.11
Cu	11 ± 3.2	0.18 ± 0.050	11.2 ± 0.8	0.18 ± 0.012
Zn	34 ± 2.1	0.53 ± 0.033	37 ± 4.4	0.6 ± 0.70

Table 3. 22 Metal Analysis of Tris:TSB medium treated with 250 µg/mL of S100A7-Ala in the presence and absence of a 2-mM Ca(II) supplement (mean ± SDM, *n* = 3)

Element	-Ca(II) (ppm)	-Ca(II) (µM)	+Ca(II) (ppm)	+Ca(II) (µM)
Mg	4000 ± 440	170 ± 19	4200 ± 109	174 ± 4.5
Ca	3700 ± 470	90 ± 12	100000 ± 3400	2500 ± 180
Mn	13 ± 1.8	0.24 ± 0.046	12 ± 2.7	0.22 ± 0.047
Fe	180 ± 31	3.2 ± 0.55	180 ± 26	3.2 ± 0.47
Co	3.1 ± 0.39	0.053 ± 0.006	3.1 ± 0.17	0.051 ± 0.004
Ni	40 ± 5.2	0.69 ± 0.089	47 ± 3.1	0.80 ± 0.053
Cu	10 ± 2.2	0.16 ± 0.035	10.0 ± 0.4	0.161 ± 0.002
Zn	40 ± 17	0.7 ± 0.27	30.9 ± 0.90	0.49 ± 0.014

Table 3. 23. Metal Analysis of Tris:TSB medium treated with 500 $\mu\text{g}/\text{mL}$ of S100A7-Ala in the presence and absence of a 2-mM Ca(II) supplement (mean \pm SDM, $n = 3$)

Element	-Ca(II) (ppm)	-Ca(II) (μM)	+Ca(II) (ppm)	+Ca(II) (μM)
Mg	3900 \pm 320	160 \pm 13	4300 \pm 320	180 \pm 13.
Ca	61000 \pm 490	1830 \pm 12	100000 \pm 3400	1000 \pm 200
Mn	13 \pm 2.5	0.23 \pm 0.033	12 \pm 2.6	0.22 \pm 0.050
Fe	180 \pm 29	3.2 \pm 0.51	180 \pm 28	3.2 \pm 0.49
Co	3.1 \pm 0.39	0.052 \pm 0.006	3.1 \pm 0.17	0.054 \pm 0.006
Ni	44 \pm 8.7	0.7 \pm 0.15	50 \pm 1.6	0.8 \pm 0.28
Cu	10 \pm 2.2	0.16 \pm 0.035	10.2 \pm 0.11	0.161 \pm 0.002
Zn	37 \pm 9.8	0.6 \pm 0.15	31.2 \pm 0.5	0.491 \pm 0.008

3. 4. 7. Evidence for a Contribution of the Intramolecular Disulfide Bonds to Antibacterial Activity

We next evaluated the antibacterial activity of S100A7_{ox}, S100A7-Ser and S100A7-Ala against *E. coli* K-12 and the $\Delta znuA$ mutant obtained from the Keio Collection⁴⁷ (Figure 3. 25, Table 3. 22). The ATP-binding cassette transport system ZnuABC is a high-affinity Zn(II) uptake system of *E. coli*.⁴⁸ ZnuA is the periplasmic Zn(II)-binding protein that delivers Zn(II) to the inner membrane transporter ZnuBC. *E. coli* that lack functional ZnuABC are more susceptible to Zn(II) deprivation compared to the parent strain.⁴⁸ We previously used the $\Delta znuA$ mutant as tool for probing Zn(II) sequestration by human S100A12,³⁴ and reasoned that experiments with this mutant would inform our understanding of S100A7. Thus, we investigated the growth inhibitory activity of S100A7_{ox}, S100A7-Ser and S100A7-Ala under conditions routinely used to study metal-sequestering host-defense proteins such as calprotectin and S100A12.^{27,33,34,45,46} We employed TSB:Tris medium with and without a 2-mM Ca(II) supplement. These conditions differ from the majority of experiments that report on the antimicrobial activity of S100A7 and employ phosphate buffer supplemented with 1% growth medium.^{10-12,15} We did not consider S100A7_{red} in these assays because S100A7_{red} converted to S100A7_{ox} during the 20-h incubation in TSB:Tris medium, even in the presence of an exogenous reducing agent (Figure 3. 26).

Under these assay conditions, untreated *E. coli* K-12 grew to an OD₆₀₀ \approx 0.45. Treatment of *E. coli* K-12 with 1000 $\mu\text{g}/\text{mL}$ (40 μM) S100A7_{ox} resulted in some growth inhibition at the 8-h

time point ($OD_{600} \approx 0.2$, $\pm Ca$), but full growth was observed at the 20-h time point (Figure 3. 25A). The presence of 1000 $\mu\text{g/mL}$ S100A7-Ser or S100A7-Ala had negligible effect on *E. coli* growth. In contrast, all three proteins inhibited growth of the $\Delta znuA$ mutant (Figure 3. 25B). Whereas full growth inhibition occurred following treatment with 1000 $\mu\text{g/mL}$ S100A7_{ox}, the S100A7-Ser and S100A7-Ala variants inhibited growth to a lesser degree at the 20-h time point ($OD_{600} \approx 0.2$). The 2-mM Ca(II) supplement had negligible effect in all cases. Taken together, these results indicate that ZnuABC can outcompete S100A7 for Zn(II) under these growth conditions. The data also suggest that, in the absence of a functional ZnuABC transport system, S100A7_{ox} is more effective than the disulfide-null variants at inhibiting *E. coli* growth.

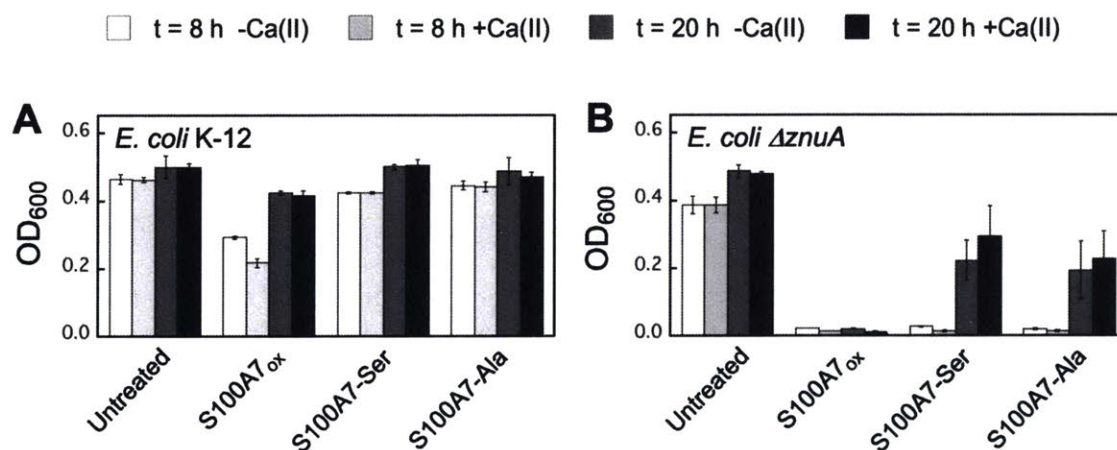


Figure 3. 25. Growth inhibitory activity of S100A7 against *E. coli* K-12 and the $\Delta znuA$ mutant in TSB:Tris medium in the absence and presence of a 2-mM Ca(II) supplement (t = 8 or 20 h, T = 37 °C). (A) *E. coli* K-12 parent strain. (B) *E. coli* $\Delta znuA$. The OD₆₀₀ values were recorded at t = 8 and 20 h (mean \pm SDM, n = 3).

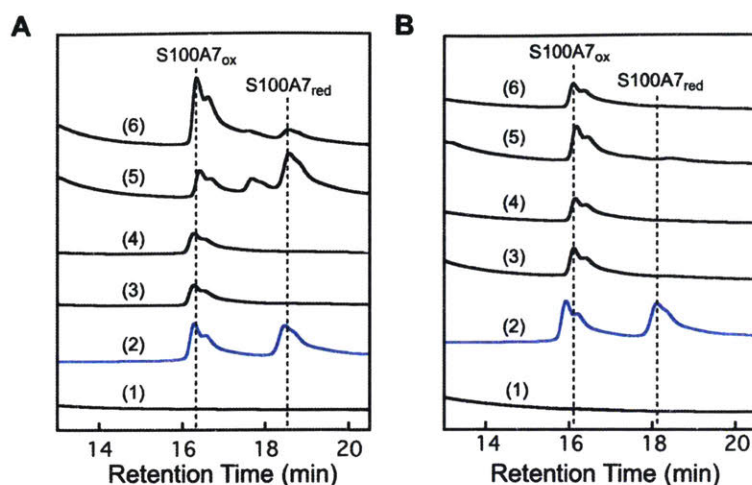


Figure 3. 26. Speciation of S100A7 after incubating a \approx 1:1 mixture (125 μ g/mL) of S100A7_{red} and S100A7_{ox} for 20 h at 37 °C in (A) TSB:Tris medium without bacteria and (B) TSB:Tris medium with *E. coli* K-12. Trace (1) is Tris:TSB medium only, trace (2) is the S100A7 mixture in AMA buffer (20 mM Tris, 100 mM NaCl, pH 7.5) that serves as a standard, trace (3) is S100A7 after 20 h at 37 °C, trace (4) is S100A7 after 20 h at 37 °C in medium supplemented with 2 mM Ca(II), trace (5) is S100A7 after 20 h at 37 °C in medium supplemented with 5 mM β -mercaptoethanol, trace (6) is S100A7 after 20 h at 37 °C in medium supplemented with 2 mM Ca(II) and 5 mM β -mercaptoethanol.

To further evaluate the *in vitro* antibacterial activity of S100A7, we screened the growth inhibitory activity of S100A7_{ox} and variants against five additional bacterial strains. On the basis of prior antimicrobial activity studies of S100A7¹⁰ as well as S100A12^{34,46} and calprotectin,^{33,44,46,49} we selected *E. coli* ATCC 25922, *Pseudomonas aeruginosa* PAO1, *Staphylococcus aureus* ATCC 25923, *Listeria monocytogenes* ATCC 19115, and *Lactobacillus plantarum* WSCF1. We treated bacteria with 1000 μ g/mL protein and monitored growth by OD₆₀₀ following a 20-h incubation (Figure 3. 27). In general, the presence of S100A7 had negligible effect on the OD₆₀₀ values for the *E. coli*, *P. aeruginosa*, and *S. aureus* strains, although slight growth inhibition was observed for *P. aeruginosa* treated with S100A7_{ox}. Growth of *L. monocytogenes* and *L. plantarum* was inhibited upon treatment with S100A7_{ox} in the absence and presence of a 2-mM Ca(II) supplement, respectively. In contrast, S100A7-Ser, S100A7-Ala, and S100A7 Δ_{ox} did not inhibit the growth of these two microbes.

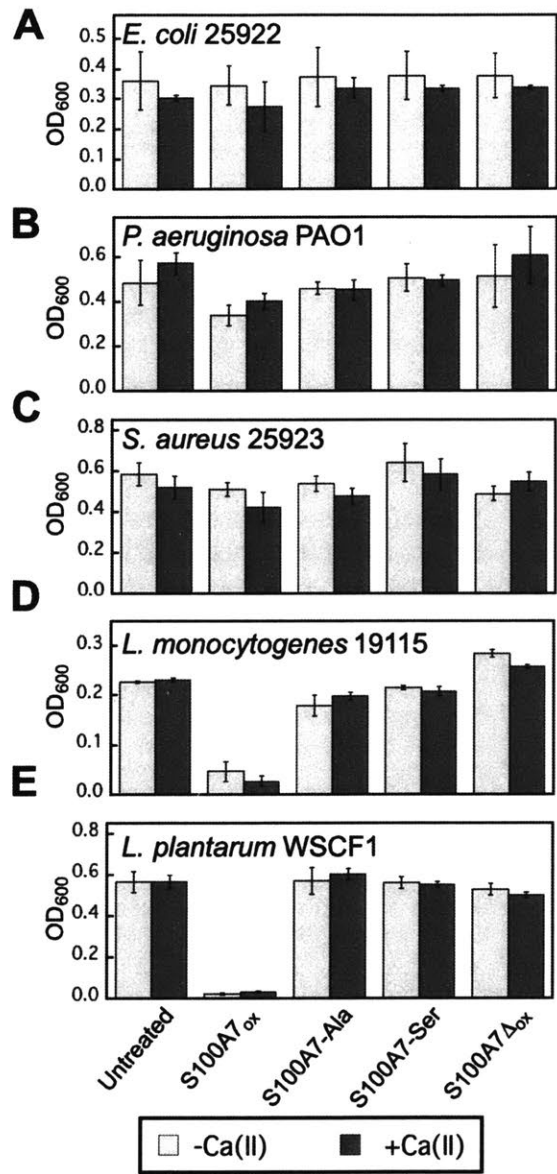


Figure 3. 27. Antibacterial activity of S100A7 (1000 µg/mL) against (A) *P. aeruginosa* PAO1, (B) *E. coli* ATCC 25922, (C) *S. aureus* ATCC 25923, (D) *L. monocytogenes* ATCC 19115, and (E) *L. plantarum* WSCF1. The experiments were conducted in TSB:Tris (*E. coli* and *S. aureus*), BHI:Tris (*L. monocytogenes*), and MRS:Tris (*L. plantarum*) in the absence (light gray bars) and presence (dark gray bars) of a 2-mM Ca(II) supplement (T = 30 or 37 °C, Table 3. 22). The OD₆₀₀ values were recorded at t = 20 h (mean ± SDM, n = 3).

A comparison of these data to the results from prior studies of the antimicrobial activity of S100A12 and calprotectin is informative. S100A12 contains two His₃Asp sites at the dimer interface and sequesters Zn(II),³⁴ whereas calprotectin harbors one His₃Asp and one His₆ site.^{46,50} The latter site allows calprotectin to sequester multiple first-row transition metals.⁴⁴ This work shows that the antibacterial activity spectrum of S100A7_{ox} is similar to that of S100A12. Under the assay conditions employed in this work, both proteins exhibit growth inhibitory activity against *E. coli* Δ *znuA*, *L. monocytogenes*, and *L. plantarum* but not *P. aeruginosa*, *S. aureus*, and *E. coli* K-12. A caveat to this comparison is that the lack of a Ca(II) effect for S100A7 observed in this work and also by others,^{10-11,13} which differs from the Ca(II)-enhanced antimicrobial activity reported for S100A12.³⁴ In contrast to S100A7_{ox} and S100A12, calprotectin displays growth inhibitory activity against all of the bacterial species considered in this work.^{33,44,46,49} Both S100A7_{ox} and S100A12 are selective and sequester Zn(II), whereas calprotectin is versatile and sequesters multiple divalent first-row transition metal ions (e.g. Mn, Fe, Ni, Zn). Thus, it is likely that organisms that exhibit inhibited growth in the presence of S100A7_{ox} and S100A12 are less able to compete with Zn(II)-chelating proteins for this metal ion and more susceptible to Zn(II) deprivation, at least under the growth conditions employed in this work, than the strains that are resistant to these proteins.

Under the antibacterial assay conditions employed in this work, we observed negligible growth inhibition of *E. coli* K-12 and ATCC 25922 by S100A7. Prior studies of S100A7 have reported that S100A7 possesses antibacterial activity against *E. coli*.¹⁰ These contrasting outcomes likely result from different experimental conditions employed in the current work and previous studies, and suggest that S100A7 exerts condition-dependent antimicrobial activity. Previous assays employed a microdilution assay in which *E. coli* cultures ($1 \times 10^4 - 10^5$ CFU/mL) were incubated in 10 mM phosphate buffer containing 1% growth medium (e.g. TSB or LB) and treated with S100A7 for 3 h at 37 °C, followed by serial dilution and plating on agar. We performed this microdilution assay with S100A7_{ox}, and consistent with prior work, we observed a \approx 2-log fold

reduction in the CFU/mL of *E. coli* K-12 and ATCC 25922 when the cultures were treated with 1000 $\mu\text{g/mL}$ ($\approx 40 \mu\text{M}$) of protein (Figure 3. 28). We tentatively propose that S100A7 exhibits different antimicrobial mechanisms under different assay conditions, and evaluating this notion is an avenue for future work.

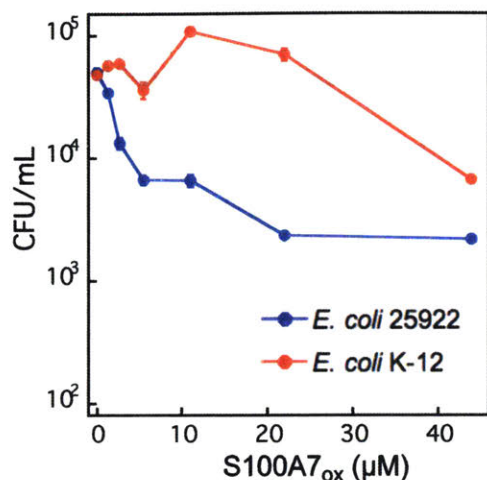


Figure 3. 28. Microdilution antimicrobial activity assay of S100A7_{ox} and *E. coli*. *E. coli* ATCC 25922 (blue) and *E. coli* K-12 (red) are killed by S100A7_{ox} under these assay conditions (3 h, 37 °C, 150 rpm; 10 mM phosphate buffer pH 7.4 supplemented with 1% TSB).

3. 4. 8. The Redox State of Human S100A7 Influences Metal Displacement at the His₃Asp Sites

Overall, our studies of Zn(II) binding and metal depletion reveal that S100A7_{ox} and the disulfide-null variants display similar Zn(II) competition with ZP4 and Zn(II) selectivity. However, the antibacterial activity assays suggest that S100A7_{ox} is more effective at Zn(II) sequestration than the disulfide-null variants. To address this matter further, we interrogated the metal-binding properties of S100A7 by monitoring Co(II) binding and probing metal substitution at the His₃Asp sites by using Co(II) as a spectroscopic probe. We first performed Co(II)-binding titrations in the absence and presence of excess Ca(II) (Figures 3. 29 and 3. 30). In all cases, solutions of S100A7 changed from colorless to pink upon addition of Co(II). The optical absorption spectra of the Co(II)-S100A7 variants exhibited *d-d* transitions centered at 563 nm ($\epsilon_{563} \approx 500$ to $580 \text{ M}^{-1}\text{cm}^{-1}$) (Figures 3. 29 and 3. 30). This spectroscopic signature is similar to the Co(II)-bound His₃Asp sites of human

calprotectin and S100A12.³³⁻³⁴ During each Co(II)-binding titration, the absorbance at 563 nm increased until ≈ 2 equivalents of Co(II) were added, indicating the expected 2:1 Co(II):S100A7 stoichiometry (Figures 3. 29 and 3. 30). The similar results obtained in the presence and absence of added Ca(II) confirm that the stoichiometry of binding of S100A7 is independent of Ca(II) binding (Figure 3. 30).

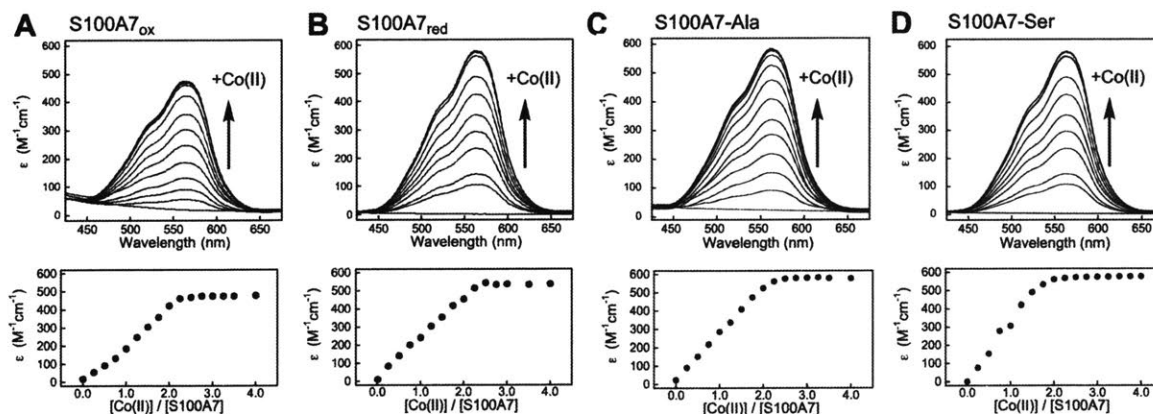


Figure 3. 29. Co(II)-binding titrations with S100A7 variants (S100A7_{ox}, S100A7_{red}, S100A7-Ser and S100A7-Ala). Optical absorption spectra titrations (top panels) and ϵ_{563} versus equivalents of Co(II) added (bottom panels) to 300 μM of S100A7 in 75 mM HEPES, 100 mM NaCl, pH 7.0 and 25 $^{\circ}\text{C}$.

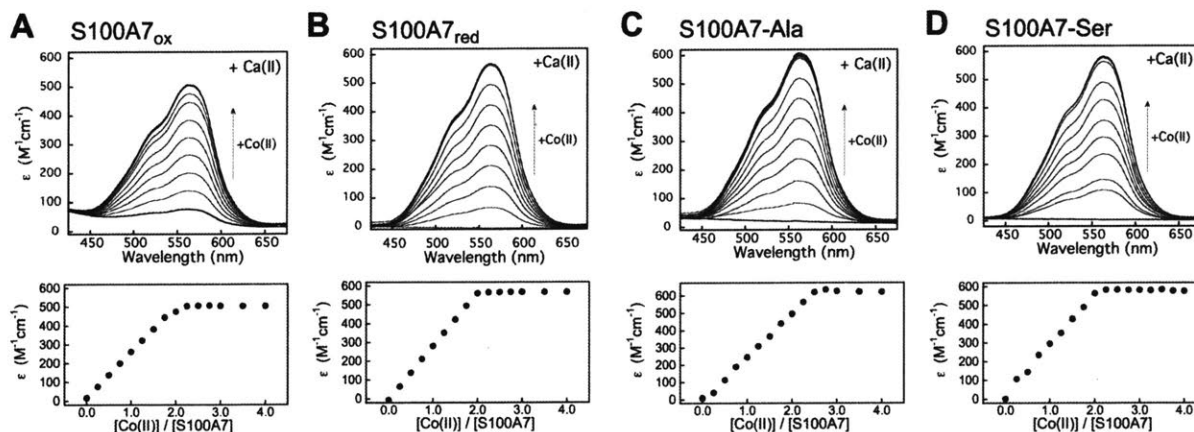


Figure 3. 30. Co(II)-binding titrations with S100A7 variants (S100A7_{ox}, S100A7_{red}, S100A7-Ser and S100A7-Ala) in the presence of 2 mM Ca(II). Optical absorption spectra titrations (top panels) and ϵ_{563} versus equivalents of Co(II) added (bottom panels) to 300 μM of S100A7 in 75 mM HEPES, 100 mM NaCl, 2 mM Ca(II), pH 7.0 and 25 $^{\circ}\text{C}$.

We subsequently examined metal substitution at the His₃Asp sites of S100A7 by monitoring the displacement of Co(II) from Co(II)-S100A7 following Zn(II) addition. On the basis of our prior Co(II)-binding studies of calprotectin³³ and S100A12,³⁴ as well as the Irving-Williams series,⁵¹ we expected that the His₃Asp sites have thermodynamic preference for Zn(II) over Co(II). Addition of Zn(II) to a solution of Co(II)-S100A7_{ox} resulted in a gradual color change from pink to colorless, and loss of the absorbance feature centered at 563 nm, consistent with loss of Co(II) from the His₃Asp sites and formation of Zn(II)-bound S100A7_{ox} (Figure 3. 31). After a 20-h incubation at room temperature, ≈20% of S100A7_{ox} remained Co(II) bound. In contrast, addition of Zn(II) to Co(II)-S100A7_{red} resulted in a comparatively rapid loss of Co(II) from the His₃Asp sites (Figure 3. 31). A comparison of the spectra obtained at the 1-h time point indicates almost complete metal substitution for S100A7_{red} whereas ≈80% of S100A7_{ox} remains Co(II) bound. This difference in metal substitution occurred both in the absence and presence of Ca(II). Addition of Zn(II) to Co(II)-S100A7-Ser and Co(II)-S100A7-Ala afforded trends similar to that of S100A7_{red} (Figure 3. 31). These results suggest that the disulfide bond decreases the kinetic lability of Co(II) ions bound to S100A7. It is possible that the Cys47–Cys96 disulfide bond limits the conformational flexibility of the S100A7 C-terminus, which pre-organize the His₃Asp binding site or stabilizes the Co(II)-bound form of the protein. Since Zn(II) and Co(II) bind to the same His₃Asp sites of S100A7, it is also possible that a similar trend occurs for Zn(II)-bound S100A7 with S100A7_{ox} more effectively entrapping the Zn(II) ion than S100A7_{red}.

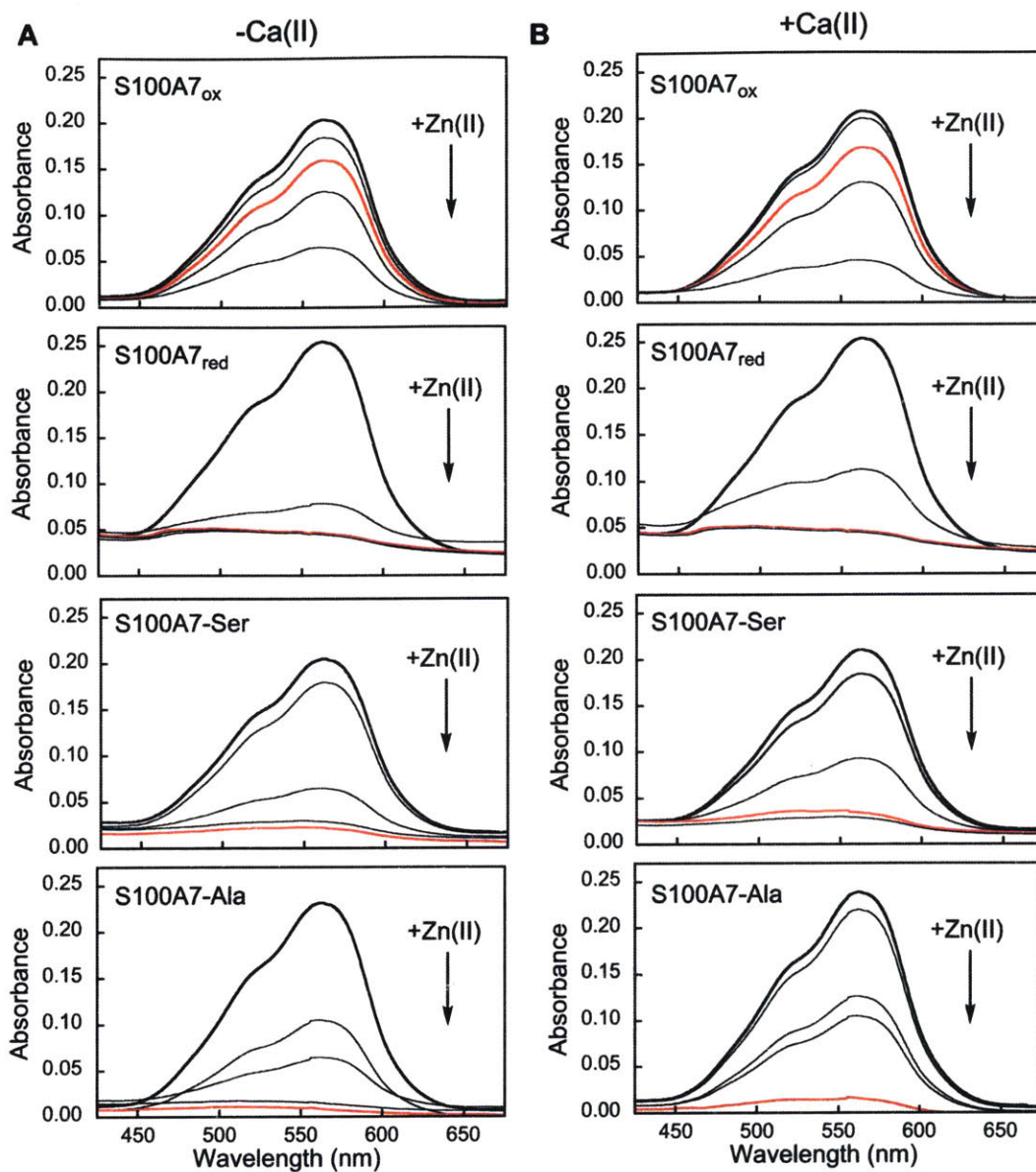


Figure 3.31. Optical absorption spectra showing the substitution of Co(II) for Zn(II) at the His₃Asp sites of S100A7 in the absence (A) and presence (B) of 2 mM Ca(II). Black trace: spectrum of S100A7 (400 μ M) in the presence of Co(II) (1.6 mM, 4.0 equiv) at pH 7.0 (75 mM HEPES, 100 mM NaCl, \pm 2 mM Ca(II)). Additional traces: after 1.6 mM Zn(II) was added to the sample. For S100A7_{ox}, time points were collected at 5, 60, 360, and 2400 min. For S100A7_{red}, S100A7-Ser and S100A7-Ala, time points were collected at 5, 20, 30 and 60 min. For all proteins, the spectrum collected at the 60 min time point is shown in red.

Furthermore, we noted a subtle but reproducible effect of Ca(II) addition for variants where the Cys47–Cys96 disulfide bond is reduced or removed by site-directed mutagenesis. For instance, an inspection of the spectra obtained 20 min after Zn(II) addition reveals that the absorbance signal corresponding to Co(II) binding was weaker in the absence of Ca(II) compared to the samples containing Ca(II) for S100A7_{red}, S100A7-Ser, and S100A7-Ala. This observation indicates that the Co(II) ion bound to these protein species is less readily substituted by Zn(II) when Ca(II) ions are present. This behavior is reminiscent of the ZP4 titration curves of S100A7_{red}, S100A7-Ser, and S100A7-Ala which indicated slightly higher Zn(II) binding affinity in the presence of excess Ca(II) (Figure 3. 18B-D). Together, these data suggest that Ca(II) binding provides some enhancement of transition-metal-binding affinities at the His₃Asp sites when the disulfide bond is not present.

3. 5. Summary and Outlook

In this work, we have examined the interplay between disulfide-bond redox chemistry, Zn(II)-binding properties, and antibacterial activity of human S100A7. Our studies provide several insights about the structure and antibacterial role of this protein and illuminate avenues for further exploration. The current data indicate that Ca(II) ions affect the redox behavior of the Cys47–Cys96 disulfide bond. By depressing the E_m value, Ca(II) binding causes the disulfide bond to be more difficult to reduce, and this phenomenon may be relevant to *in vivo* speciation and physiological function(s) of S100A7. In particular, the antibacterial activity assays and metal substitution experiments provide clues that S100A7_{ox} and S100A7_{red} exhibit differing metal-sequestering abilities with the oxidized protein showing enhanced antimicrobial activity against *E. coli* $\Delta znuA$ and relatively slow metal substitution at the His₃Asp sites. S100A7 is a cytoplasmic protein that is released from epithelial cells into the extracellular milieu where Ca(II) levels are orders of magnitude higher than those found in the cytoplasm.²⁵⁻²⁶ Hence, we reason that Ca(II)-bound S100A7 exists in the extracellular space. It is conceivable that the high Ca(II) levels in this

environment favor the formation and persistence of S100A7_{ox}, tuning the Zn(II)-binding and antibacterial properties of this protein for optimal function. We also observed that Zn(II) coordination impedes disulfide bond reduction; this behavior may indicate another related strategy that S100A7 uses to ensure that Zn(II) remains bound. Whether Ca(II) or Zn(II) binding facilitates the oxidation of S100A7_{red} to S100A7_{ox} and persistence of the latter species *in vivo* merits investigation. It is also possible that metals ions and disulfide bond formation have additional and as-yet unexplored consequences for S100A7. For example, Ca(II) and transition metal binding confers protease resistance to human calprotectin,⁵² and it is possible that metal binding and disulfide bond formation influence the stability and biological lifetime of S100A7 by modulating its proteolytic susceptibility. Moreover, the complex speciation of S100A7 may provide this protein with as-yet unappreciated functional versatility.

The ideas presented above differ from a model presented recently that focuses on S100A7_{red}.¹² Both S100A7_{ox} and S100A7_{red} have been isolated from samples of human skin, and in this prior work, S100A7_{red} was identified as an antifungal component of lesion psoriasis scale extracts.^{10,12} Subsequent antifungal susceptibility testing indicated that S100A7_{red} has greater antifungal activity than S100A7_{ox}.¹² The epidermis contains high levels of thioredoxin and thioredoxin reductase,^{53,54} and S100A7_{ox} was shown to be a substrate for the thioredoxin system *in vitro*, providing a potential mechanism for S100A7_{red} to persist in the extracellular space and confer antifungal activity.¹² Our results suggest that metal-bound S100A7_{ox} is not readily reduced by the thioredoxin system, and that apo S100A7_{ox} can be effective at inhibiting bacterial growth than S100A7_{red}.

Several different antimicrobial mechanisms for S100A7 have been proposed that include Zn(II) withholding,^{10,12} bacterial membrane permeabilization,¹⁵ and a contribution to epithelial barrier protection by forming cross-links and cellular adherence.¹³ A comparison of the current antibacterial activity assays and prior studies reveal differences in experimental outcomes depending on the assay conditions. Although the current results support a role for S100A7 in the

human Zn(II)-withholding response, further studies are required to investigate this putative function and additional antimicrobial mechanisms that may be at work. We note that there is no murine orthologue of S100A7, which limits the utility of murine model of infection for studying this protein.

The molecular basis for bacterial membrane disruption by S100A7 is unclear, and whether metal ions influence this activity remains largely unexplored. Metal ions have been shown to modulate the antimicrobial activity of other peptides that damage membranes. For example, clavanin A is a Zn(II)-binding peptide expressed by the tunicate *Styela clava* that displays enhanced pore-forming activity against *E. coli* in the presence of Zn(II).⁵⁵ It is possible that Ca(II) and Zn(II) binding modulate the ability of S100A7 to damage membranes, and further explorations of a link between metals ions and this bactericidal mode of action are warranted.

In closing, the results presented herein inform our understanding of the S100 protein family and highlight key differences between human S100A7, S100A12, and calprotectin (*vide supra*), three abundant metal-chelating human host-defense proteins. Although each protein binds Ca(II) ions at EF-hand domains, the consequences of Ca(II) ion coordination differ. Ca(II) ions modulate the quaternary structure, metal-binding properties, and antimicrobial activity of calprotectin^{33,44,56-59} and S100A12,^{34,60} whereas Ca(II) ions appear to have negligible influence on these three properties for S100A7. Instead, Ca(II) ions affect the redox behavior of the intramolecular disulfide bonds in S100A7. Nevertheless, our data suggest that this effect may provide a means for enhancing Zn(II) chelation and antibacterial activity through nutrient deprivation in the extracellular space.

3. 6. Acknowledgements

This work was supported by the National Science Foundation (NSF) (Grant CHE-1352132), the Massachusetts Institute of Technology (MIT) Department of Chemistry, and the MIT Undergraduate Research Opportunities Program (UROP, funding to Grayson Rodriguez and Hope

Flaxman). The MIT Biophysical Instrumentation Facility for the Study of Complex Macromolecular Systems is supported by NSF Grant 0070319. The ICP-MS instrument is housed in the MIT Center for Environmental Health Sciences Bioanalytical Core, which is supported by National Institutes of Health Grant P30-ES002109. We thank Dr. Megan Brophy for her training. We thank Miss Hope Flaxman and Miss Grayson Rodriguez for their help with some of the experiments. The *E. coli* K-12 and $\Delta znuA$ strains were obtained from the Keio Collection.⁴⁷

3. 7. References

1. Grice, E. A.; Segre, J. A., The skin microbiome. *Nat. Rev. Microbiol.* **2011**, *9* (4), 244-253.
2. Diamond, G.; Beckloff, N.; Weinberg, A.; Kisich, K. O., The roles of antimicrobial peptides in innate host defense. *Curr. Pharm. Des.* **2009**, *15* (21), 2377-2392.
3. McCormick, T. S.; Weinberg, A., Epithelial cell-derived antimicrobial peptides are multifunctional agents that bridge innate and adaptive immunity. *Periodontology 2000* **2010**, *54*, 195-206.
4. Madsen, P.; Rasmussen, H. H.; Leffers, H.; Honore, B.; Dejgaard, K.; Olsen, E.; Kiil, J.; Walbum, E.; Andersen, A. H.; Basse, B.; Lauridsen, J. B., Ratz, G.P., Celis, A., Vanderkeckhove, J., and Celis, J. E. Molecular cloning, occurrence, and expression of a novel partially secreted protein "psoriasin" that is highly up-regulated in psoriatic skin. *J. Invest. Dermatol.* **1991**, *97* (4), 701-712.
5. Hoffmann, H. J.; Olsen, E.; Etzerodt, M.; Madsen, P.; Thøgersen, H. C.; Kruse, T.; Celis, J. E., Psoriasin binds calcium and is upregulated by calcium to levels that resemble those observed in normal skin. *J. Invest. Dermatol.* **1994**, *103* (3), 370-375.
6. Brodersen, D. E.; Nyborg, J.; Kjeldgaard, M., Zinc-binding site of an S100 protein revealed. Two crystal structures of Ca²⁺-bound human psoriasin (S100A7) in the Zn²⁺-loaded and Zn²⁺-free states. *Biochemistry* **1999**, *38* (6), 1695-1704.

7. Tan, J. Q.; Vorum, H.; Larsen, C. G.; Madsen, P.; Rasmussen, H. H.; Gesser, B.; Etzerodt, M.; Honoré, B.; Celis, J. E.; Thestrup-Pedersen, K., Psoriasin: A novel chemotactic protein. *J. Investig. Dermatol.* **1996**, *107* (1), 5-10.
8. Vorum, H.; Madsen, P.; Rasmussen, H. H.; Etzerodt, M.; Svendsen, I.; Celis, J. E.; Honore, B., Expression and divalent cation binding properties of the novel chemotactic inflammatory protein psoriasin. *Electrophoresis* **1996**, *17* (11), 1787-1796.
9. Wolf, R.; Ruzicka, T.; Yuspa, S. H., Novel S100A7 (psoriasin)/S100A15 (koebnerisin) subfamily: highly homologous but distinct in regulation and function. *Amino Acids* **2011**, *41* (4), 789-796.
10. Gläser, R.; Harder, J.; Lange, H.; Bartels, J.; Christophers, E.; Schroder, J. M., Antimicrobial psoriasin (S100A7) protects human skin from *Escherichia coli* infection. *Nat. Immunol.* **2005**, *6* (1), 57-64.
11. Mildner, M., Stichenwirth, M., Abtin, A., Eckhart, L., Sam, C., Gläser, R., Schröder, J. M., Gmeiner, R., Mlitz, V., Pammer, J., Geusau, A., and Tschachler, E. Psoriasin (S100A7) is a major antimicrobial component of the female genital tract. *Mucosal Immunol.* **2010**, *127*, 602-609.
12. Hein, K. Z.; Takahashi, H.; Tsumori, T.; Yasui, Y.; Nanjoh, Y.; Toga, T.; Wu, Z. H.; Grotzinger, J.; Jung, S.; Wehkamp, J.; Schroeder, B. O.; Schroeder, J. M.; Morita, E., Disulphide-reduced psoriasin is a human apoptosis-inducing broad-spectrum fungicide. *Proc. Natl. Acad. Sci. U. S. A.* **2015**, *112* (42), 13039-13044.
13. Meyer, J. E.; Harder, J.; Sipos, B.; Maune, S.; Klöppel, G.; Bartels, J.; Schröder, J. M.; Gläser, R., Psoriasin (S100A7) is a principal antimicrobial peptide of the human tongue. *Mucosal Immunol.* **2008**, *1* (3), 239-243.
14. Lee, K. C.; Eckert, R. L., S100A7 (Psoriasin) - Mechanism of antibacterial action in wounds. *J. Investig. Dermatol.* **2007**, *127* (4), 945-957.

15. Michalek, M.; Gelhaus, C.; Hecht, O.; Podschun, R.; Schröder, J. M.; Leippe, M.; Grötzinger, J., The human antimicrobial protein psoriasin acts by permeabilization of bacterial membranes. *Dev. Comp. Immunol.* **2009**, *33* (6), 740-746.
16. Weinberg, E. D., Nutritional immunity: Host's attempt to withhold iron from microbial invaders. *J. Am. Med. Assoc.* **1975**, *231* (1), 39–41.
17. Hood, M. I.; Skaar, E. P., Nutritional immunity: transition metals at the pathogen–host interface. *Nat. Rev. Microbiol.* **2012**, *10* (8), 525–537.
18. Matthijs, S.; Hernalsteens, J. P.; Roelants, K., An orthologue of the host-defense protein psoriasin (S100A7) is expressed in frog skin. *Dev. Comp. Immunol.* **2017**, *67*, 395-403.
19. Gifford, J. L.; Walsh, M. P.; Vogel, H. J., Structures and metal-ion-binding properties of the Ca²⁺-binding helix-loop-helix EF-hand motifs. *Biochem. J.* **2007**, *405* (2), 199-221.
20. Brodersen, D. E.; Etzerodt, M.; Madsen, P.; Celis, J. E.; Thogersen, H. C.; Nyborg, J.; Kjeldgaard, M., EF-hands at atomic resolution: the structure of human psoriasin (S100A7) solved by MAD phasing. *Structure with Folding & Design* **1998**, *6* (4), 477-489.
21. Mely, Y.; Gerard, D., Structural and ion-binding properties of an S100b protein mixed disulfide: comparison with the reappraised native S100b protein properties. *Arch Biochem Biophys* **1990**, *279* (1), 174-182.
22. Mely, Y.; Gerard, D., Intra- and interchain disulfide bond generation in S100b protein. *J Neurochem* **1990**, *55* (4), 1100-1106.
23. Matsui Lee, I. S.; Suzuki, M.; Hayashi, N.; Hu, J.; Van Eldik, L. J.; Titani, K.; Nishikimi, M., Copper-dependent formation of disulfide-linked dimer of S100B protein. *Arch Biochem Biophys* **2000**, *374* (2), 137-141.
24. Scotto, C.; Mely, Y.; Ohshima, H.; Garin, J.; Cochet, C.; Chambaz, E.; Baudier, J., Cysteine oxidation in the mitogenic S100B protein leads to changes in phosphorylation by catalytic CKII- α subunit. *J Biol Chem* **1998**, *273* (7), 3901-3908.

25. Williams, R. J. P., Calcium binding proteins in normal and transformed cells, Perugia, May 1996. *Cell Calcium* **1996**, *20* (1), 87-93.
26. Brini, M.; Ottolini, D.; Cali, T.; Carafoli, E., Calcium in health and disease. *Met. Ions Life Sci.* **2013**, *20*, 87-93.
27. Brophy, M. B.; Nakashige, T. G.; Gaillard, A.; Nolan, E. M., Contributions of the S100A9 C-terminal tail to high-affinity Mn(II) chelation by the host-defense protein human calprotectin. *J. Am. Chem. Soc.* **2013**, *135* (47), 17804-17817.
28. Wanniarachchi, Y. A.; Kaczmarek, P.; Wan, A.; Nolan, E. M., Human defensin 5 disulfide array mutants: disulfide bond deletion attenuates antibacterial activity against *Staphylococcus aureus*. *Biochemistry* **2011**, *50* (37), 8005-8017.
29. Holmgren, A., Thioredoxin. *Ann. Rev. Biochem.* **1985**, *54*, 237-271.
30. Zhang, Y. F.; Cougnon, F. B. L.; Wanniarachchi, Y. A.; Hayden, J. A.; Nolan, E. M., Reduction of human defensin 5 affords a high-affinity zinc-chelating peptide. *ACS Chem. Biol.* **2013**, *8* (9), 1907-1911.
31. Schafer, F. Q.; Buettner, G. R., Redox environment of the cell as viewed through the redox state of the glutathione disulfide/glutathione couple. *Free Radic Biol Med* **2001**, *30* (11), 1191-1212.
32. Burdette, S. C.; Frederickson, C. J.; Bu, W. M.; Lippard, S. J., ZP4, an improved neuronal Zn²⁺ sensor of the Zinpyr family. *J. Am. Chem. Soc.* **2003**, *125* (7), 1778-1787.
33. Brophy, M. B.; Hayden, J. A.; Nolan, E. M., Calcium ion gradients modulate the zinc affinity and antibacterial activity of human calprotectin. *J. Am. Chem. Soc.* **2012**, *134* (43), 18089-18100.
34. Cunden, L. S.; Gaillard, A.; Nolan, E. M., Calcium ions tune the zinc-sequestering properties and antimicrobial activity of human S100A12. *Chem. Sci.* **2016**, *7* (2), 1338-1348.
35. Smith, R. C.; Reed, V. D., Inhibition by thiols of copper(II)-induced oxidation of oxihemoglobin. *Chem. -Biol. Interact.* **1992**, *82* (2), 209-217.

36. Lundström, J.; Holmgren, A., Determination of the reduction oxidation potential of the thioredoxin-like domains of protein disulfide-isomerase from the equilibrium with glutathione and thioredoxin. *Biochemistry* **1993**, 32 (26), 6649-6655.
37. Harrison, C. A.; Raftery, M. J.; Walsh, J.; Alewood, P.; Iismaa, S. E.; Thliveris, S.; Geczy, C. L., Oxidation regulates the inflammatory properties of the murine S100 protein S100A8. *J. Biol. Chem.* **1999**, 274 (13), 8561-8569.
38. Sokołowska, M.; Bal, W., Cu(II) complexation by "non-coordinating" N-2-hydroxyethylpiperazine-N'-2-ethanesulfonic acid (HEPES buffer). *J. Inorg. Biochem.* **2005**, 99 (8), 1653-1660.
39. Go, Y. M.; Jones, D. P., Redox compartmentalization in eukaryotic cells. *Biochimica Et Biophysica Acta-General Subjects* **2008**, 1780 (11), 1271-1290.
40. Aslund, F.; Berndt, K. D.; Holmgren, A., Redox potentials of glutaredoxins and other thiol-disulfide oxidoreductases of the thioredoxin superfamily determined by direct protein-protein redox equilibria. *J. Biol. Chem.* **1997**, 272 (49), 30780-30786.
41. Talmard, C.; Bouzan, A.; Faller, P., Zinc binding to amyloid-beta: Isothermal titration calorimetry and Zn competition experiments with Zn sensors. *Biochemistry* **2007**, 46 (47), 13658-13666.
42. Maret, W.; Vallee, B. L., Thiolate ligands in metallothionein confer redox activity on zinc clusters. *Proc. Natl. Acad. Sci. U. S. A* **1998**, 95 (7), 3478-3482.
43. Krężel, A.; Maret, W., Dual nanomolar and picomolar Zn(II) binding properties of metallothionein. *J. Am. Chem. Soc.* **2007**, 129 (35), 10911-10921.
44. Nakashige, T. G.; Zhang, B.; Krebs, C.; Nolan, E. M., Human calprotectin is an iron-sequestering host-defense protein. *Nat. Chem. Biol.* **2015**, 11 (10), 765-771.
45. Kehl-Fie, T. E.; Chitayat, S.; Hood, M. I.; Damo, S.; Restrepo, N.; Garcia, C.; Munro, Kim A.; Chazin, W. J.; Skaar, E. P., Nutrient metal sequestration by calprotectin inhibits bacterial

superoxide defense, enhancing neutrophil killing of *Staphylococcus aureus*. *Cell Host Microbe* **2011**, *10* (2), 158-164.

46. Damo, S. M.; Kehl-Fie, T. E.; Sugitani, N.; Holt, M. E.; Rathi, S.; Murphy, W. J.; Zhang, Y. F.; Betz, C.; Hench, L.; Fritz, G.; Skaar, E. P.; Chazin, W. J., Molecular basis for manganese sequestration by calprotectin and roles in the innate immune response to invading bacterial pathogens. *Proc. Natl. Acad. Sci. U. S. A.* **2013**, *110* (10), 3841-3846.

47. Baba, T.; Ara, T.; Hasegawa, M.; Takai, Y.; Okumura, Y.; Baba, M.; Datsenko, K. A.; Tomita, M.; Wanner, B. L.; Mori, H., Construction of *Escherichia coli* K-12 in-frame, single-gene knockout mutants: the Keio collection. *Mol. Syst. Biol.* **2006**, *2*, 2006 0008.

48. Patzer, S. I.; Hantke, K., The ZnuABC high-affinity zinc uptake system and its regulator zur in *Escherichia coli*. *Mol. Microbiol.* **1998**, *28* (6), 1199-1210.

49. Makthal, N.; Nguyen, K.; Do, H.; Gavagan, M.; Chandrangsu, P.; Helmann, J. D.; Olsen, R. J.; Kumaraswami, M., A critical role of zinc importer AdcABC in group A *Streptococcus*-host interactions during infection and its implications for vaccine development. *EBioMedicine* **2017**, *21*, 131-141.

50. Gagnon, D. M.; Brophy, M. B.; Bowman, S. E. J.; Stich, T. A.; Drennan, C. L.; Britt, R. D.; Nolan, E. M., Manganese binding properties of human calprotectin under conditions of high and low calcium: X-ray crystallographic and advanced electron paramagnetic resonance spectroscopic analysis. *J. Am. Chem. Soc.* **2015**, *137* (8), 3004-3016.

51. Irving, H.; Williams, R. J. P., The stability of transition-metal complexes. *J. Chem. Soc.* **1953**, *138* (37), 3192-3210.

52. Stephan, J. R.; Nolan, E. M., Calcium-induced tetramerization and zinc chelation shield human calprotectin from degradation by host and bacterial extracellular proteases. *Chem. Sci.* **2016**, *7* (3), 1962-1975.

53. Arner, E. S. J.; Holmgren, A., Physiological functions of thioredoxin and thioredoxin reductase. *Eur. J. Biochem.* **2000**, *267* (20), 6102-6109.

54. Schallreuter, K. U.; Wood, J. M., The role of thioredoxin reductase in the reduction of free-radicals at the surface of the epidermis. *Biochem. Biophys. Res. Commun.* **1986**, *136* (2), 630-637.
55. Juliano, S. A.; Pierce, S.; deMayo, J. A.; Balunas, M. J.; Angeles-Boza, A. M., Exploration of the innate immune system of *Styela clava*: Zn²⁺ binding enhances the antimicrobial activity of the tunicate peptide clavanin A. *Biochemistry* **2017**, *56* (10), 1403-1414.
56. Hunter, M. J.; Chazin, W. J., High level expression and dimer characterization of the S100 EF-hand proteins, migration inhibitory factor-related proteins 8 and 14. *J. Biol. Chem.* **1998**, *273* (20), 12427-12435.
57. Vogl, T.; Roth, J.; Sorg, C.; Hillenkamp, F.; Strupat, K., Calcium-induced noncovalently linked tetramers of MRP8 and MRP14 detected by ultraviolet matrix-assisted laser desorption/ionization mass spectrometry. *J. Am. Soc. Mass Spectrom.* **1999**, *10* (11), 1124-1130.
58. Strupat, K.; Rogniaux, H.; Van Dorsselaer, A.; Roth, J.; Vogl, T., Calcium-induced noncovalently linked tetramers of MRP8 and MRP14 are confirmed by electrospray ionization-mass analysis. *J. Am. Soc. Mass Spectrom.* **2000**, *11* (9), 780-788.
59. Hayden, J. A.; Brophy, M. B.; Cunden, L. S.; Nolan, E. M., High-Affinity manganese coordination by human calprotectin is calcium-dependent and requires the histidine-rich site formed at the dimer interface. *J. Am. Chem. Soc.* **2013**, *135* (2), 775-787.
60. Moroz, O. V.; Burkitt, W.; Wittkowski, H.; He, W.; Ianoul, A.; Novitskaya, V.; Xie, J.; Polyakova, O.; Lednev, I. K.; Shekhtman, A.; Derrick, P. J.; Bjoerk, P.; Foell, D.; Bronstein, I. B., Both Ca²⁺ and Zn²⁺ are essential for S100A12 protein oligomerization and function. *BMC Biochem.* **2009**, *10*, 11.

Chapter 4: Investigation of the Bactericidal Properties of the Host-Defense Protein Human Calprotectin

4. 1. Introduction

The human host is continually exposed to potentially pathogenic microorganisms, and the innate immune system forms a first line of defense against microbial invasion. In addition to the removal of pathogens and cell debris by phagocytes, the production of peptides or proteins that can limit infection is considered the most ancient mechanism of immunity.¹ Such peptides/proteins include antimicrobial host-defense peptides/proteins (HDPs).²⁻⁴ The modes of actions of antimicrobial HDPs are diverse; they are involved in wound healing, immune modulation, generation of reactive oxygen species, and nutrient withholding.⁴⁻⁵ Alternatively, these peptides and proteins can act directly against microbial pathogens through intracellular targeting or membrane destabilization. In this work, we refer to the antimicrobial HDPs as antimicrobial peptides (AMPs) when talking about their bactericidal activities. Of note, in addition to their antimicrobial properties, antimicrobial HDPs also possess antiviral or anticancer properties, and are now recognized to play significant immunomodulatory roles in innate immunity.⁶

In this regard, the human metal-sequestering protein calprotectin (CP), which belongs to the S100 family of proteins, is an noteworthy example of an antimicrobial HDP. CP is a heterodimer of two S100 monomers; S100A8 (93 aa, 10.8 kDa) and S100A9 (114 aa, 13.2 kDa) (Figure 4. 1A). Two transition metal-binding sites are housed at the S100A8/S100A9 heterodimer interface. One site is a His₃Asp motif (site 1) comprising H83 and H87 of S100A8 and H20 and D30 of S100A9 (Figure 4. 1B). The second site is a His₆ motif (site 2) formed by H17 and H27 of S100A8 and H91, H95, H103, and H105 of S100A9 (Figure 4. 1B). Site 2 is particularly noteworthy due to its biologically unprecedented hexahistidine coordination motif. Each monomeric unit possesses two Ca(II) EF-hands domains (Figures 4. 2D and 4. 2E). The C-terminal EF-hand of each monomer provides a calmodulin-like, seven-coordinate Ca(II)-binding site, whereas the N-terminal EF-hands are noncanonical and exhibit a five- or six-coordinate Ca(II)-binding site. Ca(II) binding by CP causes the protein to heterotetramerize, and is an important aspect of the current working model for how CP functions as a metal-sequestering HDP.

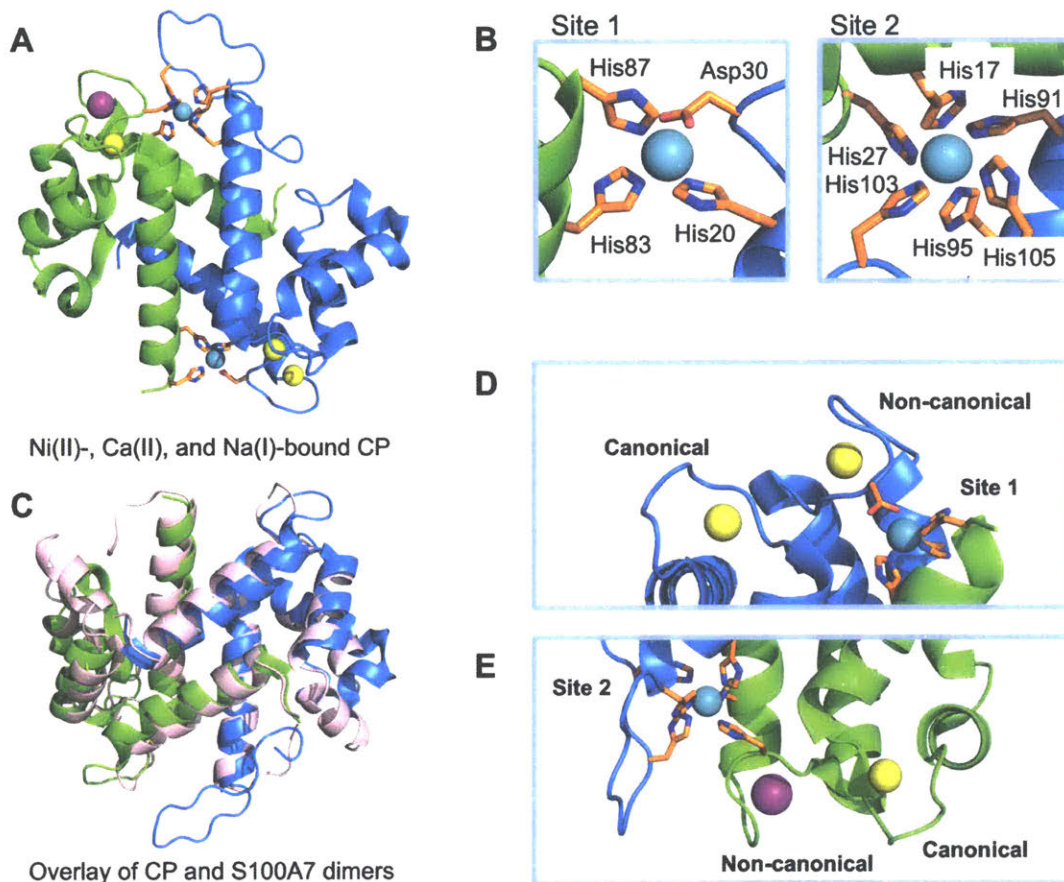


Figure 4. 1. Crystal structure of human calprotectin (CP) (PDB ID5W1F). (A) CP dimer, with S100A8 subunit shown in green, and S100A9 subunit shown in blue. (B) Zoom-in view showing the His₃Asp (site 1) and His₆ (site 2) sites (C) Overlay of CP (blue and green) and S100A7 (pink, PDB 2PSR) dimeric structures showing the similarities in secondary structural features. (D) and (E) Canonical and non-canonical EF-hand domains of CP.

In the current working model, CP is released from the cytoplasm of myeloid cell types (neutrophils, monocytes, and macrophages), as well as epithelial cells at infection sites.⁷⁻¹¹ The cytoplasmic space contains relatively low levels of Ca(II), and upon release into the extracellular space which contains orders of magnitude higher Ca(II).¹² Ca(II) coordination results in the formation of a tetrameric species with enhanced affinity for transition metals.¹³⁻²⁰ The Ca(II)-bound and tetrameric form of CP employs its metal-sequestering properties to starve microbes of essential metal nutrients, such as Zn, Mn, Ni, Cu, and Fe, resulting into growth-inhibition of

microbes.^{13-16,18-19,21-23} This process is often termed nutritional immunity.²⁴⁻²⁶ CP is recognized to be a broad-spectrum bacteriostatic agent, and has been reported to have growth-inhibitory activity against microbial pathogens that include *Candida albicans*,^{8,21,27} *Staphylococcus aureus*,²²⁻²³ *Pseudomonas aeruginosa*, and *Escherichia coli*.^{13,16,18}

The above-mentioned antimicrobial activity of CP can be accomplished without the need for physical interaction between the protein and microbe of interest, since the activity of CP comes from its ability to modify bioavailable metal levels in the extracellular environment encountered by the microbe. Intriguingly, there are studies of CP that have documented its ability to directly interact with various pathogenic microorganisms. Early studies have revealed that CP localizes with macrophages within nodules containing *Onchocerca volvulus*, a filarial nematode that causes onchocerciasis. CP displayed a staining pattern that extended beyond the margins of the cell nodule, and was found on the surface of the worm.²⁸ CP was also found to associate with *Echinococcus granulosus* larva.²⁹ The bacterial pathogen *Finnegoldia magna* employs its surface binding protein, protein L, to bind CP, thus protecting the pathogen from the antimicrobial action of CP;³⁰ consistent with this hypothesis, growth of *F. magna* strains lacking protein L was inhibited upon CP treatment.³⁰ Strains of *Neisseria*, the etiological agent of the sexually transmitted infection gonorrhea, can coordinate both apo and Zn(II)-bound CP through its CpbA receptor, to use it as a nutrient Zn(II) source.³¹

Recent work by the Culotta group has demonstrated that CP interacts with *Borrelia burgdorferi*, a bacterial pathogen that is the causative agent of Lyme disease.³² They reported that CP inhibits *B. burgdorferi* growth through a mechanism that requires physical association of CP with the bacteria, as evidenced by the presence of CP in *B. burgdorferi* whole cell lysates. Based on their findings, the authors postulated that CP inhibits growth of *B. burgdorferi* through a mechanism that does not involve metal-withholding. Instead, CP is thought to physically interact with *B. burgdorferi* and cause hypotonic stress.³²

Altogether, these studies implicate CP in a host-defense function beyond a metal-withholding response. We therefore considered the possibility that CP may function as an AMP and exert bactericidal activity because of its capability to physically interact with cell walls of microbes, its cationic charge ($pI = 6.10$), and its alpha helical character; all features that are characteristic of AMPs. Moreover, another member of the S100 family of proteins, S100A7 (psoriasin) has been identified as a bactericidal factor of the skin,³³ tongue,³⁴ and female genital tract.³⁵ As such, the structural similarities between CP and S100A7 indicate that CP may possess microbicidal properties (Figure 4. 1C).

Herein, we investigate the bactericidal properties of CP. We report that CP possesses bactericidal activity against *E. coli* as well as other Gram-negative species, but not Gram-positive species. We speculate that the selectivity of CP for Gram-negative bacteria results from an interaction between CP and negatively charged moieties on the bacterial cell surface, and further experiments are needed to test this notion. We observe that CP is most active under acidic conditions (pH 5.1) and in the absence of excess Ca(II), and retains activity at high salt concentration. Microscopy studies reveal that CP can damage the membrane of Gram-negative strains, and cause abnormal cell phenotypes in *E. coli* that include cell surface roughness, distortion, and protrusions. We also explore the roles that Zn(II)- and Ca(II)-binding play in the activity of CP and the structural features of CP that contribute to its killing activity. Our results indicate that CP may act as an AMP, and we consider physiological scenarios in which the killing activity of CP may be relevant.

4. 2. Experimental Section

4. 2.1. Materials and General Methods

All solvents and chemicals were obtained from commercial suppliers and used as received. All aqueous solutions were prepared using Milli-Q water (18.2 M Ω •cm, 0.22- μ m filter).

Commercial materials, buffers, and solvents. All precautions were taken to minimize metal ion contamination. Monobasic phosphate buffer of molecular biology grade and MES free acid ULTROL grade were obtained from Sigma-Aldrich and Calbiochem respectively. Only Teflon coated spatulas were employed to transfer reagents and make stock solutions.

For the membrane permeabilization assays, solutions of 10 mM MES (pH 5.1, 5.5, 6.0), 10 mM phosphate buffer (pH 6.5, 7.0, and 7.4) and AMA buffer (20 mM Tris, 100 mM NaCl, pH 7.5) were prepared with Milli-Q water. The pH of the buffer solutions were adjusted with potassium hydroxide, sterile-filtered (0.2- μ m filter), and stored in polypropylene bottles. Stock solutions of Ca(II) (1 M, Sigma), Zn(II) (100 mM, Sigma, anhydrous), and NaCl (1 M, Sigma) were prepared with Milli-Q water. The metal stock solutions were prepared in acid washed volumetric glassware and transferred to sterile polypropylene tubes for long-term storage. The working solutions were prepared by diluting the stock solutions in Milli-Q water. For the membrane permeabilization assays, Tryptic Soy Broth (TSB) medium (Becton Dickinson) was prepared with Milli-Q water, and added to a final concentration of 1% to the buffer of choice (phosphate or MES) for the broth microdilution assays.

4. 2. 2. Protein purification and Characterization.

Protein concentration was routinely quantified by using the calculated extinction coefficients for CP of 18,450 M⁻¹cm⁻¹ (Calculated from ProtParam (ϵ_{280})). CP and its variants were purified following a protocol we have previously published.¹³ The CP-variants employed are listed

in Table 4. 1.

Table 4. 1. Protein nomenclature and extinction coefficients

Protein	Description	ϵ_{280} ($M^{-1} cm^{-1}$)
CP-Ser	S100A8(C42S) S100A9(C3S)	18450
wtCP (wildtype CP)	S100A8, S100A9 Cys42 and Cys3 as free thiols	18450
Δ His ₃ Asp	S100A8(C42S)(H83A)(H87A) S100A9(C3S)(H20A)(D30A)	18450
Δ His ₄	S100A8(C42S)(H17A)(H27A) S100A9(C3S)(H91A)(H95A)	18450
$\Delta\Delta$	S100A8(C42S)(H17A)(H27A)(H83A)(H87A) S100A9(C3S)(H20A)(D30A)(H91A)(H95A)	18450
CP(C42S)	S100A8(C42S) S100A9	18450
FL-CP (fluorescein-CP)	S100A8(C42S) S100A9–Fluorescein	35,000

4. 2. 3. Preparation and Characterization of Fluorescein CP (FL-CP).

Purification of FL-CP. Fluorescein 5-iodoacetamide (F5I) was purchased from MilliporeSigma, and CP(C42S) was purified following the standard CP purification protocol.¹³ The preparation protocol of FL-CP was adapted from a method previously reported (Nakashige, Annual Report, 2013) and a protocol used for the purification of biotinylated CP.³⁶ The running buffers employed during the purification contained 5 mM 1,4-dithiothreitol (DTT, G Biosciences). Following purification, CP(C42S) was dialyzed overnight against 20 mM HEPES, 100 mM NaCl, pH 7.5 (1 x 4 L for 12 h, 4 °C). To a 10-mL solution of 50 μ M CP(C42S) (~10 mg of protein), 50 μ M of 50

μM tris(2-carboxyethyl)phosphine (TCEP, Alfa Aesar) was added and allowed to incubate for 15 min. F51 was dissolved in MeOH, and added to the reduced CP(C42S) solution to a final concentration of 150 μM . The mixture was covered in aluminum foil, and allowed to incubate on a rocking platform at r.t. for 1.5 h. Another aliquot of F51 was added to a final concentration of 150 μM and the mixture allowed to incubate for an additional 3.5 h, after which the mixture was quenched with 5 mM BME. Excess F51 was removed by dialyzing the mixture extensively against 20 mM HEPES, 100 mM NaCl, pH 7.5 (3 x 4L, 12 h each, 4 °C). The resulting protein was purified by preparative SEC (20 mM HEPES, 100 mM NaCl, pH 7.5). The resulting fraction containing FL-CP were combined, and dialyzed overnight against SEC buffer + chelex (20 mM HEPES, 100 mM NaCl, pH 7.5, 10 g chelex, 4 °C). The purified protein was concentrated to $\sim 500 \mu\text{M}$, flash frozen in liquid nitrogen, and stored in 50- μL aliquots at -80 °C. The purity and integrity of FL-CP was confirmed by circular dichroism (CD), and SDS-PAGE analysis (Figure 4. 16).

Quantum yield determination of FL-CP. For characterizing the quantum yield (ϕ) of FL-CP, we used fluorescein ($\phi = 0.95$ in 0. 1 N NaOH) as a standard.³⁷ The absorbance spectra of the samples were recorded, and the concentrations of fluorescein and FL-CP were adjusted such that they had equal absorbance values at the maximum excitation wavelength. The emission spectra of the samples were then recorded. This experiment was performed only once, and needs to be repeated for reproducibility. The quantum yields of two FL-CP stocks were found to be as listed in Table 4. 2.

Table 4. 2. Quantum yield determination of FL-CP

Protein	λ_{ex} (nm), ϵ ($\text{M}^{-1} \text{cm}^{-1}$)	λ_{em} (nm)	ϵ_{280} ($\text{M}^{-1} \text{cm}^{-1}$)	ϕ	Standard
FL-CP stock 1	493, 74,000	517	35,000	0.788	Fluorescein (1 N NaOH)
FL-CP stock 2 ^a	493, 74,000	517	35,000	0.596 ^b	Fluorescein (1 N NaOH)

^a Stock 2 was purified by Dr. Toshiki Nakashige

^b The lower ϕ -value appears to be due to the age of stock 2 (~2years)

Quantum yields were calculated using the equation:

$$\phi_{\text{unk}} = \phi_{\text{std}} * (F_{\text{unk}} / F_{\text{std}}) * (A_{\text{std}} / A_{\text{unk}}) * (\eta_{\text{unk}}^2 / \eta_{\text{std}}^2)$$

F is the integrated emission, A is the absorbance at λ_{ex} (equal to 1 when $A_{\text{std}} = A_{\text{unk}}$), and η is the refractive index of the solvent (assume refractive index of buffer is equal to that of water).

4. 2. 4. Metal Analysis (ICP-MS)

For these studies, 1-mL aliquots of the incubation medium for the broth microdilution assays (10 mM MES buffer pH 5.1 + 1% TSB and 10 mM phosphate buffer pH 7.4 + 1% TSB) were treated with 40 μM of CP-Ser. The mixture was allowed to incubate for 3 h at 37 $^{\circ}\text{C}$, with shaking at 150 rpm. The samples were filtered using the 4-mL Amicon spin concentrators (10 MWCO). The flow through was collected and acidified to 2.5% HNO_3 by addition of 1 mL of 5% HNO_3 . Samples were analyzed at either the Center for Environmental Health Sciences (CEHS) Core Facility at MIT with an Agilent 7900 ICP-MS used in Helium mode outfitted with integrated autosampler (I-AS). An internal standard of terbium (Agilent) was used to control for sample effects, and the concentrations of analyte were calibrated using standards prepared by serial dilution of the Agilent Environmental Calibration Standard mix. This experiment was performed

twice with two different starting stocks of incubation medium. The mean and SDM values are reported.

4. 2. 5. Membrane Permeabilization Assays

The membrane permeabilization assays were carried out following an adapted broth microdilution assay.³⁸ *E. coli* 25922 was employed for the initial solution studies to study the antimicrobial activities of S100 proteins as a function of pH, Ca(II) and NaCl, concentration, growth phase of the cell culture, and Zn(II) and/or Ca(II)-binding by the S100 proteins.

Prior to every assay:

- (i) Phosphate and MES buffer were sterile-filtered through a 0.2 μm filter, and TSB was added to a final concentration of 1%
- (ii) Unless otherwise noted, S100 proteins were buffer-exchanged three times into Milli-Q water (5 min, 13 000 rpm) to a final concentration range between 800-2000 μM

E. coli 25922 was grown overnight (37 °C, 14-16 h) with shaking in 5 mL of TSB. The overnight culture was diluted 1:100 in 5 mL of fresh TSB and grown for ~2 h at 37 °C with shaking until OD_{600} = 0.6. A 2-mL aliquot of the culture was then transferred to two 1.5-mL microcentrifuge tubes (1 mL per tube), and centrifuged at 3000 rpm for 10 min. The supernatant was discarded and the pellet washed with 1 mL of 10 mM phosphate buffer, pH 7.4 , centrifuged at 3000 rpm for 10 min. This procedure was repeated for a total of three times. The cell pellet was then resuspended to an OD_{600} of 0.6 (2.5×10^8 CFU/mL) in 10 mM phosphate buffer pH 7.4 + 1% TSB. The cell suspension was subsequently diluted to 1:2500 in four serial dilution steps (1:2.5, 1:10, 1:10, 1:10) to a final CFU count of 1×10^5 CFU/mL. A schematic of the wash and dilution steps is shown in Figure 4. 2.

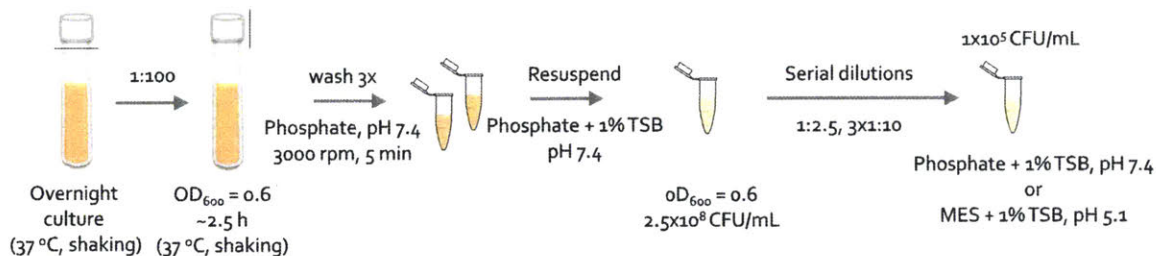


Figure 4. 2. Schematic of the wash, resuspension, and dilution steps of *E. coli* 25922 cultures for the membrane permeabilization assays.

(i) *pH titration assay.* For the pH titration assay, the washed cell suspension (2.5×10^8 CFU/mL in 10 mM phosphate buffer pH 7.4 + 1% TSB) was serially diluted by a factor of 1:2500 in four steps (1:2.5, 1:10, 1:10, 1:10) to a final bacterial density of 1×10^5 CFU/mL. The first two dilutions were done in phosphate buffer pH 7.4 + 1% TSB as followed; 1:2.5 (400 μ L in 600 μ L) and 1:10 in (100 μ L in 900 μ L). The next two dilutions were carried out in the appropriate buffer as followed; 2 x 1:10 dilution (100 μ L in 900 μ L) in 10 mM MES buffer pH 5.1/5.5/6.0 + 1% TSB or 10 mM phosphate buffer pH 6.5/7.0/7.4 + 1% TSB. For experiments requiring more than 1 mL of cell suspension, the volume of the last dilution was scaled accordingly. A 100- μ L aliquot of the diluted cell suspension (1×10^5 CFU/mL) was then added to a 96-well plate well containing the protein of interest. The plate was incubated for 3 h at 37 °C, with shaking at 150 rpm.

(ii) *Protein titration assay.* The protein titration assay was carried out at pH values of 5.1 and 7.4. The washed cell suspension (2.5×10^8 CFU/mL in 10 mM phosphate buffer pH 7.4 + 1% TSB) was serially diluted by a factor of 1:2500 in four steps (1:2.5, 1:10, 1:10, 1:10) to a final bacterial density of 1×10^5 CFU/mL. The first two dilutions were done in phosphate buffer pH 7.4 + 1% TSB, and the following two dilutions were done in the appropriate buffer (10 mM MES buffer pH 5.1 + 1% TSB or 10 mM phosphate buffer pH 7.4 + 1% TSB). For experiments requiring more than 1 mL of cell suspension, the volume of the last dilution was scaled accordingly. A 90- μ L

aliquot of the diluted cell suspension (1×10^5 CFU/mL) was then added to a 96-well plate well containing the 10 μ L of the protein of interest at a 10x concentration. The proteins were tested at the following concentrations: 0, 2.5, 5, 10, 20, and 40 μ M. The plate was incubated for 3 h at 37 $^{\circ}$ C, with shaking at 150 rpm. The % growth reported in the plots corresponding to this assay was calculated as follows:

$$\% \text{ growth} = ((\log(CFU_{\text{protein-treated}}) - 2.301) - (\log(CFU_{\text{untreated}}) - 2.301)) * 100$$

(iii) *Na(I) titration assay*. The Na(I) titration assay was carried out at pH values of 5.1 and 7.4. The washed cell suspension (2.5×10^8 CFU/mL in 10 mM phosphate buffer pH 7.4 + 1% TSB) was serially diluted by a factor of 1:2500 in four steps (1:2.5, 1:10, 1:10, 1:10) to a final bacterial density of 1×10^5 CFU/mL. The first two dilutions were done in phosphate buffer pH 7.4 + 1% TSB, and the following two dilutions were done in the appropriate buffer (10 mM MES buffer pH 5.1 + 1% TSB or 10 mM phosphate buffer pH 7.4 + 1% TSB) containing 0, 5, 10, 50, 100, 150 mM NaCl. For experiments requiring more than 1 mL of cell suspension, the volume of the last dilution was scaled accordingly. A 100- μ L aliquot of the diluted cell suspension (1×10^5 CFU/mL) was then added to a 96-well plate well containing the protein of interest. The plate was incubated for 3 h at 37 $^{\circ}$ C, with shaking at 150 rpm.

(iv) *Ca(II) titration assay*. The Ca(II) titration assay was carried out at pH values of 5.1 and 7.4. The washed cell suspension (2.5×10^8 CFU/mL in 10 mM phosphate buffer pH 7.4 + 1% TSB) was serially diluted by a factor of 1:2500 in four steps (1:2.5, 1:10, 1:10, 1:10) to a final bacterial density of 1×10^5 CFU/mL. The first two dilutions were done in phosphate buffer pH 7.4 + 1% TSB, and the following two dilutions were done in the appropriate buffer (10 mM MES buffer pH 5.1 + 1% TSB or 10 mM phosphate buffer pH 7.4 + 1% TSB) containing 0, 50, 100, 500, 1000, or 2000 μ M CaCl_2 . For experiments requiring more than 1 mL of cell suspension, the volume of the last dilution was scaled accordingly. A 100- μ L aliquot of the diluted cell suspension (1×10^5

CFU/mL) was then added to a 96-well plate well containing the protein of interest. The plate was incubated for 3 h at 37 °C, with shaking at 150 rpm. (Due to precipitation issues arising from the low solubility of CaCl₂ in phosphate buffer ($pK_{sp} = 28.9^{39}$), we did not carry out the titrations with 1000 and 2000 μM Ca(II) at pH 7.4).

(v) *Ca(II) and Zn(II) preincubation assay*. The goal of this experiment was to determine whether metal-binding by the S100 proteins affects their antimicrobial activities. We therefore decided to test the effect of Zn(II) and/or Ca(II) binding on their activities. Because we were not able to ascertain the Zn(II)-binding properties of S100 proteins at pH 5.1, the metal preincubation assay was carried out at pH 7.4 only. The washed cell suspension (2.5×10^8 CFU/mL in 10 mM phosphate buffer pH 7.4 + 1% TSB) was serially diluted by a factor of 1:2500 in four steps (1:2.5, 1:10, 1:10, 1:10) to a final bacterial density of 1×10^5 CFU/mL. The first two dilutions were done in phosphate buffer pH 7.4 + 1% TSB, and the following two dilutions were done in 10 mM phosphate buffer pH 7.4 + 1% TSB without or with a 500-μM Ca(II) supplement. Of note, we did not use a higher Ca(II) concentration due to precipitation issues observed in phosphate buffer, pH 7.4. For this assay, the buffer-exchanged S100 proteins were diluted to a 10x concentration and preincubated with either (i) 1.9 equiv of Zn(II), (ii) 500 μM Ca(II), or (iii) 1.9 equiv of Zn(II) and 500 μM Ca(II) at r.t. for at least 15 min prior to addition into the 96-well plate. A 90-μL aliquot of the diluted cell suspension (1×10^5 CFU/mL) was then added to a 96-well plate well containing 10 μL of 10x protein of interest. The plate was incubated for 3 h at 37 °C, with shaking at 150 rpm.

The membrane permeabilization assays were carried out in 96-well plates (Corning). Unless otherwise noted, each well contained 2-5 μL of CP at 20-50X concentration and 100 μL of cell suspension at 1×10^5 CFU/mL. CP was added to a final concentration of 1000 μg/mL.

Immediately after setting up the experiment, a 20- μ L aliquot of the remaining and diluted cell suspension (1×10^5 CFU/mL) was serially diluted into 180 μ L of buffer (4 x 1:10 in 10 mM phosphate buffer pH 7.4) in a 96-well plate. Aliquots of 5 μ L from the 1:10, 1:100, and 1:1000 dilution were each plated three times on TSB/agar plates; this sample was used as the t = 0 timepoint. After the 3-h incubation, another 20 μ L aliquot of the cell suspension under all the conditions tested was serially diluted into 180 μ L of buffer (4 x 1:10 in 10 mM phosphate buffer pH 7.4) in a 96-well plate. Aliquots of 5 μ L from the 1:10, 1:100, and 1:1000 dilution were each plated three times on TSB/agar plates.

The TSB/agar were allowed to incubated at 37 °C for 12-14 h. Each experiment was performed at least three times with at least two different protein and buffer stocks. Errors represent a 95% confidence interval. The limit of detection of this assay is equal to 1×10^2 CFU/mL (1 colony at the highest dilution).

For the organism screen assays, microbes were grown in the appropriate growth medium, and diluted to a final density of 1×10^5 CFU/mL based on the dilution factors reported in Table 4. 3. Cultures of *A. baumannii* were grown in MRS, phosphate and MES buffers were supplemented with 1% MRS, and the cultures were plated on MRS/agar plates (Table 4. 3). Cultures of *L. monocytogenes* were grown in BHI, phosphate and MES buffers were supplemented with 1% BHI, and the cultures were plated on BHI/agar plates. The plates *L. monocytogenes* were incubated for 20 h (Table 4. 3).

Table 4. 3. Strains and growth conditions

Strain	Source	Dilution factor	Growth conditions
<i>A. baumannii</i> ATCC 17978	ATCC	3 x 1:10	Overnight: MRS medium Incubation medium: buffer + 1% MRS Plating conditions: MRS/agar plate, 12 h
<i>E. coli</i> ATCC 25922	ATCC	1:2.5, 3 x 1:10	Overnight: TSB Incubation medium: buffer + 1% TSB
<i>E. coli</i> UTI89	ATCC	1:2.5, 3 x 1:10	Overnight: TSB Incubation medium: buffer + 1% TSB
<i>E. coli</i> cyto-GFP	MG1655/pDKR2 (dsbA _{ss} -sfgfp) transformed in <i>E. coli</i> K12 ⁴⁰	1:2.5, 3 x 1:10	Overnight: TSB Incubation medium: buffer + 1% TSB
<i>E. coli</i> cyto-GFP	pBBR1(MCS5)- P _{lac} -GFP transformed in <i>E. coli</i> K12 ⁴¹	1:2.5, 3 x 1:10	Overnight: TSB Incubation medium: buffer + 1% TSB
<i>L. monocytogenes</i> ATCC 19115	ATCC	1:5, 3 x 1:10	Overnight: BHI Incubation medium: buffer + 1% BHI Plating conditions: BHI/agar plate, 20 h
<i>P. aeruginosa</i> PAO1	ATCC	1:4, 2 x 1:10	Overnight: TSB Incubation medium: buffer + 1% TSB
<i>S. aureus</i> USA300 JE2	ATCC	3 x 1:10	Overnight: TSB Incubation medium: buffer + 1% TSB

4. 2. 6. Assay and Imaging Conditions for Phase-Contrast and Fluorescence Microscopy

Imaging was performed at the W. M. Keck Biological Imaging Facility of the Whitehead Institute (Cambridge, MA). For microscopy studies, unless otherwise noted, the standard membrane permeabilization assays were performed in 96-well plates (100- μ L sample volume per well) using 1×10^8 CFU/mL of bacteria incubated with 100 μ M of protein. The cell culture aliquots were washed in 10 mM phosphate buffer pH 7.4, resuspended in the appropriate buffer (10 mM MES buffer pH 5.1 + 1% TSB) and diluted to a bacterial density of 1×10^8 CFU/mL.

LIVE/DEAD staining Assay. Following a 3h-incubation (37 °C, 150 rpm), a 5- μ L sample from each

condition was placed on an agarose pad (1% w/w agarose/Milli-Q water) positioned on a microscope slide (VWR Cat.No. 16004-368). The sample was then covered with a coverslip (VWR Cat.No. 1600-308), and taken for imaging. A LIVE/DEAD™ BacLight Bacterial Viability Kit cell from ThermoFisher Scientific (Cat.No. L7012) was employed for viability staining of cells following the supplier instructions. The Live-Dead stain mix was added to each well 15 min before the 3-h incubation timepoint, and the sample 96-well plate covered with aluminum foil during the 15-min incubation. A Zeiss Axioplan2 upright microscope equipped with a 100x oil-immersion objective lens was employed for this experimental setup. The fluorescence images were obtained using the Texas Red (λ_{Ex} : 532-587 nm, λ_{Em} : 608-683 nm) and GFP (λ_{Ex} : 457-487 nm, λ_{Em} : 502-538 nm) channels.

Fluorescence Imaging of E. coli cyto- and per-GFP. The sources of *E. coli cyto- and per-GFP* are listed in Table 4. 3. After a 3h-incubation (37 °C, 150 rpm), a 5- μ L sample from each condition was placed on an agarose pad (1% w/w agarose/Milli-Q water) positioned on a microscope slide (VWR Cat.No. 16004-368). The sample was then covered with a coverslip (VWR Cat.No. 1600-308), and imaged with an Zeiss Axioplan2 upright microscope equipped with a 100x oil-immersion objective lens was employed for this experimental setup. The fluorescence images were obtained using the Texas Red (λ_{Ex} : 532-587 nm, λ_{Em} : 608-683 nm) and GFP (λ_{Ex} : 457-487 nm, λ_{Em} 502-538 nm) channels.

Time-lapse Studies. The time-lapse studies were carried out using poly-D-lysine coated MatTek glass bottom petri dishes of 35 mm, with a 14-mm microwell, and a No 1.5. coverglass (Part no. PG35GC-1.5-14-C). In this assay, the untreated bacteria (1×10^8 CFU/mL in 10 mM MES + 1% TSB, pH 5.1) were incubated at 37 °C on MatTek plates for 15 min and excess unbound bacteria were removed by three gentle wash steps with AMA buffer (3 x 3 mL). Next, a 2-mL portion of

100 μ M CP-Ser in 10 mM MES + 1% TSB, pH 5.1 was added to cover the microwell and petri dish. The petri dish was sealed with parafilm, and quickly positioned onto the microscope stage, which is found within an incubation chamber thermostatted at 37 °C. Image acquisition was initiated immediately. For every experiment, 10 frames were imaged at 5 min intervals over 3h. The images were collected on a Nikon-TE 2000 U wide-field inverted microscope equipped with a 100x oil-immersion objective lens.

Microscopy studies with FL-CP. For the fluorescence imaging studies with FL-CP, poly-D-lysine coated MatTek glass bottom petri dishes of 35 mm, with a 14-mm microwell, and a No 1.5. coverglass (Part no. PG35GC-1.5-14-C) were employed. The bacteria (180 μ L of a 1×10^8 CFU/mL culture in 10 mM MES buffer + 1% TSB, pH 5.1) were placed on a poly-D-lysine coated MatTek petri dish, and 20 μ L of a 10x protein stock solution was added to a final concentration of 100 μ M. The petri dish was wrapped in aluminum foil, and allowed to incubate at 37 °C for 3 h without shaking. Following the incubation, the petri dish was quickly and gently washed with AMA buffer (3 x 3 mL), which removed detached bacteria and excess FL-CP. Then, 3 mL of AMA buffer was added and the plate was covered and sealed with parafilm. The remaining immobilized cells were imaged with a Nikon-TE 2000 U wide-field inverted microscope equipped with a 100x oil-immersion objective lens. FL-CP was visualized with the GFP channel (λ_{EX} : 457-487 nm, λ_{EM} : 502-538 nm).

4. 2. 7. *Image Analysis for Phase-contrast and Fluorescence Microscopy Image Analysis.*

The microscopy images were analyzed with the FIJI software. For fluorescence images, fluorescence background subtraction was performed using a rolling ball method with a radius of 150 pixels, 8-bit image types were analyzed, and the brightness intensity was set from 0-350.

4. 2. 8. Characterization of CP Variants from the Broth-Microdilution Assay Supernatant

In order to confirm the integrity of the CP variants employed in the broth microdilution assays, the culture supernatant was analyzed after the 3-h incubation of the assay. A 90- μ L aliquot from each well was transferred to a microcentrifuge tube, and centrifuged at 13000 rpm for 5 min, after which a 70- μ L aliquot was transferred into another clean microcentrifuge tube. A 10- μ L portion from that aliquot was used for SDS-PAGE gel analysis, and the rest of the mixture was diluted to a final volume of 240 μ L (10 μ M protein) into 10 mM MES + 1% TSB, pH 5.1. This sample was used for circular dichroism (CD) analysis.

4. 2. 9. Statistical Analyses

In this chapter, we represent errors as 95% confidence interval (CI) error bars in order to facilitate the assessment of the significance between values; error bars that do not overlap therefore indicate a statistical difference between values ($P < 0.005$).⁴²⁻⁴³

4. 3. Results and Discussion

4. 3. 1. CP is an *E. coli*-cidal Factor

Initial studies we carried out with CP (CP-Ser) revealed that it was most active under acidic conditions and displayed reduced-activity as a function of increasing pH (Figure 4. 3A). At pH 5.1, CP caused complete killing of *E. coli* cultures at concentrations of 5 μ M and higher, whereas a 2-fold decrease in log (CFU/mL) was observed with 40 μ M CP under neutral conditions (Figure 4. 3B). The pH dependency of CP-Ser is reminiscent of other AMPs including human S100A7, human defensin 5, and clavanin A that are also documented to have enhanced microbicidal activity at lower pH.^{1, 33, 44-46} The origin of this behavior is likely due to increased electrostatic interactions between the cationic AMP and the negatively charged bacterial cell surface. Additionally, the concentration range at which CP is active is comparable to other AMPs⁴⁴⁻⁴⁸ and

consistent with its known physiological concentration.¹¹ Further screening showed that at acidic pH, CP is resistant to high NaCl levels; indeed, CP retained complete killing activity when supplemented with up to 50 mM NaCl, and remained moderately active in the presence of 100 mM NaCl (Figure 4. 4A). At pH 7.4, CP was only slightly active, causing a 2-fold reduction in the log (CFU/mL) compared to the untreated control (Figure 4. 4B). Interestingly, the addition of excess NaCl did not affect the activity of CP at neutral pH, hinting at the possibility that CP functions differently as a function of pH.

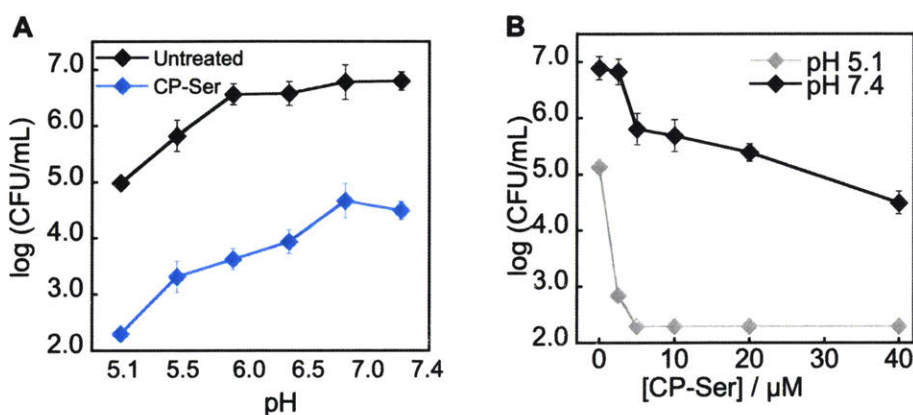


Figure 4.3. CP displays bactericidal activity against *E. coli*. (A) pH-dependency of CP-Ser activity; black trace show the untreated control, and blue trace shows the CP-treated conditions. Buffer: 10 mM MES pH 5.1, 5.5, 6.0 + 1% TSB, or 10 mM phosphate pH 6.5, 7.0, 7.4 + 1% TSB. (B) Concentration titration of CP-Ser; *E. coli* cultures were incubated with 0–40 μ M CP-Ser (grey trace). Buffer: 10 mM MES pH 5.1 + 1% TSB, or 10 mM phosphate pH 7.4 + 1% TSB. *E. coli* ATCC 25922 cultures (1×10^5 CFU/mL) were incubated with CP for 3 h at 37 °C with shaking at 150 rpm. Cultures were plated on TSB/agar plates, allowed to incubate for 12–14 h at 37 °C, and colonies counted for CFU determination. (mean \pm 95% CI, $n = 3$).

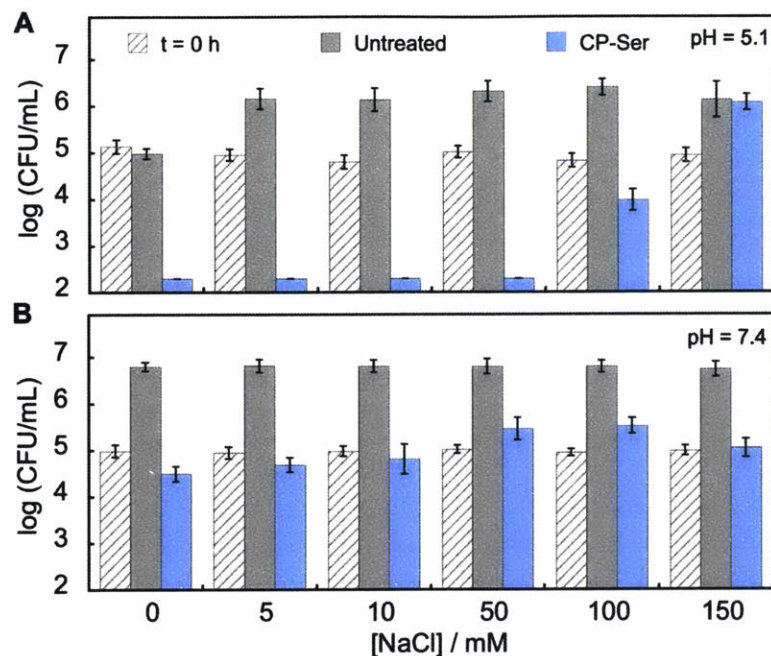


Figure 4. 4. Effect of NaCl concentration on the *E. coli*-cidal activity of CP. *E. coli* ATCC 25922 cultures (1×10^5 CFU/mL) were incubated with 40 M CP-Ser (blue) at (A) pH 5.1 and (B) pH 7.4 for 3 h at 37 °C with shaking at 150 rpm. Cultures were plated on TSB/agar plates, incubated for 12-14 h at 37 °C, and colonies counted for CFU determination. Buffer: 10 mM MES pH 5.1, or 10 mM phosphate 7.4 + 1% TSB containing 0, 5, 10, 50, 100, and 150 mM NaCl. The CFU count of the starting and untreated cultures are shown as striped and grey bars respectively. (mean \pm 95% CI, $n = 3$).

4. 3. 2. The Bactericidal Activity of CP is Independent of Metal Sequestration

CP possesses distinct Ca(II) and transition-metal binding sites (Figure 4. 1B), and the bacteriostatic effect of CP has been widely ascribed to its metal-sequestering abilities. The incubation medium used in our assay conditions are nutrient-poor. As such, we don't expect that the bactericidal activity of CP arises from its metal-sequestering properties. Nevertheless, we carried out metal-depletion experiments with CP and the incubation medium (10 mM MES + 1% TSB, pH 5.1, or 10 mM phosphate + 1% TSB, pH 7.4) under conditions similar to the broth microdilution assay. In this assay, CP was added to the incubation medium for 3 h (37 °C, with shaking at 150 rpm); the protein was then removed from the treated medium using spin filtration. We quantified the amount of unbound metal in the treated medium by inductively coupled plasma-

mass spectrometry (ICP-MS). This method provides an assessment of which metal ion can be sequestered by CP, and not an equilibrium measurement.

The phosphate and MES media, as expected are nutrient poor and, contain $\sim 2 \mu\text{M}$ total transition metals (Table 4. 4). The Ca(II) concentration of the buffers is in the single-digit micromolar range, suggesting that CP likely exists as a dimer under those assay conditions. CP treatment resulted in no measurable metal depletion at the pH values tested, corroborating the notion that CP cannot sequester Ca(II) and any of the transition metals analyzed under our assay conditions (Table 4. 4). As such, we propose that the bactericidal activity of CP is not as a result of its metal-withholding capabilities.

We also considered the possibility that a fraction of CP may exist in the metal-bound form even if it cannot sequester away metals from the incubation medium. In this scenario, metal-bound CP may interact with and affect bacterial membranes in a way that causes killing and/or growth inhibition. Notably, this mechanism was put forward to explain the antimicrobial effect of CP against *B. burgdoferi*, the causative agent of Lyme disease.³² A back-of-the-envelope calculation, which is based on CP and transition metal concentrations in our assays, revealed that $\sim 3\%$ of CP ($1 \mu\text{M}$) could potentially be metal-bound (assuming a metal:CP binding stoichiometry of 2:1). It is therefore unlikely that this small fraction of metal-bound CP would significantly contribute to the bactericidal effects of CP we observed.

Table 4. 4. Metal analysis of MES and phosphate buffers in the absence and presence of 40 μM CP-Ser (mean \pm SDM, $n = 2$).

Element	10 mM MES + 1% TSB, pH 5.1		10 mM phosphate + 1% TSB, pH 7.4	
	- CP-Ser (μM)	+ CP-Ser (μM)	- CP-Ser (μM)	+ CP-Ser (μM)
Na	4400 \pm 800	3300 \pm 600	16930 \pm 50	15940 \pm 30
Mg	6 \pm 2	14 \pm 3	3.34 \pm 0.06	7 \pm 4
K	530 \pm 160	350 \pm 110	293 \pm 1	274 \pm 1
Ca	7 \pm 2	47 \pm 6	4.8 \pm 0.9	20 \pm 10
Mn	0.05 \pm 0.06	0.016 \pm 0.002	0.007 \pm 0.001	0.014 \pm 0.002
Fe	1 \pm 0.3	1.4 \pm 0.1	0.48 \pm 0.02	1.4 \pm 0.3
Co	0.006 \pm 0.005	0.003 \pm 0.001	0.002 \pm 0.000	0.003 \pm 0.000
Ni	0.4 \pm 0.4	0.4 \pm 0.2	0.074 \pm 0.004	0.3 \pm 0.006
Cu	0.028 \pm 0.004	0.2 \pm 0.1	0.014 \pm 0.001	0.053 \pm 0.003
Zn	0.6 \pm 0.1	0.7 \pm 0.3	0.29 \pm 0.01	0.4 \pm 0.01

4. 3. 3. Divalent Metals Attenuate the *E. coli*-cidal Activity of CP

To further assess if metal-binding contributes to the bactericidal activity of CP, we examined the bactericidal activity of CP in the presence of Ca(II) and Zn(II). Ca(II) binding causes the two CP heterodimers to self-associate and form a (S100A8/S100A9)₂ heterotetramer¹³ that shows increased resistance to proteases.⁴⁹ These features caused by Ca(II)-binding are likely relevant with respect to the function of CP as an AMP and warrant further examination. We tested the activity of CP in the presence of increasing Ca(II) levels, which revealed that the activity of CP was attenuated as a function of increasing Ca(II) levels under acidic conditions (Figure 4. 5A). Indeed, there was a significant reduction in the activity of CP in the presence of 50 μM Ca(II), and no further attenuation at Ca(II) concentrations of 100 μM and higher (Figure 4. 5A). At pH 7.4, CP was mostly unaffected by Ca(II) supplementation (Figure 4. 5B).

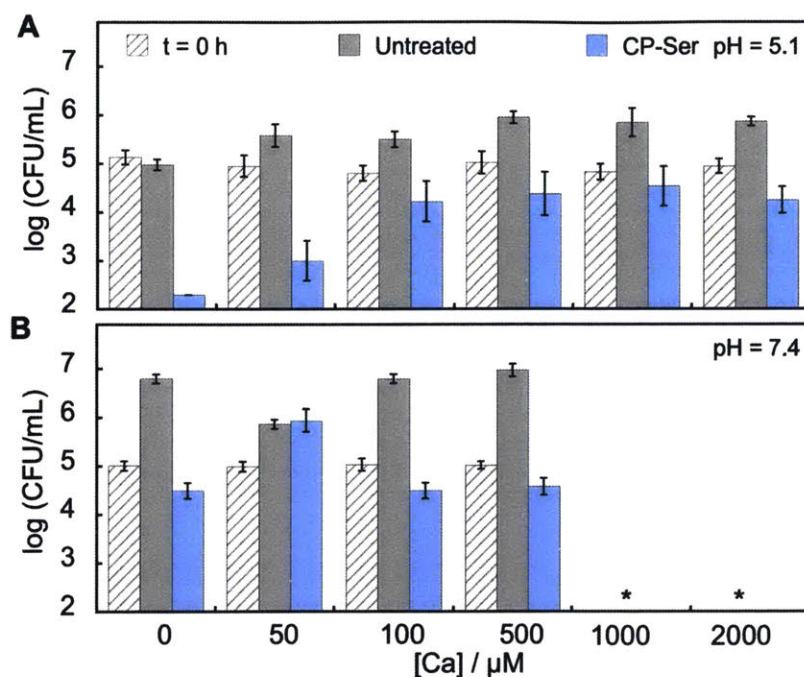


Figure 4. 5. Effect of Ca(II) concentration on the *E. coli*-cidal activity of CP. *E. coli* ATCC 25922 cultures (1×10^5 CFU/mL) were incubated with 40 μM CP-Ser (blue) at (A) pH 5.1 and (B) pH 7.4 for 3 h at 37 °C with shaking at 150 rpm. Cultures were plated on TSB/agar plates, allowed to incubate for 12-14 h at 37 °C, and colonies counted for CFU determination. Buffer: 10 mM MES pH 5.1 + 1% TSB, or 10 mM phosphate pH 7.4 + 1% TSB containing 0, 50, 100, 500, 1000, and 2000 μM Ca(II). The CFU count of the starting and untreated cultures are shown as striped and grey bars respectively. (mean \pm 95% CI, $n = 3$). * The calcium titration could not be performed under those conditions due to precipitation issues (see Experimental).³⁹

The distinct trends observed from the Ca(II) titrations at pH 5.1 and 7.4 are curious, and the molecular basis for these differences remain unclear. We postulate that Ca(II)-binding may affect either the charge distribution of CP or its structural and oligomerization state in a pH-dependent manner, and thus impact the bactericidal properties of CP differently at pH 5.1 vs 7.4. It is also possible that Ca(II) ions interact with the negatively charged lipopolysaccharides (LPS) molecules or lipoproteins on the cell surface of *E. coli* and weaken electrostatic interactions, resulting in an attenuation of CP activity. However, this scenario does not account for the pH dependency observed with Ca(II) supplementation, or the resistance that CP shows to high NaCl levels, which presumably have a similar overall effect as Ca(II) on *E. coli* cell surface charge.

Zn(II)-binding has been shown to potentiate the antimicrobial activity of clavamin A, a His-containing helical AMP.⁴⁶ In this study, substoichiometric Zn(II) (relative to the peptide concentration) was sufficient to enhance the bactericidal activity of clavamin A against *E. coli*, as seen by a reduction in cell viability compared to the apo peptide. CP is a Zn(II)-binding protein and, similarly to Ca(II) binding, CP self-associates into a tetramer upon Zn(II) coordination.¹³ A Zn(II) and Ca(II) preincubation assay was therefore designed to probe the effect of Zn(II) binding on the bactericidal activity of CP. Because we were not able to ascertain the Zn(II)-binding properties of CP under acidic conditions, we carried out the Zn(II)-preincubation assay at pH 7.4 only since we expect that CP is able to coordinate Zn(II) with at least picomolar affinity at this pH.¹⁸ Excess Zn(II) inhibits the acquisition of other essential metals, such as Mn(II), resulting in Zn(II) toxicity to microbes,⁵⁰ and consistent with this notion we found that 10 μ M free Zn(II) possesses bactericidal properties under our assay conditions. To avoid this complication and ensure that there is no free Zn(II) that may contribute *E. coli* killing, CP was preincubated with substoichiometric Zn(II) (1.9 equiv relative to protein concentration) in the absence or presence of excess Ca(II) for 15 min prior to the assay. The Zn(II)-bound protein was then incubated with *E. coli*. As expected, the untreated cells that incubated with Zn(II) only, or Zn(II) and Ca(II) resulted in complete killing of *E. coli* due to the toxic effects of Zn(II) (Figure 4. 6). Consistent with the Ca(II) titration experiments, the addition of 500 μ M Ca(II) weakened the activity of CP (Figure 4. 6). The Zn(II)-bound and Zn(II)- and Ca(II)-bound forms of CP also exhibited significantly reduced activity compared to the apo form (Figure 4. 6). Similar to Ca(II), we propose that Zn(II)-coordination by CP likely affects its oligomerization and/or electrostatic properties in a way that diminishes the *E. coli*-cidal properties of CP. Altogether these results suggest that CP is most active when in the apo form, and that divalent-metal binding abolishes the bactericidal activity of CP.

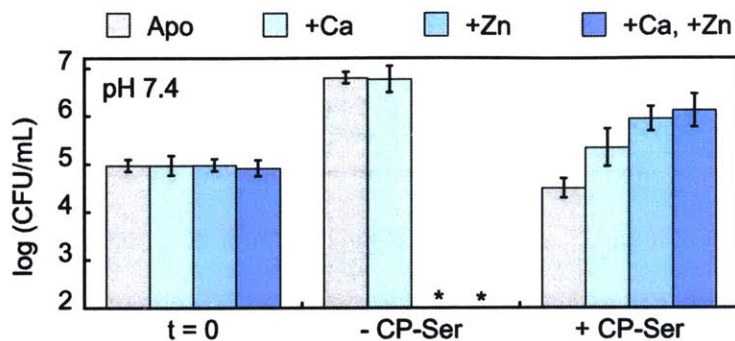


Figure 4. 6. Effect of divalent metal-binding on the *E. coli*-cidal activity of CP. CP-Ser was preincubated with 1.9 equiv of Zn(II) in the absence and presence of 500 μ M Ca(II). *E. coli* ATCC 25922 cultures (1×10^5 CFU/mL) were then treated with Zn(II)-bound CP for 3 h at 37 $^{\circ}$ C with shaking at 150 rpm. Cultures were plated on TSB/agar plates, allowed to incubate for 12-14 h at 37 $^{\circ}$ C, and colonies counted for CFU determination. Buffer: 10 mM phosphate 7.4 + 1% TSB. The CFU count of the starting and untreated cultures are also shown to demonstrated the bactericidal properties of free Zn(II) (mean \pm 95% CI, $n = 3$). * No growth was observed under these conditions due to the bactericidal properties of free Zn(II).

4. 3. 4. CP Induces Concentration-dependent Morphological Changes in *E. coli*

Next, we employed microscopy to examine the cell phenotypes caused by CP treatment. In order to allow for the visualization of enough cells, we adapted the broth microdilution by employing a greater number of cells (1×10^8 CFU/mL). We also used a higher CP concentration of 100 μ M for the imaging studies; this concentration was high enough to induce noticeable morphological cell phenotypes (Figure 4. 7), and below the MIC value of CP such that there were enough cells present for visualization (Figures 4. 7 and 4. 8). In general, CP-treated cells displayed various phenotypes that included: (i) distortion and roughness of cell wall, (ii) cell lysis, as well as (iii) cell membrane protrusions (Figure 4. 9). A quantitative analysis of these phenotypes revealed that CP treatment induced cell distortion in over 70% of cells, cell wall protrusions in ~15% of the cells, and caused cell lysis in ~10% of the cells (Figure 4. 10). While the molecular basis for these cell morphology phenotypes remains unknown, it is likely related to a perturbation of the outer and/or inner membrane architecture,⁵¹ an effect that has been reported with other AMPs.^{44, 52}

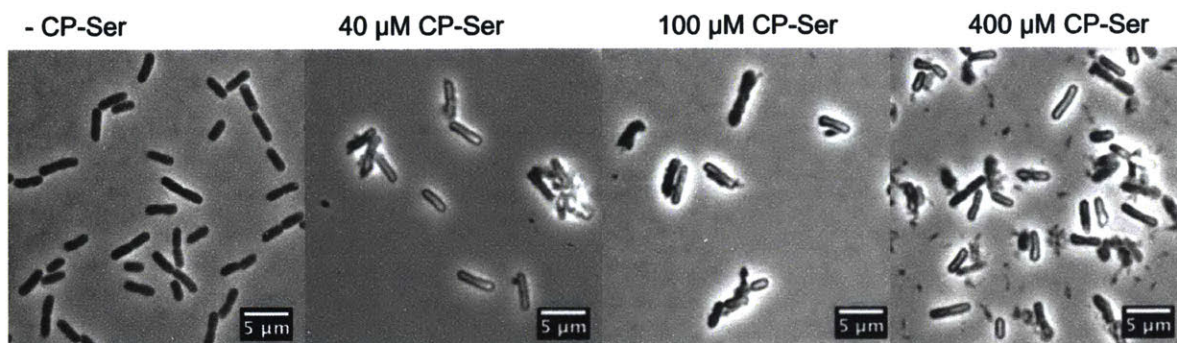


Figure 4. 7. Effect of CP on *E. coli* cell morphology. *E. coli* ATCC 25922 cultures (1×10^8 CFU/mL) were treated with 100 μ M CP for 3 h at 37 °C with shaking at 150 rpm. Buffer: 10 mM MES 5.1 + 1% TSB. Scale bar is 5 μ m.

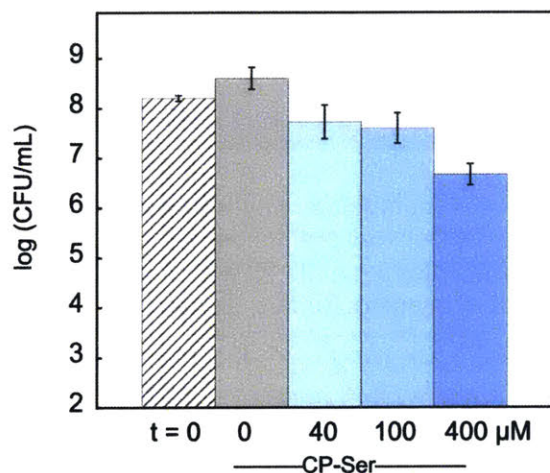


Figure 4. 8. Effect of CP concentration on *E. coli* cells. *E. coli* ATCC 25922 cultures (1×10^8 CFU/mL) were treated with the specified CP-Ser concentrations for 3 h at 37 °C with shaking at 150 rpm. Cultures were plated on TSB/agar plates, allowed to incubate for 12-14 h at 37 °C, and colonies counted for CFU determination. Buffer: 10 mM MES 5.1 + 1% TSB. The CFU count of the starting and untreated cultures are shown as striped and grey bars respectively. (mean \pm 95% CI, $n = 2$).

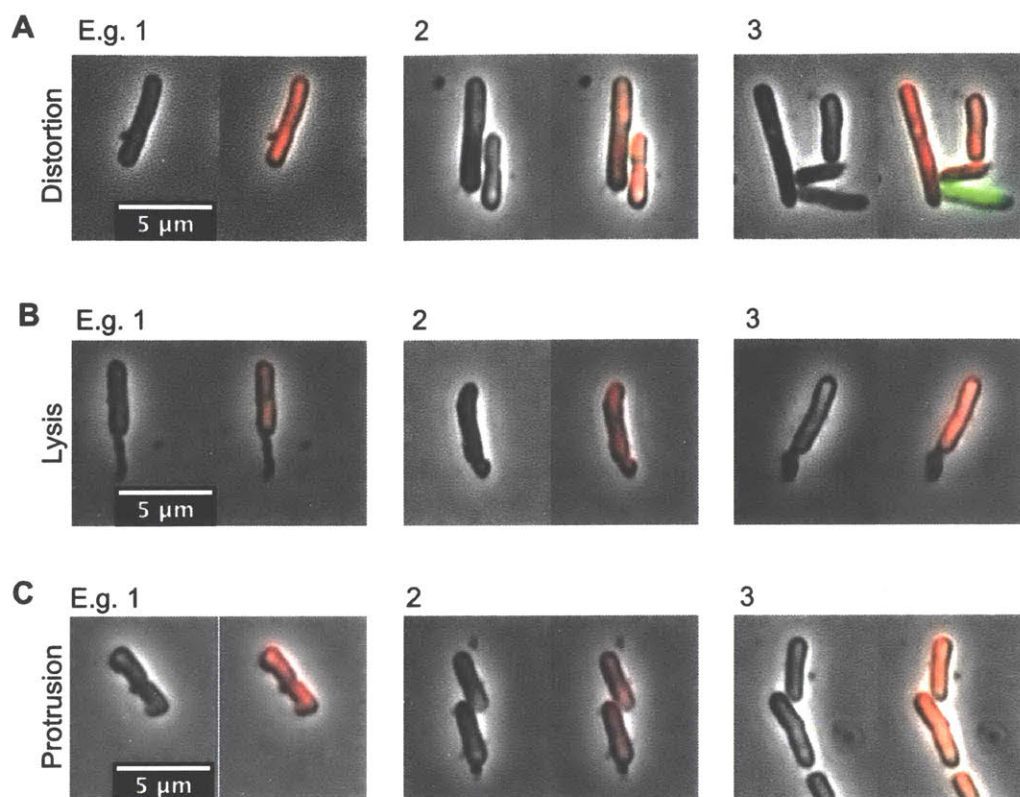


Figure 4. 9. CP induces aberrant cell morphology phenotypes in *E. coli*. (A) Distortion and cell wall roughness, (B) Cell lysis, and (C) Cell wall protrusions. *E. coli* ATCC 25922 cultures (1×10^8 CFU/mL) were treated with 100 μ M CP for 3 h at 37 °C with shaking at 150 rpm. Live-Dead stain was added to the cells 15 min prior to imaging. Buffer: 10 mM MES 5.1 + 1% TSB. Scale bar is 5 μ m.

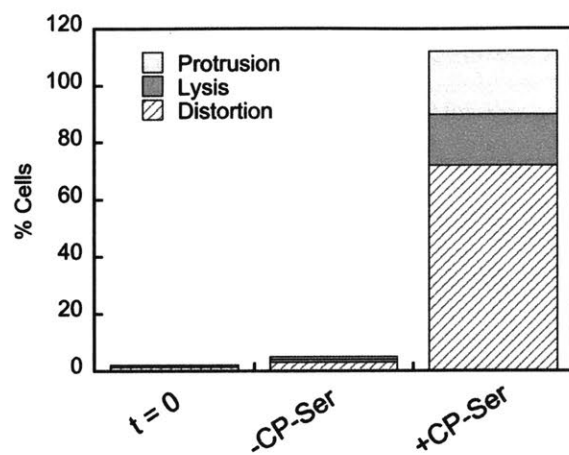


Figure 4. 10. Quantification of the CP-induced CP morphology phenotypes in *E. coli*. *E. coli* ATCC 25922 cultures (1×10^8 CFU/mL) were treated with $100 \mu\text{M}$ CP-Ser for 3 h at 37°C with shaking at 150 rpm. Buffer: 10 mM MES 5.1 + 1% TSB. A total of ~ 500 cells were counted for each condition, ($n = 3$).

We obtained temporal information about the cell morphology phenotypes by carrying real-time microscopy imaging studies of *E. coli* cells treated with CP, and examining the appearance of CP-caused cell phenotypes. As expected, the untreated cells remained smooth and divided one to two times over the 3-h incubation (Figure 4. 11). In contrast, no cell division was observed for the CP-treated cells. The cells were impaired in their ability to divide, resulting into cell distortion and elongation (Figures 4. 12D and 4. 12E). The first phenotype to appear within 15 min of treatment with CP was cell wall roughness, followed by cell wall protrusions which appeared between 15 and 60 min. Cell elongation occurred later as the cells were attempting to divide. We were not able to obtain temporal information on the cell lysis process of the cells because the cells went out of focus during that process. Altogether, the real-time imaging experiments provide valuable insights on the nature and magnitude of the membrane permeabilizing effects of CP, and corroborate that CP can be a membrane-permeabilizing factor.

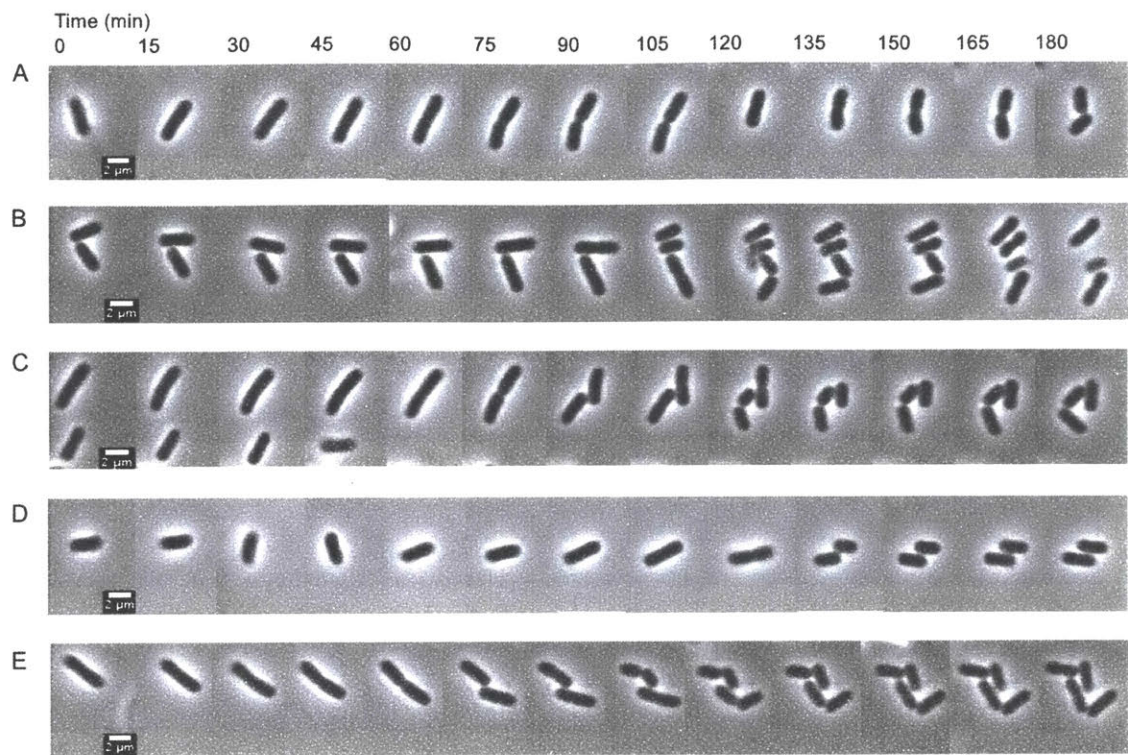


Figure 4. 11. Time-lapse imaging of select untreated *E. coli* cells. *E. coli* ATCC 25922 cultures (1×10^8 CFU/mL) were incubated for 3 h at 37 °C with shaking at 150 rpm. Buffer: 10 mM MES 5.1 + 1% TSB. Scale bar is 2 μm, ($n = 1$).

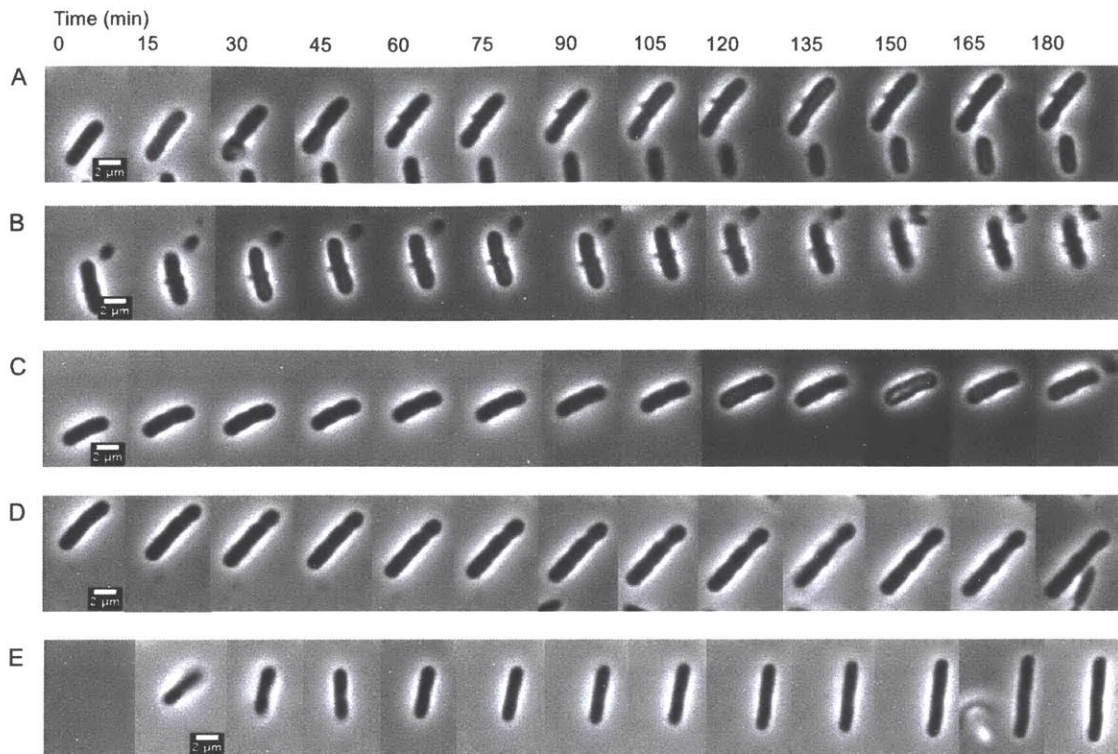


Figure 4. 12. Time-lapse imaging of select CP-treated *E. coli* cells. *E. coli* ATCC 25922 cultures (1×10^8 CFU/mL) were incubated with $100 \mu\text{M}$ CP for 3 h at 37°C with shaking at 150 rpm. Buffer: 10 mM MES 5.1 + 1% TSB. Scale bar is $2 \mu\text{m}$, ($n = 1$).

4. 3. 5. CP Binds and Permeabilizes the Bacterial Membrane

A Live-Dead staining kit was utilized to identify whether the CP-induced cell phenotypes were associated with a disruption of membrane integrity and loss of cell viability. Based on this staining kit, cells with compromised membranes stain red or yellow, whereas cells with intact membranes stain green. The results from Live-Dead staining indicated that all the CP-induced cell phenotypes we identified were associated with a disruption of membrane integrity, as evidenced by the cell red staining (Figure 4. 9). Furthermore, an analysis of the CP-treated cell population showed that 90% of cells had a compromised cell wall compared to the untreated cells that predominantly intact, with over 90% of cell staining green (Figures 4. 13). Taken together, these results suggest that CP is able to permeabilize the cell wall of *E. coli* cells, affect their

viability, and induce aberrant cell morphology phenotypes associated with a disrupted cell wall. While the majority of CP-treated cells stained red, which is indicative of cell membrane permeabilization, CFU counts showed that the effect of CP did not result in significant cell killing (Figure 4. 6). We propose two possible explanations for these results: (i) CP may either act by a mechanism whereby membrane permeabilization is not direct the cause of cell killing,^{51,53-54} or (ii) the cells are able to recover (likely during the plating step) from CP treatment. The former phenomenon is not uncommon; certain AMPs have been shown to form transient pores in the outer cell membrane of bacteria at sub-MIC levels,⁵⁴ whereas others have been reported to bind to and insert into bacterial membranes without causing significant permeabilization, and instead reaching intracellular targets.^{53,55-57}

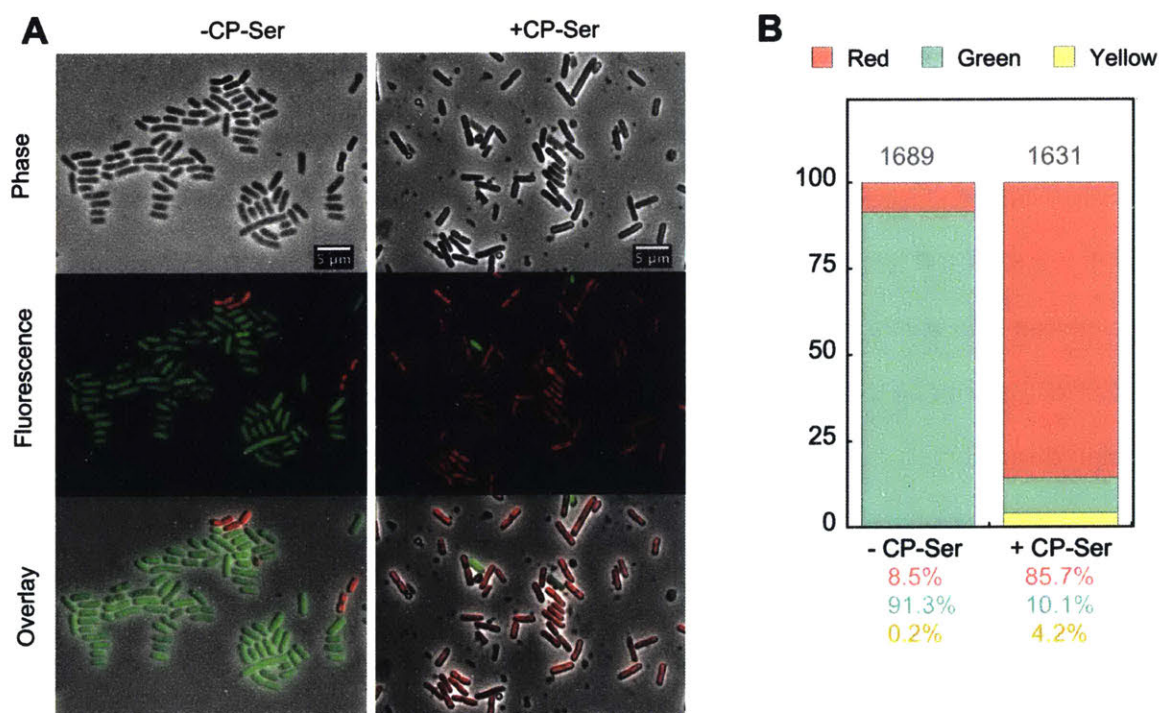


Figure 4. 13. Live-Dead staining of CP-treated *E. coli*. (A) Phase-contrast and fluorescence images of untreated and CP-treated cells. (B) Quantification of cells with intact and compromised cell wall in the absence and presence of added CP-Ser. *E. coli* ATCC 25922 cultures (1×10^8 CFU/mL) were treated with $100 \mu\text{M}$ CP for 3 h at 37°C with shaking at 150 rpm. Live-Dead stain was added to the cells 15 min prior to imaging. Buffer: 10 mM MES 5.1 + 1% TSB. Scale bar is 5 μm .

4. 3. 6. CP Treatment Causes Leakage of Periplasmic GFP

E. coli strains expressing GFP in select compartments have been used to obtain insights into the mode of action of various AMPs.⁵⁸⁻⁶¹ Guided by these studies, we utilized *E. coli* K12 strains expressing GFP in the cytoplasm (*E. coli* cyto-GFP) and the periplasm (*E. coli* peri-GFP) to visualize which cell compartment CP affects. Mid-log phase *E. coli* cyto-GFP and *E. coli* peri-GFP cells were treated with CP and examined by fluorescence microscopy. For the *E. coli* cyto-GFP expressing cells, the untreated cells exhibited a uniform green GFP emission pattern over the whole cell surface (Figure 4. 13). A similar GFP emission and localization pattern was noted for CP-treated cells (Figure 4. 13), suggesting that CP does not affect the cytoplasmic content of *E. coli*. In the case of *E. coli* peri-GFP cells, the untreated cells exhibited a more intense green halo around the cell corresponding to the periplasmic space, and a dimmer and pigmented fluorescence pattern over the whole cell, characteristic of *E. coli* peri-GFP cells (Figure 4. 14).^{58-59,61} CP-treated cells had lost this green halo and instead displayed only a mild, textured and pigmented fluorescence pattern, which was markedly less intense than the *E. coli* cyto-GFP cells, likely due to peri-GFP leaking and diffusing into the cytoplasm (Figure 4. 14). This effect has been well-reported with AMPs capable of causing periplasmic GFP diffusion due to either osmotic stress⁵⁸ or membrane permeabilization,^{59,61} and implicate a function for CP in periplasmic diffusion/disruption.

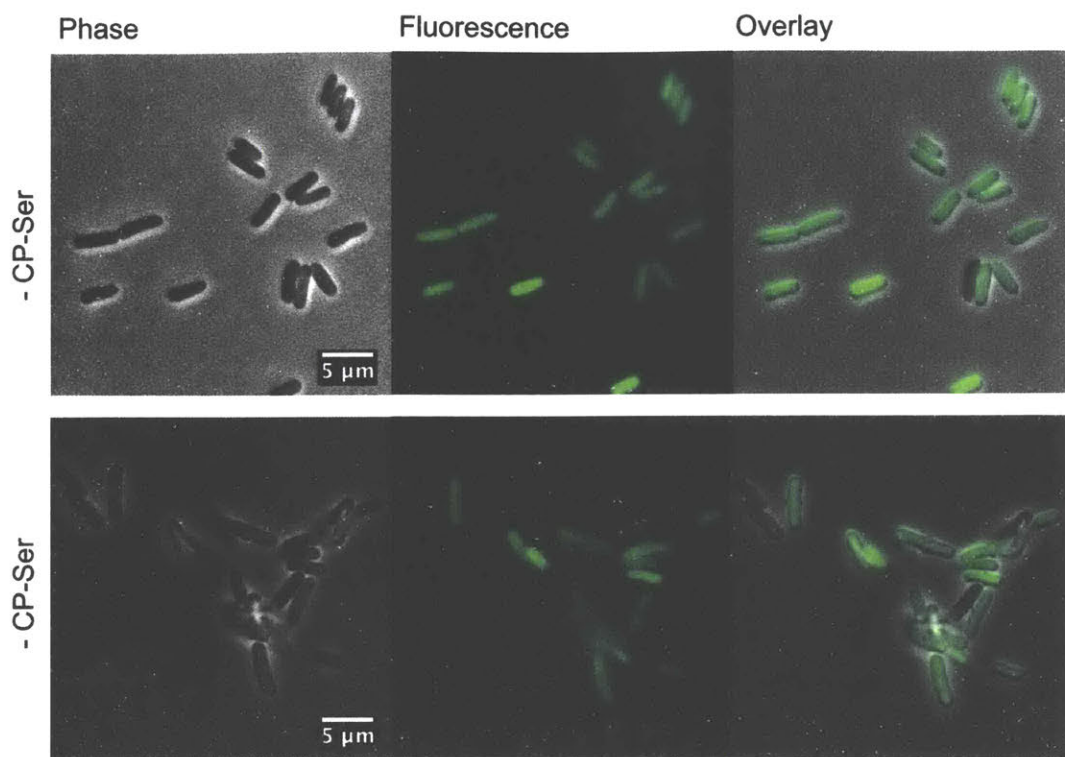


Figure 4. 14. Treatment of *E. coli* peri-GFP with CP. *E. coli* K12 peri-GFP cultures (1×10^8 CFU/mL) were treated with 100 μ M CP for 3 h at 37 °C with shaking at 150 rpm. Buffer: 10 mM MES 5.1 + 1% TSB. Scale bar is 5 μ m, ($n = 2$).

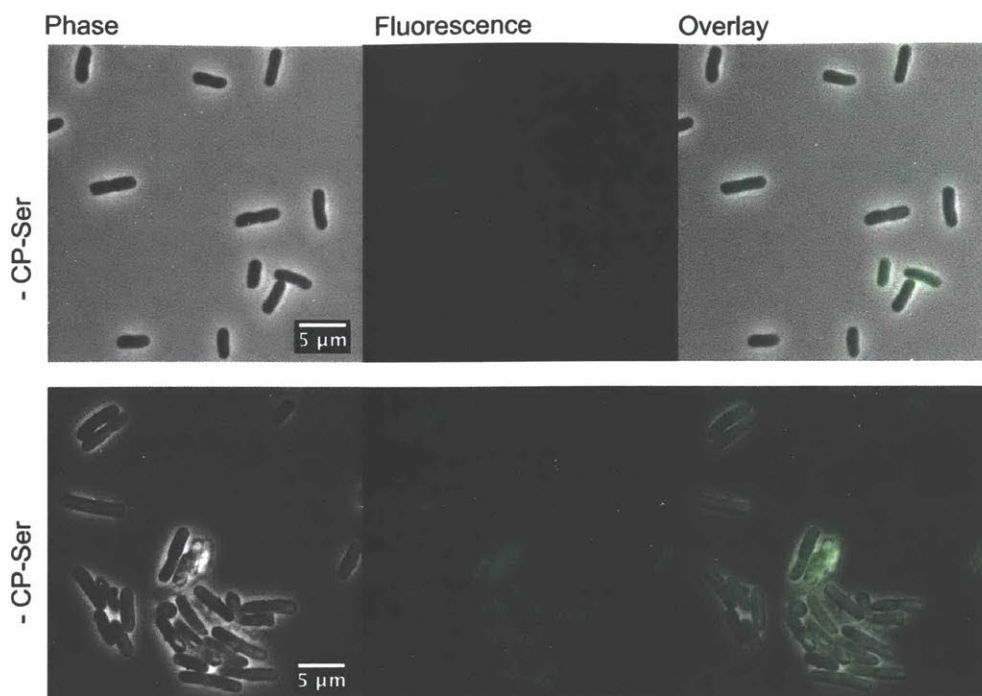


Figure 4. 15. Treatment of *E. coli* cyto-GFP with CP. *E. coli* K12 cyto-GFP cultures (1×10^8 CFU/mL) were treated with $100 \mu\text{M}$ CP for 3 h at 37°C with shaking at 150 rpm. Buffer: 10 mM MES 5.1 + 1% TSB. Scale bar is $5 \mu\text{m}$, ($n = 2$).

4. 3. 7. Synthesis and Characterization of Fluorescein-CP-Ser (FL-CP)

To probe the cellular localization of CP, we synthesized a fluorescein-CP (FI-CP) conjugate. The preparation protocol of FL-CP was adapted from a method previously reported (Nakashige, Annual Report, 2013) and a protocol used for the purification of biotinylated CP.³⁶ Briefly, the purified CP variant CP(C42S), which contains an intact Cys residues at position 3 in S100A9, was purified under reducing conditions and subsequently coupled to fluorescein-5-iodoacetamide (F5I) (Table 4. 1). The protein mixture was then dialyzed overnight to remove excess F5I, and FL-CP purified by preparative SEC. The purified FL-CP was dialyzed against Chelex, concentrated to $\sim 500 \mu\text{M}$, and stored in $50\text{-}\mu\text{L}$ aliquots at -80°C .

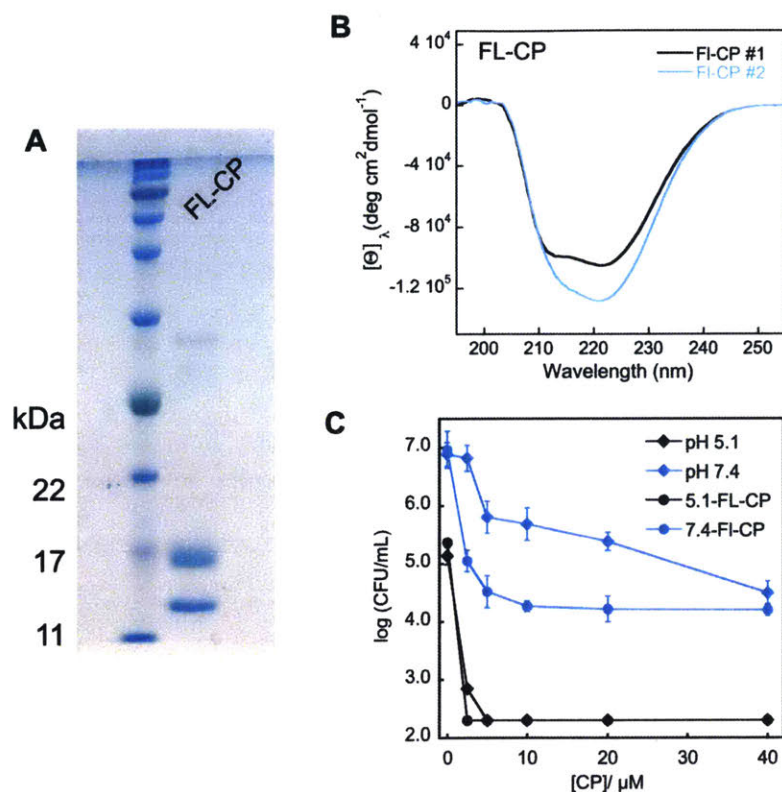


Figure 4. 16. Characterization of FL-CP. (A) SDS-PAGE (15% acrylamide Tris-HCl, glycine gel) visualized with Coomassie Blue of purified FL-CP. The ladder is P7712S from New England BioLabs. (B) Circular dichroism spectra of 10 μ M of two FL-CP. Buffer: 1 mM Tris-HCl, pH 7.0. (C) Broth microdilution assay of FL-CP and CP-Ser at pH 5.1 and 7.4 against *E. coli*. *E. coli* ATCC 25922 cultures (1×10^5 CFU/mL) were treated with the specified CP concentrations for 3 h at 37 $^{\circ}$ C with shaking at 150 rpm. Buffer: 10 mM MES 5.1 + 1% TSB, ($n = 2$).

The purity of FL-CP was confirmed SDS-PAGE, which showed two distinct bands at ~12 and ~17 kDa, corresponding to S100A8 and FL-S100A9 respectively (Figure 4. 16A). Circular dichroism (CD) analysis revealed that FL-CP was properly folded with the expected overall α -helical character for CP (Figure 4. 16B). We noted that the CD spectra of FL-CP exhibited markedly higher ellipticity compared to CP¹³ resulting from the added absorbance of the fluorescein moiety. To assess if the added fluorophore impacts the bactericidal activity of FL-CP, we carried out broth microdilution assays of FL-CP and compared it to the activity of CP-Ser. We found that the two protein variants exhibited similar *E. coli*-cidal activity at acidic pH, suggesting

that FL-CP can be used as a CP analogue for microscopy studies (Figure 4. 16.C). At neutral pH, FL-CP was slightly more potent than CP-Ser (Figure 4. 16.C); it is possible that the added charge from the fluorescein moiety enhances the killing activity of CP, or that it causes CP to undergo conformational changes that also enhances its killing activity.

4. 3. 8. *FL-CP Localizes on The Bacterial Cell Surface of E. coli*

For the microscopy studies with FL-CP, *E. coli* cells adhered to a poly-D-lysine coated culture dish were first treated with FL-CP (3 h, 37 °C, 150 rpm), followed by a gentle wash step with AMA buffer (20 mM Tris, 100 mM NaCl, pH 7.5) (3 x 3 mL), and then analyzed by microscopy. One caveat we encountered with this experimental setup was that there were not many cells that remained adhered to the poly-D-lysine culture dish after the wash step, thus precluding the analysis of a meaningful number of cells. As such, the data presented in this subsection are preliminary and more cells need to be analyzed before making conclusive statements. As expected, the untreated cells displayed no GFP emission (Figure 4. 17A). For the FL-CP-treated cells, GFP emission was observed on the entire *E. coli* cell surface (Figures 4. 17B, 4. 17C). The fluorescence pattern covered the whole cell, such that we were not able to infer on specific binding targets of CP, as well as its cellular localization. Interestingly, cells that exhibited GFP emission also displayed cell-morphology phenotypes we have shown earlier to be associated with CP-treatment (Figure 4. 9). We noted that one of the FL-CP-treated cells imaged (Figure 4. 17B) displayed a morphology phenotype that resembled a bleb, a phenotype usually associated with antibiotic exposure.^{48,51,62-63} A closer inspection of the phase-contrast image revealed that what appeared as a bleb in the fluorescence image is an artifact of the image, and seems to be an out-of-focus lysed-cell (Figure 4. 17B). Based on these initial results, we reason that CP physically interacts with *E. coli* and that this interaction results in membrane permeabilization

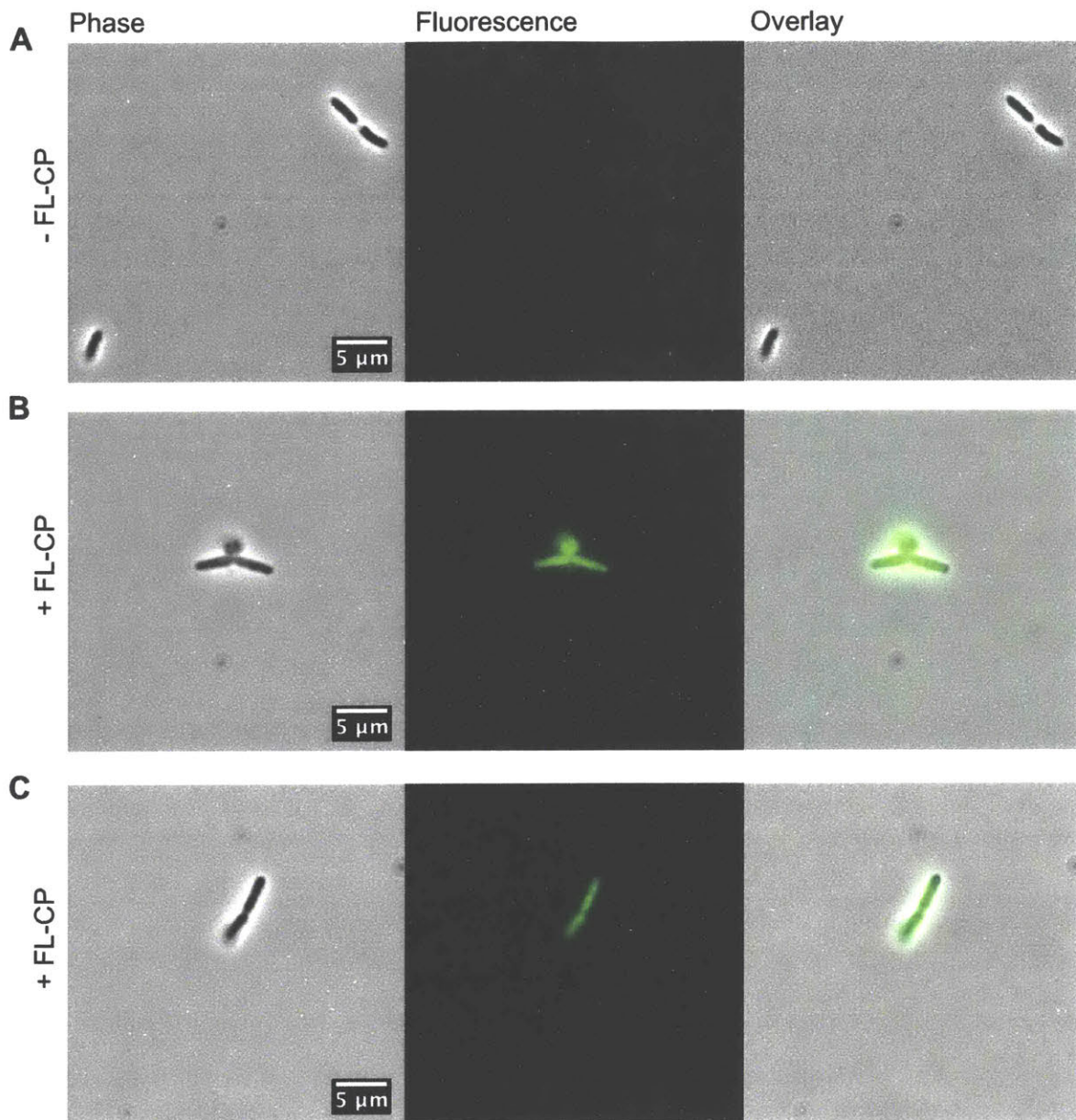


Figure 4. 17. Treatment of *E. coli* peri-GFP with FL-CP. *E. coli* ATCC 25922 cultures (1×10^8 CFU/mL) were treated with 100 μM FL-CP for 3 h at 37 °C without shaking. The cells were gently washed with AMA buffer (20mM Tris, 100 mM NaCl, pH 7.5) (3 x 3 mL), and imaged. (A) Untreated cells, (B) and (C) FL-CP-treated cells. Scale bar is 5 μm.

4. 2. 9. CP Exhibits Broad-Spectrum Bactericidal Activity against Gram-negative Strains

Select studies have shown that CP can associate with the cell wall of various microbes including parasites^{28,64-65} and bacterial pathogens.^{30-32,66} However, to the best of our knowledge, there have been no studies examining the scope of the bactericidal activity of CP. Therefore, we screened CP against a panel of bacterial species previously employed to examine the metal-mediated growth-inhibitory properties of CP.^{13-14,16,18-20} This panel of strains included the Gram-negative strains *Acinetobacter baumannii* ATCC 17978, *Escherichia coli* UTI89, and *Pseudomonas aeruginosa* PAO1, and the Gram-positive strains *Listeria monocytogenes* ATCC 19115 and *Staphylococcus aureus* USA300 JE2 (Table 4. 3). We have observed from our prior studies that CP exhibits metal-mediated bacteriostatic activity against all the strains in this panel, and it will be informative to assess how the bactericidal properties of CP compare.^{13-14,16,18-20}

In agreement with the results obtained from the broth microdilution assays with *E. coli* ATCC 25922, CP was generally more active under acidic conditions (Figure 4. 18). The three Gram-negative strains *A. baumannii*, *E. coli* UTI89, and *P. aeruginosa*, were all susceptible to CP-treatment, with complete killing of the cultures observed at pH 5.1 (Figure 4. 18). On the other hand, growth of the two Gram-positive strains *L. monocytogenes* and *S. aureus* was unaffected by CP treatment (Figure 4. 18). Concordant with results from the broth microdilution assays, microscopy studies carried out at acidic showed that the CP-treated Gram-negative cultures were composed of a high percentage of cells with a compromised cell wall (red cells), whereas for the Gram-positive strains, the ratio of intact (green) to compromised (red) cells were comparable to the untreated conditions (Figure 4. 19). Furthermore, the CP-treated Gram-negative strains displayed cell morphology phenotypes similar to the ones observed with *E. coli* ATCC 25922, whereas the Gram-negative strains displayed no obvious cell morphology phenotypes. *A. baumannii* cells, *E. coli* UTI89, *P. aeruginosa* cells were distorted with a rough outer-membrane and cell surface protrusions, and a significant number of cells were lysed as seen by the cell debris present (Figure 4. 19). Interestingly, the difference between the susceptibilities of the

strains against the bacteriostatic vs the bactericidal effects of CP indicate that the mode of action of CP as an AMP is distinct from its function as a metal-sequestering protein.

Altogether, the results from the bacterial screen suggest that CP exhibits broad-spectrum bactericidal activity against Gram-negative bacteria through a mechanism of membrane permeabilization mediated by a physical interaction between CP and the bacterial cell wall. Bacterial cell wall components are well-documented binding partners and targets for AMPs, thus supporting this our hypothesis.⁶⁷⁻⁶⁸ We consider several scenarios to explain the interaction between CP and Gram-negative bacteria: It is possible that CP interacts with the negatively-charged moieties found on the outer-membrane of Gram-negative strains.⁶⁹⁻⁷⁰ Accordingly, the resistance of *L. monocytogenes* and *S. aureus* to CP is consistent with the fact that the cell envelope of Gram-positive bacteria is not comprised of LPS moieties, and is instead made of a peptidoglycan layer coated with teichoic acids.⁶⁹⁻⁷⁰ Furthermore, both classes of bacteria have other important amphiphiles, such as lipoproteins, which may also contribute to the selectivity of CP towards Gram-negative strains over Gram-positive strains. An additional scenario involves the interaction between CP and specific cell surface proteins, as it has been reported with *Neisseria* species and *F. magna*.^{30-31,66}

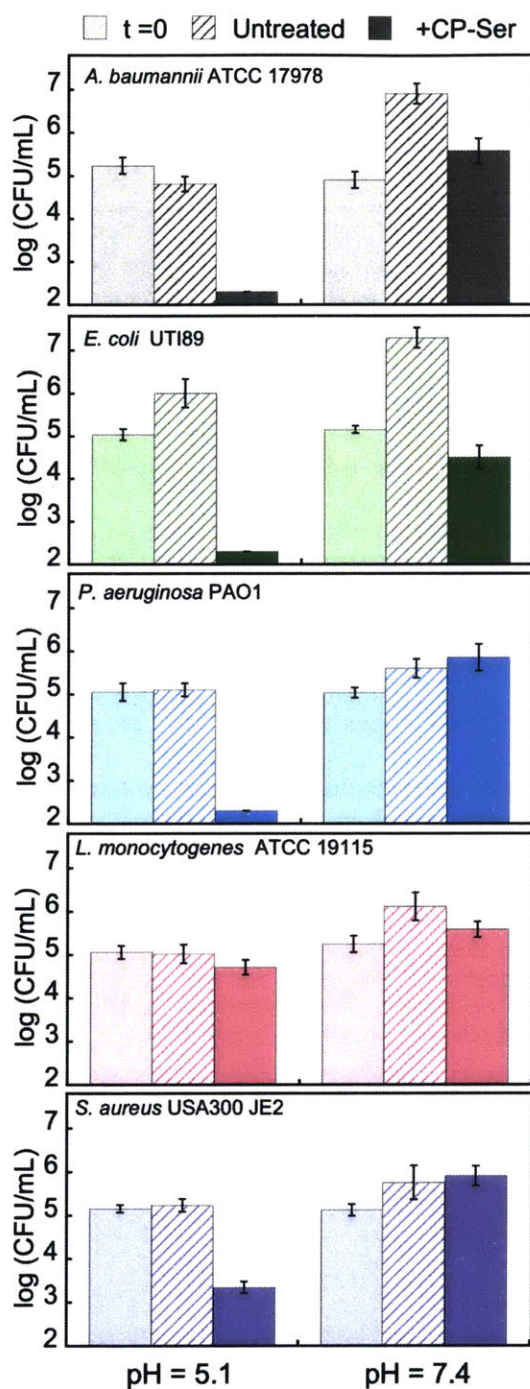


Figure 4. 18. Bactericidal activity of CP proteins against a panel of bacterial strains. Cells cultures (1×10^5 CFU/mL) of *A. baumannii* ATCC 17978 (A.B), *E. coli* UT189 (E.C), *P. aeruginosa* PAO1 (P.A), *L. monocytogenes* ATCC 19115 (L.M), and *S. aureus* USA300 JE (S.A) were incubated with 40 μ M CP for 3 h at 37 °C with shaking at 150 rpm. Cultures were plated on TSB/agar plates, allowed to incubate for 12-20 h at 37 °C, and colonies counted for CFU determination. Buffer: 10 mM MES pH 5.1, or 10 mM phosphate 7.4 + 1% TSB. (mean \pm 95% CI, $n = 3$).

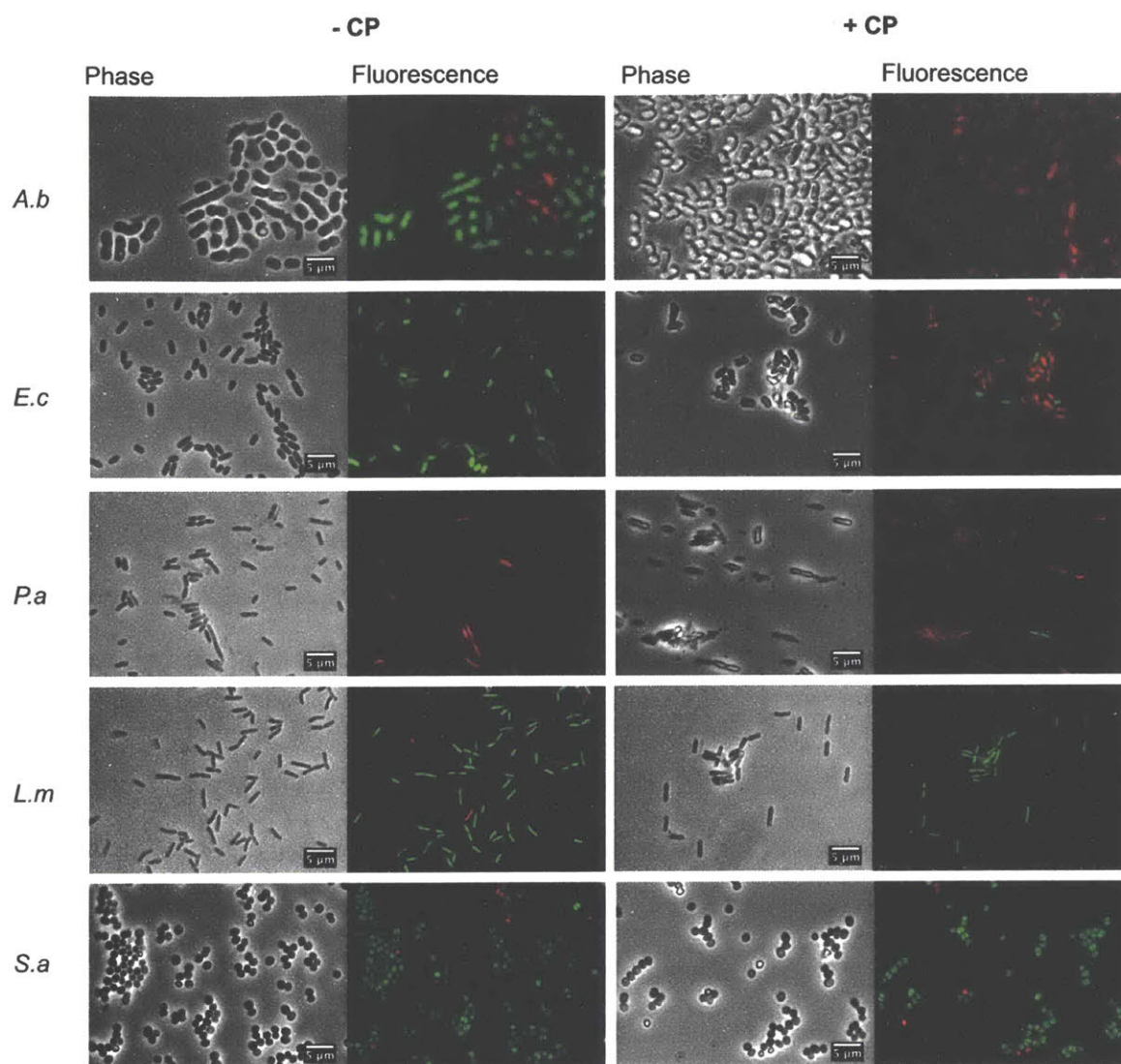


Figure 4. 19. Effect of CP-treatment on the morphology and membrane integrity on a panel of bacterial strains. Cells cultures (1×10^8 CFU/mL) of *A. baumannii* ATCC 17978 (A.B), *E. coli* UTI89 (E.C), *P. aeruginosa* PAO1 (P.A), *L. monocytogenes* ATCC 19115 (L.M), and *S. aureus* USA300 JE (S.A) were incubated with $100 \mu\text{M}$ of CP for 3 h at 37°C with shaking at 150 rpm. Live-Dead stain was added to the cells 15 min prior to imaging. Buffer: 10 mM MES 5.1 + 1% TSB. ($n = 2$) scale bar is $5 \mu\text{m}$.

4. 3. 10. *The Transition Metal-binding Sites of CP Contribute to its Function as an AMP*

In an attempt to start to understand which structural features of CP contribute to its bactericidal activity we examined the activities of a series of CP variants against *E. coli* ATCC 29522 (Table 4. 1). The variants employed included the single-site knockout variants, $\Delta\text{His}_3\text{Asp}$ and ΔHis_4 , which are defective in their abilities to coordinate transition metals, the double-site knockout variant, $\Delta\Delta$, which is missing both transition-metal binding sites and is thus incapable of coordinating transition metals, as well as the WT reduced form of CP, wtCP (wildtype CP), which contains the two original Cys residues Cys3 and Cys42. This last variant allows us to understand the contribution that the presence of Cys residues play on the activity of CP. All the CP variants were tested at acidic and neutral pH. This structure-activity assay revealed that at acidic pH wtCP and $\Delta\text{His}_3\text{Asp}$ were comparably active to CP-Ser, whereas ΔHis_4 was slightly less active, and $\Delta\Delta$ was completely inactive (Figure 4. 20). At neutral pH, the activities of all the variants were attenuated except for wtCP which displayed complete killing even at a neutral pH (Figure 4. 20).

The results obtained with the site variants are intriguing as they suggest that the transition metal-binding sites in CP contribute to its function as an AMP. We have shown that the incubation medium used in these assays are metal-poor and that CP-Ser is not capable of sequestering metals under those conditions (Table 4. 4), if anything metal-binding by CP results in an attenuation or loss of the bactericidal function of CP. Based on these observations, we reason that the presence of the site variants may contribute to AMP function by providing added protein stability or a more rigid fold. In order to test this notion, we recovered the remaining protein in the culture supernatant at the end of the assay to test this hypothesis. Circular dichroism (CD) analysis demonstrated that all the protein variants displayed the expected α -helical fold for CP suggesting that they are all properly folded under our assay conditions (Figure 4. 21). We ran an SDS-PAGE gel of the culture supernatant, which showed that all the protein variants were of comparable concentrations with two bands of similar intensities between 11 and 17 kDa,

corresponding to the S100A8 and S100A9 monomers (Figure 4. 22). These diagnostic experiments are helpful as they suggest that the proteins are not degraded over the course of the assay. However, they provide no information on the oligomerization state of the proteins, and their corresponding CD do not report on subtle or local conformational changes within the protein that may be caused by the site mutations. This overall trend is reminiscent of recent work reporting on the growth-initiatory properties of CP against *B. burgdorferi*. In this work, the author found that the antimicrobial activity of CP was not a result of metal-sequestration.³² However, the presence of the transition metal-binding sites in CP was found to contribute to the antimicrobial activity of CP. The authors proposed that metal binding causes stabilization or self-association of CP, which in turn promoted CP association with *B. burgdorferi*. Lastly, a noteworthy observation is related to the potent activity of wtCP at both acidic and neutral pH (Figure 4. 20). This behavior stands out from the other CP variants and underlines the importance of the Cys residues in CP. The functions that the Cys residues play in modulating the function CP as an AMP is an avenue for future work, and these initial results motivate us to work with wtCP in future studies.

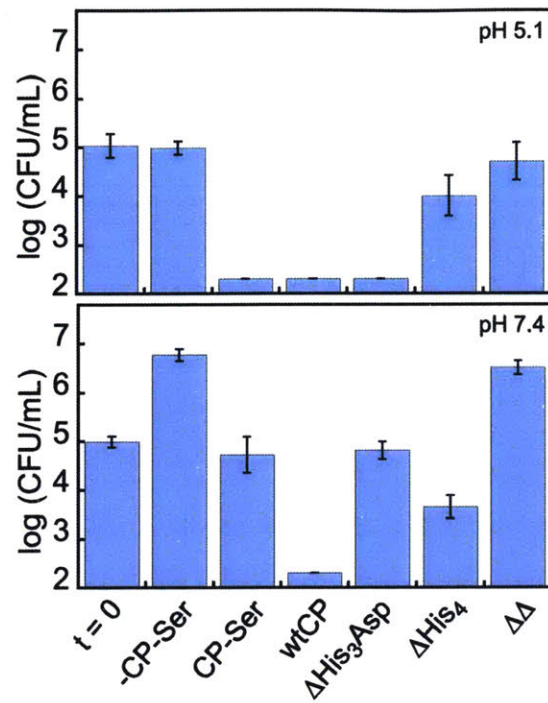


Figure 4. 20. Structure-activity assay of CP against *E. coli*. *E. coli* ATCC 25922 cultures (1×10^5 CFU/mL) were incubated with $40 \mu\text{M}$ CP for 3 h at 37°C with shaking at 150 rpm. Cultures were plated on TSB/agar plates, allowed to incubate for 12 h at 37°C , and colonies counted for CFU determination. Buffer: 10 mM MES pH 5.1, or 10 mM phosphate 7.4 + 1% TSB. (mean \pm 95% CI, $n = 3$).

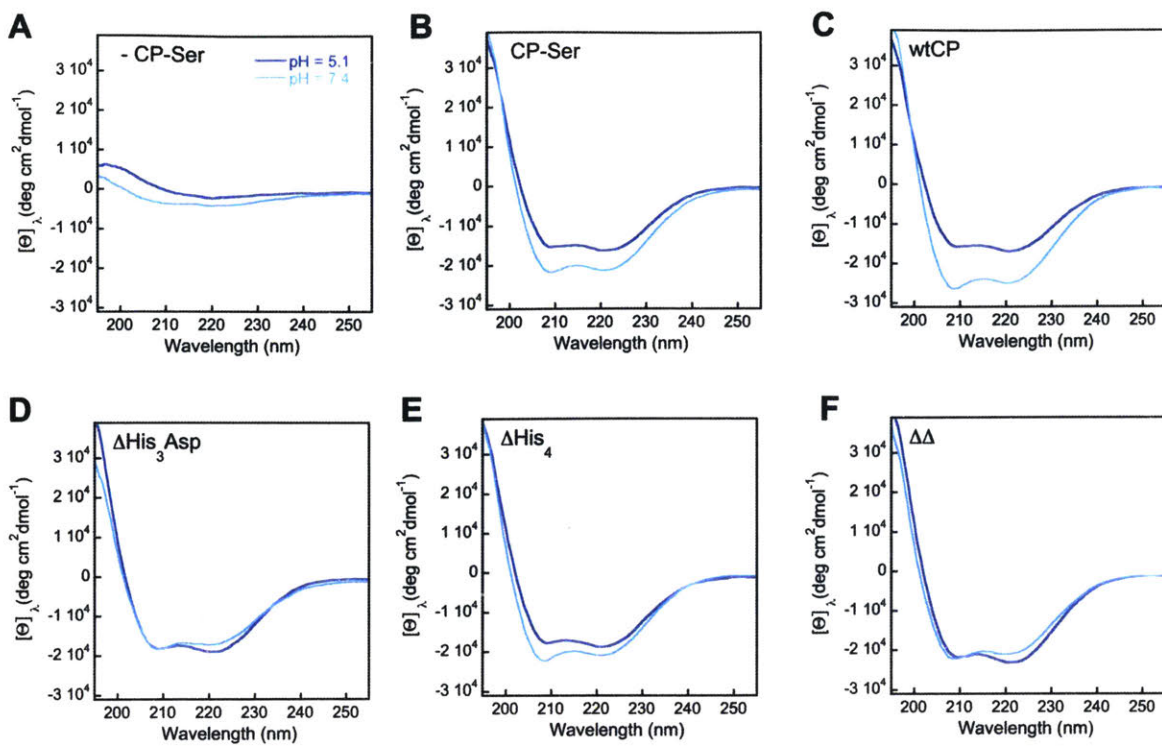


Figure 4. 21. Circular dichroism spectra of 10 μ M CP recovered from the culture supernatant of *E. coli* cells. (A) Untreated, (B) CP-Ser, (C) wtCP, (D) Δ His₃Asp, (E) Δ His₄, and (F) $\Delta\Delta$, at pH 5.1 (light blue) and 7.4 (dark blue). Buffer: 10 mM MES pH 5.1 + 1% TSB.

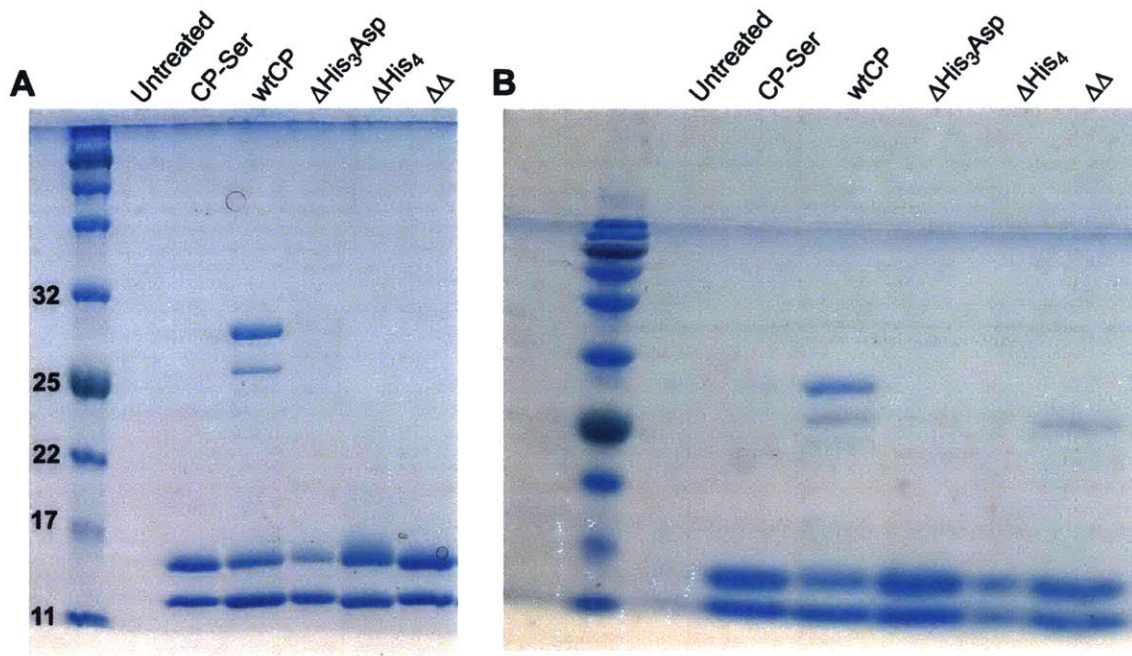


Figure 4. 22. SDS-PAGE (15% acrylamide Tris-HCl, glycine gel) of culture supernatant of CP-treated *E. coli*, visualized with Coomassie Blue at (A) pH 5.1, and (B) pH 7.4. A) The ladder is P7712S from New England BioLabs.

4. 4. Summary and Outlook

In this work, we build on prior work that documented the ability of CP to physically associate with microbial cell surfaces.^{28,30-32,64-66} We evaluate the bactericidal properties of CP, and show that CP functions as an AMP under a set of specific conditions, which include acidic pH and low divalent metal levels. We initiated phase-contrast and fluorescence microscopy studies to image the cell morphology phenotypes caused by CP, which include cell surface roughness, distortion, and protrusion, as well as cell lysis. These phenotypes have been observed for other AMPs, and indicate that CP compromises the cell membrane architecture of *E. coli*. It remains unclear which specific compartments are affected by CP treatment, as well as what the cellular target of CP is. The Live-Dead staining showed that CP compromises the cell membrane of *E. coli* cells, and fluorescence imaging studies demonstrated that CP affects the periplasmic integrity of *E. coli* cells, as evidenced by the diffusion of periplasmic GFP. However, the pore-forming

ability of CP did not correlate with direct killing as measured by CFU count, and it is possible that CP forms transient pores. Alternatively, CP can also interact reversibly with porins, as it was shown for lactoferrin.⁷¹

The bactericidal activity of CP was demonstrated towards a number of Gram-negative bacterial strains, whereas Gram-positive strains were not affected by CP treatment. The underlying molecular details for this interaction are currently unclear, and we speculate that it is mediated by electrostatic interactions between CP and the negatively-charged LPS moieties found on the outer-membrane of Gram-negative strains, or other cell surface lipoproteins. At present, it is not clear whether differences in LPS types play an important role in modulating the bactericidal properties of CP. The outer-membrane of *E. coli* ATCC 25922 and *E. coli* K12 are composed of smooth and rough LPS respectively. Therefore, it will be informative to examine how the MICs of CP for these two strains compare.

Furthermore, we provide initial results looking at structure-function relationship of CP and show that despite the fact that the bactericidal activity of CP does not result from its metal-sequestering properties, the presence of the transition the metal-binding sites in CP are important contributors to its function as an AMP. We noted that wtCP displays pH-independent activity, implicating the Cys residues in the function of CP as an AMP. Our preliminary results with wtCP and the documented importance that Cys residues play in modulating in AMP activity serve as a motivation for exploring the bactericidal properties of wtCP.^{5,44,72-75} The presence of disulfide bridges is essential for the antimicrobial functions of human defensin 5 and human defensin 6, as they confer secondary structure to the peptides and allow for proper electrostatic interactions between the peptide and bacterial cell membrane, or within the peptide itself.^{5,44,72-74} Lactoferricin B is a proteolytic fragment of lactoferrin that contains a loop region held together by a disulfide bridge. The presence of a loop within this peptide was found to be important in the antimicrobial activity of this peptide, by conferring rigidity and stability to the peptide, as observed for cyclic peptides.⁷⁶

CP is a Ca(II)-binding protein and its antimicrobial function in the extracellular space is well established. The metal-sequestering properties of CP are modulated by extracellular Ca(II) levels, and CP exhibits enhanced antimicrobial activity in the presence of excess Ca(II).^{13,77-79} In this work, we reported that excess Ca(II) attenuates the *E. coli*-cidal properties of CP, suggesting that the bactericidal properties of CP is likely not physiologically pertinent in the extracellular space. The intracellular functions of CP are not well understood and are connected to aspects of Ca(II) homeostasis, cell differentiation and regulation, and energy metabolism.⁸⁰⁻⁸¹ Within an intracellular context where Ca(II) levels are low, it is possible that CP can function as an AMP upon invasion by intracellular pathogens, or during phagocytosis of pathogens when the conditions are acidic.⁸²⁻⁸³ Intracellular pathogens have evolved elaborate ways to evade the host defense and detection mechanisms,⁸⁴ and the validity of this model needed to be tested. Therefore, an evaluation of the bactericidal activity of CP against canonical intracellular pathogens such as *Shigella* and *Salmonella* spp. will be informative.

In closing, we propose that the antimicrobial function of the human host-defense protein calprotectin is multifaceted, and modulated by environmental and chemical factors such as pH, NaCl and Ca(II) concentrations. The multifunctionality of antimicrobial HDPs has been reported for other metal-sequestering proteins, such as lactoferrin,^{5,24,71,75-76,85-86} and we noted numerous similarities between the AMP functions of CP and lactoferrin. For example, both proteins display enhanced bactericidal properties at acidic pH, both are resistant to high NaCl concentrations, and both are most active in the apo state. Remarkably, lactoferrin interacts with the lipid A region of LPS, and we speculate that a similar interaction is relevant to the function of CP as an AMP.

4. 5. Acknowledgements

We thank Dr. Wendy Salmon of the Whitehead Institute for Biomedical Research for help with the microscopy studies, and Dr. Phoom Chairatana for insightful discussions. We also thank Miss Eleane Lema for technical assistance with the assays presented in Figure 4. 20.

4. 6. References

1. Michalek, M.; Gelhaus, C.; Hecht, O.; Podschun, R.; Schroder, J. M.; Leippe, M.; Grotzinger, J., The human antimicrobial protein psoriasin acts by permeabilization of bacterial membranes. *Dev. Comp. Immunol.* **2009**, *33* (6), 740-746.
2. Jenssen, H.; Hamill, P.; Hancock, R. E. W., Peptide antimicrobial agents. *Clin. Microbiol. Rev.* **2006**, *19*, 491-511.
3. Nijnik, A.; Hancock, R. E. W., Host defence peptides: antimicrobial and immunomodulatory activity and potential applications for tackling antibiotic-resistant infections. *Emerg. Health. Threats* **2009**, *2*, e1.
4. Lai, Y.; Hancock, R. E. W., AMPed up immunity: how antimicrobial peptides have multiple roles in immune defense. *Trends Immunol.* **2009**, *30*, 131-141.
5. Wiesner, J.; Vilcinskas, A., Antimicrobial peptides: The ancient arm of the human immune system. *Virulence* **2010**, *1* (5), 440-464.
6. Hancock, R. E. W., Cationic peptides: effectors in innate immunity and novel antimicrobials. *Infect. Dis.* **2001**, *1* (3), 156-164.
7. Wilkinson, M. M.; Busuttil, A.; Hayward, C.; Brock, D. J. H.; Dorin, J. R.; Van Heyningen, V., Expression pattern of two cystic fibrosis-associated calcium-binding proteins in normal and abnormal tissues. *J. Cell Sci.* **1988**, *91*, 221-230.
8. Steinbakk, M.; Naess-Andresen, C.-F.; Fagerhol, M. K.; Lingaas, E.; Dale, I.; Brandtzaeg, P., Antimicrobial actions of calcium binding leukocyte L1 protein, caprotectin. *Lancet* **1990**, *336*, 763-765.
9. Teigelkamp, S.; Bharwaj, R. S.; Roth, J.; Meinardus-Harger, G.; Karas, M. S., C., Calcium-dependent complex assembly of the myeloid differentiation proteins MRP-8 and MRP-14. *J. Biol. Chem.* **1991**, *266* (20), 13462-13467.
10. Dale, I.; Brandtzaeg, P.; Fagerhol, M. K.; Scott, H., Distribution of a new myelomonocytic antigen (L1) in human peripheral blood leukocytes: immunofluorescence and immunoperoxidase

staining features in comparison with lysozyme and lactoferrin. *Am. J. Clin. Pathol.* **1985**, *84*, 24-34.

11. Brandtzaeg, P.; Dale, I.; Fagerhol, M. K., Distribution of a formalin-resistant myelomonocytic antigen (L1) in human tissues *Am. J. Clin. Pathol.* **1987**, *87*, 681-699.

12. Williams, R. J. P., Calcium binding proteins in normal and transformed cells. *Cell Calcium* **1996**, *20* (1), 87-93.

13. Brophy, M. B.; Hayden, J. A.; Nolan, E. M., Calcium ion gradients modulate the zinc affinity and antibacterial activity of human calprotectin. *J. Am. Chem. Soc.* **2012**, *134* (43), 18089-18100.

14. Brophy, M. B.; Nakashige, T. G.; Gaillard, A.; Nolan, E. M., Contributions of the S100A9 C-terminal tail to high-affinity Mn(II) chelation by the host-defense protein human calprotectin. *J. Am. Chem. Soc.* **2013**, *135* (47), 17804-17817.

15. Hayden, J. A.; Brophy, M. B.; Cunden, L. S.; Nolan, E. M., High-affinity manganese coordination by human calprotectin is calcium-dependent and requires the histidine-rich site formed at the dimer interface. *J. Am. Chem. Soc.* **2013**, *135* (2), 775-787.

16. Nakashige, T. G.; Zhang, B.; Krebs, C.; Nolan, E. M., Human calprotectin is an iron-sequestering host-defense protein. *Nat. Chem. Biol.* **2015**, *11* (10), 765-771.

17. Gagnon, D. M.; Brophy, M. B.; Bowman, S. E.; Stich, T. A.; Drennan, C. L.; Britt, R. D.; Nolan, E. M., Manganese binding properties of human calprotectin under conditions of high and low calcium: X-ray crystallographic and advanced electron paramagnetic resonance spectroscopic analysis. *J. Am. Chem. Soc.* **2015**, *137* (8), 3004-3016.

18. Nakashige, T. G.; Stephan, J. R.; Cunden, L. S.; Brophy, M. B.; Wommack, A. J.; Keegan, B. C.; Shearer, J. M.; Nolan, E. M., The hexahistidine motif of host-defense protein human calprotectin contributes to zinc withholding and its functional versatility. *J. Am. Chem. Soc.* **2016**, *138* (37), 12243-12251.

19. Nakashige, T. G.; Zygiel, E. M.; Drennan, C. L.; Nolan, E. M., Nickel sequestration by the host-defense protein human calprotectin. *J. Am. Chem. Soc.* **2017**, *139* (26), 8828-8836.

20. Zygiel, E. M.; Nolan, E. M., Transition metal sequestration by the host-defense protein calprotectin. *Ann. Rev. Biochem.* **2018**, *87*, 621-643.
21. Besold, A. N.; Gilston, B. A.; Radin, J. N.; Ramsoomair, C.; Culbertson, E. M.; Li, C. X.; Cormack, B. P.; Chazin, W. J.; Kehl-Fie, T. E.; Culotta, V. C., The role of calprotectin in withholding zinc and copper from *Candida albicans*. *Infect. Immun.* **2017**, *86* (2), e00779-17.
22. Damo, S. M.; Kehl-Fie, T. E.; Sugitani, N.; Holt, M. E.; Rathi, S.; Murphy, W. J.; Zhang, Y.; Betz, C.; Hench, L.; Fritz, G.; Skaar, E. P.; Chazin, W. J., Molecular basis for manganese sequestration by calprotectin and roles in the innate immune response to invading bacterial pathogens. *Proc. Natl. Acad. Sci. U. S. A.* **2013**, *110* (10), 3841-3846.
23. Corbin, B. D.; Seeley, E. H.; Raab, A.; Feldmann, J.; Miller, M. R.; Torres, V. J.; Anderson, K. L.; Dattilo, B. M.; Dunman, P. M.; Gerads, R.; Caprioli, R. M.; Nacken, W.; Chazin, W. J.; Skaar, E. P., Metal chelation and inhibition of bacterial growth in tissue abscesses. *Science* **2008**, *319* (5865), 962-965.
24. Weinberg, E. D., Nutritional immunity: Host's attempt to withhold iron from microbial invaders. *J. Am. Med. Assoc.* **1975**, *231* (1), 39-41.
25. Hood, M. I.; Skaar, E. P., Nutritional immunity: transition metals at the pathogen-host interface. *Nat. Rev. Microbiol.* **2012**, *10* (8), 525-537.
26. Zackular, J. P.; Chazin, W. J.; Skaar, E. P., Nutritional immunity: S100 proteins at the host-pathogen interface. *J. Biol. Chem.* **2015**, *290* (31), 18991-18998.
27. McNamara, M. P.; Wiessner, J. H.; Collins-Lech, C.; Hahn, B. L.; Sohnle, P. G., Neutrophil death as a defence mechanism against *Candida albicans* infection. *Lancet* **1988**, *336*, 763-763.
28. Edgeworth, J. D.; Abiose, A.; Jones, B. R., An immunohistochemical analysis of onchocercal nodules: evidence for an interaction between macrophage MRP8/MRP14 and adult *Clin. Exp. Immunol.* **1993**, *92*, 84-92.

29. Basika, T.; Muñoz, N.; Casaravilla, C.; Irigoín, F.; Batthyány, C.; Bonilla, M.; Salinas, G.; Pacheco, J. P.; Roth, J.; Durán, R.; Díaz, A., Phagocyte-specific S100 proteins in the local response to the *Echinococcus granulosus* larva. *Parasitology* **2012**, *139*, 271-283.
30. Akerström, B.; Bjorck, L., Bacterial surface protein L binds and inactivates neutrophil proteins S100A8/A9. *J. Immunol.* **2009**, (183), 4583-4592.
31. Stork, M.; Grijpstra, J.; Bos, M. P.; Torres, C. M.; Devos, N.; Poolman, J. T.; Chazin, W. J.; Tommassen, J., Zinc piracy as a mechanism of *Neisseria meningitidis* for evasion of nutritional immunity. *PLoS Pathog.* **2013**, *9* (10), e1003733.
32. Besold, A. N.; Culbertson, E. M.; Nama, L.; Hobbs, R. P.; Boyko, A.; Maxwell, C. N.; Chazin, W. J.; Marques, A. R.; Culotta, A. C., Antimicrobial action of calprotectin that does not involve metal withholding. *Metalomics* **2018**, 10.1039/c8mt00133b.
33. Gläser, R.; Harder, J.; Lange, H.; Bartels, J.; Christophers, E.; Schröder, J. M., Antimicrobial psoriasin (S100A7) protects human skin from *Escherichia coli* infection. *Nat. Immunol.* **2005**, *6* (1), 57-64.
34. Meyer, J. E.; Harder, J.; Sipos, B.; Maune, S.; Klöppel, G.; Bartels, J.; Schröder, J. M.; Gläser, R., Psoriasin (S100A7) is a principal antimicrobial peptide of the human tongue. *Mucosal Immunol.* **2008**, *1* (3), 239-243.
35. Mildner, M.; Stichenwirth, M.; Abtin, A.; Eckhart, L.; Sam, C.; Gläser, R.; Schröder, J. M.; Gmeiner, R.; Mlitz, V.; Pammer, J.; Geusau, A.; Tschachler, E., Psoriasin (S100A7) is a major antimicrobial component of the female genital tract. *Mucosal Immunol.* **2010**, *127*, 602-609.
36. Hadley, R. C.; Gagnon, D. M.; Brophy, M. B.; Gu, Y.; Nakashige, T. G.; Britt, R. D.; Nolan, E. M., Biochemical and spectroscopic observation of Mn(II) sequestration from bacterial Mn(II) transport machinery by calprotectin. *J. Am. Chem. Soc.* **2018**, *140*, 110-113.
37. Lakowicz, J. R., Principles of fluorescence spectroscopy. **1999**.
38. Steinberg, D. A.; Lehrer, R. I., Designer assays for antimicrobial peptides. Disputing the "one-size-fits-all" theory. *Methods. Mol. Biol.* **1997**, *78*, 169-186.

39. Gregory, T. M.; Moreno, E. C.; Patel, J. M.; Brown, W. E., Solubility of β - $\text{Ca}_3(\text{PO}_4)_2$ in the system $\text{Ca}(\text{OH})_2$ - H_3PO_4 - H_2O at 5, 15, 25, and 37 °C, *J. Res. Natl. Bur. Stand* **1974**, *78* (A), 667-674.
40. Ranjit, D. K.; Young, K. D., The rcc stress response and accessory envelope proteins are required to *de novo* generation of cell shape in *Escherichia coli*. *J. Bacteriol.* **2013**, *195*, 2452-2462.
41. Billings, N.; Millan, M. R.; Caldara, M.; Rusconi, R.; Tarasova, Y.; Stocker, R.; Ribbeck, K., The extracellular matrix component Psl provides fast acting antibiotic defense in *Pseudomonas aeruginosa* biofilms. *PLoS Pathog.* **2013**, *9*, e1003526.
42. Error bars. *Nat. Methods* **2013**, *10*, 921-922.
43. Significance, P values and *t*-tests. *Nat. Methods* **2013**, *10*, 1041-1042.
44. Chileveru, H. R.; Lim, S. A.; Chairatana, P.; Nolan, E. M., Visualizing attack of *Escherichia coli* by the antimicrobial peptide Human Defensin 5. *Biochemistry* **2015**, *54*, 1767-1777.
45. Lee, H.; Cho, Y.; I., L. R., Effects of pH and salinity on the antimicrobial properties of clavanins. *Infect. Immun.* **1997**, *65* (7), 2898-2903.
46. Juliano, S. A.; Pierce, S.; deMayo, J. A.; Balunas, M. J.; Angeles-Boza, A. M., Exploration of the innate immune system of *Styela clava*: Zn^{2+} binding enhances the antimicrobial activity of the tunicate peptide clavanin A. *Biochemistry* **2017**, *56*, 1403-1414.
47. Schneider, V. A. F.; Coorens, M.; Ordonez, S. R.; Tjeerdsma-van Bokhoven, J. L. M.; Posthuma, G.; van Dijk, A.; Haagsman, H. P.; Veldhuizen, E. J. A., Imaging the antimicrobial mechanism(s) of cathelicidin-2. *Sci. Rep.* **2016**, *6* (1), 1-11.
48. Schitteck, B.; Hipfel, R.; Sauer, B.; Bauer, J.; Kalbacher, H.; Stevanovic, S.; Schirle, M.; Schroeder, K.; Blin, N.; Meier, F.; Rassner, G.; Garbe, G., Dermcidin: a novel human antibiotic peptide secreted by sweat glands. *Nat. Immunol.* **2001**, *2*, 1133-1137.

49. Stephan, J. R.; Nolan, E. M., Calcium-induced tetramerization and zinc chelation shield human calprotectin from degradation by host and bacterial extracellular proteases. *Chem. Sci.* **2016**, 7 (3), 1962-1975.
50. McDevitt, C. A.; Ogunniyi, A. D.; Valkov, E.; Lawrence, M. C.; Kobe, B.; McEwan, A. G.; Paton, J. C., A molecular mechanism for bacterial susceptibility to Zinc. *PLoS Pathog.* **2011**, 7 (11), e1002357.
51. Epand, R. M.; Walker, C.; Epand, R. F.; Magarvey, N. A., Molecular mechanisms of membrane targeting antibiotics. *Biochim. Biophys. Acta* **2016**, 1858, 980-987.
52. Bindman, N. A.; van der Donk, W. A., A general method for fluorescent labeling of the N-termini of lanthipeptides and its application to visualize their cellular location. *J. Am. Chem. Soc.* **2013**, 135, 10362-10371.
53. Brogden, K. A., Antimicrobial peptides: pore formers or metabolic inhibitors in bacteria? *Nat. Rev. Microbiol.* **2005**, 3, 238-250.
54. Frantz, J.; Elezgaray, J.; Berson, P.; Vacher, P.; Dufourc, E. J., Pore formation induced by an antimicrobial peptide: electrostatic effects. *Biophys. J.* **2008**, 95 (12), 5748-5756.
55. Park, C. B.; Kim, H. S.; Kim, S. C., Mechanism of action of the antimicrobial peptide buforin II: buforin II kills microorganisms by penetrating the cell membrane and inhibiting cellular functions. *Biochem. Biophys. Res. Commun.* **1998**, 244 (1), 253-257.
56. Li, L.; Shi, Y.; Cheng, X.; Xia, S.; Cheserek, M. J.; Le, G., A cell-penetrating peptide analogue, P7, exerts antimicrobial activity against *Escherichia coli* ATCC 25922 via penetrating cell membrane and targeting intracellular DNA. *Food Chem.* **2015**, 166, 231-239.
57. Podda, E.; Benincasa, M.; Pacor, S.; Micali, F.; Mattiuzzo, M.; Gennaro, R.; Scocchi, M., Dual mode of action of Bac7, a proline-rich antibacterial peptide. *Biochim. Biophys. Acta* **2006**, 1760 (11), 1732-1740.
58. Sochacki, K. A.; Shkel, I. A.; Record, M. T.; Weisshaar, J. C., Protein diffusion in the periplasm of *E. coli* under osmotic stress. *Biophys. J.* **2011**, 100 (1), 22-32.

59. Rangarajan, N.; Bakshi, S.; Weisshaar, J. C., Localized permeabilization of *E. coli* membranes by the antimicrobial peptide cecropin A. *Biochemistry* **2013**, *52* (38), 6584-6495.
60. Choi, H.; Nambirajan, R.; Weisshaar, J. C., Lights, camera, action! Antimicrobial peptide mechanisms imaged in space and time. *Trends Microbiol.* **2016**, *24* (2), 111-122.
61. Yang, Z.; Choi, H.; Weisshaar, J. C., Melittin-induced permeabilization, re-sealing, and re-permeabilization of *E. coli* membranes. *Biophys. J.* **2018**, *114* (2), 368-379.
62. Ganz, T., Defensins. Natural peptide antibiotics of human neutrophils. *Nat. Rev. Immunol.* **2003**, *3*, 710-720.
63. Afacan, N. J.; Yeung, A. T. Y.; Pena, O. M.; Hancock, R. E. W., Therapeutic potential of host defense peptides in antibiotic-resistant infections. *Curr. Pharma. Design* **2012**, *18*, 807-819.
64. Marti, T.; Erttmann, K. D.; Gallin, M. Y., Host-parasite interaction in human onchocerciasis: identification and sequence analysis of a novel human calgranulin. *Biochem. Biophys. Res. Commun.* **1996**, *221* (2), 454-458.
65. Gottsch, J. D.; Eisinger, S. W.; Liu, S. H.; L., S. A., Calgranulin C has filariacidal and filariastatic activity. *Infect. Immun.* **1999**, *67* (12), 6631-6636.
66. Jean, S.; Juneau, R. A.; Criss, A. K.; Cornelissen, C. N., *Neisseria gonorrhoeae* evades calprotectin-mediated nutritional immunity and survives neutrophil extracellular traps by production of TdfH. *Infect. Immun.* **2016**, *84*, 2982-2994.
67. Martinez de Tejada, G.; Sánchez-Gómez, S.; Kowalski, I.; Kaconis, Y.; Andrä, J.; Schürholz, T.; Hornef, M.; Dupont, A.; Garidel, P.; Gutschmann, T.; David, S. A.; Brandenburg, K., Bacterial cell wall compounds as promising targets of antimicrobial agents I. Antimicrobial peptides and lipopolyamines. *Curr. Drug. Targets* **2012**, *13* (9), 1221-1130.
68. Papo, N.; Shai, Y., A molecular mechanism for lipopolysaccharide protection of Gram-negative bacteria from antimicrobial peptides. *J. Biol. Chem.* **2005**, *280*, 10378-10387.
69. Silhavy, T. J.; Kahne, D.; Walker, S., The bacterial cell envelope. *Cold Spring Harb. Perspect. Biol.* **2010**, *2*:a000414.

70. Brown, L.; Wolf, J. M.; Prados-Rosales, R.; Casadevall, A., Through the wall: extracellular vesicles in Gram-positive bacteria, mycobacteria and fungi. *Nat. Rev. Microbiol.* **2015**, *13*, 620-630.
71. Naidu, S. S.; Svensson, U.; Kishore, A. R.; Naidu, A. S., Relationship between antibacterial activity and porin binding of lactoferrin in *Escherichia coli* and *Salmonella typhimurium*. *Antimicrob. Agents. Chemother.* **1993**, *37* (2), 240-245.
72. Chu, H.; Pazgier, M.; Jung, G.; Nuccio, S.-P.; Castillo, P. A.; deJong, M. F.; Winter, M. G.; Winter, S. E.; Wehkamp, J.; Shen, B.; Salzman, N. H.; Underwood, M. A.; Tsois, R. M.; Young, G. M.; Lu, W.; Lehrer, R. I.; Baumler, A. J.; Bevins, C. L., Human α -defensin 6 promotes mucosal innate immunity through self-assembled peptide nanonets. *Science* **2012**, *337*, 477-481.
73. Zhang, Y. F.; Cougnon, F. B. L.; Wanniarachchi, Y. A.; Hayden, J. A.; Nolan, E. M., Reduction of human defensin 5 affords a high-affinity zinc-chelating peptide. *ACS Chem. Biol.* **2013**, *8*, 1907-1911.
74. Chairatana, P.; Nolan, E. M., Human α -Defensin 6: A small peptide that self-assembles and protects the host by entangling microbes. *Acc. Chem. Res.* **2017**, *50*, 960-967.
75. Bellamy, W.; Takase, M.; Yamauchi, K.; Wakabayashi, H.; Kawase, K.; Tomita, M., Identification of the bactericidal domain of lactoferrin. *Biochim. Biophys. Acta* **1992**, *1121*, 130-136.
76. Farnaud, S.; Evans, R. W., Lactoferrin - a multifunctional protein with antimicrobial properties. *Mol. Immunol.* **2003**, *40*, 395-405.
77. Cunden, L. S.; Gaillard, A.; Nolan, E. M., Calcium ions tune the zinc-sequestering properties and antimicrobial activity of human S100A12. *Chem. Sci.* **2016**, *7* (2), 1338-1348.
78. Cunden, L. S.; Brophy, M. B.; Rodriguez, G. E.; Flaxman, H. A.; Nolan, E. M., Biochemical and functional evaluation of the intramolecular disulfide bonds in the zinc-chelating antimicrobial protein human S100A7 (Psoriasin). *Biochemistry* **2017**, *56*, 5726-5738.

79. Cunden, L. S.; Nolan, E. M., Bioinorganic explorations of Zn(II) sequestration by human S100 host-defense proteins. *Biochemistry* **2018**, *57* (11), 1673-1680.
80. Donato, R.; Canon, B. R.; Sorci, G.; Riuzzi, F.; Hsu, K.; Weber, D. J.; Geczy, C. L., Functions of S100 proteins. *Curr. Mol. Med.* **2013**, *13*, 24-57.
81. Donato, R., Intracellular and extracellular roles of S100 proteins. *Microsc. Res. Tech.* **2003**, *60* (6), 540-541.
82. Styrt, B.; Klempner, M. S., Internal pH of human neutrophil lysosomes. *FEBS Lett.* **1982**, *149*, 113-116.
83. Reeves, E. M.; Lu, H.; Jacobs, H. L.; Messina, C. G. M.; Bolsover, S.; Gabella, G.; Potma, E. O.; Warley, A.; Roes, J.; Segal, A. W., Killing activity of neutrophils is mediated through activation of proteases by K⁺ flux. *Nature* **2002**, *416*, 291-297.
84. Pizarro-Cerda, J.; Cossart, P., Bacterial adhesion and entry into host cells. *Cell* **2006**, *124*, 715-727.
85. Saito, H.; Miyakawa, H.; Tamura, Y.; Shimamura, S.; Tomita, M., Potent bactericidal activity of bovine lactoferrin hydrolysate produced by heat treatment at acidic pH. *J. Dairy Sci.* **1991**, *74*, , 3724-3730.
86. Bellamy, W.; Takase, M.; Wakabayashi, H.; Kawase, K.; Tomita, M., Antibacterial spectrum of lactoferricin B, a potent bactericidal peptide derived from the N-terminal region of bovine lactoferrin. *J. Appl. Bacteriol.* **1992**, *73*, 472-479.

Chapter 5: Biochemical Investigation of the Bactericidal Properties of Four Human S100 Proteins: Calprotectin, S100A7, S100A15, and S100A12

5. 1. Introduction.

Antimicrobial peptides (AMPs), which are a subgroup of host-defense peptides (HDPs), are an evolutionarily conserved component of the innate immune response. They are found across all the classes of life and defend against invading bacteria, fungi, and viruses.¹⁻⁴ With the rise of hospital-acquired and multidrug resistant (MDRs) infections, peptide-based antibiotics are widely considered a potential answer to the growing problem of resistance to conventional antibiotics.⁵⁻⁷ As such, fundamental research on the chemistry and biology of these peptides can be used as a paradigm for the design of antibiotic analogues. Furthermore, increasing efforts must be devoted to elucidate host-defense systems, and membrane-protein interactions within the context of infectious diseases. Decades of intensive study have shown that the mechanisms by which AMPs kill specific microbes exhibit remarkable variety from peptide to peptide. Clear relationships between AMP structure and killing mechanisms have not yet emerged, and further investigations in their structure-function activities are needed.

AMPs act by rapidly inhibiting microbial proliferation within the host through metabolic or membrane disruption.⁸⁻⁹ Their synthesis and secretion can be constitutive or inducible by microbial products or pro-inflammatory cytokines, and the modes of action by which they kill microbes are varied and may differ for different bacterial species. AMPs can destabilize biological membranes,¹⁰ form transmembrane channels,¹¹ withhold essential nutrients from pathogens,¹²⁻¹³ and have the ability to enhance immunity by functioning as immunomodulators.¹⁴ Alternatively, AMPs can also penetrate into cells to interfere with DNA and RNA,¹⁵ target intracellular processes such as protein synthesis and folding,¹⁶ cell wall synthesis,¹⁷⁻¹⁸ and inhibit key metabolic enzymes.¹⁹

One of the commonly studied AMPs include the host-defense protein S100A7. S100A7 is part of the human S100 protein family of proteins, which includes 21 relatively small (≈ 10 kDa) α -helical Ca(II)-binding host-defense peptides,²⁰⁻²¹ including CP, S100A15, and S100A12. The

S100 proteins are found in the human host and play key roles in innate immunity. They are multifaceted, and at least two distinct mechanisms of action have been proposed to explain the antimicrobial activities of CP, S100A7, and S100A12. One involves metal-mediated growth inhibition, whereby the proteins are able to starve pathogen of essential metal nutrients, namely Mn, Fe, Cu, Ni, and Zn. This mode of action is a common theme observed amongst the S100 proteins and is often termed nutritional immunity.²²⁻³¹ This metal-mediated growth inhibitory mechanism is generally thought to be a bacteriostatic one that does not require a physical interaction between the protein and pathogen. The other mechanism of action is a microbicidal activity, resulting in direct killing of pathogens. The molecular details for this mode of action are currently unclear.

The S100 proteins are interesting candidates as potential AMPs due to their high helical character, overall cationic charge, relatively small size, and localization patterns (Figure 5.1).^{20,32-}
³³ A comparison of the structure of S100A7 (pI = 6.27) to its S100 counterparts, namely CP (pI = 6.11), S100A12 (pI = 5.81), and S100A15 (pI = 6.89) highlights noteworthy structural similarities. In the apo state, the four S100 proteins exist as homodimers, or as a heterodimer in the case of CP, of comparable sizes (21-24 kDa), with each dimer forming a stable four-helix domain with a hydrophobic core (Figure 5. 1). Each S100 polypeptide contains two EF-hand domains where the C-terminal EF-hand is described as “canonical” or “calmodulin-like” and the N-terminal EF-hand is described as “non-canonical.” A “canonical” EF-hand domain affords a heptadentate coordination sphere for Ca(II), whereas a “non-canonical” EF-hand binds Ca(II) with lower coordination number.²¹ Furthermore, each dimer exhibits two transition-metal-binding sites, distinct from the Ca(II)-binding sites. The transition-metal-binding sites form at the dimer interface and are composed of metal-binding residues from each subunit (Figure 5.1).

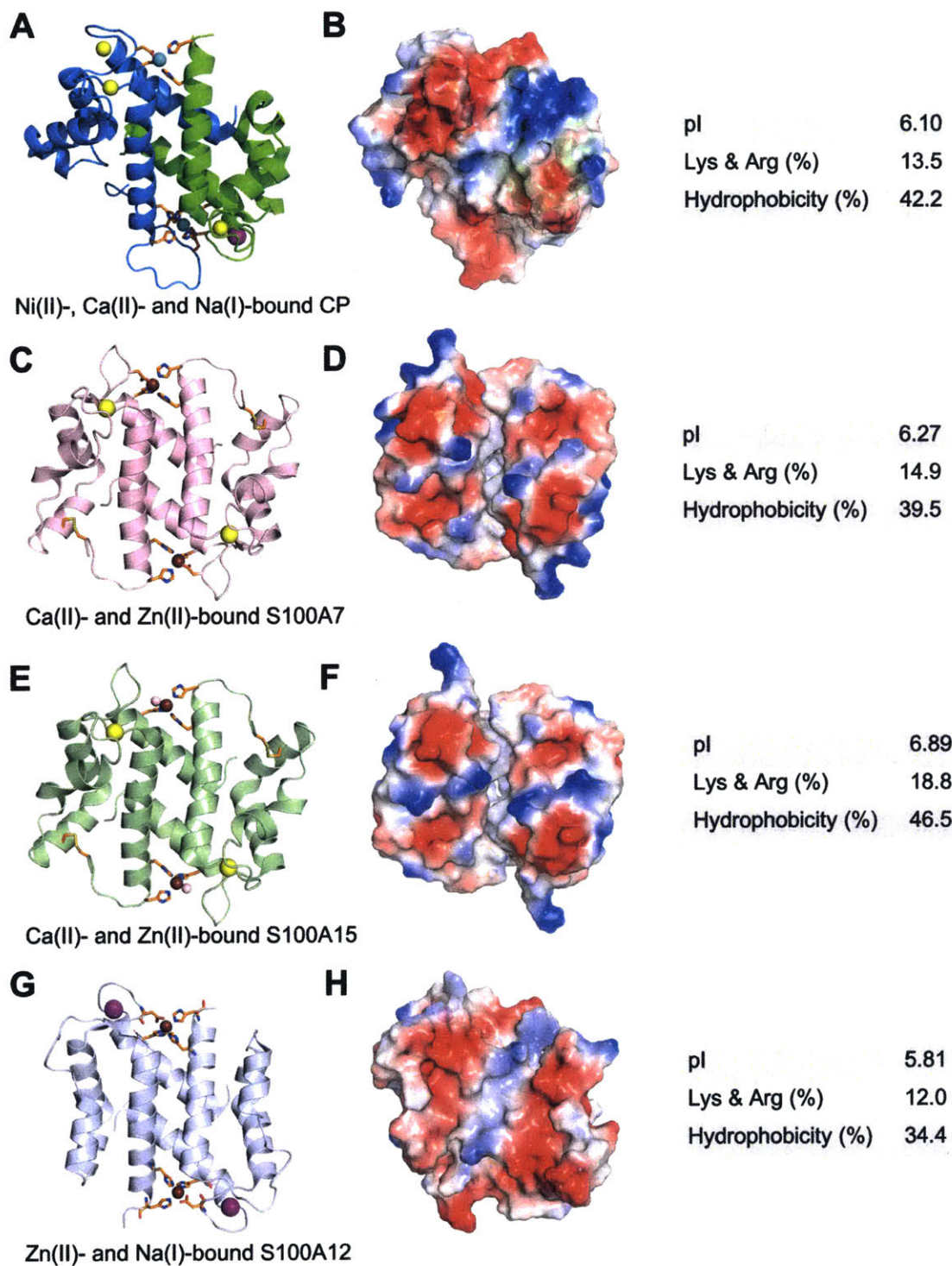


Figure 5. 1. Crystal structures and charge electrostatics of (A, B) CP (PDB 5W1F), (C, D) S100A7 (PDB 2PSR), (E, F) S100A15 (PDB 4AQL), and (G, H) S100A12 (PDB 2WC8). Electron potential maps are shown from -75 (red) to +73 (blue).

A few studies of CP and S100A12 have shown that the proteins are capable of physically interacting with the cell walls of microbes,³⁴⁻³⁸ while studies with S100A7 have established that it possesses membrane-permeabilizing properties.³⁹⁻⁴¹ Human S100A7 (psoriasin) was first isolated as an AMP from keratinocytes of psoriatic skin lesions in 1996,⁴²⁻⁴³ and is recognized as an antimicrobial factor of the skin as well as the human tongue, esophagus and female genital tract.^{39,41,44-45} Early studies of CP detected the protein associated with the cell surface of larva,³⁵ and CP and S100A12 have been shown to interact with the surface of adult *Onchocerca volvulus*.⁴⁶⁻⁴⁷ Furthermore, studies have documented the ability of CP to physically interact with the bacterial cell wall,⁴⁵ as well as cell wall-associated bacterial proteins,^{36-37,48} We recently studied the microbicidal properties of CP as described in Chapter 4, and demonstrated that CP possesses broad-spectrum bactericidal activity against Gram-negative bacteria, while it is generally less active or inactive against Gram-positive bacteria. The bactericidal activity was condition-specific; CP was found to be most active at acidic pH, and its activity is attenuated in the presence of high salinity, a behavior typical of AMPs.⁴⁹⁻⁵⁰ Fluorescence microscopy studies revealed that CP physically interacts with cell surface of *E. coli*, further supporting the notion that CP can affect the cell wall integrity of Gram-negative bacteria.

On the basis of studies with CP, S100A7 that implicate these proteins as having microbicidal functions, and motivated by the structural similarities between CP, S100A7, S100A15, and S100A12, we decided to (i) further probe the scope of the bactericidal activities of these four proteins, (ii) investigate the chemical and environmental factors that affect their antimicrobial properties, and (iii) employ microscopy studies to further understand the molecular basis of their activities. In the experiments presented below, we employ an experimental setup that involves broth microdilution assays slightly modified from an established protocol in order to study the bactericidal properties of the S100 proteins.⁵¹ This work is a systematic screen for the bactericidal properties of the S100 proteins and highlights similarities and differences between these HDPs . Throughout this study, we compare the activities of the S100 proteins to CP and other AMPs. As

a starting point, we screened the *E. coli*-cidal properties of the S100 proteins at varying salt, metal, and pH, factors that are pertinent to the physiological environments of the proteins. We found that the proteins were most active at acidic (pH 5.1) in the absence of added NaCl and Ca(II), against cultures in the mid-log phase. We therefore employ these conditions for all our solution studies, and microscopy studies. Furthermore, we employ microscopy to visualize protein-specific cell phenotypes, and probe the scope of the bactericidal activities of the proteins.

5. 2. Experimental Section

5. 2.1. Materials and General Methods

All solvents and chemicals were obtained from commercial suppliers and used as received. All aqueous solutions were prepared using Milli-Q water (18.2 M Ω •cm, 0.22- μ m filter). Protein concentrations were routinely quantified by using the calculated extinction coefficients as followed:

Table 5. 1. Protein extinction coefficient

Protein	Extinction coefficient* (M ⁻¹ cm ⁻¹) (per dimer)
CP (CP-Ser, calprotectin)	18, 450
S100A12	5960
S100A7 (S100A7 _{ox})	9190
S100A15 (S100A15 _{ox})	9190

*Calculated from ProtParam (ϵ_{280})

The S100A7 and S100A15 protein variants in this study are the oxidized forms of the proteins, with the Cys residues 47 and 96 forming an intramolecular disulfide bond within each monomer. We confirmed by HPLC that the proteins remained oxidized over the time course of the experiments presented in this chapter.

5. 2. 2. Purification of CP, S100A7, S100A15, and S100A12

The S100 proteins were prepared following the protocols listed below:

Table 5. 2. Purification protocols for S100 proteins

Protein	Reference
CP (CP-Ser, calprotectin)	52
S100A12	53
S100A7 and variants	54
S100A15 and variants	54

- The membrane permeabilization assays were carried out as reported in Section 4. 2. 5 of Chapter 4.
- The microscopy studies and analysis were carried out as reported in Sections 4. 2. 6 and 4. 2. 7 of Chapter 4
- The list of bacterial strains employed and the conditions used for growth are listed in Table 4. 3 of Chapter 4.
- For the broth microdilution assays, the protein of interest (POI) was used at a final concentration of 1000 µg/mL (40 µM for CP, S100A7, S100A15, and 44 µM for S100A12).
- For the microscopy experiments, the protein of interest (POI) was used at final concentration of 100 µM.

5. 3. Results and Discussion

Our solution and microscopy studies revealed that CP and S100A7 were most potent, followed by S100A15. S100A12 was negligibly active under any of the conditions tested. We therefore focus our discussion on CP, S100A7, and S100A15.

5. 3. 1. The *E. coli*-cidal Activity of the S100 Proteins are pH-Dependent

As a first step, we decided to test the bactericidal activities of the four S100 proteins, CP, S100A7, S100A15, and S100A12 over pH values ranging from 5.1 to 7.4. Based on the studies carried out with S100A7, we speculated that the S100 proteins would be generally more active at acidic pH, and our data agree (Figure 5. 2). Additionally, in Chapter 4, we showed that CP displays a pH-dependent activity where the protein becomes more potent under acidic conditions. Upon incubation with 1000 $\mu\text{g/mL}$ of the protein at acidic pH, we observed complete bacterial killing with CP and S100A7, significant cell killing with S100A15, and no killing with S100A12 (Figure 5. 2). As the pH of the buffer was increased, the activities of the CP, S100A7, and S100A15 were attenuated. At pH of 7.4, CP and S100A7 were moderately bactericidal, while S100A15 was almost inactive. The pH-dependent bactericidal activities of CP, S100A7, and S100A15 are consistent with the studies on the antimicrobial activity of clavanins against *E. coli* ML-35p.⁵⁰ Clavanins are a class of His-rich amidated α -helical AMPs originally isolated from leukocytes the tunicate, *Styela clava*. *In vitro* assays have shown that clavanins are generally more active under acidic conditions.^{2,10,13,40,50} Furthermore, the MICs (minimal inhibitory concentration) of CP, S100A7, and S100A15 are in the micromolar range and comparable to other AMPs,^{10,13,17} suggesting that the proteins may function as AMPs in a physiological milieu. Since we observed the most significant difference in the activities of the proteins at pH 5.1 and 7.4, we decided to carry out future screening tests probing the effects of salt and Ca(II) concentrations at these two pH values.

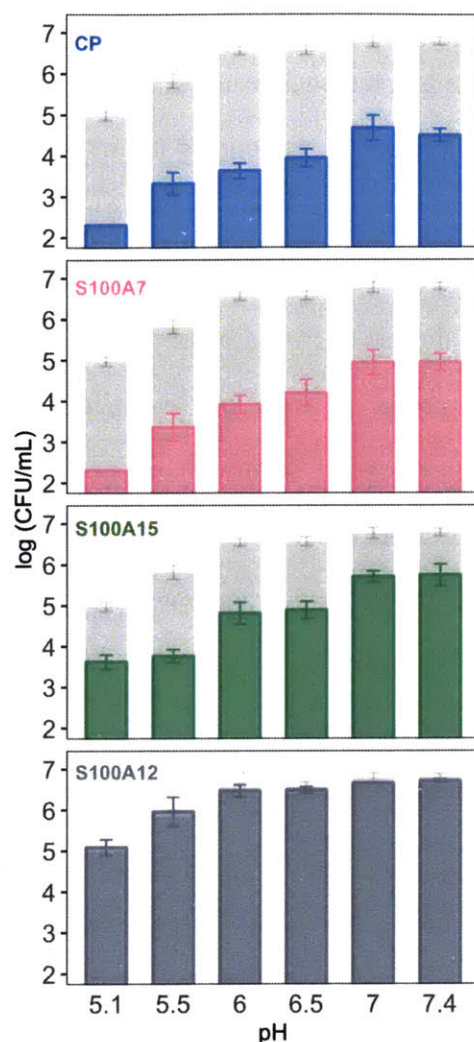


Figure 5. 2. Effects of pH on the *E. coli*-cidal activity of the S100 proteins. *E. coli* ATCC 25922 cultures (1×10^5 CFU/mL) were incubated with 1000 μ g/mL of CP (blue), or S100A7 (pink), or S100A15 (green), or S100A12 (grey) for 3 h at 37 °C with shaking at 150 rpm. Cultures were plated on TSB/agar plates, allowed to incubate for 12-14 h at 37 °C, and colonies counted for CFU determination. Buffer: 10 mM MES pH 5.1, 5.5, 6.0 + 1% TSB, or 10 mM phosphate pH 6.5, 7.0, 7.4 + 1% TSB. The untreated cultures are shown in light grey. (mean \pm 95% CI, $n = 3$).

5. 3. 2. The *E. coli*-cidal Activity of S100 Proteins are Concentration-Dependent

Next, we investigated how the bactericidal properties of the proteins vary as a function of their concentration. We expected that these results would allow us to compare the activities of the S100 proteins relative to one another. Indeed, all of the S100 proteins, except for S100A12,

displayed concentration-dependent bactericidal activities and enhanced activity at acidic pH under all concentrations tested (Figure 5. 3). CP was the most potent protein, exhibiting 100% killing at pH 5.1 at concentrations of 125 $\mu\text{g}/\text{mL}$ and higher. S100A7 and S100A15 exhibited 100% and 60% killing respectively at 1000 $\mu\text{g}/\text{mL}$ under acidic conditions (Figure 5. 3). At 1000 $\mu\text{g}/\text{mL}$ of protein, we were able to detect differences in the protein activities relative to one another, and therefore decided to employ this protein concentration value in our next assays.

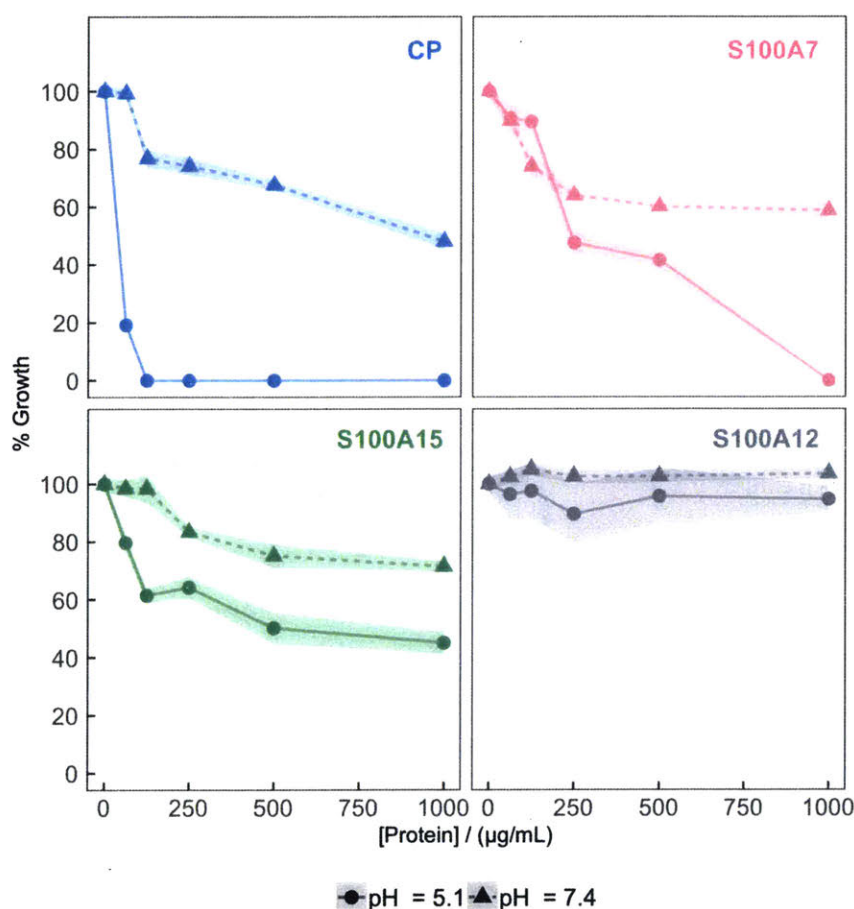


Figure 5. 3. Effects of protein concentration on the activity of the S100 proteins. *E. coli* ATCC 25922 cultures (1×10^5 CFU/mL) were incubated with 0–1000 $\mu\text{g}/\text{mL}$ of CP (blue), or S100A7 (pink), or S100A15 (green), or S100A12 (grey) for 3 h at 37 $^{\circ}\text{C}$, with shaking at 150 rpm. Cultures were plated on TSB/agar plates, allowed to incubate for 12–14 h at 37 $^{\circ}\text{C}$, and colonies counted for CFU determination. Buffer: 10 mM MES pH 5.1, or 10 mM phosphate 7.4 + 1% TSB. Errors are displayed as shaded regions and show 95% CI of the mean ($n = 3$).

5. 3. 3. Ionic Strength and Salinity Affect the *E. coli*-cidal Activities of S100 Proteins

Prior work by others showed that S100A7 retains its bactericidal activity at high NaCl levels,³⁹ and we reported a similar behavior with CP in Chapter 4. To further examine the notion that resistance to high salt is an inherent property of the S100 proteins, we tested the activities of the S100 proteins against a range of NaCl concentrations from 0 to 150 mM. CP retained full activity in the presence of 50 mM NaCl; S100A7 displayed a gradual loss in activity, and remained moderately active in the presence of up to 100 mM of NaCl, consistent with previously published studies;³⁹ S100A15 exhibited a salt-dependent behavior similar to S100A7, whereas S100A12 was inactive under all the conditions tested (Figure 5. 4). These results are noteworthy as they suggest that the proteins are active at salt concentrations present in sweat, which are in the range between 18 and 60 mM.⁵⁹ Increasing the NaCl levels did not significantly affect the activities of CP, S100A7, and S100A15 at pH 7.4 (Figure 5. 4).

The S100 proteins are Ca(II)-binding proteins and their functions are pertinent to their local Ca(II) concentrations. For instance, when found in the intracellular space, Ca(II) levels are relatively low, in the sub-micromolar range. Once the S100 proteins are secreted into the extracellular space, they experience Ca(II) concentrations that are orders of magnitude higher.⁶⁰ Therefore, we decided to investigate the effect of Ca(II) supplementation on the bactericidal activities of the proteins. We previously reported that at acidic pH, excess Ca(II) weakens the *E. coli*-cidal activity of CP (Chapter 4). Indeed, there was a significant reduction in the activity of CP in the presence of 50 μ M Ca(II), after which its activity did not diminish further (Figure 5. 5). We observed similar trends as CP for S100A7 and S100A15, under acidic conditions (Figure 5. 5). Interestingly, the degree of attenuation for S100A7 and S100A15 was lower than CP; S100A7 and S100A15 both retained full activity when incubated with up to 50 and 100 μ M of Ca(II) respectively (Figure 5. 5).

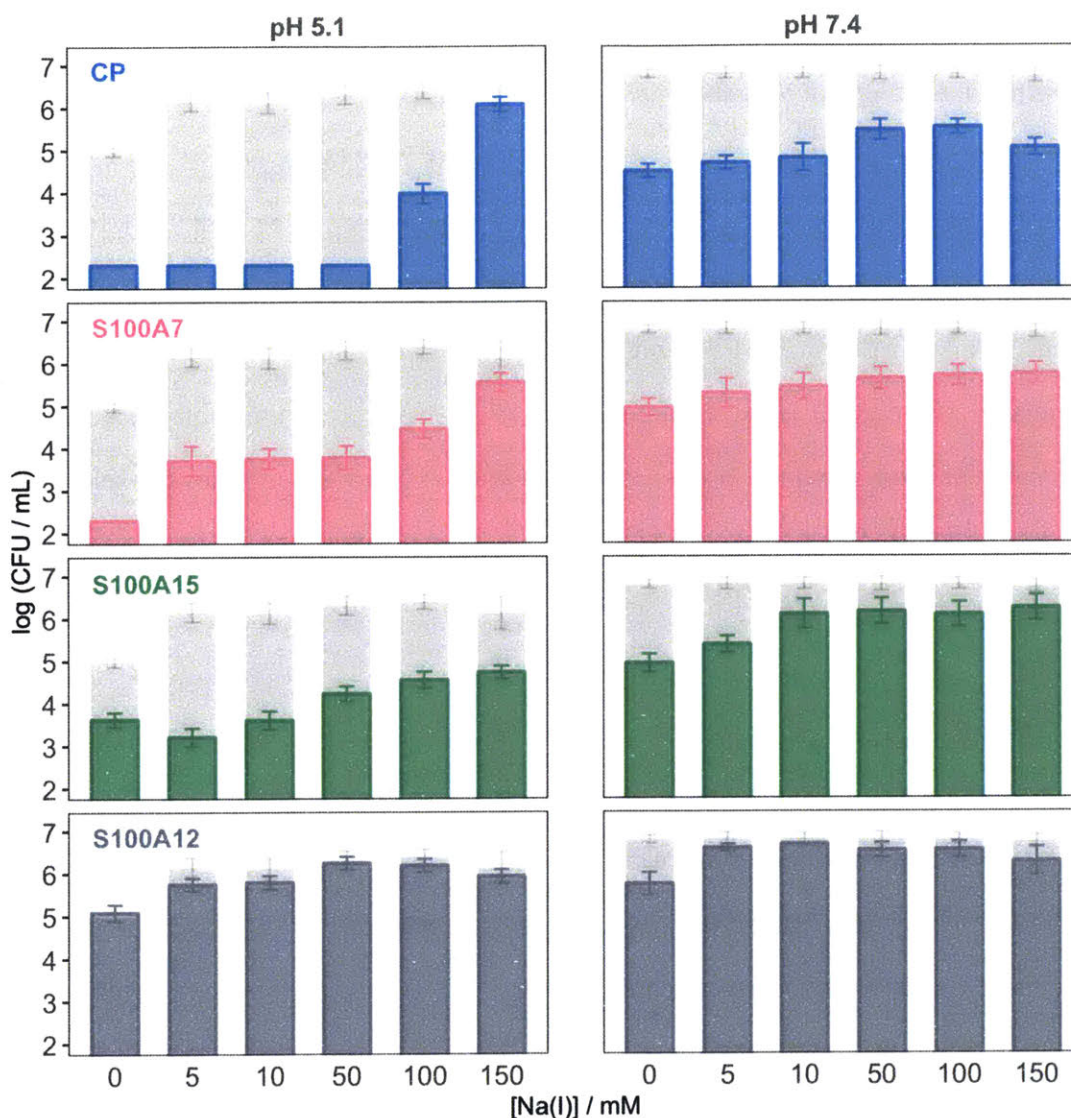


Figure 5. 4. Effects of NaCl concentration on the *E. coli*-cidal activity of the S100 proteins. *E. coli* ATCC 25922 cultures (1×10^5 CFU/mL) were incubated with 1000 μ g/mL of CP (blue), or S100A7 (pink), or S100A15 (green), or S100A12 (grey) for 3 h at 37 °C with shaking at 150 rpm. Cultures were plated on TSB/agar plates, allowed to incubate for 12-14 h at 37 °C, and colonies counted for CFU determination. Buffer: 10 mM MES pH 5.1 + 1% TSB, or 10 mM phosphate pH 7.4 + 1% TSB. The untreated cultures are shown in light grey. (mean \pm 95% CI, $n = 3$).

The results obtained from the Ca(II) titrations point to differences in the Ca(II)-binding properties of S100A7 and S100A15 compared to CP. Along those lines, the N-terminal EF-hand domains of S100A7 and S100A15 are particularly noteworthy because their loop region is three residues shorter when compared to those of S100A8, S100A9, and S100A12. In addition, they

contain a Ser residue at position 30,^{54,56,61} whereas at this position, the other S100 proteins have a Glu/Asp residue, which is a bidentate ligand that binds Ca(II) at the N-terminal EF-hand.⁶¹ These structural features suggest that the N-terminal EF-hands of S100A7 and S100A15 may be defective in Ca(II) binding. Hence, it is possible that the attenuated effect that Ca(II) has on the activities of S100A7 and S100A15 is due to their lower affinities for Ca(II) as a result of their non-functional or defective N-terminal EF-hands. Alternatively, Ca(II) supplementation may neutralize the negatively charged *E. coli* cell membrane and disfavor protein-membrane electrostatic interactions, thus weakening the killing activities of the S100 proteins. The latter explanation is unlikely since addition of NaCl, which presumably has a similar effect as Ca(II) on the cell surface charge, did not affect the activities of the S100 proteins at concentrations as high as 50 mM (Figure 5. 4).

Different from the trends observed under acidic conditions, addition of Ca(II) had no apparent effect on the activities of the S100 proteins at neutral pH (Figure 5. 5). The origins of this discrepancy are not clear, and similarly to what we proposed with CP in Chapter 4, it is possible that the proteins undergo distinct structural changes upon Ca(II) binding at pH 5.1 and 7.4 that affect their killing activities differently.

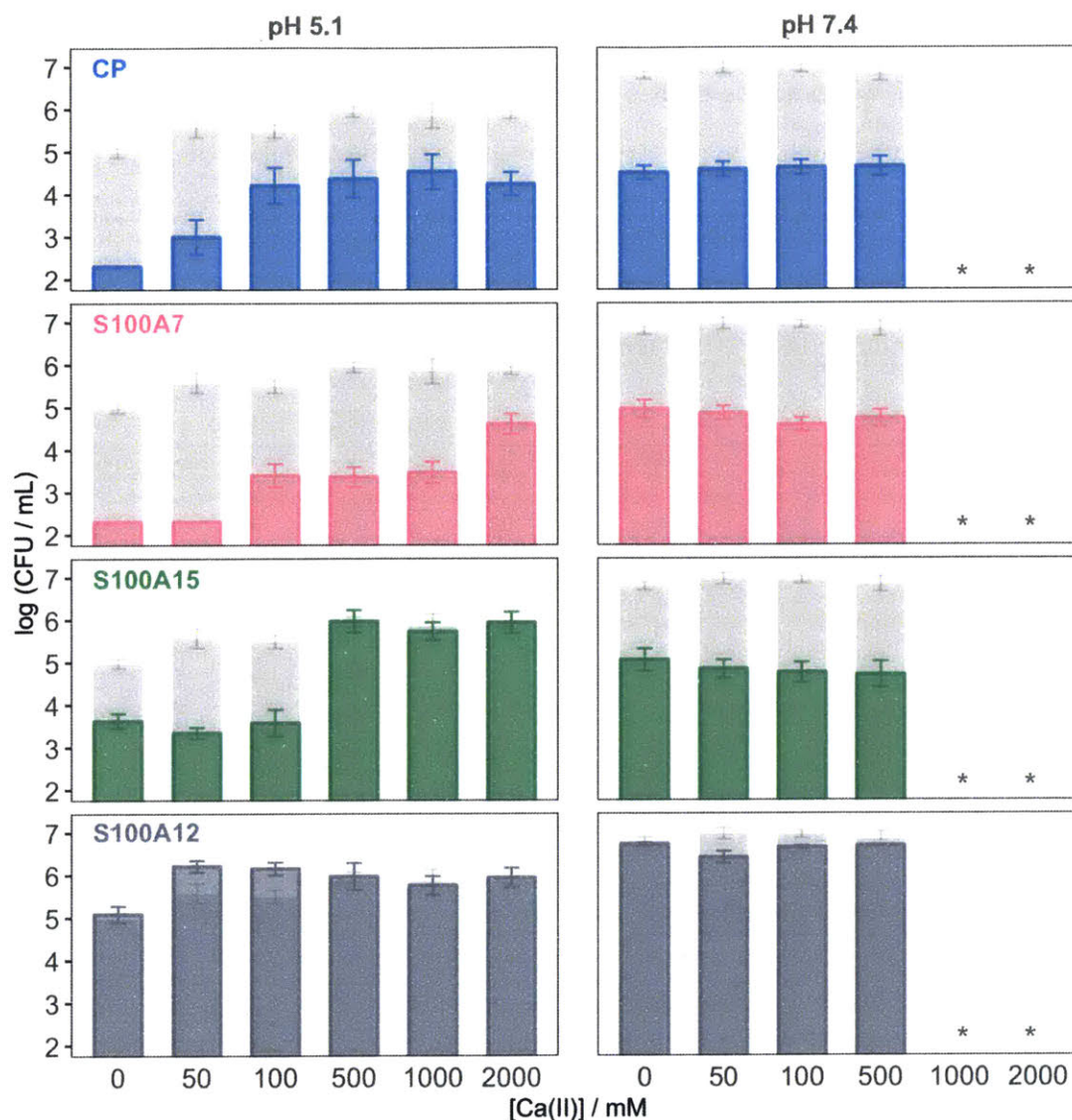


Figure 5. 5. Effects of Ca(II) concentration on the *E. coli*-cidal activity of S100 proteins. *E. coli* ATCC 25922 cultures (1×10^5 CFU/mL) were incubated with 1000 μ g/mL of CP (blue), or S100A7 (pink), or S100A15 (green), or S100A12 (grey) for 3 h at 37 °C with shaking at 150 rpm. Cultures were plated on TSB/agar plates, allowed to incubate for 12-14 h at 37 °C, and colonies counted for CFU determination. Buffer: 10 mM MES pH 5.1 + 1% TSB, or 10 mM phosphate pH 7.4 + 1% TSB. The untreated cultures are shown in light grey. (mean \pm 95% CI, $n = 3$). * The Ca(II) titration could not be carried out at these Ca(II) concentrations due to precipitation issues.

5. 3. 4. Growth Stage of *E. coli* Cultures Affects the Activities of the S100 Proteins

In agreement with previous studies looking at other AMPs, the S100 proteins were found to be less active against cultures in the stationary phase over mid-log phase at acidic pH (Figure 5. 6).^{2,10} Whilst the degree of attenuation was not negligible, CP and S100A7 still retained substantial activity at pH 5.1 against *E. coli* cultures in the stationary phase (Figure 5. 6). At pH 7.4, CP, S100A7, and S100A15 all had comparable activities against cultures in the mid-log and stationary phase (Figure 5. 6).

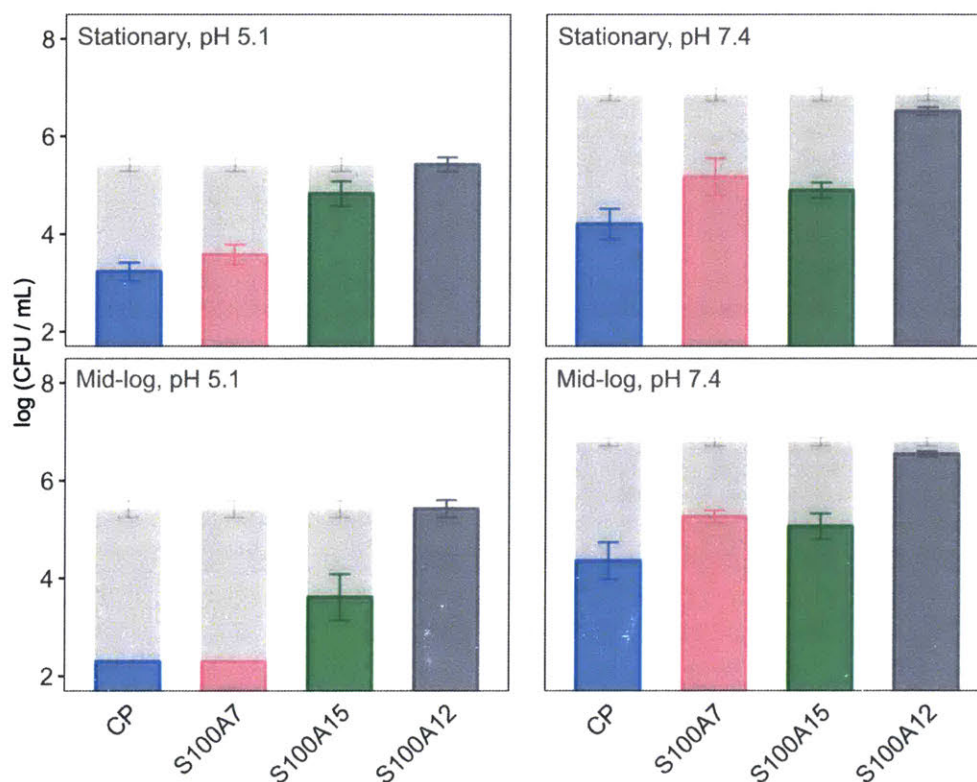


Figure 5. 6. Effects of *E. coli* growth stage on the activity of the S100 proteins. *E. coli* ATCC 25922 cultures (1×10^5 CFU/mL) were incubated with 1000 μ g/mL of CP (blue), or S100A7 (pink), or S100A15 (green), or S100A12 (grey) for 3 h at 37 °C with shaking at 150 rpm. Cultures were plated on TSB/agar plates, allowed to incubate for 12-14 h at 37 °C, and colonies counted for CFU determination. Buffer: 10 mM MES pH 5.1 + 1% TSB, or 10 mM phosphate pH 7.4 + 1% TSB. The untreated cultures are shown in light grey. (mean \pm 95% CI, $n = 3$).

Taken together, the results from our solution studies suggest that CP, S100A7, and S100A15 possess *E. coli*-cidal properties, and are the most active at acidic pH against cultures in the mid-log phase. The proteins seem relatively resistant to the effect of high salt but are inactivated in presence of excess Ca(II) under acidic conditions. Interestingly, Ca(II) or NaCl supplementation, as well as the growth stage of the *E. coli* cultures did not affect the killing activities of the proteins at pH 7.4. This observation is unusual as it contrasts to the behaviors of the proteins at acidic pH, and hints at the possibility of different antimicrobial mechanisms of action at pH 5.1 vs 7.4. How those mechanisms differ is not clear. However, a scenario whereby the proteins turn on their functions as metal-sequestering factors at pH 7.4, and display a bacteriostatic mechanism of action is plausible. For instance, Lactoferrin, a well-recognized host-defense peptide possesses both bacteriostatic and bactericidal properties.¹²

5. 3. 5. *The S100 Proteins Compromise the Bacterial Membrane of E. coli*

On the basis of the results from our solution studies, we then conducted microscopy studies to investigate the effects S100 proteins on *E. coli* cells. Phase-contrast and fluorescence microscopy were previously employed to probe the effect of CP treatment on cells (Chapter 4). CP was found to permeabilize the cell wall of *E. coli* and other Gram-negative strains, cause distinct morphological cell phenotypes, and physically interact with *E. coli* cells under acidic conditions. In order to facilitate the visualization of more cells per microscopy experiment, we modified the broth microdilution assays that employed mid-log phase bacteria at 1×10^5 CFU/mL. Instead, we used a greater number of cells (1×10^8 CFU/mL) and higher protein concentration (100 μ M), and carried out the microscopy studies at pH 5.1. Under those conditions, CP, S100A7, and S100A15 were at concentrations below their MICs, and were nonetheless capable of permeabilizing the membrane of cells resulting into morphological phenotypes. Therefore, these conditions allowed us to visualize enough cells as well as quantify cell morphology phenotypes.

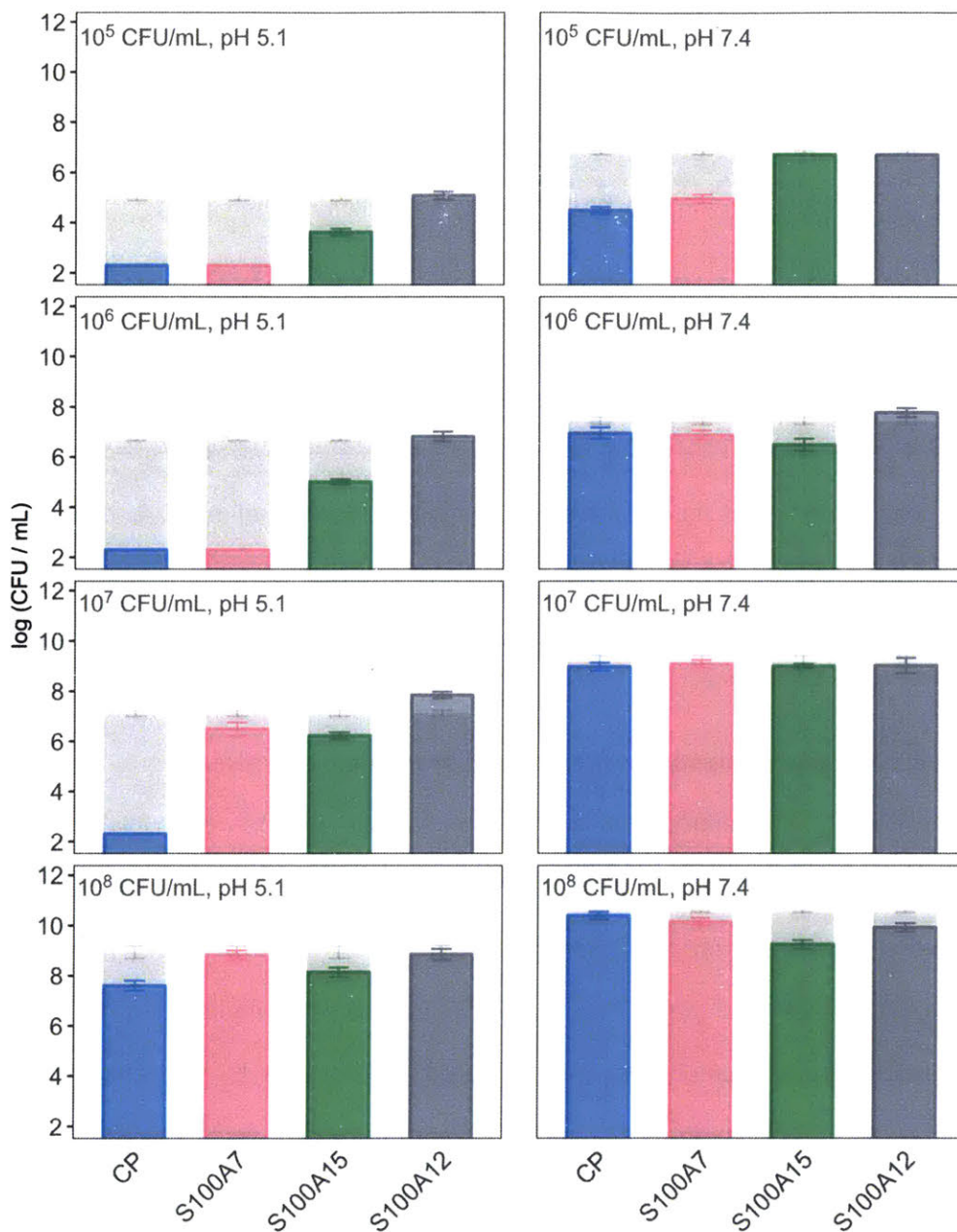


Figure 5. 7. Effects of CFU on the activity of the S100 proteins. *E. coli* ATCC 25922 cultures were incubated with 1000 µg/mL of CP (blue), or S100A7 (pink), or S100A15 (green), or S100A12 (grey) for 3 h at 37 °C with shaking at 150 rpm. Cultures were plated on TSB/agar plates, allowed to incubate for 12-14 h at 37 °C, and colonies counted for CFU determination. Buffer: 10 mM MES pH 5.1 + 1% TSB, or 10 mM phosphate pH 7.4 + 1% TSB. The untreated cultures are shown in light grey. (mean ± 95% CI, n = 3).

First, a Live-Dead stain was employed to quantify the number of cells with compromised membranes due to S100 treatment; cells with compromised membranes stained red or less frequently yellow, and cells with intact membranes stained green. As expected, the untreated cells were found to stain mostly green, with less than 10% of cells staining red (Figure 5. 8, Figure 5. 9). Upon treatment with CP, S100A7, and S100A15, 88%, 77%, and 62% of cells had compromised cell membranes respectively, whereas only 16% of cells stained red upon S100A12 treatment (Figure 5. 8, Figure 5. 9). The number of cells with a compromised cell wall was consistent with the results on the *E. coli*-cidal activities of the proteins determined by the broth microdilution assays (Figure 5. 2). It is worth noting that under this experimental setup we found that the Live-Dead stain did not directly report on live and dead cells, but instead reported on cells with compromised cell walls as evidenced by CFU titrations where we observed no decrease in CFU count at the two highest CFU tested (Figure 5. 7). We have reported a similar observation with CP in Chapter 4, and postulate that the membrane pores caused by the S100 proteins may not be the direct cause of their *E. coli*-cidal activity. This phenomenon has been reported with a multitude of other AMPs that can bind and insert into bacterial membranes without causing significant permeabilization.⁶²⁻⁶⁵ The discrepancy between the membrane-permeabilizing and effective killing properties of the S100 proteins are unclear and warrant further exploration.

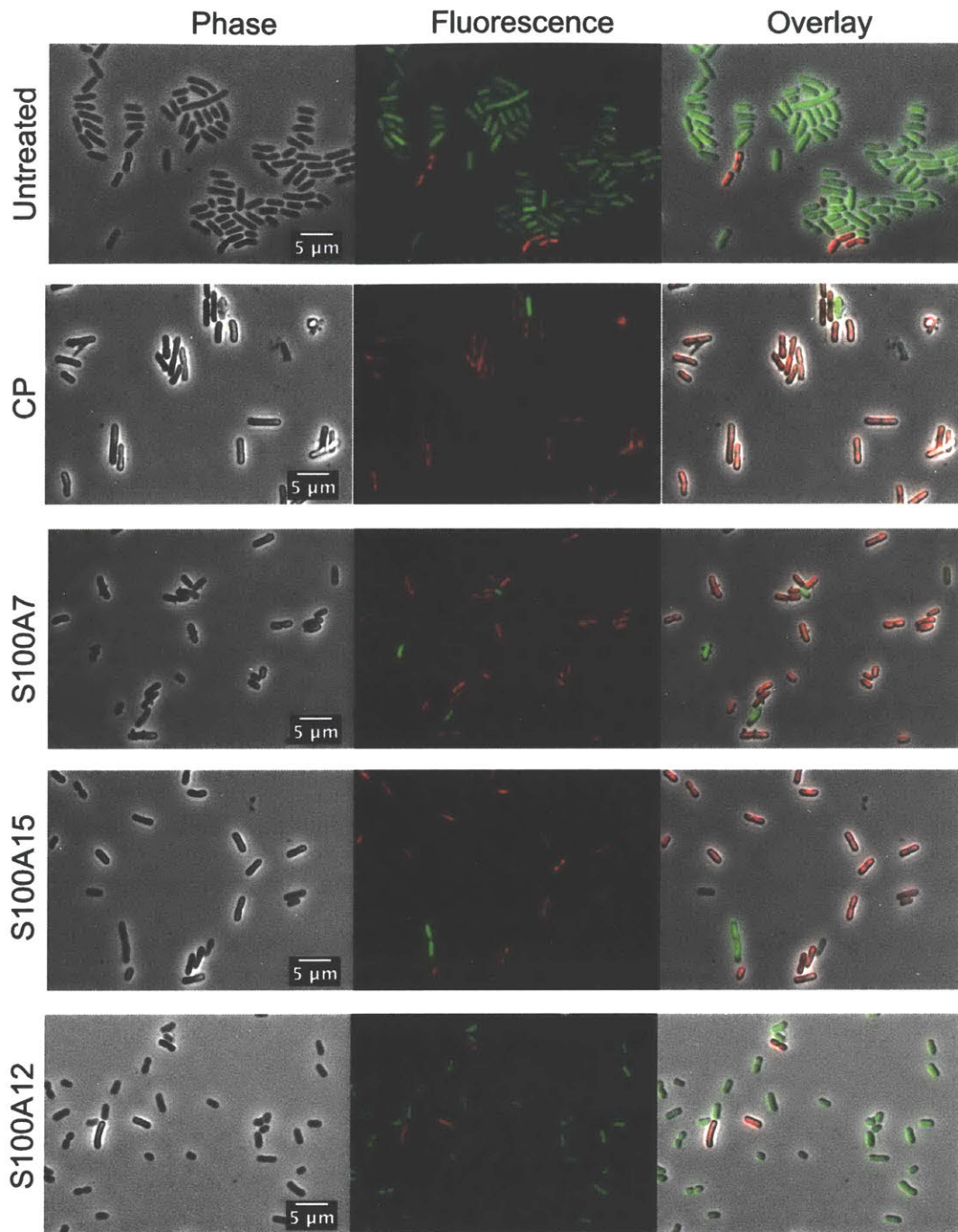


Figure 5. 8. The S100 proteins affect the cell wall integrity of *E. coli* ATCC 25922. Phase-contrast and fluorescence imaging of *E. coli* 25922 (1×10^8 CFU/mL) in the absence and presence of 100 μ M of S100 protein. Cells were incubated for 3 h at 37 °C and shaking at 150 rpm prior to imaging. The Live-Dead stain was added 15 min prior to imaging. Buffer: 10 mM MES pH 5.1 + 1% TSB, ($n = 3$). Scale bar is 5 μ m.

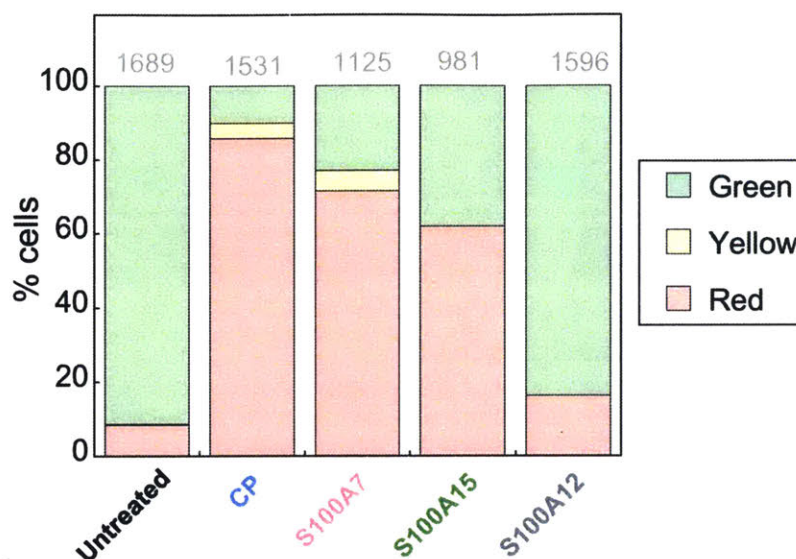
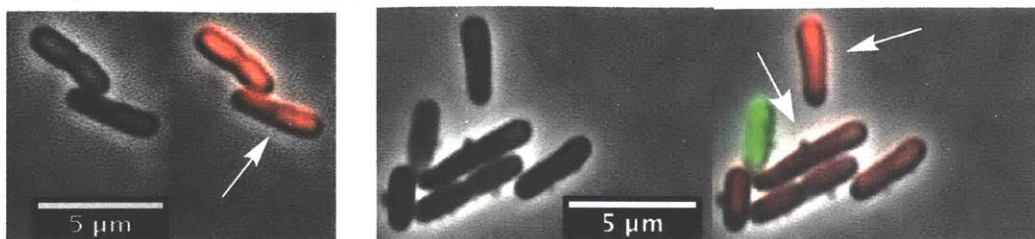


Figure 5. 9. Effects of S100 treatment on *E. coli* ATCC 25922 cell wall integrity. Number of cells staining green, yellow, or red was counted. *E. coli* ATCC 25922 (1×10^8 CFU/mL) were treated with 100 μ M of S100 protein. Cells were incubated for 3 h at 37 °C and shaking at 150 rpm prior to imaging. The Live-Dead stain was added 15 min prior to imaging. The number above each bar indicates the number of cells counted. Buffer: 10 mM MES pH 5.1 + 1% TSB ($n = 3$).

5. 3. 6. The S100 Proteins Induce Morphological Changes in *E. coli*

E. coli cells treated with S100A7 and S100A15 exhibited membrane curvature, distortion, and roughness (Figure 5. 9, Figure 5. 10), phenotypes that were observed with CP treatment (Chapter 4); these phenotypes are likely caused by a perturbation in the outer and/or inner membrane morphology.⁶⁶ In the case of S100A7, the occurrence of protrusion from the cell wall at cell division sites was also observed (Figure 5. 9). While these morphology studies do not provide direct information on the mechanisms of actions of S100A7 and S100A15, they suggest that the proteins are able to bind and interact with the bacterial cell membrane of *E. coli*, and cause the observed morphological changes. Interestingly, S100A12-treated cells were indistinguishable from the untreated cells, and displayed a comparable Live-Dead staining pattern (Figure 5. 8, Figure 5. 9).

A Phenotype 1: Cell membrane curvature and roughness



B Phenotype 2: Protrusion at cell division site

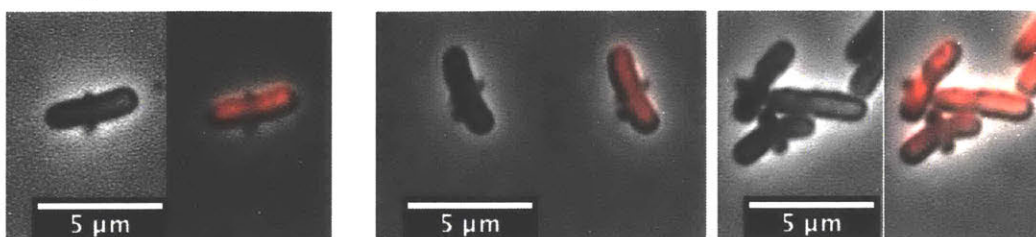


Figure 5. 10. S100A7 causes distinct morphological changes to *E. coli* cells. Phase-contrast and fluorescence imaging of *E. coli* 25922 (1×10^8 CFU/mL) in the absence and presence of 100 μ M S100A7. **(A)** Curvature, roughness, and distortion of cells observed upon S100A7 treatment. **(B)** Protrusions on the cell surface of cells observed upon S100A7 treatment. Cells were incubated for 3 h at 37 $^{\circ}$ C, with shaking at 150 rpm prior to imaging. The Live-Dead stain was added 15 min prior to imaging. Buffer: 10 mM MES pH 5.1 + 1% TSB, ($n = 3$). Scale bar is 5 μ m.

A Phenotype 1: Cell membrane curvature

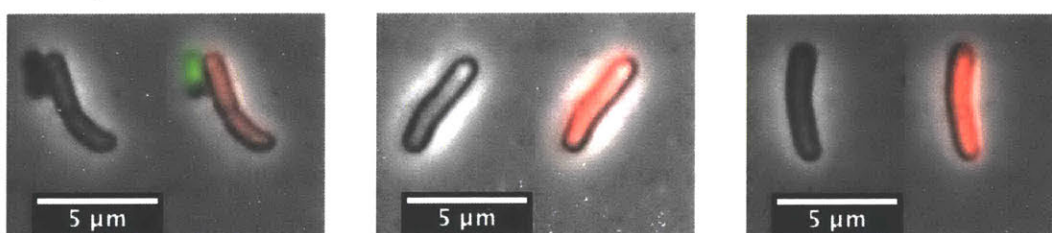


Figure 5. 11. S100A15 causes distinct morphological treatment on *E. coli* cells. Phase-contrast and fluorescence imaging of *E. coli* 25922 (1×10^8 CFU/mL) in the absence and presence of 100 μ M S100A15. **(A)** Curvature of cells observed upon S100A7 treatment. Cells were incubated for 3 h at 37 $^{\circ}$ C, with shaking at 150 rpm prior to imaging. The Live-Dead stain was added 15 min prior to imaging. Buffer: 10 mM MES pH 5.1 + 1% TSB, ($n = 3$). Scale bar is 5 μ m.

5. 3. 7. The S100 Proteins Affect the Cell-Length Distribution of *E. coli*

Because the S100-treated cells were a mix of cells staining green, red, and yellow, we divided the S100-treated cells into two categories based on their Live-Dead staining. Cells that stained red or yellow were considered to have a compromised cell wall, and grouped together as “red” cells (Figure 5. 12A), while cells that stained green were considered to have an intact cell wall and grouped together as “green” cells (Figure 5. 12B). This categorization simplified the analysis for the cell length distribution for S100-treated and untreated cells. To further simplify our analysis, we only considered cells that stained green for the untreated cell population, as less than 10% of the untreated cells stained red (Figure 5. 9).

A comparison of the bacterial cell length distribution of CP- and S100A7-treated “red” cells to the untreated cells showed that these two cell populations were statistically different from the untreated population ($P < 0.001$), whereas the S100A15- and S100A12-treated cell populations were not ($P > 0.05$) (Figure 5. 12A). These trends are consonant with the killing activities of the S100 proteins reported from the broth microdilution assays, whereby CP and S100A7 are the most potent ones, followed by S100A15, while S100A12 displayed no killing activity (Figure 5. 2). On average, the CP-treated red cells were longer than the untreated cells ($2.34 \pm 0.05 \mu\text{m}$), and S100A7-treated red cells were shorter than the untreated cells ($2.09 \pm 0.07 \mu\text{m}$) (Figure 5. 13). When this comparison was extended to S100-treated “green” cells, we remarked that S100-treated “green” cells were on average shorter than the untreated control (Figure 5. 13). Interestingly, the cell length profile of green cells treated with S100A7, S100A15, and S100A12 were statistically different ($P < 0.001$) from the untreated cells (Figure 5. 12B), whereas CP-treated cells were not (Figure 5. 12B, Figure 5. 13). We speculate that the root of this discrepancy is due to the small number of CP-treated “green” cells ($n = 70$). Taken together, these results show that CP-treated cells with a compromised cell wall display aberrant cell phenotypes in the form of cell elongation. On the other hand, S100A7, S100A15 and S100A12 treatment results in cell

shortening, implying that the proteins inhibit cell growth and may act through a bacteriostatic mode of action.

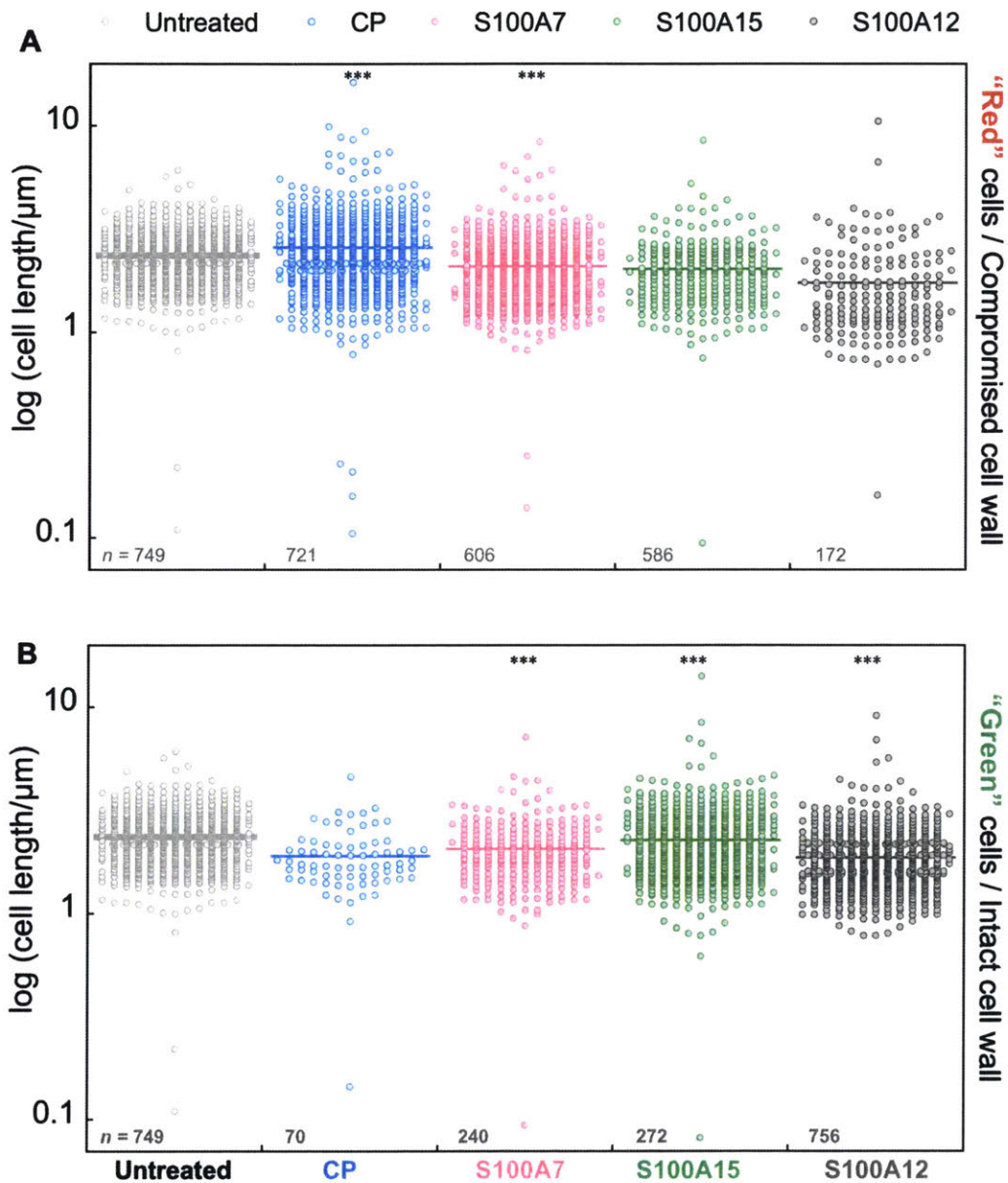


Figure 5. 12. Cell length profile upon S100 treatment. The cell length of untreated cells were compared to S100-treated "green" (A) and "red" (B) cells. *E. coli* ATCC 25922 (10^8 CFU/mL) were treated with 100 μM of S100 protein. Cells were incubated for 3 h at 37 $^\circ\text{C}$ and shaking at 150 rpm prior to imaging. The Live-Dead stain was added 15 min prior to imaging. Buffer: 10 mM MES pH 5.1 + 1% TSB ($n = 3$). The number in the bottom left corner indicates the number of cells measured. *** $P < 0.001$.

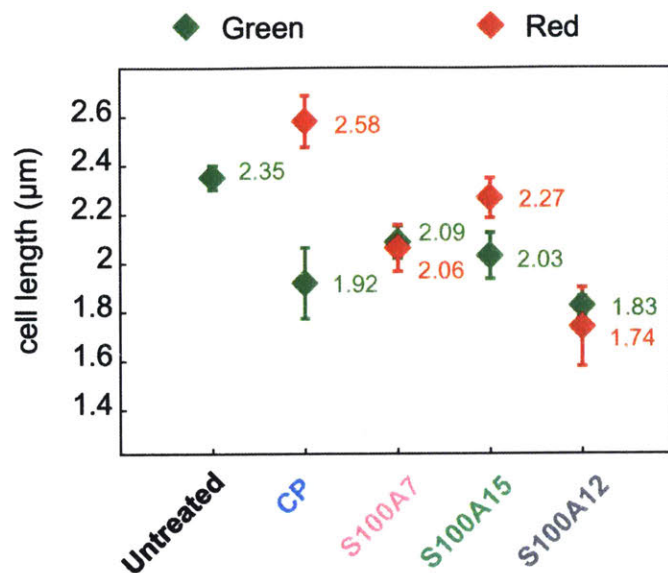


Figure 5. 13. Cell length average of untreated and S100-treated cells. The cell length average of untreated cells were compared to S100-treated “green” and “red” cells. *E. coli* ATCC 25922 (10^8 CFU/mL) were treated with 100 μ M of S100 protein. Cells were incubated for 3 h at 37 °C and shaking at 150 rpm prior to imaging. The Live-Dead stain was added 15 min prior to imaging. Buffer: 10 mM MES pH 5.1 + 1% TSB (mean \pm 95% CI, $n = 3$). The values presented in the plot represent the cell length mean (μ m) for each condition.

5. 3. 8. The S100 Proteins Display Broad-Spectrum Bactericidal Activity against Gram-negative Strains

The scope of the bactericidal activities of the S100 proteins are limited to a few studies and warrant further assessment. Early studies of CP and S100A12 have documented that they can associate with the cell surface of parasites^{35,46-47} and bacterial pathogens,³⁸ but no direct evaluation of their killing activities was provided. In the case of S100A7, it is well documented to be an *E. coli*-cidal factor,³⁹⁻⁴⁰ and a study reported that it was slightly active against *Bacillus megaterium*.⁴⁰ To the best of our knowledge, there have been no studies documenting the microbicidal activities of S100A12 and S100A15. We recently probed the bactericidal activity of CP against a panel of bacterial strains and found that it was a broad-spectrum Gram-negative AMP, whereas it was less active or inactive against Gram-positive strains (Chapter 4). We

therefore decided to expand upon the scope of the bactericidal activities of S100A7, S100A15, and S100A12 by testing them against the same panel of bacterial strains that was used with CP. This panel of strains included the Gram-negative strains *Acinetobacter baumannii* ATCC 17978, *Escherichia coli* UTI89, and *Pseudomonas aeruginosa* PAO1, and the Gram-positive strains *Listeria monocytogenes* ATCC 19115 and *Staphylococcus aureus* JE2.

In agreement with the results obtained from our assays with *E. coli*, the proteins were generally more active at acidic pH, and S100A12 was found to be inactive against all the strains tested (Figure 5. 14). Treatment of *A. baumannii*, *E. coli*, and *P. aeruginosa* with CP, S100A7, and S100A15 resulted into complete killing of the cultures under acidic conditions, while the growth of the Gram-Positive strains *L. monocytogenes* and *S. aureus* were unaffected (Figure 5. 14). These results suggest that the bactericidal properties of CP, S100A7, and S100A15 can be generalized to include Gram-negative strains but not Gram-positive strains. Of note, *L. monocytogenes* was found to be slightly susceptible to CP, S100A7, and S100A15 at neutral pH but not at acidic pH. The origins of this trend remain unknown, but could point to a mechanism of Zn(II)-mediated growth-inhibition, a mechanism previously described for CP, S100A7, and S100A12.^{53-54,67}

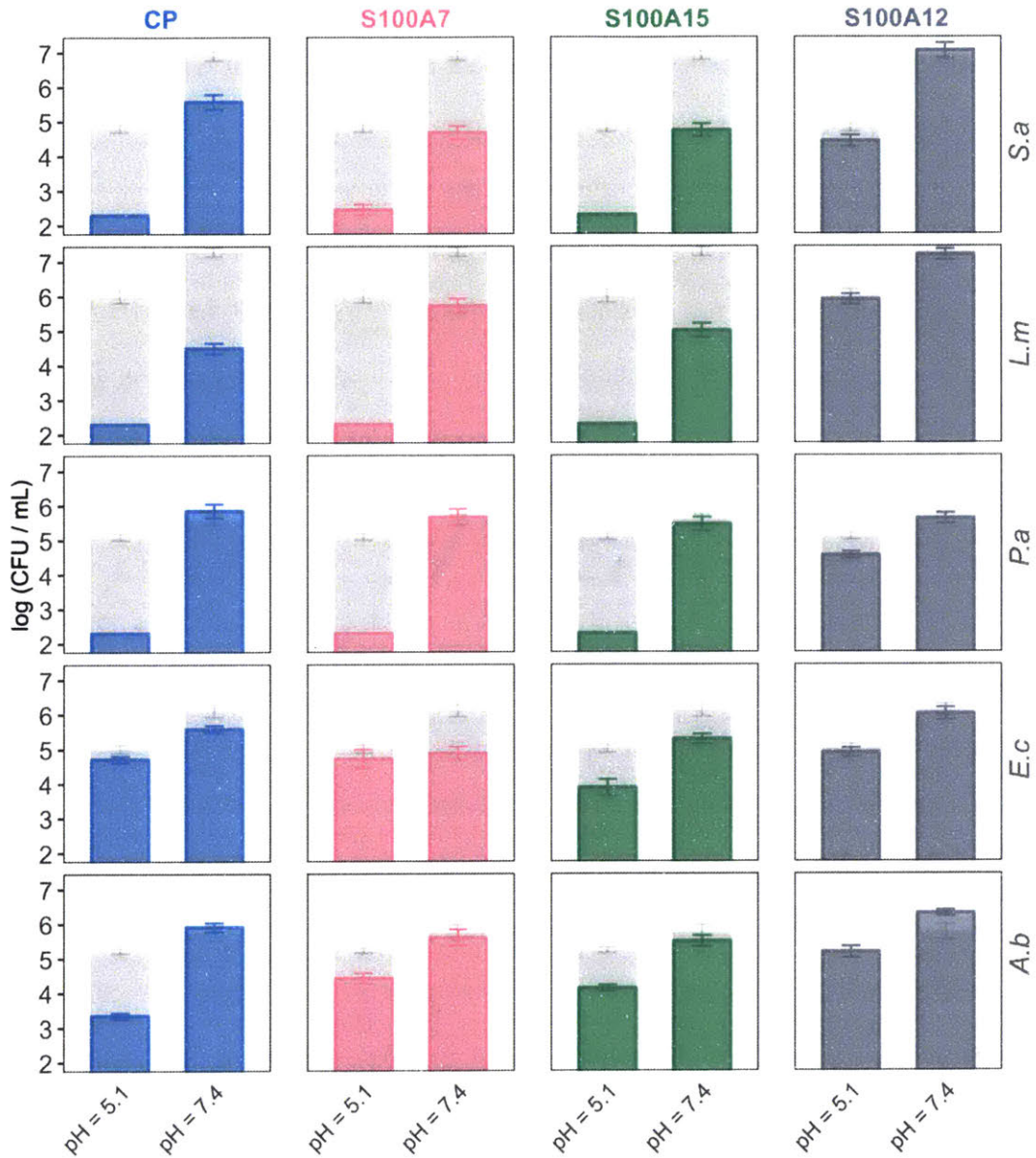


Figure 5. 14. Antibacterial activities of the S100 proteins against *A. baumannii* ATCC 17978 (A.b), *E. coli* UT189 (E.c), *P. aeruginosa* PAO1 (P.a), *L. monocytogenes* ATCC 19115 (L.m), and *S. aureus* JE (S.a). Cell cultures (1×10^8 CFU/mL) were incubated with 1000 μ g/mL of CP (blue), or S100A7 (pink), or S100A15 (green), or S100A12 (grey) for 3 h at 37 °C with shaking at 150 rpm. Cultures were plated on TSB/agar plates, allowed to incubate for 12-20 h at 37 °C, and colonies counted for CFU determination. Buffer: 10 mM MES pH 5.1 + 1% TSB, or 10 mM phosphate pH 7.4 + 1% TSB. The untreated cultures are shown in light grey. (mean \pm 95% CI, $n = 3$).

5. 4. Summary and Outlook

In summary, we have screened the bactericidal properties of four S100 proteins that include CP, S100A7, S100A15, and S100A12, and have shown that all but S100A12 possess bactericidal properties. We have characterized conditions under which they are most active and have found that the proteins are effective bactericidal agents under acidic conditions, and remain active at salt concentrations that are physiologically relevant. CP, S100A7, and S100A15 were found to be active against all the Gram-negative strains tested suggesting that they are broad-spectrum AMPs against Gram-negative strains. We postulate that such activity is as a result of the electrostatic interaction between the cationic the S100 proteins, and anionic LPS moieties on the cell outer-membrane of Gram-negative strains.⁶⁸

S100A12 stands out from the other S100 proteins as the only one that does not possess bactericidal activity under any of the conditions tested. S100A12 possess similar secondary features and pI value as the other S100 proteins (Figure 5. 1), and the molecular basis for this difference in activity is not apparent to us. Prior studies have reported that a C-terminal fragment of S100A12 isolated from human nasal airways named calcitermin, possesses bactericidal activity against *Candida albicans*, *E. coli*, *L. monocytogenes* and *P. aeruginosa* at acidic pH.⁶⁹ Hence, it is possible that while the full-length S100A12 is inactive as an AMP, proteolytic cleavage of S100A12 by the host or microbes generates a potent S100A12-derived AMP. This strategy of AMP activation upon proteolytic processing has been observed with other AMPs, including human defensin 6 (HD6), dermcidin-1, and lactoferrin.^{2,12,70-71} Indeed, HD6 it is stored as a premature inactive form with an N-terminal extension, and subsequent cleavage of this region by trypsin generates an active form of the peptide with host-defense function.^{70,72-73} Dermcidin-1 (DCD-1) is a processed form of dermcidin, a human AMP secreted by sweat glands, which shows antimicrobial activity against a variety of pathogen microorganisms.⁷¹ In the case of lactoferrin, Saito and coworkers demonstrated that limited acid proteolysis of bovine lactoferrin yielded a hydrolysate that had greater antibacterial activity than lactoferrin,⁷⁴ and Bellamy and coworkers

described the generation of lactoferrin fragments from pepsin hydrolysis, termed lactoferricins, that showed enhanced bactericidal activity but no iron-binding capacities.⁷⁵⁻⁷⁶ As such, proteolytic cleavage products of S100A12 and other S100 proteins warrant consideration since this regulation would conveniently allow for spatial and temporal activation of S100-derived AMPs.

Taken together, this work demonstrates the multifunctionality of the antimicrobial functions of the S100 proteins, and sets the groundwork for understanding factors that modulate the killing activities of the S100 proteins. However, several unanswered questions remain and warrant further investigation; it is unclear what processes regulate the bacteriostatic and bactericidal activities of the S100 proteins. Furthermore, the synergistic effect on the antimicrobial activities of the S100 proteins is another avenue for future investigation since CP and S100A12, and S100A7 and S100A15 are co-expressed and co-released.^{58,61,77-79} Therefore, efforts to further investigate these notions will be informative.

5. 5. Acknowledgements

We thank Dr. Wendy Salmon of the Whitehead Institute for Biomedical Research for help with the microscopy studies, and Dr. Phoom Chairatana for insightful discussions.

5. 6. References

1. Ganz, T., The role of antimicrobial peptides in innate immunity. *Integr. Compt. Biol.* **2003**, 43, 300-304.
2. Wiesner, J.; Vilcinskas, A., Antimicrobial peptides: The ancient arm of the human immune system. *Virulence* **2010**, 1 (5), 440-464.
3. Ganz, T., Defensins. Natural peptide antibiotics of human neutrophils. *Nat. Rev. Immunol.* **2003**, 3, 710-720.
4. Parkin, J.; Cohen, B., An overview of the immune system. *Lancet* **2001**, 357, 1777-1789.

5. Walker, D.; Fowler, T., Annual report of the chief medical officer: Volume two, 2011: Infections and the rise of antimicrobial resistance. **2011**, (Department of Health, 2011).
6. Forum, W. E., Global risks 2014 report. **2014**.
7. Blair, J. M. A.; Webber, M. A.; Baylay, A. J.; Ogbolu, D. O.; Piddock, L. J. V., Molecular mechanisms of antibiotic resistance. *Nat. Rev. Microbiol.* **2015**, *13*, 42-51.
8. Dale, B. A.; Fredericks, L. P., Antimicrobial peptides in the oral environment: expression and function in health and disease. *Curr. Issues. Mol. Biol.* **2005**, *7*, 119-133.
9. Harder, J.; Meyer-Hoffert, U.; Wehkamp, K.; Schwichtenberg, L.; Schröder, J. M., Differential gene induction of human beta-defensins (hBD-1, -2, -3, and -4) in keratinocytes is inhibited by retinoic acid. *J. Invest. Dermatol.* **2004**, *123*, 522-529.
10. Chileveru, H. R.; Lim, S. A.; Chairatana, P.; Nolan, E. M., Visualizing attack of *Escherichia coli* by the antimicrobial peptide human defensin 5. *Biochemistry* **2015**, *54*, 1767-1777.
11. Wang, Y.; Chen, C. H.; Hu, D.; Ulmschneider, M. B.; Ulmschneider, J. P., Spontaneous formation of structurally diverse membrane channel architectures from a single antimicrobial peptide. *Nat. Comm.* **2016**, DOI: 10.1038/ncomms13535.
12. Farnaud, S.; Evans, R. W., Lactoferrin - a multifunctional protein with antimicrobial properties. *Mol. Immunol.* **2003**, *40*, 395-405.
13. Juliano, S. A.; Pierce, S.; deMayo, J. A.; Balunas, M. J.; Angeles-Boza, A. M., Exploration of the innate immune system of *Styela clava*: Zn²⁺ binding enhances the antimicrobial activity of the tunicate peptide clavanin A. *Biochemistry* **2017**, *56*, 1403-1414.
14. Nguyen, L. T.; Haney, E. F.; Vogel, H. J., The expanding scope of antimicrobial peptide structures and their modes of action. *Trends Biotechnol.* **2011**, *29* (9), 464-72.
15. Yan, J.; Wang, K.; Dang, W.; Chen, R.; Xie, J.; Zhang, B.; Song, J.; Wang, R., Two hits are better than one: membrane-active and DNA binding-related double-action mechanism of NK-18, a novel antimicrobial peptide derived from mammalian NK-Lysin. *Antimicrob. Agents. Chemother.* **2013**, *57* (1), 220-228.

16. Haukland, H. H.; Ulvatne, H.; Sandvik, K.; H., V. L., The antimicrobial peptides lactoferricin B and magainin 2 cross over the bacterial cytoplasmic membrane and reside in the cytoplasm. *FEBS Lett.* **2001**, *508*, 389-393.
17. Wilmes, M.; Stockem, M.; Bierbaum, G.; Schlag, M.; Gotz, F.; Tran, D. Q.; Schaal, J. B.; Ouellette, A. J.; Selsted, M. E.; Sahl, H. G., Killing of staphylococci by theta-defensins involves membrane impairment and activation of autolytic enzymes. *Antibiotics (Basel)* **2017**, *3* (4), 617-631.
18. Tran, D.; Tran, P. A.; Tang, Y. Q.; Yuan, J.; Cole, T.; Selsted, M. E. H., Homodimeric theta-defensins from rhesus macaque leukocytes: isolation, synthesis, antimicrobial activities, and bacterial binding properties of the cyclic peptides. *J. Biol. Chem.* **2002**, *277* (5), 3079-3084.
19. Scheit, K. H.; Reddy, E. S.; Bhargava, P. M., Seminaplasmin is a potent inhibitor of *E. coli* RNA polymerase in vivo. *Nature* **1979**, (279), 728-731.
20. Donato, R.; Canon, B. R.; Sorci, G.; Riuzzi, F.; Hsu, K.; Weber, D. J.; Geczy, C. L., Functions of S100 proteins. *Curr. Mol. Med.* **2013**, *13*, 24-57.
21. Gifford, J. L.; Walsh, M. P.; Vogel, H. J., Structures and metal-ion-binding properties of the Ca²⁺-binding helix-loop-helix EF-hand motifs. *Biochem. J.* **2007**, *405* (2), 199-221.
22. Gagnon, D. M.; Brophy, M. B.; Bowman, S. E. J.; Stich, T. A.; Drennan, C. L.; Britt, R. D.; Nolan, E. M., Manganese binding properties of human calprotectin under conditions of high and low calcium: X-ray crystallographic and advanced electron paramagnetic resonance spectroscopic analysis. *J. Am. Chem. Soc.* **2015**, *137* (8), 3004-3016.
23. Nakashige, T. G.; Zhang, B.; Krebs, C.; Nolan, E. M., Human calprotectin is an iron-sequestering host-defense protein. *Nat. Chem. Biol.* **2015**, *11* (10), 765-771.
24. Hayden, J. A.; Brophy, M. B.; Cunden, L. S.; Nolan, E. M., High-affinity manganese coordination by human calprotectin is calcium-dependent and requires the histidine-rich site formed at the dimer interface. *J. Am. Chem. Soc.* **2013**, *135* (2), 775-787.

25. Nakashige, T. G.; Stephan, J. R.; Cunden, L. S.; Brophy, M. B.; Wommack, A. J.; Keegan, B. C.; Shearer, J. M.; Nolan, E. M., The hexahistidine motif of host-defense protein human calprotectin contributes to zinc withholding and its functional versatility. *J. Am. Chem. Soc.* **2016**, *138* (37), 12243-12251.
26. Stephan, J. R.; Nolan, E. M., Calcium-induced tetramerization and zinc chelation shield human calprotectin from degradation by host and bacterial extracellular proteases. *Chem. Sci.* **2016**, *7* (3), 1962-1975.
27. Cunden, L. S.; Gaillard, A.; Nolan, E. M., Calcium ions tune the zinc-sequestering properties and antimicrobial activity of human S100A12. *Chem. Sci.* **2016**, *7* (2), 1338-1348.
28. Zackular, J. P.; Chazin, W. J.; Skaar, E. P., Nutritional Immunity: S100 proteins at the host-pathogen interface. *J. Biol. Chem.* **2015**, *290* (31), 18991-18998.
29. Damo, S. M.; Kehl-Fie, T. E.; Sugitani, N.; Holt, M. E.; Rathi, S.; Murphy, W. J.; Zhang, Y. F.; Betz, C.; Hench, L.; Fritz, G.; Skaar, E. P.; Chazin, W. J., Molecular basis for manganese sequestration by calprotectin and roles in the innate immune response to invading bacterial pathogens. *Proc. Natl. Acad. Sci. U. S. A.* **2013**, *110* (10), 3841-3846.
30. Gilston, B. A.; Skaar, E. P.; Chazin, W. J., Binding of transition metals to S100 proteins. *Sci. China Life Sci.* **2016**, *59* (8), 792-801.
31. Brophy, M. B.; Nolan, E. M., Manganese and microbial pathogenesis: sequestration by the mammalian immune system and utilization by microorganisms. *ACS Chem. Biol.* **2015**, *10* (3), 641-651.
32. Sohnle, P. G.; Collins-Lech, C.; Wiessner, J. H., The zinc-reversible antimicrobial activity of neutrophil lysates and abscess fluid supernatants. *J. Infect. Dis.* **1991**, *164* (1), 137-142.
33. Donato, R., Functional roles of S100 proteins, calcium-binding proteins of the EF-hand type *Biochim. Biophys. Acta* **1999**, (1450), 191-231.
34. Eversole, L. R.; Miyasaki, T. M.; Christenten, R. E., The distribution of the antimicrobial protein, calprotectin, in normal oral keratinocytes. *Archs. Oral. Biol.* **1992**, *11*, 963-968.

35. Edgeworth, J. D.; Abiose, A.; Jones, B. R., An immunohistochemical analysis of onchocercal nodules: evidence for an interaction between macrophage MRP8/MRP14 and adult *Clin. Exp. Immunol.* **1993**, *92*, 84-92.
36. Stork, M.; Grijpstra, J.; Bos, M. P.; Torres, C. M.; Devos, N.; Poolman, J. T.; Chazin, W. J.; Tommassen, J., Zinc piracy as a mechanism of *Neisseria meningitidis* for evasion of nutritional immunity. *PLoS Pathog.* **2013**, *9* (10), e1003733.
37. Jean, S.; Juneau, R. A.; Criss, A. K.; Cornelissen, C. N., *Neisseria gonorrhoeae* evades calprotectin-mediated nutritional immunity and survives neutrophil extracellular traps by production of TdfH. *Infect. Immun.* **2016**, *84*, 2982-2994.
38. Besold, A. N.; Culbertson, E. M.; Nama, L.; Hobbs, R. P.; Boyko, A.; Maxwell, C. N.; Chazin, W. J.; Marques, A. R.; Culotta, A. C., Antimicrobial action of calprotectin that does not involve metal withholding. *Metallomics* **2018**, 10.1039/c8mt00133b.
39. Gläser, R.; Harder, J.; Lange, H.; Bartels, J.; Christophers, E.; Schröder, J. M., Antimicrobial psoriasin (S100A7) protects human skin from *Escherichia coli* infection. *Nat. Immunol.* **2005**, *6* (1), 57-64.
40. Michalek, M.; Gelhaus, C.; Hecht, O.; Podschun, R.; Schröder, J. M.; Leippe, M.; Grotzinger, J., The human antimicrobial protein psoriasin acts by permeabilization of bacterial membranes. *Dev. Comp. Immunol.* **2009**, *33* (6), 740-746.
41. Mildner, M.; Abtin, A.; Gmeiner, R.; Sam, C.; Gläser, R.; Schröder, J. M.; Mlitz, V.; Stichenwirth, M.; Pammer, J.; Geusau, A.; Tschachler, E., Psoriasin (S100A7) is a major antimicrobial component of the female genital tract. *Mucosal Immunol.* **2010**, *127*, 602-609.
42. Jinquan, T.; Vorum, H.; Larsen, C. G.; Madsen, P.; Rasmussen, H. H.; Gesser, B.; Etzerodt, M.; Honoré, B.; Celis, J. E.; Thestrup-Pedersen, K., Psoriasin: A novel chemotactic protein. *J. Invest. Dermatol.* **1996**, *107* (1), 5-10.

43. Vorum, H.; Madsen, P.; Rasmussen, H. H.; Etzerodt, M.; Svendsen, I.; Celis, J. E.; Honore, B., Expression and divalent cation binding properties of the novel chemotactic inflammatory protein psoriasin. *Electrophoresis* **1996**, *17* (11), 1787-1796.
44. Hein, K. Z.; Takahashi, H.; Tsumori, T.; Yasui, Y.; Nanjoh, Y.; Toga, T.; Wu, Z. H.; Grotzinger, J.; Jung, S.; Wehkamp, J.; Schroeder, B. O.; Schröder, J. M.; Morita, E., Disulphide-reduced psoriasin is a human apoptosis-inducing broad-spectrum fungicide. *Proc. Natl. Acad. Sci. U. S. A.* **2015**, *112* (42), 13039-13044.
45. Meyer, J. E.; Harder, J.; Sipos, B.; Maune, S.; Kloppel, G.; Bartels, J.; Schröder, J. M.; Glaser, R., Psoriasin (S100A7) is a principal antimicrobial peptide of the human tongue. *Mucosal Immunology* **2008**, *1* (3), 239-243.
46. Marti, T.; Erttmann, K. D.; Gallin, M. Y., Host-parasite interaction in human onchocerciasis: identification and sequence analysis of a novel human calgranulin. *Biochem. Biophys. Res. Commun.* **1996**, *221* (2), 454-458.
47. Gottsch, J. D.; Eisinger, S. W.; Liu, S. H.; L., S. A., Calgranulin C has filariacidal and filariastatic activity. *Infect. Immun.* **1999**, *67* (12), 6631-6636.
48. Akerström, B.; Bjorck, L., Bacterial surface protein L binds and inactivates neutrophil proteins S100A8/A9. *J. Immunol.* **2009**, (183), 4583-4592.
49. Jenssen, H.; Hamill, P.; Hancock, R. E. W., Peptide antimicrobial agents. *Clin. Microbiol. Rev.* **2006**, *19*, 491-511.
50. Lee, H.; Cho, Y.; I., L. R., Effects of pH and salinity on the antimicrobial properties of clavanins. *Infect. Immun.* **1997**, *65* (7), 2898-2903.
51. Steinberg, D. A.; Lehrer, R. I., Designer assays for antimicrobial peptides. Disputing the "one-size-fits-all" theory. *Methods. Mol. Biol.* **1997**, *78*, 169-186.
52. Brophy, M. B.; Hayden, J. A.; Nolan, E. M., Calcium ion gradients modulate the zinc affinity and antibacterial activity of human calprotectin. *J. Am. Chem. Soc.* **2012**, *134* (43), 18089-18100.

53. Cunden, L. S.; Gaillard, A.; Nolan, E. M., Calcium ions tune the zinc-sequestering properties and antimicrobial activity of human S100A12. *Chem. Sci.* **2016**, *7* (2), 1338-1348.
54. Cunden, L. S.; Brophy, M. B.; Rodriguez, G. E.; Flaxman, H. A.; Nolan, E. M., Biochemical and functional evaluation of the intramolecular disulfide bonds in the zinc-chelating antimicrobial protein human S100A7 (Psoriasin). *Biochemistry* **2017**, *56*, 5726-5738.
55. Gregory, T. M.; Moreno, E. C.; Patel, J. M.; Brown, W. E., Solubility of β -Ca₃(PO₄)₂ in the system Ca(OH)₂-H₃PO₄-H₂O at 5, 15, 25, and 37 °C, . *J. Res. Natl. Bur. Stand.* **1974**, *78* (A), 667-674.
56. Brodersen, D. E.; Etzerodt, M.; Madsen, P.; Celis, J. E.; Thøgersen, H. C.; Nyborg, J.; Kjeldgaard, M., EF-hands at atomic resolution: the structure of human psoriasin (S100A7) solved by MAD phasing. *Structure with Folding & Design* **1998**, *6* (4), 477-489.
57. Murray, J. I.; Tonkin, M. L.; Whiting, A. L.; Peng, F.; Farnell, B.; Cullen, J. T.; Hof, F.; Boulange, M. J., Structural characterization of S100A15 reveals a novel zinc coordination site among S100 proteins and altered surface chemistry with functional implications for receptor binding. *MBC Struc. Biol.* **2012**, (12:16).
58. Wolf, R.; Ruzicka, T.; Yuspa, S. H., Novel S100A7 (psoriasin)/S100A15 (koebnerisin) subfamily: highly homologous but distinct in regulation and function. *Amino acids* **2011**, *41* (4), 789-796.
59. van der Merwe, D. E.; Ubbink, J. B.; Delpont, R.; Becker, P.; Dhatt, G. S.; Vermaak, W. J., Biological variation in sweat sodium chloride conductivity. *Ann. Clin. Biochem.* **2002**, *39*, 39-43.
60. Williams, R. J. P., Calcium binding proteins in normal and transformed cells. *Cell Calcium* **1996**, *20* (1), 87-93.
61. Cunden, L. S.; Nolan, E. M., Bioinorganic explorations of Zn(II) sequestration by human S100 host-defense proteins. *Biochemistry* **2018**, *57* (11), 1673-1680.

62. Park, C. B.; Kim, H. S.; Kim, S. C., Mechanism of action of the antimicrobial peptide buforin II: buforin II kills microorganisms by penetrating the cell membrane and inhibiting cellular functions. *Biochem. Biophys. Res. Commun.* **1998**, *244* (1), 253-257.
63. Li, L.; Shi, Y.; Cheng, X.; Xia, S.; Cheserek, M. J.; Le, G., A cell-penetrating peptide analogue, P7, exerts antimicrobial activity against *Escherichia coli* ATCC 25922 via penetrating cell membrane and targeting intracellular DNA. *Food Chem.* **2015**, *166*, 231-239.
64. Podda, E.; Benincasa, M.; Pacor, S.; Micali, F.; Mattiuzzo, M.; Gennaro, R.; Scocchi, M., Dual mode of action of Bac7, a proline-rich antibacterial peptide. *Biochim. Biophys. Acta* **2006**, *1760* (11), 1732-1740.
65. Brogden, K. A., Antimicrobial peptides: pore formers or metabolic inhibitors in bacteria? *Nat. Rev. Microbiol.* **2005**, *3*, 238-250.
66. Epand, R. M.; Walker, C.; Epand, R. F.; Magarvey, N. A., Molecular mechanisms of membrane targeting antibiotics. *Biochim. Biophys. Acta* **2016**, *1858*, 980-987.
67. Zaia, A. A.; Sappington, K. J.; Nisapakultorn, K.; Chazin, W. J.; Dietrich, E. A.; Ross, K. F.; Herzberg, M. C., Subversion of antimicrobial calprotectin (S100A8/S100A9 complex) in the cytoplasm of TR146 epithelial cells after invasion by *Listeria monocytogenes*. *Mucosal Immunol.* **2009**, (2), 43-53.
68. Li, J.; Koh, J. J.; Liu, S.; Lakshminarayanan, R.; Verma, C. S.; Beuerman, R. W., Membrane active antimicrobial peptides: Translating mechanistic insights to design. *Front. Neurosci.* **2017**, *11* (73), 10.3389/fnins.2017.00073.
69. Cole, A. M.; Kim, Y.-H.; Tahk, S.; Hong, T.; Weis, P.; Waring, A. J.; Ganz, T., Calcitermin, a novel antimicrobial peptide isolated from human airway secretions. *FEBS Lett.* **2001**, *504*, 5-10.
70. Chairatana, P.; Nolan, E. M., Human α -defensin 6: A small peptide that self-assembles and protects the host by entangling microbes. *Acc. Chem. Res.* **2017**, *50*, 960-967.

71. Schitteck, B.; Hipfel, R.; Sauer, B.; Bauer, J.; Kalbacher, H.; Stevanovic, S.; Schirle, M.; Schroeder, K.; Blin, N.; Meier, F.; Rassner, G.; Garbe, G., Dermcidin: a novel human antibiotic peptide secreted by sweat glands. *Nat. Immunol.* **2001**, *2*, 1133-1137.
72. Chairatana, P.; Nolan, E. M., Molecular basis for self-assembly of a human host-defense peptide that entraps bacterial pathogens. *J. Am. Chem. Soc.* **2014**, *136*, 13267-13276.
73. Chu, H.; Pazgier, M.; Jung, G.; Nuccio, S.-P.; Castillo, P. A.; deJong, M. F.; Winter, M. G.; Winter, S. E.; Wehkamp, J.; Shen, B.; Salzman, N. H.; Underwood, M. A.; Tsohis, R. M.; Young, G. M.; Lu, W.; Lehrer, R. I.; Baumler, A. J.; Bevins, C. L., Human α -defensin 6 promotes mucosal innate immunity through self-assembled peptide nanonets. *Science* **2012**, *337*, 477-481.
74. Saito, H.; Miyakawa, H.; Tamura, Y.; Shimamura, S.; Tomita, M., Potent bactericidal activity of bovine lactoferrin hydrolysate produced by heat treatment at acidic pH. *J. Dairy Sci.* **1991**, *74*, 3724-3730.
75. Bellamy, W.; Takase, M.; Wakabayashi, H.; Kawase, K.; Tomita, M., Antibacterial spectrum of lactoferricin B, a potent bactericidal peptide derived from the N-terminal region of bovine lactoferrin. *J. Appl. Bacteriol.* **1992**, *73*, 472-479.
76. Bellamy, W.; Takase, M.; Yamauchi, K.; Wakabayashi, H.; Kawase, K.; Tomita, M., Identification of the bactericidal domain of lactoferrin. *Biochim. Biophys. Acta* **1992**, *1121*, 130-136.
77. Ilg, E. C.; Troxler, H.; Bürgisser, D. M.; Kuster, T.; Markert, M.; Guignard, F.; Hunziker, P.; Birchler, N.; Heizmann, C. W., Amino acid sequence determination of human S100A12 (P6, calgranulin C, CGRP, CAAF1) by tandem mass spectrometry. *Biochem. Biophys. Res. Commun.* **1996**, *225* (1), 146-150.
78. Robinson, M. J.; Hogg, N., A comparison of human S100A12 with MRP-14 (S100A9). *Biochem. Biophys. Res. Commun.* **2000**, *275* (3), 865-70.

79. Büchau, A. S.; Mohamed, H.; Kukova, G.; Lewerenz, V.; Kellermann, S.; Würthner, J. U.; Wolf, R.; Walz, M.; Gallo, R. L.; Ruzicka, T., S100A15, an antimicrobial protein of the skin: regulation by *E. coli* through Toll-Like Receptor 4. *J. Invest. Dermatol.* **2007**, *127* (11), 2596-2604.

Appendix A: Preparation of the Oxidized and Reduced Forms of Psoriasin (S100A7)

This Chapter is adapted from Meth. Mol. Biol. 2018, *Accepted*.

A. 1. Introduction

Human S100A7 (psoriasin), is a metal-chelating host-defense protein that is a member of the S100 family of Ca(II)-binding proteins.¹⁻⁴ Its antimicrobial activity has been the subject of several investigations. S100A7 has been reported to be an *E. coli*-cidal factor on the skin, human tongue, and female genital tract,⁵⁻⁷ and to have the capacity to permeabilize bacterial membranes.⁸ Furthermore, S100A7 has been shown to exhibit Zn(II)-mediated growth inhibitory properties against select bacterial and fungal species.^{9, 10} S100A7 may also act as a solid-phase barrier at the surface of epithelial cells, thus preventing microbial invasion during wound healing.¹¹ These examples indicate that the contributions of S100A7 to host defense are complex and multifaceted, and we reason that further biochemical and biophysical studies of the protein will inform the molecular basis for how it performs known and as-yet unidentified biological functions.

In its native state, apo S100A7 exists as a 22-kDa homodimer composed of two non-covalently linked antiparallel monomer subunits (101 residues, 11 kDa).^{12, 13} Each S100A7 monomer contains two Ca(II)-binding EF-hand domains. The C-terminal EF-hand domain is referred to as “canonical” and binds Ca(II) in a 7-coordinate manner. The “noncanonical” N-terminal EF-hand coordinates Ca(II) in a 6-coordinate geometry.^{1, 14} In addition to the Ca(II)-binding sites, S100A7 houses two His₃Asp motifs at the dimer interface, composed of residues His87 and His91 of one monomer, and residues His18 and Asp25 of the other monomer. The His₃Asp sites each coordinate Zn(II) in a distorted tetrahedral geometry to afford a 2:1 Zn(II):S100A7 homodimer complex.¹³

Each S100A7 polypeptide contains two Cys residues, Cys47 and Cys96, that can exist as free thiols (S100A7_{red}), or can form an intramolecular disulfide bond (S100A7_{ox}). Cys96, and hence the disulfide bond, is in close proximity to His91 of the metal-binding motif,¹²⁻¹⁴ and disulfide bond formation and reduction are reported to affect the transition-metal-binding properties and antimicrobial activity of S100A7.^{9, 10} Furthermore, both S100A7_{ox} and S100A7_{red} have been detected in human specimens,^{5-7,10} and biochemical studies support the notion that both redox

forms of S100A7 are physiologically relevant.^{9, 10}

Herein, we present a procedure for the purification of S100A7_{ox} and S100A7_{red}, and provide an overview of methods that can be employed to evaluate the redox state and integrity of the purified proteins. These methods are based on published biochemical studies of S100A7.⁹ Briefly, S100A7 is obtained in high yield and purity following recombinant expression in *E. coli* BL21(DE3) cells, two chromatography steps, and dialysis. The chromatography steps involve anion-exchange chromatography (AEC), followed by size-exclusion chromatography (SEC). S100A7_{red} is obtained by dialyzing and storing the protein in the presence of DTT, and a procedure that involves the Cu(II)-catalyzed oxidation of thiols to disulfides is employed to obtain S100A7_{ox}. While unusual, this oxidation method has been utilized to generate intra- and intermolecular disulfide bonds in other proteins, including S100B and oxyhemoglobin.¹⁵⁻¹⁷ The assays described in this chapter include analytical RP-HPLC, mass spectrometry, thiol quantification, and a competition titration for determining the stoichiometry of Zn(II) binding by S100A7.

A. 2. Materials

1. All solvents and chemicals are obtained from commercial suppliers and used as received.
2. All aqueous solutions are prepared using Milli-Q water (18.2 M Ω •cm, 0.22- μ m filter).
3. Protein concentrations are routinely quantified by using the calculated extinction coefficients for the S100A7 homodimer (ProtParam: ϵ_{280} = 9190 M⁻¹cm⁻¹ for S100A7_{ox} and ϵ_{280} = 8940 M⁻¹cm⁻¹ for S100A7_{red}). All protein concentrations are for the S100A7 homodimer and reported stoichiometries are for the S100A7 homodimer.

A. 2. 1. Commercial Materials and Reagents Preparations

1. The S100A7 synthetic gene is obtained from ATUM (formerly DNA2.0).

2. The pET41a expression vector is obtained from Invitrogen.
3. To reduce metal-ion contamination,¹ plastic spatulas are used to transfer reagents.
4. All metal stock solutions are prepared in acid-washed volumetric glassware and transferred to sterile polypropylene tubes for long-term storage.
5. Stock solutions of Zn(II) (100 mM, 100 mL) and Cu(II) (100 mM, 100 mL) are prepared from 99.999% anhydrous ZnCl₂ and 99.999% CuCl₂, respectively, and Milli-Q water.² Working solutions are prepared by diluting the stock solutions in Milli-Q water.
6. Stock solutions of Ca(II) (1 M, 100 mL) are prepared from 99.999% CaCl₂ and Milli-Q water. Working solutions are prepared by diluting the stock solutions in Milli-Q water.
7. Reagents employed for the indicated purposes were purchased from the following suppliers:

Purpose	Reagent	Supplier
Protein overexpression & purification	Luria Bertani (LB) 99.5% HEPES TraceSELECT NaCl Guanidinium hydrochloride (GuHCl) Dithiothreitol (DTT) EDTA disodium salt dehydrate Chelex resin	Becton Dickinson MilliporeSigma MilliporeSigma MilliporeSigma VWR Life Science VWR Life Science Bio-Rad
Solution studies	Ultral grade HEPES (free acid) Tris Hydrochloride DMSO Zincon monosodium salt ³	Calbiochem J. T. Baker MilliporeSigma MilliporeSigma
pH adjustment	TraceSELECT aqueous NaOH	Fisher Scientific

A. 2. 2. Zincon preparation

For the Zn(II) competition titration experiment, the competitor Zincon is employed.^{18, 19}

1. Stock solutions (≈ 10 mM) of Zincon are prepared in methanol, aliquoted into 200- μ L portions, and lyophilized to dryness.³
2. Each aliquot is thawed only once and dissolved in 200 μ L of Milli-Q water.
3. The Zincon concentration is confirmed (≈ 10 mM) by preparing a sample of Zn(II)-bound Zincon (≈ 20 μ M) and using the reported extinction coefficient of this complex at 621 nm.¹⁸⁻

20

A. 2. 3. Buffer for Protein Purification

Buffers employed for the purification of S100A7 are prepared with the compositions described below, and sterile-filtered through a 0.22- μ m bottle-top filter prior to use.

Buffer (1 L)	Composition
lysis buffer A:	50 mM Tris, 100 mM NaCl, 1 mM EDTA, 0.5% Triton X-100, pH 8.0, 5 mM DTT, 1 mM PMSF*
lysis buffer B:	50 mM Tris, 100 mM NaCl, 4 M GuHCl, pH 8.0
MonoQ buffer A:	20 mM HEPES, pH 8.0
dialysis buffer:	20 mM HEPES, pH 8.0
MonoQ buffer B:	20 mM HEPES, 1 M NaCl, pH 8.0
S75 buffer:	20 mM Tris, 100 mM NaCl, pH 7.5
metal-binding buffer:	75 mM HEPES, 100 mM NaCl, pH 7.0

* PMSF stock solutions (100 mM) are prepared in ethanol, stored at -20 °C, and added to lysis buffer A prior to lysis.

A. 2. 4. Equipment for Protein Purification.

1. An ÄKTA purifier (GE Lifesciences) housed at 4 °C and outfitted with a 150-mL Superloop (GE Lifesciences) is employed for chromatographic purification.
2. S100A7 is purified in two chromatographic steps: anion-exchange chromatography (AEC) is first performed using a MonoQ 10/100 GL column (GE Lifesciences), followed by size-exclusion chromatography (SEC) using a Superdex 75 10/300 GL column (GE Lifesciences).

A. 2. 5. Equipment for Optical Absorption Spectroscopy.

1. Optical absorption spectra are collected on a Beckman Coulter DU 800 spectrophotometer thermostatted at 25 °C with a Peltier temperature controller.
2. Quartz cuvettes (1-cm path length, Starna) are employed for all optical absorption measurements of samples of purified proteins.
3. Plastic cuvettes (1-cm path length, VWR) are employed for monitoring bacterial culture growth by the culture optical density at 600 nm (OD_{600}).
4. Observed OD_{600} values are reported throughout this protocol as benchmarks; however, these values will vary from instrument to instrument.

A. 3. Methods

The general methods described in this section can be used to purify S100A7 variants obtained by site-directed mutagenesis, as well as S100A15.⁴ S100A15 shares high sequence homology with S100A7, and the S100A15 homodimer has two His₃ sites that coordinate Zn(II).²¹⁻²⁴

A. 3. 1. Design of the synthetic gene for S100A7. A synthetic gene for human S100A7 optimized for *E. coli* codon usage includes an N-terminal *Nde*I restriction site (N-terminal Met residue

encoded by the *NdeI* site) and a C-terminal stop codon followed by an *XhoI* restriction site.

***E. coli* optimized nucleotide sequence *NdeI*-S100A7-*Stop-XhoI*:**

**CATATGAGCAACACCCAGGCAGAACGTAGCATTATTGGTATGATTGACATGTTTCACAAAT
ACACGCGCCGTGATGATAAGATCGACAAACCGTCGCTGCTGACGATGATGAAAGAGAACT
TCCCGAATTTTCTGTCTGCCTGCGATAAGAAAGGCACCAATTATCTGGCGGACGTGTTCGA
AAAGAAAGACAAAACGAGGACAAGAAGATCGACTTTAGCGAGTTCTTGTCCCTGCTGGGT
GATATCGCGACCGATTACCATAAGCAAAGCCACGGCGCTGCGCCGTGTAGCGGTGGTAGC
CAGTAACTCGAG**

**Translated sequence for *NdeI*-S100A7-*Stop-XhoI*: H M S N T Q A E R S I I G M I D M F H K Y
T R R D D K I D K P S L L T M M K E N F P N F L S A C D K K G T N Y L A D V F E K K D K N
E D K K I D F S E F L S L L G D I A T D Y H K Q S H G A A P C S G G S Q Stop L E**

A. 3. 2. Sub-cloning of the Human S100A7 Gene

1. The codon-optimized gene is obtained in the pJ201 vector from DNA 2.0.
2. The gene is amplified by PCR, digested with *NdeI/XhoI*, ligated into the pET-41a vector with T4 DNA ligase to afford pET41a-S100A7, and the resulting plasmids are transformed into chemically-competent *E. coli* TOP10 cells. This plasmid affords full-length S100A7 with no tags attached.
3. The pET41a-S100A7 expression plasmids (verified by DNA sequencing) are transformed into chemically-competent *E. coli* BL21(DE3) cells for protein overexpression.
4. Cell stocks of *E. coli* BL21(DE3) containing pET41a-S100A7 are prepared by growing *E. coli* in LB containing 50 µg/mL kanamycin to saturation. Aliquots were frozen in 25% glycerol and stored at -80 °C.

A. 3. 3. Purification of Human S100A7

The protein purification is described for an overexpression carried out in 2 L of culture, and the procedure affords protein yields that range from ≈30-50 mg/L.

Day 1 - Plating of *E. coli* BL21(DE3)

1. Using an inoculating loop, streak *E. coli* BL21(DE3) that contain pET41a-S100A7 onto a LB/agar plate containing 50 µg/mL kanamycin and incubate the plate for ≈20 h at 37 °C.

Day 2 - Overnight culture

2. To a sterile 250-mL baffled flask, add 40 mL of LB medium supplemented with 50 µg/mL kanamycin, inoculate the medium with a single colony from the LB/agar plate, and incubate the culture overnight (14-16 h, 37 °C, 150 rpm).
3. Prepare and autoclave 2 L of LB medium in a 4 L flask, and incubate the medium overnight at 37 °C.

Day 3 - Overexpression

4. Measure the optical density of the overnight culture at 600 nm (OD₆₀₀), which should be ≈1.5-2.5.
5. Add 50 µg/mL kanamycin (final concentration, 1:100 dilution from a 50 mg/mL stock solution in water) into the 4-L baffled flask containing 2 L of LB medium, and dilute a 20-mL volume (1:100 dilution) of the overnight culture into the medium. Transfer the resulting culture to an incubator-shaker (37 °C, 150 rpm).
6. Record the OD₆₀₀ of the bacterial culture every 30 min and induce overexpression at OD₆₀₀ ≈0.4 by adding IPTG to a final concentration of 125 µM. The cultures should reach an OD₆₀₀ ≈0.4 after about ≈1.5 h if the LB medium was pre-warmed overnight.
7. Incubate the culture (37 °C, 150 rpm) for an additional 4-4.5 h after induction, and measure the OD₆₀₀ of the cell culture, which should be ≈3.
8. Harvest the cells by centrifugation (3210 g, 15 min, 4 °C) and discard the supernatant.
9. Transfer the cell pellet to a sterile 50-mL centrifuge tube. Flash freeze the pellet in liquid nitrogen and store at -80 °C until future use.

This procedure typically yields ca. 4 g of cells / 2 L of culture (wet weight), which can be stored at -80 °C for up to four months. The overexpression can be evaluated by SDS-PAGE analysis (Coomassie stain) of the pre- and post-induction cell samples (whole cell lysate) using a 15% tricine gel. Successful overexpression should show an intense band at ≈11 kDa in the post-induction sample, corresponding to the S100A7 monomer (Figure A. 1).

Days 4-5 - Cell lysis and protein refolding

The following steps should be carried out at 4 °C and buffers should be equilibrated and stored at 4 °C (in a cold room or on ice).

10. Thaw a cell pellet from a 2-L culture on ice, and resuspend the pellet in 100 mL of lysis buffer A.
11. Transfer the resuspension to an ice-cold stainless-steel beaker and sonicate the resuspension on ice at 40% amplitude for 5 min (30 s on, 10 s off).
12. Centrifuge the resulting cell lysate (20,200 g, 10 min, 4 °C).
13. Transfer the supernatant, which contains soluble aggregated S100A7, to a 150-mL glass beaker housing a magnetic stir bar in the 4 °C cold room.
14. Weigh out 38 g of ammonium sulfate, and slowly add the entire portion to the supernatant over 15-20 min with constant stirring. This step yields a 60% saturated ammonium sulfate solution and causes contaminating proteins to precipitate.⁵

S100A7 is soluble in up to 80% saturated ammonium sulfate and remains in the soluble portion of the mixture.

15. Once the entire portion of ammonium sulfate has been added, allow the solution to stir gently at 4 °C for 60 min.
16. Centrifuge the mixture (20,200 g, 10 min, 4 °C) and quickly transfer the supernatant to an ice-cold clean glass beaker. If necessary, use a plastic spatula to remove any greasy clumps.

17. Weigh out 25 g of ammonium sulfate, and slowly add the entire portion to the supernatant over 10 min while stirring to bring the final saturation level of ammonium sulfate to 90%.

S100A7 precipitates at an ammonium sulfate saturation level of 90%.

18. Once the entire portion of ammonium sulfate has been added, allow the solution to stir gently at 4 °C for 60 min.

19. Centrifuge the mixture (20,200 g, 10 min, 4 °C). Quickly decant the supernatant to prevent the pellet, which contains S100A7, from re-dissolving.

20. Keep the pellet at 4 °C, and add a 100-mL portion of lysis buffer B to resolubilize the pellet. Incubate the mixture on ice or in the cold room with occasional and gentle swirling to dissolve the S100A7 pellet.

This steps typically requires ca. 30 min and affords S100A7 in a soluble and denatured state. The following step allows for the refolding of S100A7.

21. Transfer the resulting supernatant, which contains denatured S100A7, to a dialysis bag (Spectropor3 10 KDa MWCO) for three rounds of dialysis against 4L of dialysis buffer for >12 h each. Include 1 mM DTT in the dialysis buffer for the first round of dialysis, but not for the latter rounds.⁶

After dialysis, the refolded protein is purified by AEC and SEC – see Days 6-7.

22. The day before the chromatography steps, pre-equilibrate the S75 column with 1 column volume (CV) of S75 buffer.⁷

Days 6-7 - Protein purification using an FPLC ÄKTA purifier (AEC and SEC)

Over the course of the refolding process described above, a small portion of S100A7 forms an insoluble aggregate and accumulates at the bottom of the dialysis bag as a white precipitate.

23. Pellet the precipitated protein from the dialysate by centrifugation (20,200 g, 10 min, 4 °C). Decant and vacuum filter the supernatant using a 0.22- μ m bottle-top filter.⁸

24. Load the filtrate (\approx 120 mL) onto the Superloop.

25. Wash the MonoQ column with 2 CV of Milli-Q water, followed by equilibration with 2 CV of MonoQ buffer A, 2 CV of MonoQ buffer B, and 2 CV of MonoQ buffer A (2 mL / min flow rate).
26. Load ≈60 mL of the protein solution from the Superloop onto the MonoQ column and elute the proteins with a gradient of 0–10% B (A: MonoQ buffer A, B: MonoQ buffer B) over 12 CV at a flow rate of 2 mL / min. (Figure A. 2). This step should take between 110-130 min depending on the injection volume. The fractions corresponding to the folded S100A7 homodimer elute at ≈5% B (Figure A. 2).
27. Repeat steps 25 and 26, loading the rest of the protein sample from the Superloop.
28. Collect and pool the fractions containing dimeric S100A7 (Figure A. 2) and concentrate the protein by centrifugation to a final volume of ≈10 mL (15-mL Amicon 10-kDa MWCO spin filter). This step typically requires 2-3 rounds of centrifugation (3210 g, 20 min per round, 4 °C).
29. Load the concentrated S100A7 sample onto the pre-equilibrated S75 column,^{vii} and elute the protein over 1 CV at a flow rate of 1 mL / min.
30. Collect and pool the fractions containing S100A7 (Figure A. 3) and measure the protein concentration using the calculated extinction coefficient for S100A7_{red}. At this stage, the protocol should yield ≈20-25 mL of ≈90 μM protein that is predominantly S100A7_{red} (Figure A. 4).

Steps 31-35 describe the step to obtain homogeneous S100A7_{red} and S100A7_{ox}.⁹

31. For S100A7_{red}, dialyze the purified protein against 1 L of metal-binding buffer, containing 1 mM DTT and ≈10 g Chelex resin (Biorad), at 4 °C for ≈12 h (Spectropor3 3500 Da MWCO dialysis bag). Analytical HPLC (Table A. D. 1, Figure A. 4) may be employed to ascertain the speciation of S100A7 and confirm it is fully reduced prior to the next steps.
32. The dialysate containing S100A7_{red} is then passed through a 0.22-μm syringe filter to remove any contaminating Chelex.

33. Go to step 38 for the storage of S100A7_{red}.
34. For the Cu(II)-catalyzed oxidation to obtain S100A7_{ox}, dilute the purified protein from step 30 \approx 4-fold to \approx 20 μ M in S75 buffer (equilibrated at room temperature), and transfer the solution to a 150-mL glass beaker.
35. Add three equivalents of Cu(II) (60 μ L from a 100-mM Cu(II) stock solution for 100 mL of 20 μ M S100A7) dropwise to the protein solution, and incubate the mixture at room temperature for 2 h with stirring.¹⁰ Some precipitate may form over the course of the oxidation, and can be removed by centrifugation (3210 g, 10 min, 4 °C). After 2 h, analyze a reaction aliquot by analytical RP-HPLC to confirm that the reaction reached completion (Figure A. 4).
36. Transfer the resulting solution of S100A7_{ox} to a Spectropor3 3500 MWCO dialysis bag and dialyze overnight against 1 L of metal-binding buffer containing \approx 10 g Chelex resin, and 1 mM EDTA at 4 °C.
37. Remove the EDTA by two rounds of dialysis against the metal-binding buffer (2 x 4 L, \approx 12 h per dialysis, 4 °C).
38. Following dialysis, S100A7_{red} and S100A7_{ox} are concentrated using a 15-mL Amicon 10-kDa MWCO spin filter (3210 g, 4 °C) to $>$ 500 μ M, partitioned into sterile microcentrifuge tubes as 50- μ L aliquots, flashed frozen in liquid nitrogen, and stored at -80 °C until further use. Prior to any experiments, the proteins are analyzed by SDS-PAGE and analytical RP-HPLC (Figure A. 5).¹¹

A. 3. 4. Zinc Competition Titration between S100A7 and Zincon

This procedure allows for the Zn(II):S100A7 homodimer stoichiometry to be ascertained. The titration should provide a 2:1 stoichiometry. This titration can be performed at 25 °C or room temperature. Experiments with Zincon are performed in the dark.

1. In an acid-washed quartz cuvette, prepare a 2-mL solution containing Zincon (20 μM) from the Zincon stock solution in the metal-binding buffer, $\pm 2 \text{ mM Ca(II)}$, and record the optical absorption spectrum. Check that the spectrum agrees with the literature spectrum of the metal-free Zincon.²⁰
2. Add an aliquot of the S100A7 stock solution (10 μM final concentration, reduced or oxidized form) to the Zincon solution, gently swirl the cuvette to mix the sample, and record the optical absorption spectrum of this mixture. Provided a negligible dilution factor, the Zincon spectrum should be unchanged in the absence and presence of apo S100A7.
3. Titrate the mixture containing Zincon and S100A7 with Zn(II) by adding Zn(II) in 2.5 μM increments until the Zn(II) concentration is 40 μM (1 μL from a 5-mM Zn(II) stock solution per addition). After each Zn(II) addition, gently swirl the cuvette and allow the sample to equilibrate for 2 min before the optical absorption spectrum is collected.
4. Plot the absorbance at 621 nm versus the $[\text{Zn(II)}] / [\text{S100A7}]$ ratio.

For the competition titration with S100A7_{red}, the thawed protein sample must be immediately buffer-exchanged to remove DTT (3 x 5 min, 20,200 g, 4 °C), mixed with Zincon, and then titrated with Zn(II). We observed no air-oxidation of S100A7_{red} over the course of the titration (≈ 30 min) as ascertained by analytical RP-HPLC.

A. 4. Biochemical characterization of human S100A7

Following the purification of S100A7, we recommend employing standard biochemical techniques to evaluate the integrity of the purified protein.⁹ These methods include SDS-PAGE, mass spectrometry, metal analysis by inductively-coupled plasma mass spectrometry (ICP-MS), analytical RP-HPLC, thiol quantification assays using DTDP (Table A.1, Figure A. 5). The experimental conditions for these procedures, as well as circular dichroism spectroscopy and inductively coupled plasma mass spectrometry, are found in *reference 9*.

Moreover, a competition titration between S100A7 and the colorimetric Zn(II) indicator Zincon ($K_{d,Zn} \approx 10$ M)^{18, 19} should be carried out to confirm that the purified protein has the correct Zn(II)-binding stoichiometry (Section 3.4). Zincon is a colorimetric probe that displays an increase in absorbance at 621 nm upon binding Zn(II) (Figure A. 6). When Zn(II) is titrated to a solution mixture containing Zincon and S100A7, both S100A7_{ox} and S100A7_{red} outcompete Zincon for two equivalents of Zn(II). This behavior is expected because the protein has two His₃Asp sites that coordinate Zn(II) with sub-nanomolar affinity.^{9, 12, 13} If the competition shows that S100A7 outcompetes Zincon for less than two equivalents of Zn(II), then the purified protein may have a metal contamination.

A. 5. Notes

1. Because S100A7 is a metal-binding protein, we employ high-purity buffer reagents and plastic or Teflon-coated spatulas to minimize the risk of metal contamination from buffers. These precautions, as well as extensive dialysis against Chelex resin (and EDTA for S100A7_{ox} obtained by Cu(II)-catalyzed oxidation), afford apo S100A7 in high yield and purity.
2. ZnCl₂ is hygroscopic and is therefore stored in a desiccator to prevent exposure to moisture.
3. We have found that the quality of the Zincon reagent depends on the supplier. We recommend purchasing Zincon monosodium salt from MilliporeSigma. Furthermore, we have observed decomposition of the compound when stored at -20 °C in DMSO. If stored as a stock solution at -20 or -80 °C, we recommend checking the integrity of the Zincon stock solution by optical absorption spectroscopy prior to use. We also recommend storing Zincon as a powder at -80 °C if the reagent will be used infrequently, and we recommend making a new stock solution (10 mM) immediately prior to each experiment.
4. The expression and purification procedure described herein can be adapted for other S100A7 variants as follows:
 - a. For non-Cys containing variants of S100A7, including S100A7-Ala and S100A7-

Ser that contain Cys47→Ser/Ala and Cys96→Ser/Ala mutations,⁹ the protocol for purification of S100A7_{red} can be followed, with the addition of DTT in the first dialysis step after SEC (Step 31) omitted.

- b. We have designed and evaluated S100A7 Δ , a variant of S100A7 that lacks the His₃Asp metal-binding sites because the four residues that comprise the His₃Asp motif of S100A7 (His18, Asp25, His87, and His91) have been replaced by noncoordinating Ala residues.⁹ S100A7 Δ_{ox} can be obtained by modifying the Cu(II)-catalyzed oxidation protocol for S100A7 such that two equivalents of Cu(II) are employed rather than three equivalents. During the oxidation reaction, a precipitate will slowly appear. Following a 2-h incubation at room temperature, the precipitate is removed by centrifugation, and the resulting soluble protein-Cu mixture is allowed to stir overnight at room temperature. This procedure results in the complete oxidation of S100A7 Δ to S100A7 Δ_{ox} .
 - c. The protocols described for preparing S100A7_{ox} and S100A7_{red} can be used to obtain S100A15_{ox} and S100A15_{red} (unpublished work). The Cys residues of S100A7 are conserved in S100A15.
5. This step should be carried out with caution by slow addition of ammonium sulfate in a scoop-by-scoop manner and gentle stirring, in order to minimize S100A7 precipitation.
 6. For the dialysis procedure described in Step 21, DTT is preferred as a reducing agent over TCEP because it is less expensive and because more protein precipitation occurs during the refolding process when TCEP is employed. Furthermore, we find that including 1 mM DTT only in the first round of dialysis minimizes protein precipitation during refolding, as well as formation of an S100A7 adduct (observed by SDS-PAGE) that appears to form and persist when DTT is included in two or more rounds of dialysis (data not shown). We suspect that the identity of the protein-adduct is S100A7-DTT.

7. We chose to purify S100A7 in Tris buffer for the SEC step (S75 buffer; 20 mM Tris, 100 mM NaCl, pH 7.0) because we observed significant precipitation during the subsequent Cu(II)-catalyzed oxidation step when using HEPES buffer.
8. We recommend using vacuum filtration over gravity filtration for step 23 because the sample tends to clog the filter membrane, making gravity filtration more time-consuming.
9. The protein collected after SEC can be split into two batches for subsequent purification of S100A7_{ox} and S100A7_{red}. The volume given in Step 34 (100 mL of 20 μ M S100A7) assumes that the protein batch is not split at step 30.
10. Upon addition of Cu(II), the clear and colorless solution turns yellowish. The origin of this color change is unclear.
11. The metal content of purified S100A7_{ox} can be analyzed by inductively coupled plasma–mass spectrometry (ICP-MS). We routinely find that S100A7_{ox} contains \approx 0.03 and \approx 0.04 equivalents of Cu and Zn, respectively. These results indicate that the dialysis step removed the Cu(II) introduced during the oxidation step.

A. 6. Figures and Tables

Table A.1. Characterization of S100A7

Protein	HPLC Retention Time (min) ^a	Free thiol ^b	Calculated Mass (g/mol)	Observed Mass (g/mol) ^c
S100A7 _{ox}	16.4	0.11 ± 0.03	11 454.9	11 455.4 11 324.0 (-Met1)
S100A7 _{red}	18.4	4.16 ± 0.45	11 456.9	11 457.4 11 326.0 (-Met1)

a Retention times determined by analytical RP-HPLC. A 45- μ L aliquot of 30 μ M protein was mixed with 100 μ L of 6 M GuHCl, and 5 μ L of 6% aqueous TFA. The sample was centrifuged (5 min, 20,200 g, 4 °C) and a 120- μ L portion of supernatant was transferred to an HPLC vial. Analytical RP-HPLC was performed using a Proto C4 column (5- μ m pore, 4.6 x 250 mm, Higgins Analytical Inc.), an 100- μ L injection volume, a gradient of 35–50% B over 30 min, and a flow rate of 1 mL/min (solvent A : water + 0.1% TFA, solvent B: MeCN + 0.1% TFA). **b** Free thiol content determined by using the DTDP assay.⁹ The reported errors are the SDM (n=2). **c** High-resolution mass spectrometry was performed on an Agilent 1290 series LC system equipped with an Agilent 6230 TOF system housing Agilent Jetstream ESI source. An Agilent Poroshell 300SB-C18 column (5- μ m pore) was employed with a flow rate of 0.2 mL / min (solvent A: water + 0.1% formic acid, solvent B: MeCN + 0.1% formic acid). Protein samples (10 μ M) were prepared in Milli-Q water and 1 μ L was injected for each analysis.

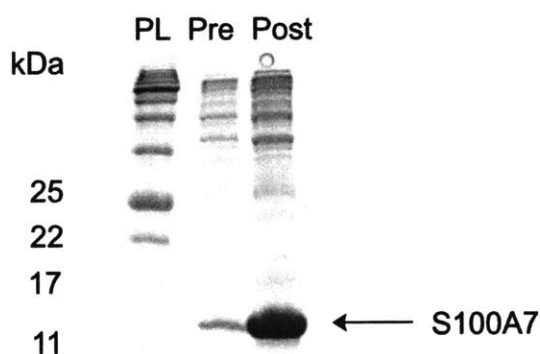


Figure A. 1. Expression of S100A7. SDS-PAGE gel (15% Tris-HCl, tricine gel) of pre- and post-induction samples of S100A7. Protein Ladder (PL): P7712s color prestained protein standard broad range (New England Biolabs).

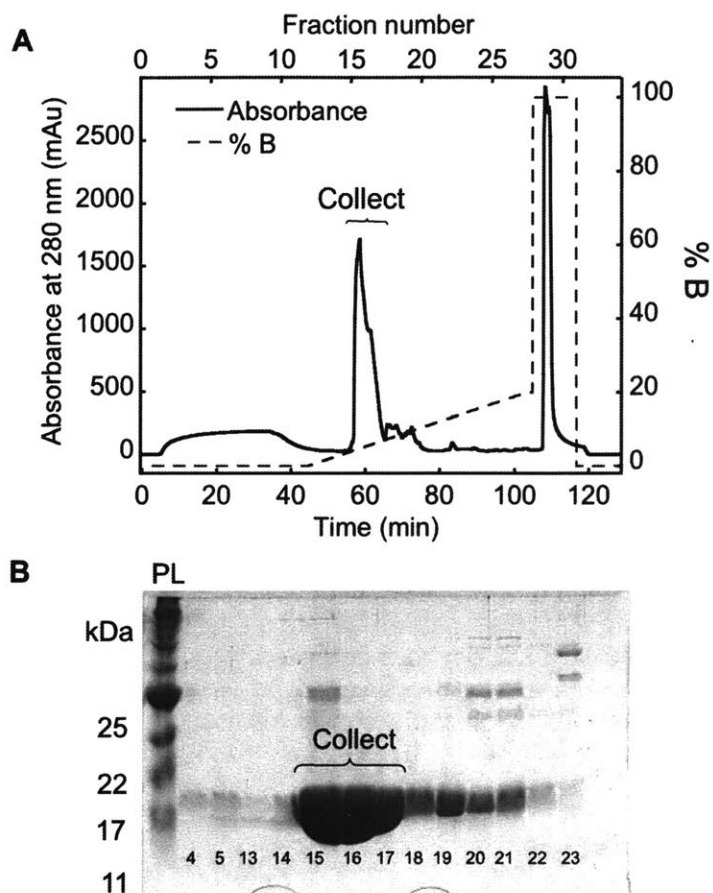


Figure A. 2. Elution profile of S100A7 from the MonoQ column. (A) S100A7 was eluted over 12 CV with a gradient of 0–10 % MonoQ buffer B at a flow rate of 2 mL/min. Fractions 15–17 were collected and pooled for the next chromatography step. (B) SDS-PAGE gel (15% Tris-HCl, tricine gel) of select fractions from the MonoQ purification step. Protein Ladder (PL): P7712s color prestained protein standard broad range (New England Biolabs). As a precaution, the flow through is routinely collected, which corresponds to fractions 1–10.

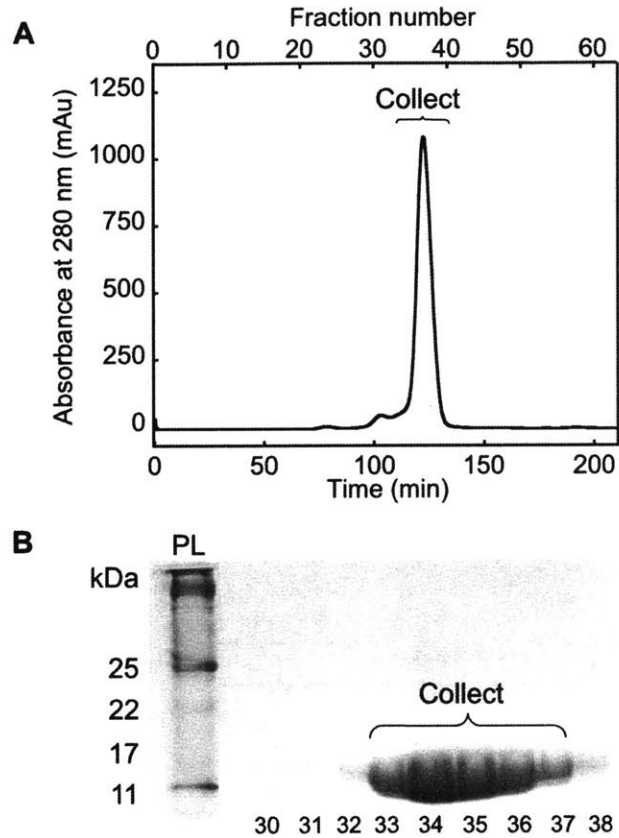


Figure A. 3. Elution profile of S100A7 from the S75 column. (A) S100A7 was eluted over 1 CV in S75 buffer at a flow rate of 1 mL/min. Fractions 33–37 were collected and pooled for the subsequent step. (B) SDS-PAGE gel (15% Tris-HCl, tricine gel) of select fractions from the S75 purification step. Protein Ladder (PL): P7712s color prestained protein standard broad range (New England Biolabs).

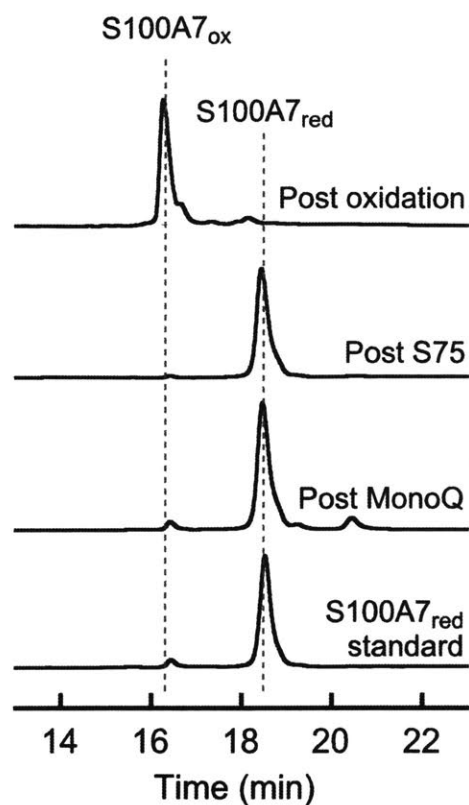


Figure A. 4. Analytical HPLC traces showing S100A7 over the course of the purification and Cu(II)-catalyzed oxidation. A 45- μ L aliquot of 30 μ M protein was mixed with 100 μ L of 6 M GuHCl, and 5 μ L of 6% aqueous TFA. The sample was centrifuged and a 120- μ L portion was transferred to an HPLC vial. An 100- μ L aliquot was injected onto the HPLC outfitted with a C4 column. A gradient of 35–50% B over 30 min at 0.5 mL / min was employed. Solvent A: water + 0.1 % TFA, solvent B: MeCN + 0.1 % TFA.

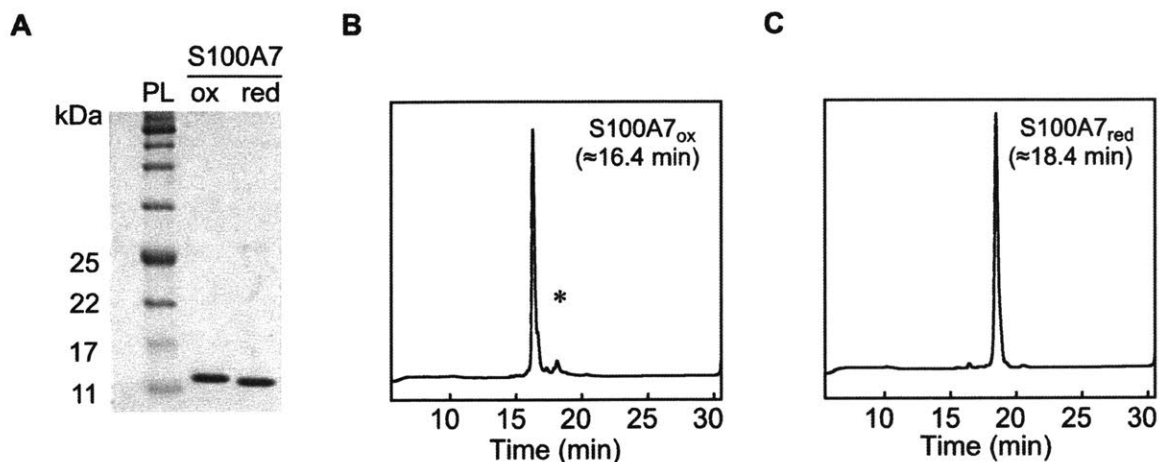


Figure A. 5. SDS-PAGE purity gel and analytical HPLC traces of S100A7_{ox} and S100A7_{red}. (A) SDS-PAGE purity gel (15% Tris-HCl, tricine gel) of S100A7_{ox} and S100A7_{red}. Protein Ladder (PL): P7712s color prestained protein standard broad range (New England Biolabs). (B) and (C) HPLC chromatograms (220 nm absorption) of S100A7_{ox} and S100A7_{red}, respectively. A 45- μ L aliquot of 30 μ M protein was mixed with 100 μ L of 6 M GuHCl, and 5 μ L of 6% aqueous TFA. The sample was centrifuged and a 120- μ L portion was transferred to an HPLC vial. An 100- μ L aliquot was injected onto the HPLC outfitted with a C4 column. A gradient of 35–50% B over 30 min at 0.5 mL / min was employed. Solvent A: water + 0.1 % TFA, solvent B: MeCN + 0.1 % TFA. An asterisk (*) indicates the position of the isoform of S100A7 missing the N-terminal methionine.

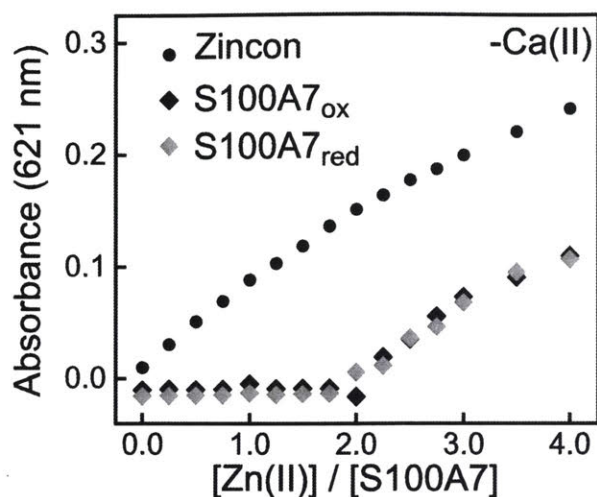


Figure A. 6. S100A7 outcompetes Zincon for two equivalents of Zn(II). Representative plot showing the response of 20 μM Zincon to Zn(II) in the presence of 10 μM S100A7 proteins in metal-binding buffer at 25 $^{\circ}\text{C}$.

A. 7. Acknowledgements

Our current studies of psoriasin are supported by the National Science Foundation (CHE-1352132).

A. 8. References

1. Donato, R.; Canon, B. R.; Sorci, G.; Riuzzi, F.; Hsu, K.; Weber, D. J.; Geczy, C. L., Functions of S100 proteins. *Curr. Mol. Med.* **2013**, *13*, 24-57.
2. Zackular, J. P.; Chazin, W. J.; Skaar, E. P., Nutritional immunity: S100 proteins at the host-pathogen interface. *J. Biol. Chem.* **2015**, *290* (31), 18991-18998.
3. Cunden, L. S.; Nolan, E. M., Bioinorganic explorations of Zn(II) sequestration by human S100 host-defense proteins. *Biochemistry* **2018**, *57* (11), 1673-1680.

4. Jinquan, T.; Vorum, H.; Larsen, C. G.; Madsen, P.; Rasmussen, H. H.; Gesser, B.; Etzerodt, M.; Honoré, B.; Celis, J. E.; Thestrup-Pedersen, K., Psoriasin: A novel chemotactic protein. *J. Invest. Dermatol.* **1996**, *107* (1), 5-10.
5. Meyer, J. E.; Harder, J.; Sipos, B.; Maune, S.; Klöppel, G.; Bartels, J.; Schröder, J. M.; Gläser, R., Psoriasin (S100A7) is a principal antimicrobial peptide of the human tongue. *Mucosal Immunol.* **2008**, *1* (3), 239-243.
6. Mildner, M.; Stichenwirth, M.; Abtin, A.; Eckhart, L.; Sam, C.; Gläser, R.; Schröder, J. M.; Gmeiner, R.; Mlitz, V.; Pammer, J.; Geusau, A.; Tschachler, E., Psoriasin (S100A7) is a major antimicrobial component of the female genital tract. *Mucosal Immunol.* **2010**, *127*, 602-609.
7. Gläser, R.; Harder, J.; Lange, H.; Bartels, J.; Christophers, E.; Schröder, J. M., Antimicrobial psoriasin (S100A7) protects human skin from *Escherichia coli* infection. *Nat. Immunol.* **2005**, *6* (1), 57-64.
8. Michalek, M.; Gelhaus, C.; Hecht, O.; Podschun, R.; Schröder, J. M.; Leippe, M.; Grötzinger, J., The human antimicrobial protein psoriasin acts by permeabilization of bacterial membranes. *Dev. Comp. Immunol.* **2009**, *33* (6), 740-746.
9. Cunden, L. S.; Brophy, M. B.; Rodriguez, G. E.; Flaxman, H. A.; Nolan, E. M., Biochemical and functional evaluation of the intramolecular disulfide bonds in the zinc-chelating antimicrobial protein human S100A7 (Psoriasin). *Biochemistry* **2017**, *56* (43), 5726-5738.
10. Hein, K. Z.; Takahashi, H.; Tsumori, T.; Yasui, Y.; Nanjoh, Y.; Toga, T.; Wu, Z. H.; Grötzinger, J.; Jung, S.; Wehkamp, J.; Schroeder, B. O.; Schröder, J. M.; Morita, E., Disulphide-reduced psoriasin is a human apoptosis-inducing broad-spectrum fungicide. *Proc. Natl. Acad. Sci. U. S. A.* **2015**, *112* (42), 13039-13044.
11. Lee, K. C.; Eckert, R. L., S100A7 (Psoriasin) - Mechanism of antibacterial action in wounds. *J. Invest. Dermatol.* **2007**, *127* (4), 945-957.

12. Brodersen, D. E.; Etzerodt, M.; Madsen, P.; Celis, J. E.; Thøgersen, H. C.; Nyborg, J.; Kjeldgaard, M., EF-hands at atomic resolution: the structure of human psoriasin (S100A7) solved by MAD phasing. *Structure* **1998**, *6* (4), 477-489.
13. Brodersen, D. E.; Nyborg, J.; Kjeldgaard, M., Zinc-binding site of an S100 protein revealed. Two crystal structures of Ca²⁺-bound human psoriasin (S100A7) in the Zn²⁺-loaded and Zn²⁺-free states. *Biochemistry* **1999**, *38* (6), 1695-1704.
14. Gifford, J. L.; Walsh, M. P.; Vogel, H. J., Structures and metal-ion-binding properties of the Ca²⁺-binding helix-loop-helix EF-hand motifs. *Biochem. J.* **2007**, *405* (2), 199-221.
15. Matsui Lee, I. S.; Suzuki, M.; Hayashi, N.; Hu, J.; Van Eldik, L. J.; Titani, K.; Nishikimi, M., Copper-dependent formation of disulfide-linked dimer of S100B protein. *Arch Biochem Biophys* **2000**, *374* (2), 137-141.
16. Harrison, C. A.; Raftery, M. J.; Walsh, J.; Alewood, P.; Iismaa, S. E.; Thliveris, S.; Geczy, C. L., Oxidation regulates the inflammatory properties of the murine S100 protein S100A8. *J. Biol. Chem* **1999**, *274* (13), 8561-8569.
17. Smith, R. C.; Reed, V. D., Inhibition by thiols of copper(II)-induced oxidation of oxihemoglobin *Chem.-Biol. Interact.* **1992**, *82* (2), 209-217.
18. Talmard, C.; Bouzan, A.; Faller, P., Zinc binding to amyloid-beta: Isothermal titration calorimetry and Zn competition experiments with Zn sensors. *Biochemistry* **2007**, *46* (47), 13658-13666.
19. Maret, W.; Vallee, B. L., Thiolate ligands in metallothionein confer redox activity on zinc clusters. *Proc. Natl. Acad. Sci. U. S. A.* **1998**, *95* (7), 3478-3482.
20. Kocyla, A.; Pomorski, A.; Krezel, A., Molar absorption coefficients and stability constants of Zincon metal complexes for determination of metal ions and bioinorganic applications. *J. Inorg. Biochem.* **2017**, *176*, 53-65.

Appendix B: S100A12 and Pra1: Competition for Zn(II) at the Host-Pathogen Interface

B. 1. Introduction

In order to survive in a nutrient starved environment, such as in the human host, and cause infection, pathogens have developed elaborate ways to acquire essential metal ions from the host, through the use of high-affinity metal transporters and metallophores.^{1,2} High-affinity metallo-transporters can be upregulated under conditions of growth within the host. One example includes the high-affinity metal transporter of *C. albicans*, Zrt1 that has been found to be upregulated under *in vitro* growth conditions in Zn(II)-deprived medium.^{3,4} Metallophores are small molecules or proteins that are released in the extracellular space to scavenge essential metal ions—such as Zn(II)—and deliver the metal of interest back to the pathogen through a transporter system. *C. albicans* possesses a zincophore system, whereby it secretes a scavenger protein Pra1, which goes in the extracellular space and coordinates Zn(II).^{5,6} Pra1 can then deliver Zn(II) to *C. albicans* by associating with the high-affinity Zn(II) transporter Zrt1, and hand off Zn(II) to Zrt1, which then transports Zn(II) into the fungus (Figure B. 1).⁶ The host fights back by releasing a number of antimicrobial factors at sites of infection to combat the growth of invading pathogens by sequestering Zn(II) and other essential metal ions.⁷ This process is often termed nutritional immunity.^{1,2,7} One such antimicrobial factor is S100A12. S100A12 is released from neutrophils, and possesses antifungal activity as a result of Zn(II) sequestration.⁸ We therefore question whether treatment of *C. albicans* cultures with S100A12 would result in the upregulation of Pra1 and/or other components of the Zn(II) uptake machinery of *C. albicans*. We postulate that the Zn(II)-starved environment created by S100A12 encourages deployment of such fungal factors.

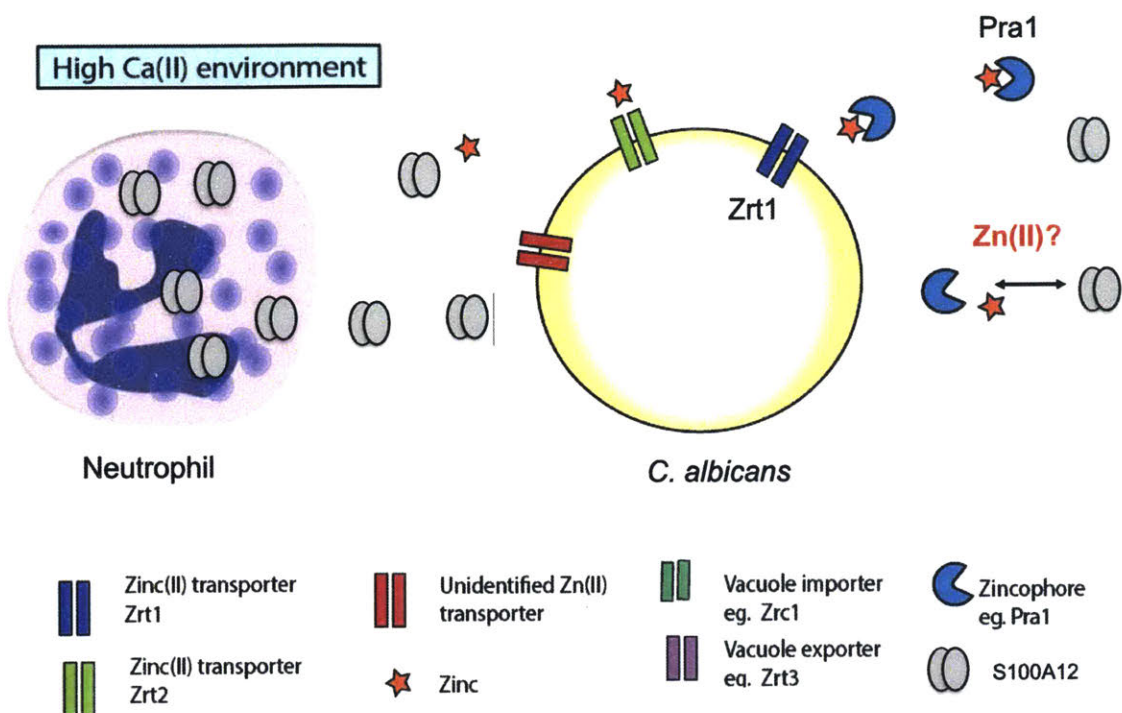


Figure B. 1. Schematic of Zn(II) competition between *C. albicans* and S100A12 at the host-pathogen interface. Pra 1 (blue) competes with S100A12 (grey) for bioavailable Zn(II).

In order to test the notion that Pra1 and S100A12 compete under our assay conditions, we obtained single knockout strains of *C. albicans* *PRA1*^{-/-} and *ZRT1*^{-/-}, which are missing the proteins Pra1 and Zrt1 respectively.⁹ We expect that these single knockout strains will be more susceptible to S100A12 if these proteins are involved in Zn(II) acquisition and competition against S100A12 under our assay conditions. To the best of our knowledge, there has been no thorough characterization of the Zn(II)-binding properties of Pra1, and there are no available crystal structures of Pra1 that inform us on structural features of the protein, such as its oligomerization state, and/or the coordination and stoichiometry of Zn(II) binding.

The set of preliminary data obtained so far provides evidence for competition between Pra1⁶—the first fungal metallophore characterized—and S100A12, and suggests that these two players may compete for Zn(II) at sites of infections.

B. 2. Experimental Section

B. 2. 1. Antifungal Assays with S100A12

The antifungal activity of S100A12 was tested against the *C. albicans* SC5314 WT strain, and the single knockout strains, *PRA1*^{-/-} and *ZRT1*^{-/-}. Fungal strains were stored as glycerol stocks (75% YPD, 25 % glycerol) at -80 °C. For assays performed in Zn(II)-replete conditions, the medium used for the overnight culture was YPD, and the medium used for antifungal assays was AMA medium (Tris:YPD). The recipe for the AMA medium is as follows; 32:68 (v:v) ratio of YPD and AMA buffer (20 mM Tris-HCl, 100 mM NaCl, pH 7.5). For antifungal assays under Zn(II)-deplete conditions, the overnight cultures were grown in Zn(II)-depleted YPD, and the antifungal assays performed with Zn(II)-depleted AMA medium. Briefly, YPD or AMA medium (Tris:YPD) was depleted of Zn(II) by pretreating it with 125 µg/mL of S100A12 for 1 h at r.t. The samples were then centrifuged (3750 rpm, 20 min) using a spin filter with MWCO of 10 kDa to separate S100A12 from the medium. The flow-through was collected and used as a Zn(II)-depleted medium. ICP-MS analysis revealed that Zn(II)-depleted YPD and Zn(II)-depleted AMA medium typically contained about 1-1.5 µM and 400-600 nM Zn respectively. Overnight cultures were inoculated from single colonies on agar plates into 10 mL of YPD or Zn(II)-depleted YPD in a 250-mL baffled flask and grown for 20-24 h (37 °C, 150 rpm). The next day, the overnight cultures were diluted 1:50 into 10 mL of YPD or Zn(II)-depleted YPD and allowed to grow to mid-log phase (OD₆₀₀ = 1.0) in a 250-mL baffled flask (37 °C, 150 rpm). The cultures took about 3.5 h and 6 h to reach mid-log phase in YPD and Zn(II)-depleted YPD respectively. The cultures were then diluted 1:500 into Tris:YPD or Zn(II)-depleted Tris:YPD medium. A 90 µL aliquot of the dilution added to a well containing 10 µL of the 10x protein stock in 96-well plates (Corning, Inc.). For samples containing excess Ca(II), the AMA buffer was supplemented with 3 mM Ca(II). Each condition was repeated in three wells, and values for each experiment was averaged from these three wells. The plates were then covered with a wet paper towel, and wrapped in saran wrap to minimize

evaporation over the course of incubation. The plates were incubated in an incubator-shaker (37 °C, 150 rpm, t = 24 h). The growth was monitored by OD₆₀₀ at regular intervals using a Synergy HT plate reader (BioTek). To resuspend cultures that formed clumping at the bottom of the wells, the plates were shaken vigorously prior to OD₆₀₀ measurement. Each set of experiments was performed twice with two different protein and medium stocks. The mean and SEM are reported.

B. 2. 2. Extraction of RNA and Synthesis of cDNA from C. albicans Cultures Treated with S100A12

Antifungal assays were set up as described for the antifungal assays with S100A12 (vide supra), except for the steps described below. In order to obtain enough genomic RNA, these assays were set up in 24-well plates (Corning, Inc.), and each well contained 2 mL of culture. Only one well per condition was setup. Instead of adding 90- μ L of *C. albicans* culture and 10 μ L of 10x protein, 2 mL of *C. albicans* culture (previously diluted 1:500 in Tris:YPD) was added to the well, and concentrated S100A12 (previously buffer-exchanged into AMA buffer) was added directly to the well to a final concentration of 125 μ g/mL (-Ca(II)) and 62.5 μ g/mL (+Ca(II)). Typically, less than 50 μ L of protein was added per well. The plates were then covered with a wet paper towel, and wrapped in saran wrap to minimize evaporation over the course of incubation, and were incubated in an incubator-shaker (37 °C, 150 rpm, t = 24 h). In order to analyze the effect of S100A12 on the transcriptional levels of Zn(II)-acquisition-related machinery in *C. albicans*, total RNA was extracted from *C. albicans* after 24 h of incubation with the MasterPure Yeast RNA Purification Kit (Epicentre).¹⁰ cDNA was generated from 1 μ g of extracted RNA by using the High-Capacity cDNA Reverse Transcription Kit (Thermo Fisher).¹¹ cDNA samples were stored at -80 °C until use. Each set of experiments was performed at least three times with at least two different protein and medium stocks. The mean and STD are reported.

B. 2. 3. Quantitative Real-time PCR

All oligonucleotide primers used in these experiments are listed in Table B.1. Real-time PCR was performed using the LightCycler 480 SYBR Green I Master (Roche, Indianapolis, IN) and the Roche Lightcycler 480 II Real-time machine (MIT MicroBio Center) with the following run protocol: 50 °C (2 min), 95°C (3 min), and then 45 cycles of 95 °C (15 s), 50 °C (15 s), and 60 °C (1 min). Cycle threshold (C_T) values were obtained and used for analysis. The efficiency of each PCR reaction was calculated using Real-time PCR Miner online software (<http://ewindup.info/miner/index.htm>).¹² Fold changes were calculated using the $\Delta\Delta$ -C_T method in comparison to the average transcription levels of reference genes ACT1 and PMA1.¹³ The C_T values were obtained using two pairs of primers for each gene. The experiments were conducted in three independent trials and the results are presented with errors shown as STD.

Table B. 1. List and sequences of primers used for qRT-PCR analysis.

Primer Name	Sequence
Pra1 F1	TAGCTAACATGCCAGGGAC
Pra1 R1	ACCTCAGCACTTGCAGTCTC
Pra1 F2	TACAGGTTACGATTGGCGGG
Pra1 R2	TGAGCTTCTTGCAACCCAGT
Zrt1 F1	AGCTGACCCCTACTGATGGT
Zrt1 R1	AGCAGACAGGTTTCAGTGGTG
Zrt1 F2	TCCATGCTGGTGTGAGCAT
Zrt1 R2	GGACCAAAGACCCGATACCA
Gat2 F1	GTCTACCGTTGGCGGTACTION
Gat2 R1	ACTTTGACAGGCAATGTAGGTG
Zrt1 F1	GATCCAGACGTGATGGGGAC
Zrt2 R1	AACCGCCAAAGCAAGACCTA
Zrt1 F2	TAGGTCTTGCTTTGGCGGTT
Zrt2 R2	CTGGCCAATTGGTAGTTGC

B. 3. Results and Discussion

We have previously reported that S100A12 possesses antifungal activity and acts through a mechanism of Zn(II) sequestration.⁸ We therefore questioned whether a major fungal pathogen, *C. albicans*, responds to Zn(II) deprivation, and what acquisition systems it can utilize to fight back. We obtained *C. albicans* strains *PRA1*^{-/-} and *ZRT1*^{-/-} from the Noble collection.⁹ The *PRA1*^{-/-} and *ZRT1*^{-/-} strains are defective in expressing the Zn(II) uptake proteins Pra1 and Zrt1, respectively. We expect them to be more susceptible to S100A12 treatment compared to the WT strain if they are functionally relevant with respect to Zn(II) acquisition. Upon S100A12 treatment, we observed a Ca(II) effect with the three strains, whereby S100A12 has enhanced antifungal in the presence of excess Ca(II) (Figure B. 2. A). This trend is consistent with the reported mechanism of action of S100A12.⁸ Under our Zn(II)-rich conditions (Tris:YPD medium), the three strains were equally susceptible to S100A12 in the absence of Ca(II), which suggests that at high Zn(II) levels, Pra1 and Zrt1 are not being utilized for Zn(II) acquisition under these *in vitro* conditions (Figure B. 2. A). In the presence of excess Ca(II), S100A12-treatment of the parent and *ZRT1*^{-/-} strains resulted in growth inhibition to OD₆₀₀ values of 0.2 and 0.25 respectively, while the *PRA1*^{-/-} strain was slightly more susceptible to A12 treatment compared to the parent and *ZRT1*^{-/-} strains (Figure B. 2. A). *C. albicans* possesses intracellular Zn(II)-storage compartments,⁴ and we speculate that no significant growth defect compared to the parent strain was observed due to use of these Zn(II) storage sources.

The difference in growth observed in the presence of Ca(II) across the three strains tested are within the experimental errors of this assay. We decided to repeat this experiment with various S100A12 concentrations in a Zn(II)-depleted growth medium in an attempt to parse out differences in susceptibilities of the strains to S100A12. A Zn(II)-depleted growth medium was made by pretreating Tris:YPD with 125 µg/mL of S100A12 for 1h at r.t. The medium was then spin filtered to remove S100A12, and ICP-MS analyses confirmed the Zn content of the resulting Zn(II)-depleted medium to be between 400-600 nM.

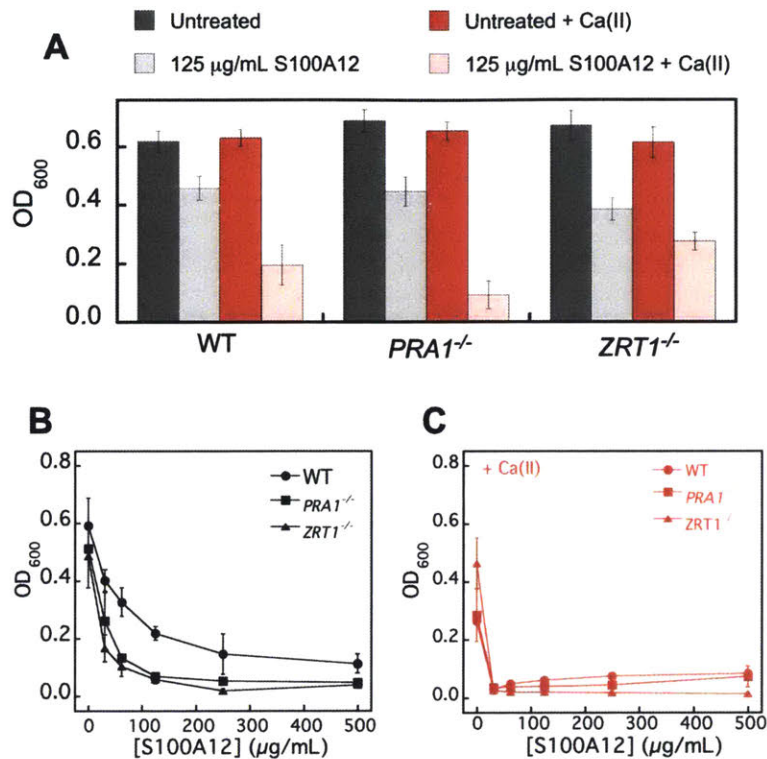


Figure B. 2. Antifungal activity of 125 µg/mL of S100A12 (\pm 2 mM Ca(II)) against *C. albicans* WT, *PRA1*^{-/-}, and *ZRT1*^{-/-} in Tris:YPD (t = 20 h, mean \pm SEM, n = 2). **B** Antifungal activity of A12 against *C. albicans* WT, *PRA1*^{-/-}, and *ZRT1*^{-/-} in Zn(II)-depleted Tris:YPD (t = 20 h, mean \pm SEM, n = 2). **C** Antifungal activity of A12 against *C. albicans* WT, *PRA1*^{-/-}, and *ZRT1*^{-/-} in Zn(II)-depleted Tris:YPD, + 2Mm Ca(II) (t = 20 h, mean \pm SEM, n = 2).

The data show that in the presence of Ca(II), growth of the three strains is completely inhibited even at the lowest S100A12 concentration (31.25 µg/mL) (Figure B. 2. C). This suggests that under Zn(II)-depleted condition and in the presence of excess Ca(II), the Zn(II)-uptake machinery of *C. albicans* cannot compete with the high-affinity form of S100A12. However in the absence of Ca(II), when S100A12 is not activated by Ca(II), the strains are able to compete with S100A12 for Zn(II), and a concentration-dependent growth inhibition is observed with S100A12 (Figure B. 2. B). The parent strain is more resistant to S100A12 treatment compared to the single-knockout mutants under all concentrations of S100A12 tested, implicating Pra1 and Zrt1 in Zn(II) acquisition under Zn(II)-depleted conditions (Figure B. 2. B); complete growth inhibition is

observed with the single knockout strains at 125 $\mu\text{g}/\text{mL}$ of S100A12, while the parent strain grows to an $\text{OD}_{600} = 0.2$ (Figure B. 2. B).

The results from the antimicrobial assays suggest that Pra1 and Zrt1 are involved in Zn(II) acquisition. As such, we wanted to obtain transcriptional insights about the mechanism of Zn(II) acquisition that *C. albicans* employs upon treatment with S100A12. We therefore decided to employ qRT-PCR to monitor changes in transcriptional levels of Zn(II)-regulated genes. The efficiency of the primers was confirmed, two primer sets per genes were employed, and two housekeeping genes *pma1* and *actin* were chosen (Table B. 1). The genes of interest we monitored are *PRA1*, *ZRT1*, *ZRT2* and *ZAP1*. The functions of each of these proteins are listed in Table B. 2.

The qRT-PCR results show that treatment of *C. albicans* WT with 125 $\mu\text{g}/\text{mL}$ of S100A12, or 62.5 $\mu\text{g}/\text{mL}$ of S100A12 with excess Ca(II) results in the upregulation of *PRA1* mRNA levels by 2.1- and 2.2-fold, respectively (Figure B. 3. B). The high-affinity transporter *ZRT1* is also upregulated by 3- (-Ca) and 3.2-fold (+Ca) (Figure B. 3). Interestingly, the low-affinity Zn(II)-transporter *ZRT2*, and the transcription factor *ZAP1* are upregulated to smaller extents, by less than 2-fold in the absence and presence of Ca(II) (Figure B. 3). Zap1 is an autoregulated Zn(II)-finger transcription factor protein that regulates *ZRT1* and *ZRT2* expression by binding to the zinc-response element (ZRE) in the promoter region of these genes. Its affinity for DNA is controlled by Zn(II) levels. In general we observe similar upregulation patterns in the absence and presence of excess Ca(II) added, which suggest that the same Zn(II)-acquisition mechanisms are activated by *C. albicans* upon treatment with S100A12 and Ca(II)-bound S100A12.

The trend in the expression levels of *ZAP1*, *ZRT1*, and *ZRT2* agrees with previous literature that studied the mRNA levels of *ZAP1*, *ZRT1*, and *ZRT2* in *Saccharomyces cerevisiae*. *S. cerevisiae* and *C. albicans* are both yeasts that are closely related from an evolutionary perspective, with conserved Zn(II) transporters.¹⁴ This pattern of expression levels correlates well

with our understanding of the different functions of these genes. High levels of the Zrt1 transporter are needed under Zn(II) limitation because of its critical role in supplying Zn(II) to the cell under these extreme conditions. Zrt2, the low affinity transporter, plays more of a housekeeping function, supplying Zn(II) to the cell under Zn(II)-replete conditions,¹⁵ and Zap1 is expressed only at low levels because of its role as a transcriptional regulator.^{4, 5}

Table B. 2. *C. albicans* genes monitored through qRT-PCR and their functions.

Gene	Function	Ref.
<i>PRA1</i>	Cell-wall associated and secreted protein. Zincophore	5,6
<i>ZRT1</i>	High-affinity Zn(II) transporter. Presumably interacts with Pra1 to deliver Zn(II) to <i>C. albicans</i>	3, 6
<i>ZRT2</i>	Low-affinity Zn(II) transporter. Considered a housekeeping gene.	15
<i>ZAP1</i>	Zn(II)-finger transcription factor of Pra1, Zrt1 and Zrt2	16-17

Interestingly, a greater fold change in mRNA expression levels are observed for the single knockout strains, *PRA1*^{-/-} and *ZRT1*^{-/-}, compared to WT strain upon treatment with S100A12 (±Ca) (Figure B. 3). For the *PRA1*^{-/-} strain, mRNA levels of *ZRT1* increased by 4 (-Ca) and 7 (+Ca) fold, while in *ZRT1*^{-/-}, *PRA1* levels increased by 7-fold (±Ca) (Figure B. 3). Furthermore, greater than a 2-fold increase in *ZRT2* levels is observed for both knockouts (Fig. A. 3). The higher fold increase observed overall with the single knockouts compared to the WT strain implicates a “compensation” mechanism, whereby the strains defective in Zn(II) uptake upregulate other functional components of their Zn(II) acquisition system to make up for this shortcoming. Furthermore, the upregulation of *ZRT2* in the *ZRT1*^{-/-} knockout agrees with previous studies carried out by *Eide and coworkers*, where they reported that overexpression of a plasmid containing *ZRT2* suppresses the Zn(II)-limited growth defect in *S. cerevisiae* in a *ZRT1*^{-/-} mutant.³

⁴ We speculate that a similar mechanism is possible with Pra1, hence explaining the fold-increase of *ZRT1* and *ZRT2* mRNA levels in the *PRA1*^{-/-} mutant.

The qRT-PCR experiments were repeated with S100A12 ΔHis₃Asp, a mutant of S100A12

that cannot coordinate Zn(II). As expected, S100A12 Δ His₃Asp produced no response in the genes monitored under all conditions tested (Figure B. 3), confirming that the genotypes observed are as a result of Zn(II)-starvation by S100A12, and not due to a physical interaction between *C. albicans* and S100A12.

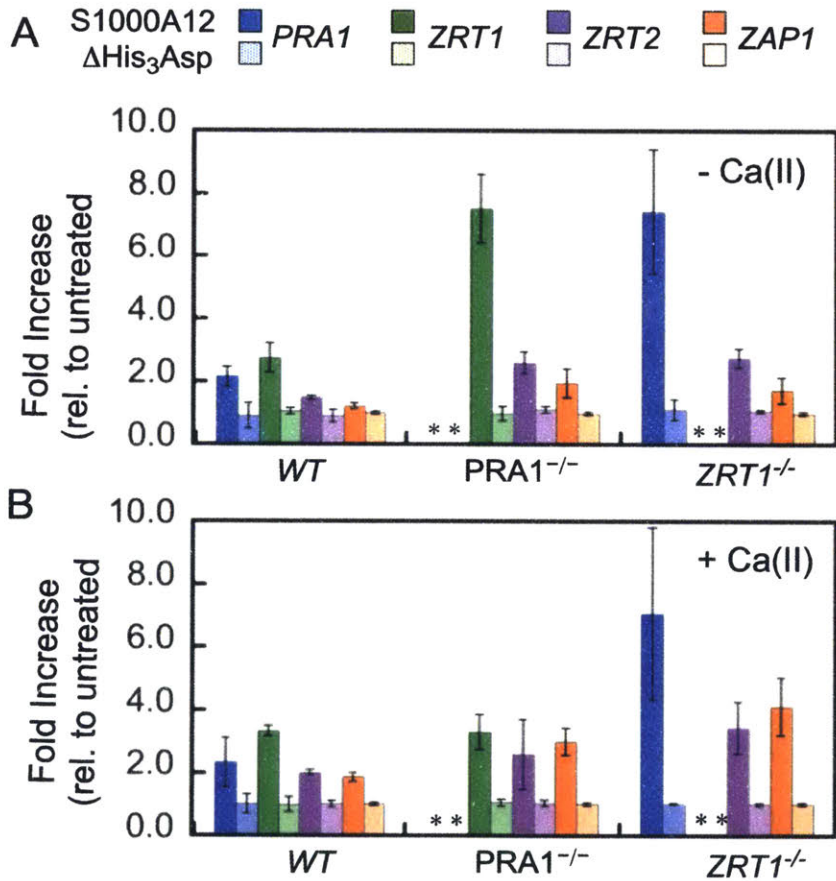


Figure B. 3. qRT-PCR data of *C. albicans* WT, *PRA1*^{-/-} and *ZRT1*^{-/-} treated with **A** 125 μ g/mL of S100A12, or **B** 62.5 μ g/mL of S100A12 with 2 mM Ca(II). The bars shaded in lighter colors correspond to S100A12 Δ His₃Asp-treated cultures at concentrations identical to S100A12. (t = 24 h, mean \pm STD, n = 3). Asterisks denote Ct values below the detection limit.

B. 4. Summary and Outlook

In summary, we have shown that Pra1 is expressed under conditions of S100A12-mediated Zn(II) starvation, and that Pra1 and Zrt1 are needed for growth of the fungal pathogen under Zn(II)-deplete conditions. The Zn(II) acquisition machinery of *C. albicans* is upregulated at the transcriptional level in response to S100A12 treatment, supporting the notion that S100A12 acts through a mechanism of Zn(II) sequestration. Future work will involve the purification and characterization of the Zn(II)-binding properties of Pra1. Furthermore, we would like to employ solution studies to investigate the competition between S100A12 and Pra1 for Zn(II). We expect that these studies will provide molecular insights on the competition for Zn(II) between host and pathogen factors for Zn(II).

B. 5. References

1. Hood, M. I.; Skaar, E. P., Nutritional immunity: transition metals at the pathogen-host interface. *Nat. Rev. Microbiol.* **2012**, *10* (8), 525-537.
2. Zackular, J. P.; Chazin, W. J.; Skaar, E. P., Nutritional immunity: S100 proteins at the host-pathogen interface. *J. Biol. Chem.* **2015**, *290* (31), 18991-18998.
3. Zhao, H.; Eide, D., The yeast ZRT1 gene encodes the zinc transporter protein of a high-affinity uptake system induced by zinc limitation. *Proc. Natl. Acad. Sci. U. S. A.* **1996**, *93*, 2454-2458.
4. Wilson, D.; Citiulo, F.; Hube, B., Zinc exploitation by pathogenic fungi. *PLoS Pathog.* **2012**, *8* (12), e1003034.
5. Marcil, A.; Gadoury, C.; Ash, J.; Zhang, J.; Nantel, A.; Whiteway, M., Analysis of PRA1 and its relationship to *Candida albicans*- macrophage interactions. *Infect Immun* **2008**, *76* (9), 4345-4358.

6. Citiulo, F.; Jacobsen, I. D.; Miramon, P.; Schild, L.; Brunke, S.; Zipfel, P.; Brock, M.; Hube, B.; Wilson, D., *Candida albicans* scavenges host zinc via Pra1 during endothelial invasion. *PLoS Pathog.* **2012**, *8* (6), e1002777.
7. Bardoel, B. W.; Kenny, E. F.; Sollberger, G.; Zychlinsky, A., The balancing act of neutrophils. *Cell Host Microbe* **2014**, *15* (5), 526-536.
8. Cunden, L. S.; Gaillard, A.; Nolan, E. M., Calcium ions tune the zinc-sequestering properties and antimicrobial activity of human S100A12. *Chem. Sci.* **2016**, *7* (2), 1338-1348.
9. Noble, S. M.; French, S.; Kohn, L. A.; Chen, V.; Johnson, A. D., Systematic screens of a *Candida albicans* homozygous deletion library decouple morphogenetic switching and pathogenicity. *Nat. Genet.* **2010**, *42* (7), 590-598.
10. Epicentre, MasterPure™ Yeast RNA Purification Kit. **2012**.
11. Biosystems, A., High capacity cDNA reverse transcription kits for 200 and 1000 reactions protocol. **2010**.
12. Zhao, S.; Fernald, R. D., Comprehensive algorithm for quantitative real-time polymerase chain reaction. *J. Comput. Biol.* **2005**, *12* (8), 1047-1064.
13. Nailis, H.; Coenye, T.; Van Nieuwerburgh, F.; Deforce, D.; Nelis, H. J., Development and evaluation of different normalization strategies for gene expression studies in *Candida albicans* biofilms by real-time PCR. *BMC Mol Biol* **2006**, *7*, 25.
14. Diezmann, S.; Cox, C. J.; Schonian, G.; Vilgalys, R. J.; Mitchell, T. G., Phylogeny and evolution of medical species of *Candida* and related taxa: a multigenic analysis. *J. Clin. Microbiol.* **2004**, *42* (12), 5624-35.
15. Zhao, H.; Eide, D., ZRT2 gene encodes the low affinity zinc transporter in *Saccharomyces cerevisiae*. *J. Biol. Chem.* **1996**, *271* (38), 23302 - 23210.
16. Zhao, H.; Eide, D., Zap1p, a metalloregulatory protein involved in zinc-responsive transcriptional regulation in *Saccharomyces cerevisiae*. *Mol. Cell. Biol.* **1997**, *17* (9), 5044-5052.

17. Zhao, H.; Butler, E.; Rodgers, J.; Spizzo, T.; Dueterhoeft, S.; Eide, D., Regulation of zinc homeostasis in yeast by binding of the ZAP1 transcriptional activator to zinc-responsive promoter elements. *J. Biol. Chem.* **1998**, *273* (44), 28713-28720.

Biographical Note

Lisa S. Cunden was born to Lysie Henri and Steve Cunden. She was born and raised in Trianon, Mauritius, surrounded by three annoying siblings and a multitude of less-annoying pets. She attended the all-girls catholic high school, Loreto College of Quatre-Bornes (LCQB), and ranked nationally in Chemistry for the Cambridge International Advanced-Level examination. In 2009, Lisa moved to the United States with a one-way ticket, two suitcases, and three scarves (ready to face the New England winters). She attended Smith College and graduated *magna cum laude* in 2013 with a B. A. in Chemistry. During her undergraduate time, she performed research in the laboratories of Prof. Bob Linck and Prof. Betsy Jamieson, and her undergraduate thesis focused on understanding the entropic and enthalpic contributions to the Chelate Effect. Lisa moved to San Francisco in the Spring of 2013 and worked at Novartis Institute for Biomedical Research (NIBR), to gain experience in the field of oncology-proteomics. Lisa came to MIT in the summer of 2014 to join the laboratory of Prof. Elizabeth Nolan. At MIT, Lisa focused on investigating the antimicrobial modes of action of the host-defense peptides, calprotectin, S100A12, S100A7, and S100A15. She was also a board member of CGSC and WIC. Outside of MIT, you can usually find Lisa training for her next half-marathon or marathon, daydreaming about her next scuba-diving vacation by means of Instagram, scrolling through pictures of her nieces Charlotte and Lucy, or petting other people's dogs.

Lisa S. Cunden

Education

Ph.D. Chemistry
2014–2018

Massachusetts Institute of Technology
Advisor: Professor Elizabeth M. Nolan

B. A. Chemistry
2009–2013

Smith College
Advisor: Professor Bob Linck

Publications

1. Cunden, L. S. and Nolan, E. M. "Preparation of the Oxidized and Reduced Forms of Psoriasin (S100A7)." *Meth. Mol. Biol.* **2018**, accepted.
2. Cunden L. S. and Nolan E. M., Bioinorganic Explorations of Zn(II) Sequestration by Human S100 Host-Defense Proteins, *Biochemistry* **2018**, 57(11), 1673–1680
3. Richardson C. E. R, Cunden L. S., Butty V. L., Nolan E. M, Lippard S. J., Shoulders M. D., A Method for Selective Depletion of Zn (II) Ions from Complex Biological Media and Evaluation of Cellular Consequences of Zn (II) Deficiency, *J. Am. Chem. Soc.* **2018**, 140(7), 2413–2416
4. Cunden L. S., Brophy M. B., Rodriguez G. E., Flaxman H. A., Nolan E. M., Biochemical and Functional Evaluation of the Intramolecular Disulfide Bonds in the Zinc-Chelating Antimicrobial Protein Human S100A7 (Psoriasin), *Biochemistry* **2017**, 56(43), 5726–5738
5. Nakashige T.G., Stephan J.R, Cunden L. S., Brophy M. B., Wommack A. J., Keegan B. C., Shearer J. M., Nolan E. M., The Hexahistidine Motif of Host-Defense Protein Human Calprotectin Contributes to Zinc Withholding and Its Functional Versatility, *J. Am. Chem. Soc.* **2016**, 138(37), 12243–12251
6. Cunden L. S., Gaillard A., Nolan E. M., Calcium Ions Tune the Zinc-Sequestering Properties and Antimicrobial Activity of Human S100A12, *Chem. Sci.* **2015**, 7, 1338–1348
7. Hayden J. A., Brophy, M. B., Cunden L. S., Nolan E. M., "High-affinity Manganese Coordination by the Host-defense Protein Human Calprotectin is Calcium-dependent and Requires the Histidine-rich Site Formed at the Dimer Interface." *J. Am. Chem. Soc.* **2013**, 135(2), 775–787
8. Cunden L. S., Linck R. G., "Fe(CO)₄ and Related Compounds as Isolobal Fragments", *Inorg. Chem.*, **2011**, 50(10), 4428–4436

Patent

Richardson C. E. R, Cunden L. S., Butty V. L., Nolan E. M, Lippard S. J., Shoulders M. D. Composition and Methods for Selectively Sequestering Metal ions. December 29 2017, U.S provisional application, pending.